

Catalytic Hydrogels with a Prebiotic Nature

Kirsten Hawkins

Doctor of Philosophy

Chemistry

University of York

October 2019

Abstract:

Low-molecular-weight-gelators (LMWGs) form a network *via* non-covalent interactions, these interactions immobilise the surrounding bulk solvent and form a gel. As a result, these gels are highly responsive, dynamic and highly porous solvated materials. It has been suggested that prior to the evolution of the membranes, gels may have provided an appropriate medium for the organisation of simple components, which could constitute early life. The research presented here attempts to develop a protocell by using LMWGs and form hydrogels that are both simplistic in nature and catalytically proficient. Three single amino acid amides, based upon L-valine, L-serine and L-glutamine were initially synthesised and tested for their ability to gel in water as well as their catalytic ability in the aldol condensations. It was found that all the amides were catalytically active and formed organo- and hydrogels. In addition glutamine amide was found to spontaneously form more effective hydrogels in the presence of 4-nitrobenzaldehyde in water. This two-component gel system was examined further and was found to work with many aromatic aldehydes including benzaldehyde, and demonstrated to be based on dynamic formation of a self-assembling imine.

A second generation of gelators was generated by coupling glutamine amide and benzaldehyde followed by reduction and tested for gelation ability and catalytic ability. It was found that this benzyl glutamine amide was able to form hydrogels and was catalytically proficient for the aldol reaction in solution phase. After establishing the catalytic potential and gelling ability of the new hydrogelator, the gel was also tested for the dimerization of glycolaldehyde, as this is a prebiotically relevant reaction. The results indicated good conversion to threose and erythrose without the loss of the gel network. Furthermore there was a degree of enantioselectivity induced by the chirality of the catalytic gel.

The formation of the prebiotically relevant 2-deoxy-D-ribose was also studied, unfortunately the gel was lost and no product was produced. However, the formation of 2,4-diphosphate tetrose products *via* the dimerization of glycolaldehyde phosphate on the hydrogel was shown to be effective.

Table of contents

Catalytic Hydrogels with a Prebiotic Nature	i
Abstract:.....	i
Table of contents	ii
List of Figures.....	v
List of Schemes	xiii
List of Tables.....	xv
Acknowledgements	xvii
1.0 Introduction.....	1
1.1 Gels and Low Molecular Weight Gelators (LMWGs).....	1
1.2 Two component gels:	3
1.2.1 Two-component gel systems:.....	4
1.3 Catalytic supramolecular LMWGs.....	8
1.4 Supramolecular structures and the origins of life	22
1.5 Origins of sugars	27
1.6 Prebiotic interest in phosphates.....	29
1.7 Prebiotic interest of amino acids	32
1.8 Amino acids a prebiotic catalysts	37
1.9 LMWGs as a catalytic media for prebiotic chemistry.....	48
1.10 Conclusions and project aims	51
2.0 Amino acid amides as catalysts and hydrogelators	53
2.1 Aims:.....	53
2.2 Results and discussion.....	55
2.2.1 Synthesis of valine (206), serine (209) and glutamine amide (210)	55
2.2.2 Solvent screening for valine (206), serine (209) and glutamine (210) amides for gelation:	56
2.2.3 Simple catalysis of 4-nitrobenzaldehyde (47) and cyclohexanone (49) in a direct aldol reaction:	62
2.3 Conclusions	74
3.0 A novel Two-component hydrogel	75
3.1 Aims:.....	75
3.2 Results and discussion:.....	76

3.2.1 Evidence for Schiff base formation	76
3.2.2 Two-component gel system	78
3.2.3 Optimising synthesis of glutamine amide	79
3.2.4 Identifying the minimum ratio of aldehyde to amide required to form a gel.....	80
3.2.5 Identifying the minimum gelation concentration of a 1:1 aldehyde: amide system	85
3.2.6 Physical properties and characteristics of the two component system.....	86
3.2.7 Dynamic light scattering (DLS)	89
3.2.8 Circular Dichroism spectroscopy:.....	91
3.2.9 pH screening.....	94
3.2.10 Self-healing properties	97
3.2.11 Aldehyde screening.....	99
3.2.12 Physical properties and characterising different aldehyde gels.....	106
3.2.13 Rheology.....	108
3.3 Conclusions	114
4.0 Developing a prebiotic protocell	115
4.1 Aims.....	115
4.2 Results and discussion:.....	118
4.2.1 Synthesis of benzylglutamine amide (230)	118
4.2.2 Solution phase catalysis of 4-nitrobenzaldehyde and cyclohexanone.....	122
4.2.3 Gelation and characterisation	130
4.2.4 Catalysis on the gel.....	135
4.3 Conclusion:	145
5.0 A prebiotic route to 2-deoxy-D-ribose and phosphorylated sugars	146
5.1 Aims.....	146
5.1 Results and Discussion	147
5.2 Conclusions.....	161
6.0 Conclusions and Future work	162
7.0 Experimental.....	164
7.1 Synthesis of L-Boc-serine dodecylamine (248)	165
7.2 Synthesis of L-serine dodecylamine (209)	166
7.3 Method one for the synthesis of L-Boc-glutamine dodecylamine (249).....	167
7.4 Method two for the synthesis of L-Boc-glutamine dodecylamine (249).....	168
7.5 Synthesis of L-Glutamine dodecylamine (210)	168
7.6 Synthesis of (E)-2-(benzylideneamino)-N¹-dodecyl-L-glutamine amide (231).....	169
7.7 Synthesis of 2-Benzylamino-N¹-dodecyl-L-glutamine amide (230).....	170

7.8 Synthesis of (2 <i>R</i> , 3 <i>S</i>) <i>E</i> -4-(2,2-diphenylhydrazone)-butane-1,2,3-triol (232) ¹⁴⁶	171
7.9 Synthesis of (2 <i>S</i> , 3 <i>R</i>) <i>E</i> -4-(2,2-diphenylhydrazone)-butane-1,2,3-triol (233) ¹⁴⁶	172
7.10 Synthesis of (2 <i>S</i> , 3 <i>S</i>) <i>E</i> -4-(2,2-diphenylhydrazone)-butane-1,2,3-triol (234) ¹⁴⁶	172
7.11 Synthesis of (2 <i>R</i> , 3 <i>R</i>) <i>E</i> -4-(2,2-diphenylhydrazone)-butane-1,2,3-triol (235) ¹⁴⁶	173
7.12 Synthesis of 2-(2,2-diphenylhydrazone)-ethanol (235) ¹⁴⁶	174
7.13 Synthesis of Bis(cyclohexyl-1-ammonium)-allyl-phosphate (238) ⁹⁷	174
7.14 Synthesis of 2-(Phosphonoxy)acetaldehyde (239) ⁹⁷	175
7.15 Synthesis of 2-(Phosphonoxy)acetaldehyde calcium salt (97) ⁹⁷	176
7.16 General procedure for solution phase catalysis of 4-nitrobenzaldehyde (47) and cyclohexanone (49) ³⁸	176
7.17 General procedure for the dimerization of glycolaldehyde on the hydrogel.....	177
7.18 General procedure of Aldol condensation of D-glyceraldehyde and acetaldehyde on the hydrogel	178
7.19 General procedure for the dimerization of glycolaldehyde phosphate calcium salt on the hydrogel	179
7.20 General procedure for the dimerization of glycolaldehyde phosphate on the hydrogel	179
7.21 Solvent screening for valine, serine and glutamine amides for gelation	180
7.22 General procedure for gelation of L-glutamine amide (210) and aldehyde.....	180
7.23 Gelation of 2-benzylamino-N ¹ -dodecyl-L-glutamine amide (230)	180
7.24 TEM sample preparation	180
7.25 SEM sample preparation	181
7.26: General procedure for Circular dichroism samples with glutamine amide (210) and 4- nitrobenzaldehyde (47).....	181
7.27: General procedure for Circular dichroism samples with benzylglutamine amide (230)	181
7.28: General procedure for rheology samples with glutamine amide (210) and 4- nitrobenzaldehyde (47).....	182
7.29: General procedure for Circular dichroism samples with benzylglutamine amide (230)	182
Abbreviations	183
8.0 Appendix:	186
References.....	205

List of Figures

Figure 1: Examples of polymeric gelators	1
Figure 2: 1,3:2,4-Dibenzylidene-D-sorbitol (DBS)	2
Figure 3: Low molecular weight supramolecular gel assembly process	2
Figure 4: Illustration of three main classes of two-component supramolecular gels ⁴	3
Figure 5: Barbituric acid and pyrimidine units studied by Hanabusa in a two-component gelation system. 4	
Figure 6: Diamine Lysine carboxylic acid two-component system structure	5
Figure 7: Assembly of guanosine hydrazide into G-quartets and further reversible reaction with aldehydes leading to hydrogels	7
Figure 8: Formation of acyl hydrazone gelator from commercial building blocks	7
Figure 9: Three categories of supramolecular approaches to catalysis	8
Figure 10: Metallogel for oxidative reduction of benzyl alcohol to benzaldehyde	9
Figure 11: 1,3:2,4-Dibenzylidene sorbitol modified with acyl hydrazides used for reduction of PdNPs	9
Figure 12: Agarose, used for structural robustness	10
Figure 13: Schematic of the 'waste-to-wealth' approach using DBS-CONHNH ₂ /agarose hybrid hydrogels to remediate waste, generating PdNPs in situ then using the resulting material to catalyse Suzuki cross-coupling reactions. ³¹	10
Figure 14: Proposed hydrogen bonding of cyclodipeptide result in gelation during cyanohydrin addition reactions ³⁴	12
Figure 15: Histidine-functionalized self-assembling peptide amphiphiles studied by Stupp	13
Figure 16: Organogelator developed by Tu and co-workers	13
Figure 17: L-Valine bolaamphiphilic 36 scaffold used to design the L-proline derived bolaamphiphilic 39 14	
Figure 18: Cooperation of neighbouring proline moieties organised as a charge relay system	15
Figure 19: Amphiphilic hydrogelator with proline moiety	16
Figure 20: Sample spanning network structure showing hydrogen bonding interactions	17
Figure 21: Short lipophilic peptide hydrogelator	18
Figure 22: Structure of triazolyl functionalised gelator	19
Figure 23: Asymmetric alcoholysis of anhydrides	20
Figure 24: Gelator structure	21
Figure 25: Ionic solvents used	21
Figure 26: Chiral catalysts	21
Figure 27: Prokaryotic cell	22
Figure 28: Structure of a micelle and a vesicle	24
Figure 29: Structure of alkyl amine and fatty acid used to form stabilised vesicles	24
Figure 30: Synthesis of dipeptide derivative 85 inside a vesicle by the catalysis of Ser-His 82. Once synthesised the product moved to the bilayer of the vesicle. The group found vesicles with the product would grow, where as those with-out would shrink	25
Figure 31: Droplet formation in a hydrogel	26
Figure 32: Compounds used to form vesicle with hydrogel encapsulated with in	27
Figure 33: Biologically important phosphates	29

Figure 34: An overview of suggested prebiotic routes to phosphates.....	30
Figure 35: Dimerization of glycolaldehyde phosphate in aqueous sodium hydroxide	30
Figure 36: Dimerization of glycolaldehyde phosphate with formaldehyde in aqueous sodium hydroxide	31
Figure 37: Potential prebiotic pathway to phosphorylate pyruvate.....	32
Figure 38: Miller-Urey electric discharge experiment set up	33
Figure 39: Amino acid structures identified in Miller-Urey electric discharge experiment.	33
Figure 40: Amino acids identified in reaction replicating hydrothermal events	35
Figure 41: Carbon-carbon bond formation in direct aldol condensation.....	37
Figure 42: Zimmerman-Traxler model for the <i>E</i> -enolate.....	38
Figure 43: Product from favoured six-membered transition state using the Zimmerman-Traxler model ..	38
Figure 44: L-proline catalyst six-membered transition state involving a hydroxylated ketone	41
Figure 45: Bifunctional organocatalyst.....	42
Figure 46: Short lipophilic peptide hydrogelator	48
Figure 47: Products observed in the dimerization of TIPS protected glycolaldehyde	49
Figure 48: Structure of the lipopeptide	50
Figure 49: Valine amide hydrogelator	50
Figure 50: Proposed structure of amino acid amide	52
Figure 51: L-Proline.....	53
Figure 52: L-Valine (208), L-serine (119) and L-glutamine (145)	54
Figure 53: Amino acid amide targets to be synthesised.....	54
Figure 54: Hydrogel formed: 1= L-valine amide (206), 2= L-serine amide (209), 3= L-glutamine amide (210)	56
Figure 55: Two-dimensional projection (A-C) and a 3D rendering (D) of the Hansen space using minimal enclosing spheres and appearance at the CGC. The blue sphere encloses DBS solutions, the green sphere encloses opaque gels, and the red sphere encloses clear gels ¹⁵²	59
Figure 56: Valine amide (206) 3-D Hansen parameter plot	60
Figure 57: Serine amide (209) 3-D Hansen parameter plot	61
Figure 58: Glutamine amide (210) 3-D Hansen parameter plot.....	61
Figure 59: 1H NMR of crude reaction material for the aldol condensation of 4-nitrobenzaldehyde (47) and cyclohexanone (49) in CDCl ₃ . Showing the aromatic region only used for conversion calculations ..	64
Figure 60: 1H NMR of crude reaction material for the aldol condensation of 4-nitrobenzaldehyde (47) and cyclohexanone (49) in CDCl ₃ . Showing the aliphatic region only used for diastereoselectivity calculations	65
Figure 61: Graph showing the percentage of conversion at time intervals of 24 h, 48 h and 72 h with different amino acid amides. Data reported here is an average of three experiments, error bars show the deviation in the data repeats	67
Figure 62: Graph showing percentage <i>anti</i> product for different catalysts	67
Figure 63: Suspected new compound formed in situ due to appearance of new aromatic peaks in ¹ H NMR	68
Figure 64: Zimmerman-Traxler like transition state of L-proline.....	68

Figure 65: HPLC trace of crude aldol condensation of 4-nitrobenzaldehyde (47) and cyclohexanone (49). IB Chiral Pak, 1 mL/min, 97:3 Hexane: IPA	69
Figure 66: Graph showing HPLC ee% of crude material after 72 h with different catalysts.....	70
Figure 67: Transition state required to give the stereochemistry observed when <i>anti</i> -favours.....	72
Figure 68: Transition state required to give the stereoselectivity observed when <i>syn</i> favours.....	73
Figure 69: Aldol reaction containing glutamine amide (210), cyclohexanone and 4-nitrobenzaldehyde (47) in water (20 mL) that resulted in gelation of most of the reaction mixture	74
Figure 70: Mass spectroscopy of sample proposed to be a Schiff base formed from glutamine amide (210) and 4-nitrobenzaldehyde (47).....	77
Figure 71: ¹ H NMR of dehydrated two-component gel system	77
Figure 72: ¹ H NMR of 4-nitrobenzaldehyde (47) (670 μg) and glutamine amide (210) (1.5mg) hydrogel with chloroform spike (2 μL). Obtained in D ₂ O (0.7 mL) 400 MHz	82
Figure 73: Gel NMR of 4-nitrobenzaldehyde (47) and glutamine amide (210) (1:1, 1.48 mg mL ⁻¹) with DMSO solvent spike (2μL).....	84
Figure 74: Gel NMR of 4-nitrobenzaldehyde (47) and glutamine amide (210) (1:1, 1.48 mg mL ⁻¹) with MeOH solvent spike (2μL).....	84
Figure 75: TEM image 1 mg / mL glutamine amide (210) and 480 μg 4-nitrobenzaldehyde (47) (1:1)	88
Figure 76: SEM image 1 mg / mL glutamine amide (210) and 480 μg 4-nitrobenzaldehyde (47) (1:1)	88
Figure 77: TEM image 2 mg / mL glutamine amide (210) and 960 μg 4-nitrobenzaldehyde (47) (1:1)	89
Figure 78: TEM image 3 mg / mL glutamine amide (210) and 1.44 mg 4-nitrobenzaldehyde (47) (1:1).....	89
Figure 79: TEM image 5 mg / mL glutamine amide (210) 2.4 mg 4-nitrobenzaldehyde (47) (1:1)	89
Figure 80: DLS data of glutamine amide (210) 1 mg/ mL	90
Figure 81: a) Initial DLS of 1:1 glutamine amide (210) and 4-nitrobenzaldehyde (47) in 1 mL water (ca 100 °C).....	90
Figure 82: DLS of 1:1 glutamine amide (210) and 4-nitrobenzaldehyde (47) in 1 mL water after standing for 5 h.....	91
Figure 83: CD spectrum of 1:1 glutamine amide (210), 4-nitrobenzaldehyde (47) (solution 0.0625 mM) ..	92
Figure 84: CD spectrum of 1:1 glutamine amide (210) 4-nitrobenzaldehyde (47) solution 0.25 mM.....	93
Figure 85: Variable temperature of 1:1 glutamine amide (210) 4-nitrobenzaldehyde (47) gel CD spectra 1.48 mg total loading in 1 mL. 450 μL sample taken and transferred to 1 mm quartz cuvette for analysis	94
Figure 86: Acid catalysed imine formation	97
Figure 87: Injection gel method	98
Figure 88: π-π stacking interactions	101
Figure 89: Non-covalent interactions involved with self-assembly when aromatic ring is present	101
Figure 90: Non-covalent interactions involved with self-assembly when aliphatic chain is present	102
Figure 91: 2-Nitrobenzaldehyde glutamine amide gel compared to 4-Nitrobenzaldehyde (47) glutamine gel	102
Figure 92: Mass spectrum of 9-anthraldehyde (220) and glutamine amide (210) imine formed in gelation. RMM = 503.34.....	103

Figure 93: Mass spectrum of benzaldehyde (221) and glutamine amide (210) imine formed in gelation. RMM = 402.31, 424.29.....	103
Figure 94: Mass spectrum of cinnamaldehyde (222) and glutamine amide (210) imine formed in gelation. RMM = 427.32, 450.80.....	104
Figure 95: Mass spectrum of 4-methoxybenzaldehyde (226) and glutamine amide (210) imine formed in solution. RMM = 432.22, 454.30	104
Figure 96: Mass spectrum of vanillin (225) and glutamine amide (210) imine formed in solution. RMM = 448.31, 470.29	105
Figure 97: Graph of T_{gels} for different aldehyde derivatives of the aldehyde : glutamine amide (210) hydrogel 1:1 5 mg of glutamine amide in 1 mL water.....	106
Figure 98: SEM of 9-anthraldehyde (220) two-component hydrogel with glutamine amide (210).....	107
Figure 99: SEM of benzaldehyde (221) two-component hydrogel with glutamine amide (210).....	107
Figure 100: SEM of Cinnamaldehyde (222) two-component hydrogel with glutamine amide (210)	107
Figure 101: SEM of 2-nitrobenzaldehyde (223) two-component hydrogel with glutamine amide (210) ..	107
Figure 102: Bottomless vial, and bottomless vial attached to glass plate with sealant	108
Figure 103: Bottomless vial in suba-seal	108
Figure 104: Left bottomless vial in suba-seal, no glass bottom, Right suba-seal with glass bottom.....	109
Figure 105: Rheology sample made with 4-nitrobenzaldehyde (47) and glutamine amide (210) (1.48 mg 1 mL) with pH 2.90 solution.....	109
Figure 106: 4-Nitrobenzaldehyde (47) (480 μ g) and glutamine amide (210) (1 mg) Gel 1:1 in 1 mL pH 2.9. Elastic (G' , blue circles) and loss (G'' , orange circles) moduli of hydrogels with varying shear strain (frequency = 1 Hz).	111
Figure 107: 4-Nitrobenzaldehyde (47) and glutamine amide (210) gel 1:1 pH 2.9. Elastic (G' , blue circles) and loss (G'' , orange circles) moduli of hydrogels with varying frequency	111
Figure 108: Benzaldehyde and glutamine amide (210) (5 mg) 1:1 rheology sample prepared using a bottomless vial and sealant.	112
Figure 109: Rheology sample made with 2-nitrobenzaldehyde (223) and glutamine amide (210).....	112
Figure 110: 2-Nitrobenzaldehyde (223) (1.2 mg) and glutamine amide (210) (2.4 mg) Gel 1:1 in 1 mL water Elastic (G' , blue circles) and loss (G'' , orange circles) moduli of hydrogels with varying shear strain (frequency = 1 Hz).	113
Figure 111: 2-Nitrobenzaldehyde (223) (1.2 mg) and glutamine amide (210) (2.4 mg) hydrogel (1:1) in 1 mL water. Elastic (G' , blue circles) and loss (G'' , orange circles) moduli of hydrogels with varying frequency	113
Figure 112: Amine target molecule with catalytic site (in blue) available	116
Figure 113: Proposed new hydrogelator with catalytic activity (shown in red).....	117
Figure 114: Proposed new scaffold for gelator, benzylglutamine amide (230).....	118
Figure 115: ^1H NMR of benzylglutamine imine (231) in deuterated DMSO. 400 MHz.....	119
Figure 116: ^1H NMR of benzylglutamine amide (230) in deuterated DMSO	122
Figure 117: Percentage conversion of start material to product over time using benzylglutamine amide (230) 10 mol% in water.....	124

Figure 118: NMR dr % for Anti product using 10 mol% benzylglutamine amide (230) in water	125
Figure 119: HPLC <i>Syn Anti</i> ee% with benzylglutamine amide (230) in water	125
Figure 120: Example of HPLC trace of 4-nitrobenzaldehyde (47) and cyclohexanone (49) aldol condensation in water catalysed by benzylglutamine amide (230) at 48 h crude reaction.....	126
Figure 121: Graph showing percentage conversion of start material to product in 24 h at different pH and with or without catalyst (231)	127
Figure 122: Graph showing percentage <i>anti</i> product at different pH in 24 h with and without catalyst (231)	128
Figure 123: Graph showing <i>syn</i> and <i>anti</i> ee% at different pH with catalyst (231) in 24 h	128
Figure 124: Proposed transition state for the major and minor <i>anti</i> products	129
Figure 125: Proposed transition states for the major <i>syn</i> products.....	130
Figure 126: Results of the highly concentrated gelation of benzylglutamine amide (230) (3 mg) water (0.1 mL) using tube inversion test. Heat cool induced	130
Figure 127: Result of highly concentrated gelation on benzylglutamine amide (230) (6 mg) in water (0.2 mL) using tube inversion test. Heat then sonicate induced gelation.....	131
Figure 128: 1 mg mL ⁻¹ benzylglutamine amide (230) gel and SEM image of the gel network	132
Figure 129: Minimum gelation concentration mg mL ⁻¹	132
Figure 130: Variable temperature of CD spectrum of benzylglutamine amide (230) gel 1mg in 1 mL transferred 450 µL 1mm quartz cuvette	132
Figure 131: ¹ H NMR of benzylglutamine amide (230) hydrogel. 0.7 mg in 0.7 mL D ₂ O, 2 µL DMSO	133
Figure 132: Benzylglutamine amide (230) Gel 4 mg in 1 mL water. Elastic (G', blue circles) and loss (G'', orange circles) moduli of hydrogels with varying shear strain (frequency = 1 Hz).	134
Figure 133: Benzylglutamine amide (230) Gel 4 mg in 1 mL water. Elastic (G', blue circles) and loss (G'', orange circles) moduli of hydrogels with varying frequency.....	135
Figure 134: a) Benzylglutamine amide (230) gel before reagents pipetted on top of the surface. b) Once reagents added to the surface of the gel.....	136
Figure 135: c) Benzylglutamine amide (230) gel before reaction. d) Benzylglutamine amide (230) gel after aldol reaction has been on the gel for 48 h	137
Figure 136: Erythrose and Threose Hydrazone HPLC traces Chiralpak AD column (85:15 <i>n</i> -hexane: IPA)	139
Figure 137: Mixed hydrazone HPLC trace Chiralpak AD column (85:15 <i>n</i> -hexane: IPA)	139
Figure 138: Erythrose and Threose Hydrazone HPLC traces Chiralpak IC column (90:10 <i>n</i> -hexane: IPA) 40 °C	140
Figure 139: Mixed Hydrazone HPLC trace Chiralpak IC column (90:10 <i>n</i> -hexane: IPA) 40 °C. L-erythrose hydrazone = 18.414 min, D-threose Hydrazone = 21.506 min, D-erythrose = 26.264 min, L-threose = 33.021 min	140
Figure 140: An authentic crude ¹ H NMR of the dimerization of glycolaldehyde (89) on the benzylglutamine amide (230) gel. Protected as the hydrazone	141
Figure 141: Percentage conversion to threose (234/235) and erythrose (232/233) in water and pH7 analysed as the hydrazone	143

Figure 142: Diastereomeric ratio of erythrose (232/233) to threose (234/235) in pH7 and water analysed as the hydrazone	144
Figure 143: Enantioselectivity of erythrose (232/233) and threose (234/235) in water and pH7 analysed at the hydrazone	144
Figure 144: Formation of 2-deoxy-D-ribose (186) and 2-deoxythreopentose (187)	146
Figure 145: Formation of 2,4-threosephosphate and 2,4-erythrosephosphate (98) from the dimerization of glycolaldehyde phosphate (97)	147
Figure 146: Image a gel with reagents on the surface. Image b shows the layer of reagents on the gel ..	148
Figure 147: ¹ H NMR spectrum of 2-deoxy-D-ribose diphenyl hydrazide standard (188)	149
Figure 148: ¹ H NMR spectrum of crude reaction taken place on benzyl glutamine amide hydrogel after 7 days, diphenyl hydrazine trapped	150
Figure 149: Gels left for 7 days image c at the start of reaction, image d after 7 days	150
Figure 150: Images of the gel at the start of the reaction with reagents added (e), and after 7 days (f) ..	152
Figure 151: Glycolaldehyde phosphate reaction on the gel using the free acid (239) at the start (g) and after 48h (h)	153
Figure 152: (i) Benzylglutamine amide (230) gel before reagents loaded, (j) once reagents (239) added resulting in the loss of the gel network	154
Figure 153: In situ gel during the dimerization of glycolaldehyde phosphate (239) catalysed by benzylglutamine amide (230)	154
Figure 154: Electrospray mass spectrum of gel formed <i>in situ</i>	155
Figure 155: ¹ H NMR spectrum of crude glycolaldehyde phosphate (239) dimerization ¹ H NMR (700 MHz) D ₂ O	156
Figure 156: SEM image of gel formed <i>in situ</i> 1000 magnification	157
Figure 157: SEM image of gel formed <i>in situ</i> 5000 magnification	158
Figure 158: ¹ H NMR of hydrogel formed in the catalysis of glycolaldehyde phosphate (239) dimerization. 10uL DMSO spike	159
Figure 159: HPLC trace for stands for the aldol condensation of 4-nitrobenzaldehyde with using D/L proline	187
Figure 160: HPLC trace for aldol condensation of 4-nitrobenzaldehyde with cyclohexanone at 72 h run 1 catalysed by valine amide in solution phase	188
Figure 161: HPLC trace for aldol condensation of 4-nitrobenzaldehyde with cyclohexanone at 72 h run 2 catalysed by valine amide in solution phase	188
Figure 162: HPLC trace for aldol condensation of 4-nitrobenzaldehyde with cyclohexanone at 72 h run 3 catalysed by valine amide in solution phase	189
Figure 163: HPLC trace for aldol condensation of 4-nitrobenzaldehyde with cyclohexanone at 72 h run 1 catalysed by serine amide in solution phase	189
Figure 164: HPLC trace for aldol condensation of 4-nitrobenzaldehyde with cyclohexanone at 72 h run 2 catalysed by serine amide in solution phase	190
Figure 165: HPLC trace for aldol condensation of 4-nitrobenzaldehyde with cyclohexanone at 72 h run 1 catalysed by glutamine amide in solution phase	190

Figure 166: HPLC trace for aldol condensation of 4-nitrobenzaldehyde with cyclohexanone at 72 h run 2 catalysed by glutamine amide in solution phase	191
Figure 167: HPLC trace for aldol condensation of 4-nitrobenzaldehyde with cyclohexanone at 72 h run 3 catalysed by glutamine amide in solution phase	191
Figure 168: HPLC standard for the aldol condensation of 4-nitrobenzaldehyde and cyclohexanone using D/L proline as a catalyst	193
Figure 169: HPLC trace for aldol condensation of 4-nitrobenzaldehyde with cyclohexanone at 24 h run 1 catalysed by benzyl glutamine amide in solution phase	193
Figure 170: HPLC trace for aldol condensation of 4-nitrobenzaldehyde with cyclohexanone at 24 h run 2 catalysed by benzyl glutamine amide in solution phase	194
Figure 171: HPLC trace for aldol condensation of 4-nitrobenzaldehyde with cyclohexanone at 24 h run 3 catalysed by benzyl glutamine amide in solution phase	194
Figure 172: HPLC trace for aldol condensation of 4-nitrobenzaldehyde with cyclohexanone at 48 h run 1 catalysed by benzyl glutamine amide in solution phase	195
Figure 173: HPLC trace for aldol condensation of 4-nitrobenzaldehyde with cyclohexanone at 48 h run 2 catalysed by benzyl glutamine amide in solution phase	195
Figure 174: HPLC trace for aldol condensation of 4-nitrobenzaldehyde with cyclohexanone at 48 h run 3 catalysed by benzyl glutamine amide in solution phase	196
Figure 175: HPLC trace for aldol condensation of 4-nitrobenzaldehyde with cyclohexanone at 72 h run 1 catalysed by benzyl glutamine amide in solution phase	196
Figure 176: HPLC trace for aldol condensation of 4-nitrobenzaldehyde with cyclohexanone at 72 h run 2 catalysed by benzyl glutamine amide in solution phase	196
Figure 177: HPLC trace for aldol condensation of 4-nitrobenzaldehyde with cyclohexanone at 72 h run 3 catalysed by benzyl glutamine amide in solution phase	197
Figure 178: HPLC trace for aldol condensation of 4-nitrobenzaldehyde with cyclohexanone at 72 h run 1 pH 8.6 buffer control reaction	198
Figure 179: HPLC trace for aldol condensation of 4-nitrobenzaldehyde with cyclohexanone at pH 7 with benzylglutamine amide control reaction 24 h run 1	198
Figure 180: HPLC trace for aldol condensation of 4-nitrobenzaldehyde with cyclohexanone at pH 7 with benzylglutamine amide control reaction 24 h run 2	198
Figure 181: HPLC trace for aldol condensation of 4-nitrobenzaldehyde with cyclohexanone at pH 7 with benzylglutamine amide control reaction 24 h run 3	199
Figure 182: HPLC trace for aldol condensation of 4-nitrobenzaldehyde with cyclohexanone at pH 4 with benzylglutamine amide control reaction 24 h run 1	199
Figure 183: HPLC trace for aldol condensation of 4-nitrobenzaldehyde with cyclohexanone at pH 4 with benzylglutamine amide control reaction 24 h run 2	199
Figure 184: HPLC trace for aldol condensation of 4-nitrobenzaldehyde with cyclohexanone at pH 4 with benzylglutamine amide control reaction 24 h run 3	200
Figure 185: HPLC trace for aldol condensation of 4-nitrobenzaldehyde with cyclohexanone at pH 7 no catalyst control reaction	200

Figure 186: HPLC trace for aldol condensation of 4-nitrobenzaldehyde with cyclohexanone at pH 7 no catalyst control reaction	200
Figure 187: HPLC trace for dimerization of glycolaldehyde with benzylglutamine amide as a gel 48 h run 1	201
Figure 188: HPLC trace for dimerization of glycolaldehyde with benzylglutamine amide as a gel 48 h run 2	202
Figure 189: HPLC trace for dimerization of glycolaldehyde with benzylglutamine amide as a gel 48 h run 3	202
Figure 190: HPLC trace for dimerization of glycolaldehyde with benzylglutamine amide as a gel 48 h at pH 7 run 1.....	203
Figure 191: HPLC trace for dimerization of glycolaldehyde with benzylglutamine amide as a gel 48 h at pH 7 run 2.....	203
Figure 192: HPLC trace for dimerization of glycolaldehyde with benzylglutamine amide as a gel 48 h at pH 7 run 3.....	204

List of Schemes

Scheme 1: Asymmetric addition of HCN to 3-phenoxybenzaldehyde catalysed by cyclodi-peptide.....	11
Scheme 2: Ester hydrolysis being performed by nanostructures developed by Stupp.....	13
Scheme 3: Phase-transfer catalysed N-alkylation of benzimidazole.	14
Scheme 4: Mechanism of L-proline as an organocatalyst for aldol condensation reactions	15
Scheme 5: Aldol condensation of acetone and 4-nitrobenzaldehyde	15
Scheme 6: The 1,4-conjugate addition of cyclohexanone to trans- β -nitro-styrene	16
Scheme 7: Aldol condensation of 4-nitrobenzaldehyde and cyclohexanone.....	19
Scheme 8: Huisgen 1,3-dipolar cycloaddition between phenylacetylene and benzylazide	20
Scheme 9: Synthesis of PG, PGP and PA from glycerol and n-dodecylic acid.....	23
Scheme 10: Synthesis of further phospholipid MPGP, DPGP and cMPGP	23
Scheme 11: Reaction pathway for the formose reaction conceived by Breslow	28
Scheme 12: Reaction pathway from formaldehyde to amino acids ¹¹¹	36
Scheme 13: Reaction pathway from acetylene to amino acids	36
Scheme 14: Aldol reaction of the aldolase type I enzyme.....	38
Scheme 15: Aldol type II reaction mechanism using a zinc-cofactor	39
Scheme 16: The Eder-Sauer-Wiechert-Hajos-Parrish Reaction	39
Scheme 17: Aldol condensation of acetone and 4-nitrobenzaldehyde in DMSO with 30 mol% catalytic loading	39
Scheme 18: Organocatalysed aldol reaction in water	42
Scheme 19: The nor nicotine-catalysed aldol reaction investigated by Janda <i>et al.</i> electron ^{134,135}	43
Scheme 20: TIPS protected glycolaldehyde dimerization with different amino ester catalysts	44
Scheme 21: Leu-catalyzed (183) direct asymmetric aldol reactions of unprotected glycolaldehyde.....	45
Scheme 22: Synthesis of diphenyl hydrazone protected 2-deoxy-D-ribose 186 and 2-deoxy-D-threopentose 187 by amino ester and amino nitrile promoters	46
Scheme 23: Formation of D-glyceraldehyde in pH 7.0 buffer, concentration of 0.33 M with respect to glycolaldehyde	47
Scheme 24: One pot approach to ribose sugars 203	47
Scheme 25: Aldol condensation of glycolaldehyde.....	49
Scheme 26: Aldol condensation of TIPS-protected glycolaldehyde.....	49
Scheme 27: Aldol condensation of 4-nitrobenzaldehyde and cyclohexanone with tripeptide.....	50
Scheme 28: Model aldol condensation reaction of 4-nitrobenzaldehyde (49) and cyclohexanone (47).....	52
Scheme 29: Dimerization of glycolaldehyde.....	52
Scheme 30: Aldol condensation of acetaldehyde (127) and D-glyceraldehyde (106)	52
Scheme 31: Synthesis of L-valine amide (206)	55
Scheme 32: Synthesis of L-serine amide (209).....	55
Scheme 33: Synthesis of L-glutamine amide (210).....	55
Scheme 34: Direct Aldol condensation of 4-nitrobenzaldehyde (47) and cyclohexanone (49) in water catalysed by simple amino acid amides	62
Scheme 35: The proposed two-component hydrogelation system	76

Scheme 36: Initial synthesis of glutamine amide (210).....	80
Scheme 37: Optimised synthesis of glutamine amide	80
Scheme 38: Direct aldol condensation in water catalysed by valine (206), serine (209) and glutamine (210) amides as hydrogels or organogels	116
Scheme 39: Synthesis of the imine (231).....	118
Scheme 40: Reduction of imine (231) to amine using sodium borohydride	120
Scheme 41: Reduction of imine (231) to amide using sodium cyanoborohydride	120
Scheme 42: Synthesis of the imine (231).....	121
Scheme 43: Reduction of imine (231) with sodium borohydride to yield benzylglutamine amide (230)..	121
Scheme 44: Aldol condensation of 4-nitrobenzaldehyde (49) and cyclohexanone (47) in water	122
Scheme 45: Dimerization of glycolaldehyde (89).....	136
Scheme 46: Acylation of threose and erythrose for analysis of dimerization of glycolaldehyde by chiral GC	137
Scheme 47: Synthesis of diphenyl hydrazone.....	138
Scheme 48: <i>N,N</i> -Diphenyl hydrazine trapping of reaction mixture	148
Scheme 49: Synthesis of allyl phosphate biscyclohexylamine salt (238)	151
Scheme 50: Synthesis of glycolaldehyde phosphate calcium salt (97).....	151
Scheme 51: Dimerisation of glycolaldehyde phosphate calcium salt (97)	151
Scheme 52: Dimerization of glycolaldehyde phosphate free acid (240)	152
Scheme 53: Dimerization of glycolaldehyde phosphate (239) with higher catalytic and therefore gelator loading of benzylglutamine amide (230)	153
Scheme 54: Method for the phosphorylation of diphenyl hydrazine trapped L-erythrose (233)	160
Scheme 55: Method 1 of diphenylhydrazine trapping of glycolaldehyde phosphate (239)	160
Scheme 56: Method 2 of diphenylhydrazine trapping of glycolaldehyde phosphate (239)	160
Scheme 57: Aldol condensation of formaldehyde and glycolaldehyde phosphate by benzylglutamine amide hydrogel	161

List of Tables

Table 1: Table of results for the asymmetric addition of HCN to 3-phenoxybenzaldehyde catalysed by cyclodipeptide purified in different ways ³³	11
Table 2: Catalytic performance of amphiphilic hydrogel	17
Table 3: Catalytic results for the aldol condensation reaction using compounds 55 and 56 as catalysts ...	19
Table 4: Amino acid derivatives tested as catalysts for the asymmetric aldol reaction of acetone with 4-nitrobenzaldehyde	40
Table 5: TIPS protected glycolaldehyde dimerization using amino ester catalysts	44
Table 6: Result of the formation of 2-deoxy-D-ribose 186 and 2-deoxy- D-threopentose 187 in water.....	46
Table 7: Solvent screening for gelation with amides, 3 mg gelator in 0.1 mL solvent	57
Table 8 Valine amide (206) catalysed aldol condensation of 4-nitrobenzaldehyde (47) and cyclohexanone (49) in water.....	66
Table 9: Serine amide (209) catalysed aldol condensation of 4-nitrobenzaldehyde (47) and cyclohexanone (49) in water.....	66
Table 10: Glutamine amide (210) catalysed aldol condensation of 4-nitrobenzaldehyde (47) and cyclohexanone (49) in water.....	66
Table 11: Retention times of enantiomers from HPLC traces reported by Rolando and co-workers ¹⁵³	69
Table 12: L-valine amide (206) catalysis HPLC ee%	70
Table 13: L-serine amide (209) catalysed HPLC data	70
Table 14: L-glutamine amide (210) catalysis HPLC data	70
Table 15: Method to initiate gelation with varying concentrations of 4-nitrobenzaldehyde (47). Gelation determined by tube inversion.	79
Table 16: Identifying the minimum ratio of 4-nitrobenzaldehyde (47) to glutamine amide (210) (1mg, 3.16 mmol) required to form a hydrogel in 1 mL water. Gelation determined by tube inversion.	81
Table 17: Varying the concentration of the 1:1 system to find the minimum gelation concentration (MGC) and most robust gel, 1 mL water	85
Table 18: T _{gel} of glutamine amide (210) and 4-nitrobenzaldehyde (47) hydrogel 1:1 (1 mL water)	86
Table 19: T _{gel} of glutamine amide (210) (1 mg, 3.16 mmol) and 4-nitrobenzaldehyde (47) hydrogel with varying equivalents of 4-nitrobenzaldehyde (47) (1mL water)	86
Table 20: pH buffer solution screen for a 1:1 two-component system with glutamine amide (210) (1mg, 3.19 mmol) and 4-nitrobenzaldehyde (47) in 1 mL	95
Table 21: HCl or NaOH adjusted solution pH screen for a 1:1 two-component system using glutamine amide (210) (1 mg, 3.19 mmol) and 4-nitrobenzaldehyde (47) 1mL.....	95
Table 22: Self-healing test 1:1 4-nitrobenzaldehyde (47) glutamine amide (210) gel 3.16 μmol in 1 mL water	98
Table 23: Aldehyde screen of the 1:1 two-component system glutamine amide (210) (5 mg, 15.97 mmol) 1mL	99
Table 25: Benzylglutamine amide catalysed aldol condensation of 4-nitrobenzaldehyde and cyclohexanone in solution in water	123

Table 26: Controlled pH reactions * D.R ratio approximate due to poor conversion therefore peaks unclear	127
Table 27: pH screen (0.01 M buffer) of benzylglutamine amide (230) (3 mg / 0.1 mL, 0.1 M).....	133
Table 28: Solvent screen of benzylglutamine amide (230) (3 mg / 0.1 mL, 0.1 M).....	133
Table 29: Dimerization of glycolaldehyde (89) with benzylglutamine amide (230) data on the hydrogel over 48h	143
Table 30: Dimerization of glycolaldehyde phosphate (239) with benzylglutamine amide (230) hydrogel pH7	157
Table 31 Valine amide catalysed aldol condensation of 4-nitrobenzaldehyde and cyclohexanone in water	186
Table 32: Serine amide catalysed aldol condensation of 4-nitrobenzaldehyde and cyclohexanone in water	186
Table 33: Glutamine amide catalysed aldol condensation of 4-nitrobenzaldehyde and cyclohexanone in water	187
Table 34: L-valine amide catalysis HPLC ee%.....	187
Table 35: L-serine amide catalysed HPLC data.....	189
Table 36: L-glutamine amide catalysis HPLC data	190
Table 37: Benzylglutamine amide catalysed aldol condensation of 4-nitrobenzaldehyde and cyclohexanone in solution in water	192
Table 38: Controlled pH reactions.....	197
Table 39: Dimerization of glycolaldehyde with benzylglutamine amide data on the hydrogel over 48h .	201

Acknowledgements

First of all I would like to thank both of my supervisors Prof David Smith and Prof Paul Clarke for giving the opportunity to work on such a challenging and exciting project. Over the course of the last three years they have provided a lot of valuable advice and discussions about the direction of the project. It has been a fun project to be part of, if challenging at times, and has given me the chance to develop lab skills in multiple areas of chemistry.

I would like to thank all the members of both the Smith group and Clarke group over the last couple of years, I'd list you all but that would be a long list! Phill, thank you for making me feel so welcome when I started and bringing me out of my shell and for constantly making the lab a fun place to be and for answering my questions. Jack, thank you for being you and for always making us all laugh there was never a dull moment! Nik, thank you for being there with me in group meeting and helping with the HPLC it was great to finally have someone on a similar(ish) project to me! Chris – don't really know where to start you've always been a great help in so many different ways the lab really wouldn't function without you! Your singing will most likely be missed but your one-liners...not so much! Branna just thank you for being the friend I could have only wished for! Not only are you great to work with you are amazing to talk to about anything and everything. Thank you Branna for the many evening walks and pub trips we took setting the world to rights!

I would also like to mention Heather Fish and Karl Hale for all of their assistance with acquiring NMR and mass spectrometry data and Meg Stark for assistance with acquiring TEM/SEM images.

Other people to mention are Liz my wonderful tutor who helped me so much with being organised and helping me break my workload down so that I could manage it all in bite size chunks. Thank you to the Wentworth squash team who have been a great group to be with – So thank you Sam for making me go along when I started! A massive thank you to the various Mchem students (Alex, Jamie, Max, Johnny and Dan) that have work with or alongside me, and the team down in teaching labs! Finally I'd like to thank my family for helping me when I needed it.

Declaration

I hereby declare that the substance of this thesis has not been submitted, nor is currently being submitted, in candidature for any other degree.

I also declare that the work embodied in this thesis is the result of my own investigations and in the event the work of others has been used this has been fully acknowledged in the text.

1.0 Introduction

1.1 Gels and Low Molecular Weight Gelators (LMWGs)

Gels are a colloidal state of matter where a small amount of a solid-like network (a gelator) immobilizes the bulk flow of a larger amount of liquid-like phase. Typically a gel will consist of ca. 1% solid-like network in 99% liquid-like phase. It is this mixed nature that gives gels their unique soft-solid properties for use in a wide variety of applications due to the tuneability of both solvent and gelator.¹

Gelators can be separated into two categories, each with their own advantages and disadvantages.² The first of these are polymer gelators (PGs)³ which can be found in products such as hair gel. As the name implies, these are long-chain polymeric molecules, which upon covalent or non-covalent cross-linking, are able to form a sample spanning network. Polymer gels can be either naturally derived, such as agarose (**1**) or synthetic, such as poly(acrylic acid) (**2**) (Figure 1). As a consequence of entanglement/interactions or covalent cross-links, present in some PGs, between the polymers and/or the large size of the polymeric molecules these gels are mechanically strong. However, these materials are often unresponsive to stimuli, which can limit their usefulness.

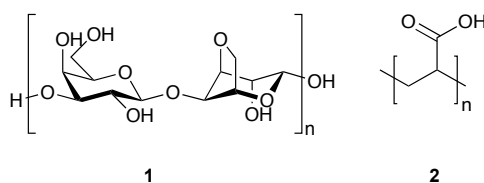


Figure 1: Examples of polymeric gelators

The second category of gelators are low molecular weight gelators (LMWGs). Low-molecular-weight-gelators such as 1,3:2,4-dibenzylidene-D-sorbitol (DBS) (Figure 2) are gelator molecules that have a molecular weight less than ca. 2000 Da and gel organic solvents, water and in some cases they can gel ionic liquids or deep eutectics. The gels that form from these smaller molecules assemble *via* non-covalent interactions such as hydrogen bonds, van der Waals forces, solvophobic effects, π - π stacking, *etc.* For example, in the case of 1,3:2,4-dibenzyl-D-sorbitol the gel network assembles *via* hydrogen bond

interactions between the sugar hydroxyls and oxygens and π - π stacking and solvophobic effect associated with the aromatic rings.

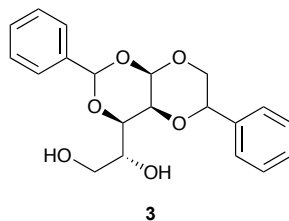


Figure 2: 1,3:2,4-Dibenzylidene-D-sorbitol (DBS)

Low-molecular-weight-gelators undergo hierarchical self-assembly, with non-covalent interactions driving the formation of nanofibrils, which then aggregate together to form nanofibres, that eventually entangle and interact to form a sample-spanning network (Figure 3)⁴.

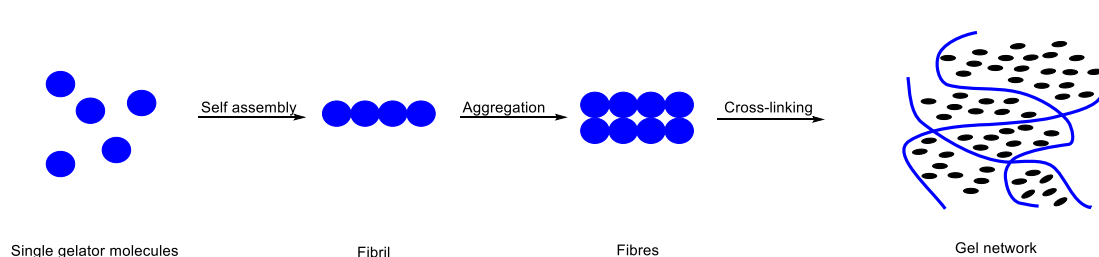


Figure 3: Low molecular weight supramolecular gel assembly process

Due to the solid-like gel network structure being formed by non-covalent interactions these gels are usually rheologically weaker than PGs.^{5,6} However, this can be advantageous because the non-covalent interactions between the small molecules can enable reversible self-assembly. This allows the network to be broken down or formed upon variation of external stimuli such as temperature, pH, enzyme addition, *etc*, providing an excellent degree of responsiveness. Furthermore, because the composition of these materials is based on small molecules, dynamics within the gels can be very fast. The responsive, tunable and programmable nature of supramolecular gels has captured the interest of academic chemists with high-tech applications in mind; and nanoscale electronics, sensors, biomaterials, tissue engineering and drug delivery have all received considerable interest^{1,7-11}.

1.2 Two component gels:

In addition to forming gels using a single small molecule, gels can be self-assembled using more than one molecular component to form the supramolecular gel (*i.e.*, a multi-component gel), or combining the LMWGs with polymers in some way.

A two-component gel, as the name suggests, is made up of two different components (excluding the solvent). In a landmark review, Buerkle and Rowan⁴ categorised such systems into three main types (Figure 4):

1. Two-component gel where neither individual component is a gelator and both components are required in combination to form a gel.
2. Two-component gel where both components are gelators in their own right and can interact either to form co-fibres¹²⁻¹⁴ or self sort¹⁵ into their own individual networks.
3. Two-component gel based on a single component gelator and an additive, where the non-gelator modifies the gel's physical properties.

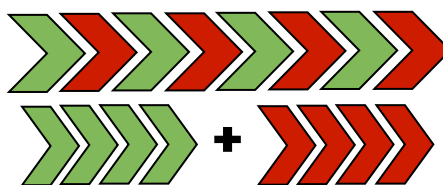
1)



Two component gel-phase:

Both components necessary to access gel

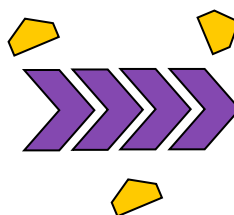
2)



Two gelator component:

Co-gel or self-sorting gel

3)



Gelator plus non-gelling additive component:

Addition of non-gelling additive to influence gel properties

Figure 4: Illustration of three main classes of two-component supramolecular gels⁴

Two-component gel systems can exhibit some unique properties, such as forming gels simply upon mixing, which potentially allow the development of materials with truly new, synergistic forms of behaviour. Two-component systems can be based on either non-covalent or covalent interactions to form an active gelator. As a result, they are highly tuneable, as either component can be easily modified to change the performance of the gel or introduce additional functionality. This is unlike a one-component gel system where there is only one component that can be modified.

1.2.1 Two-component gel systems:

Two-component gels are far less common than one-component gels. In 1993, Hanabusa and co-workers reported the first two-component gel.¹⁶ This gel was based on the well-known interaction between pyrimidine (e.g **4** or **5**) and barbituric acid (e.g. **6** or **7**) units (Figure 5). The molecules were modified with alkyl chains to modify solubility and encourage the formation of a sample-spanning network. It was found that a 1:1 ratio of the two components was required for the formation of a gel; although high concentrations (40-160 mM) were required depending on the solvent used. Both IR spectroscopy and transmission electron microscopy (TEM) were employed to understand the system. The data showed that hydrogen bond interactions were forming and a nanoscale architecture consisting of fibres with a diameter of 80 nm were created.

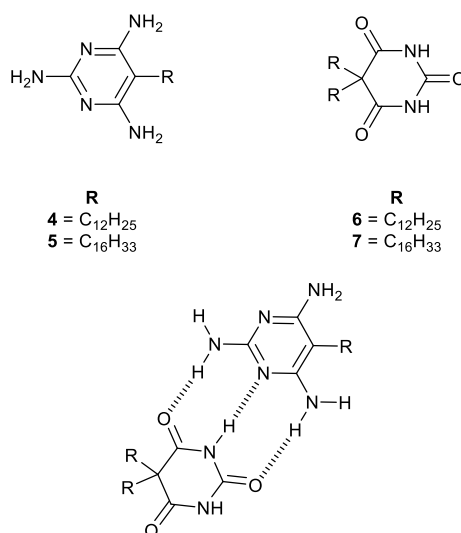


Figure 5: Barbituric acid and pyrimidine units studied by Hanabusa in a two-component gelation system

Smith reported a multi-component gelling system.¹⁷⁻¹⁹ The two-components that made up this system were a dendritic branch, which contained a free carboxylic acid unit, and a diamine that contained basic amine sites. The acid-base interaction of these two components resulted in formation of a complex (Figure 6). This complex then self-assembled into a sample-spanning network as a result of intramolecular hydrogen bonds between the dendritic peptide building blocks. This is a Type 1 two-component gelator system. In this example it was shown that both the length of the diamine spacer and the ratio of the aliphatic diamine to dendritic acid affected thermal stability as well as the nanoscale morphology. For example, when the length of the diamine spacer was 12 carbons, and the ratio of the two components was 2:1 (dendritic branch: diamine spacer) the morphology indicated fibres with diameters of 20 nm and a T_{gel} value of 37, but when the ratio was changed to 1:4.5, flattened 1 μm platelets formed with no gel at room temperature. Aside from the length of the spacer unit, it was also demonstrated that the geometry of the aromatic diamine could impact the morphology of the gel. Mixing dendron (**8**) with either 1,4-diaminobenzene (**9**), 1,3-diaminobenzene (**10**) or 1,2-diaminobenzene (**11**) in toluene led to very different behaviour: formation of a gel, partial gel formation or no gel respectively.²⁰ This clearly illustrated the tuneability of two-component systems.

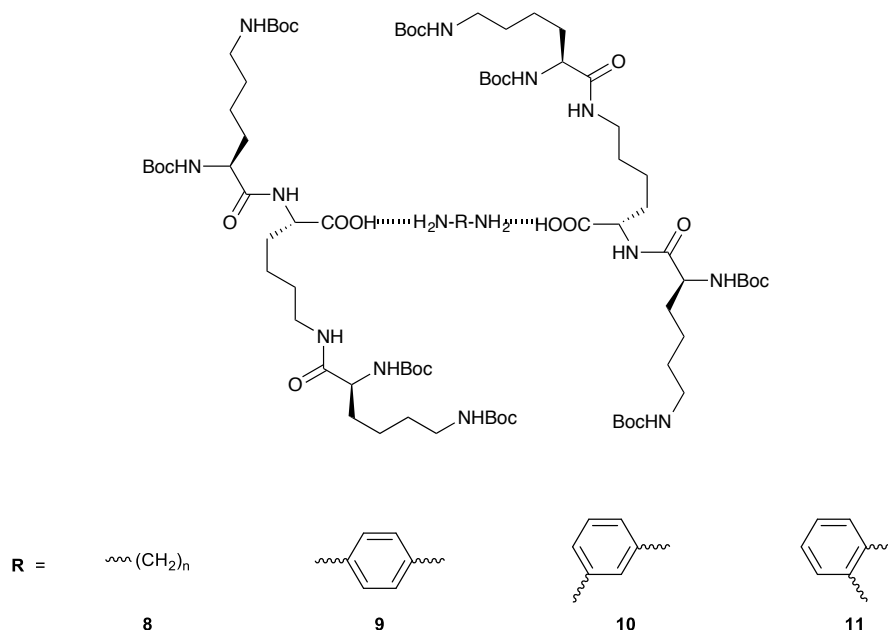


Figure 6: Diamine Lysine carboxylic acid two-component system structure

Aside from multi-component gels forming via non-covalent interactions between the two components, there are also systems in which covalent bonds form

between the two components. This results in a new molecule forming *in situ* that is capable of forming gels. These systems are often referred to as dynamic multi-component systems as the reaction-taking place can be reversible. The reversibility of the reaction can be exploited to access a new range of gels. Lehn and co-workers²¹ reported the generation of dynamic covalent libraries by reaction of guanosine hydrazide with different aldehydes. In the presence of a metal cation these molecules form G-quartets, which are able to self-assemble and form hydrogels (Figure 7). It was found that varying the aldehyde could impact the strength of the hydrogel that formed. In 2013 Smith presented related work with simpler molecules avoiding the need for metals. In this work commercially available lauric hydrazide, formed a sample-spanning network in dimethylsulfoxide (DMSO), and different aldehydes were then added to change the properties of the gel such as T_{gel} , as a result of dynamic reaction with hydrazide (Figure 8) to generate a modified gelator.²²

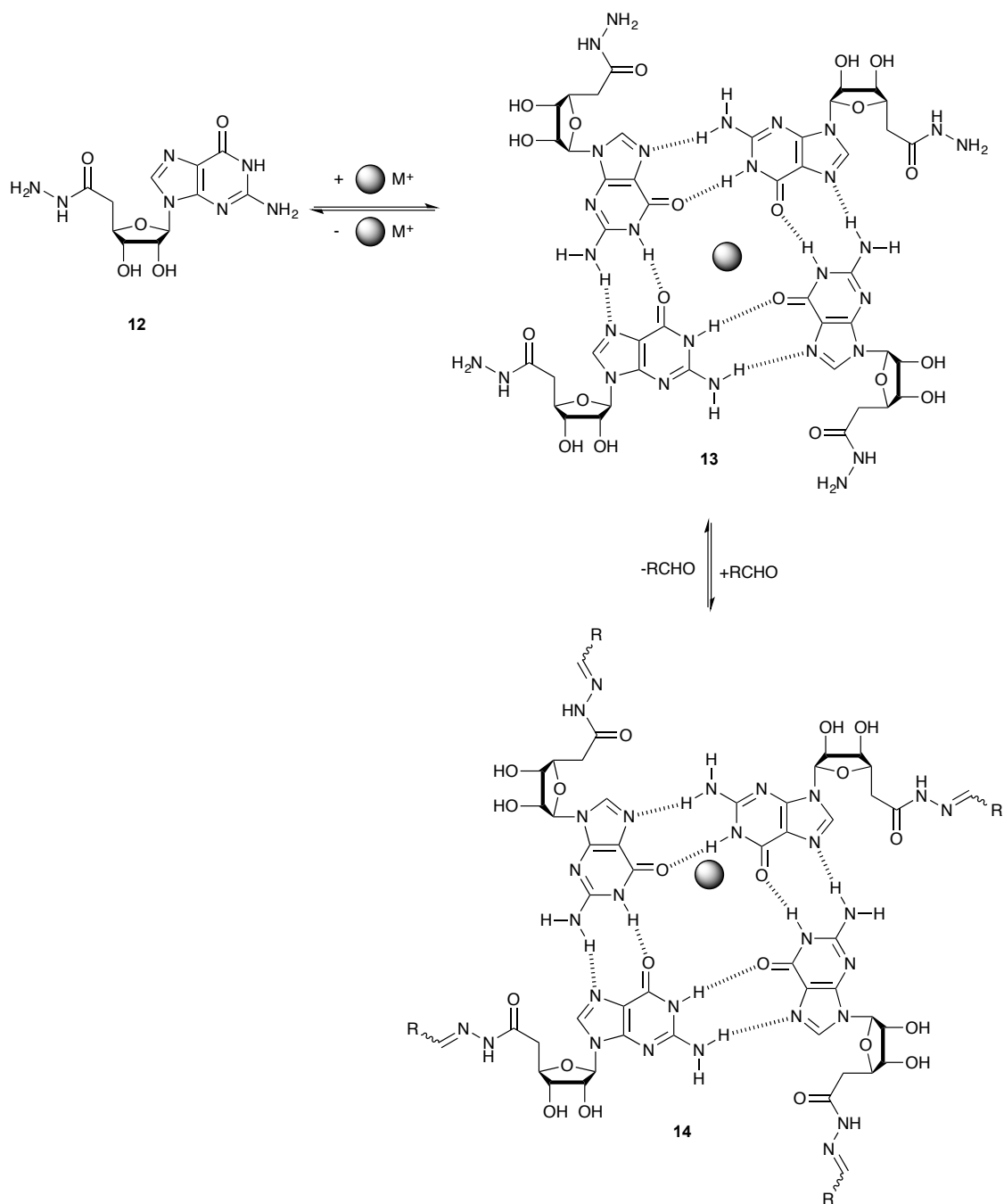


Figure 7: Assembly of guanosine hydrazide into G-quartets and further reversible reaction with aldehydes leading to hydrogels

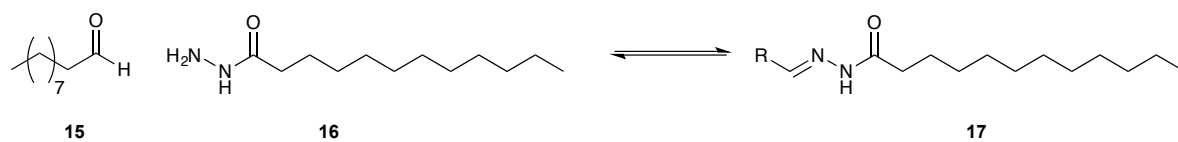


Figure 8: Formation of acyl hydrazone gelator from commercial building blocks

1.3 Catalytic supramolecular LMWGs

Within the chemical community, the development of new methods to perform reactions that enhance certain aspects such as selectivity or efficiency through catalysis, is highly desirable. Catalysis is also one of the main goals of supramolecular chemistry, an area of research that was started 40 years ago by Pedersen, Cram and Lehn in molecular recognition.^{23–25} Since then, supramolecular approaches to catalysis have been divided into three main categories by Ballester and Vidal-Ferran^{26,27,28} (Figure 9):

1. Molecular receptors that place a binding site close to a catalytic centre
2. Molecular receptors that simultaneously bind two reactants and promote their reaction
3. Systems in which supramolecular interactions are used to construct a catalytic centre

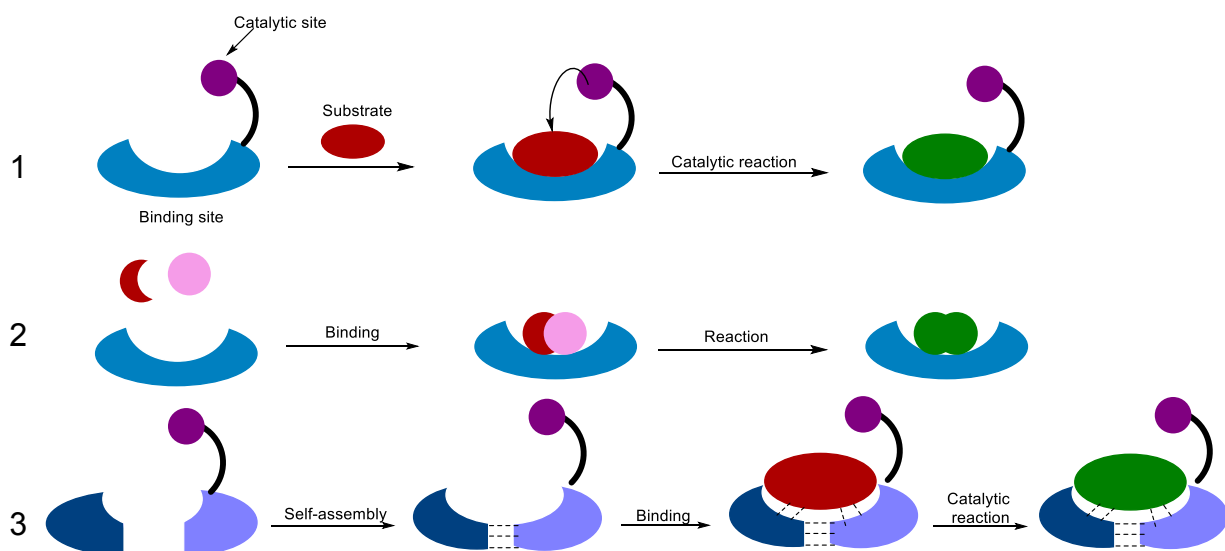


Figure 9: Three categories of supramolecular approaches to catalysis

In recent years, gels have been of particular interest in catalysis.²⁹ Gels are highly solvated but also immobilised and hence combine aspects of homogeneous and heterogeneous catalysis. They allow access of reagents *via* diffusion in the liquid-like phase, but can immobilise the catalyst preventing contamination of the product.

One area that is increasingly using LMWGs is precious metal based catalysis. A palladium-binding ligand can be incorporated in the gelator structure. Xu and co-workers³⁰ reported an early example of Pd(II)-coordination metallogels which catalysed the oxidation of benzyl alcohol to aldehydes (Figure 10). Palladium salts

were directly incorporated into a multidentate ligand. It was found that the metallogel demonstrated catalytic turnover in the aerobic oxidative reaction. It was further found that the solvated gel was better suited to catalysis compared to the dehydrated metallogel to give the xerogel. This was thought to be due to the more effective delivery of substrate to the metal sites in the solvated gel compared to the dehydrated xerogel. Since the work by Xu and co-workers, there has been a significant amount of research using gels for metal-catalysed reactions such as Suzuki-Miyaura cross coupling.

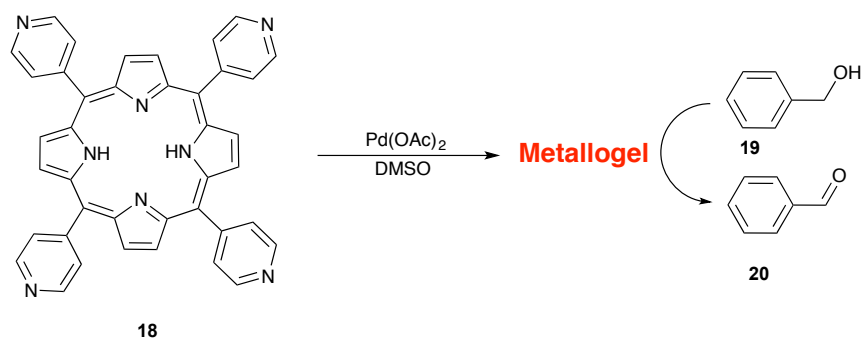


Figure 10: Metallogel for oxidative reduction of benzyl alcohol to benzaldehyde

In addition to binding Pd to a ligand, the use of Pd nanoparticles (PdNP) within a gel material has also been reported.³¹ The Smith group used 1,3:2,4-dibenzylidene-D-sorbitol (DBS) modified with acyl hydrazides (**21**) (Figure 11) combined with agarose (Figure 12) for metal based catalysis. This hydrogel bound Pd(II) and was then capable of *in situ* reduction of Pd (II) to Pd (0) without the need of an external reducing agent. The hybrid hydrogel with embedded palladium nanoparticles was used as a catalyst for Suzuki-Miyaura cross coupling reactions. The gel limited PdNP aggregation/leaching, and was recycled more than 10 times without the metal catalyst being inhibited and losing catalytic efficiency (Figure 13).

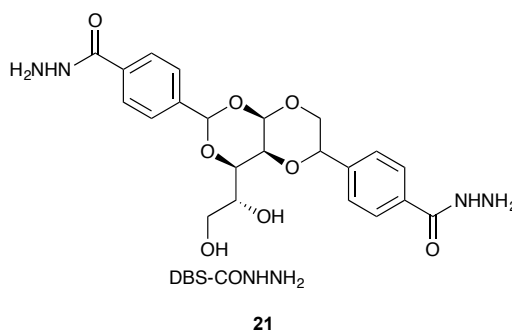
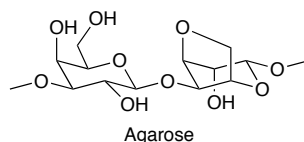


Figure 11: 1,3:2,4-Dibenzylidene sorbitol modified with acyl hydrazides used for reduction of PdNPs



2

Figure 12: Agarose, used for structural robustness

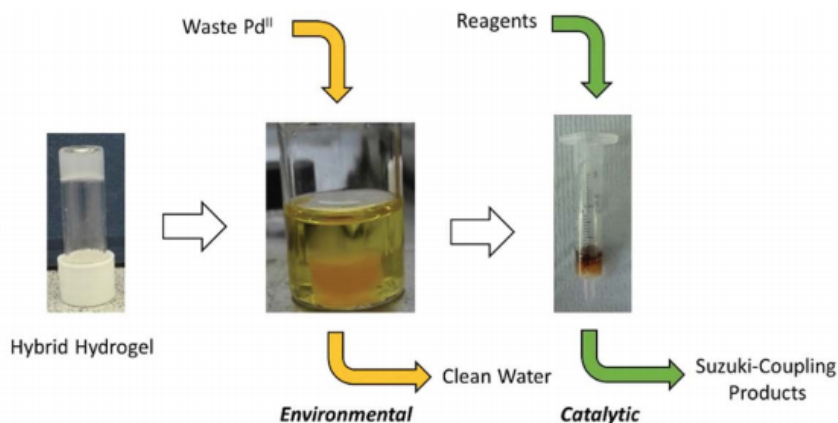
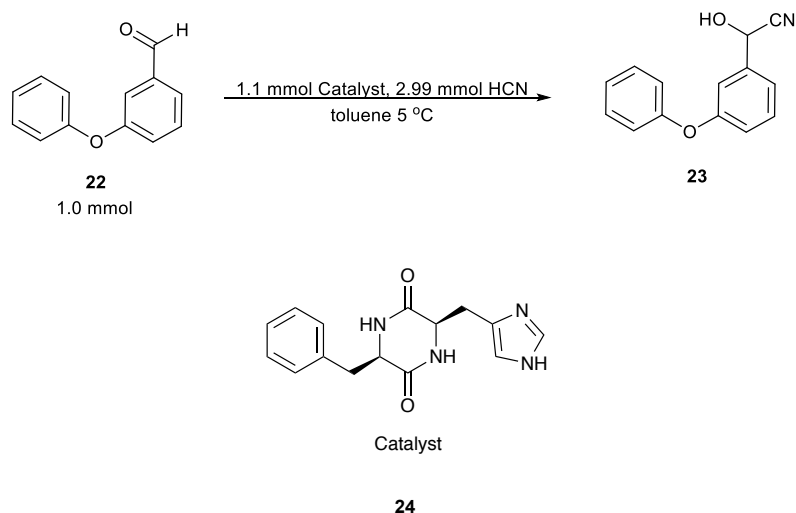


Figure 13: Schematic of the 'waste-to-wealth' approach using DBS-CONHNH₂/agarose hybrid hydrogels to remediate waste, generating PdNPs in situ then using the resulting material to catalyse Suzuki cross-coupling reactions.³¹

Another concept in catalytic supramolecular gels of great interest, is the potential for the gelator itself to be catalytically active. This, however, can be potentially problematic as it can be difficult for the gel structure to be maintained throughout the catalytic cycle. As a result there is relatively limited research using organogels or hydrogels for direct catalysis.²⁹

During studies of organocatalysed asymmetric addition of hydrogen cyanide to *m*-phenoxybenzaldehyde by cyclodipeptide, (Scheme 1) Inoue *et al.* reported the presence of a supramolecular gel.³² The formation of a gel was observed at low temperatures alongside an increase in stereoselectivity. Later it was found³³ that depending on the purification technique used for the catalyst, either a transparent or opaque gel was seen when the reaction solvent was toluene (Table 1). The gels that formed were thixotropic, and it was found that on increasing stirring the viscosity decreased and as a consequence enantioselectivities increased from 74% ee to 92 % ee.



Scheme 1: Asymmetric addition of HCN to 3-phenoxybenzaldehyde catalysed by cyclodipeptide

Table 1: Table of results for the asymmetric addition of HCN to 3-phenoxybenzaldehyde catalysed by cyclodipeptide purified in different ways³³

Time h	Yield %	ee %	State of reaction mixture	State of catalyst	Method of activation of catalyst
6	97	92	Clear gel	Amorphous	A
6	97	91	Clear gel	Amorphous	B
7	86	70	Slightly opaque gel	Slightly crystalline	C
125	79	22	suspension	needles	D

A: Rapid evaporation of aqueous methanol solution at 120 °C, *B*: Precipitated in methanol-ether under vigorous stirring, *C*: Precipitated in methanol-ether under slow stirring, *D*: Purified from aqueous methanol

In 1996, Youval Shvo reasoned that the ability of the diketopiperazine to hydrogen bond is the reason for gel formation.³⁴ Shvo also suggested that the solid state intermolecular hydrogen bonding interactions between the monomers is responsible for the chemical and stereochemical course of the hydrocyanation reaction. This is due to the way the monomers can align head to head, **25**, or head to **26** tail. However no formal mechanisms have been proposed.

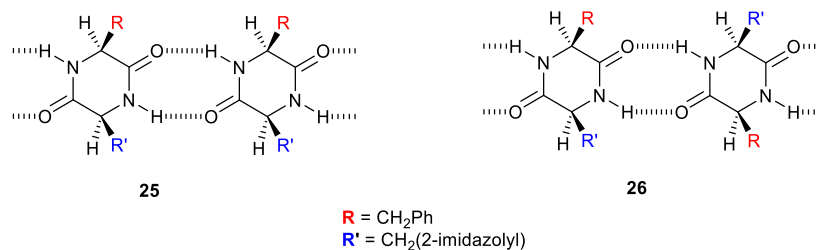


Figure 14: Proposed hydrogen bonding of cyclodipeptide result in gelation during cyanohydrin addition reactions³⁴

In 2007, the catalytic properties of supramolecular gels were investigated by Stupp *et al.*³⁵ In this work, histidine-functionalized self-assembling peptide amphiphiles (Figure 15) were synthesised, and then used to form self-assembled high-aspect-ratio nanofibers. The histidine residues are the organocatalytic reactive sites for the ester hydrolysis shown in Scheme 2. It was found that nanofibers were better catalysts than smaller aggregates due to the higher density of catalytic sites on their surface. The density of catalytic sites is due to the alignment of gelator molecules required for the formation of nanofibres, which make up the hydrogel network. It was also found that upon changing the R group different supramolecular structures could be obtained, for example compound **27** is soluble in water at pH 4 and forms gels at pH 6.5 and above where as compounds **28-30** at soluble at pH 7.4 and form poly disperse aggregates rather than gels. Since 2007, when Stupp presented the catalytic potential of these supramolecular structures there has been an increase in research into these systems.³⁶⁻³⁹

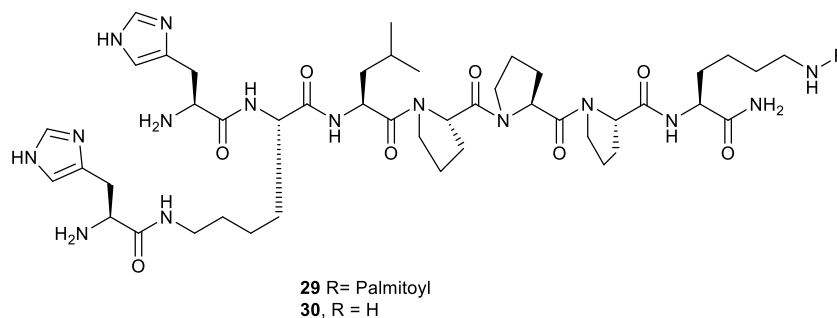
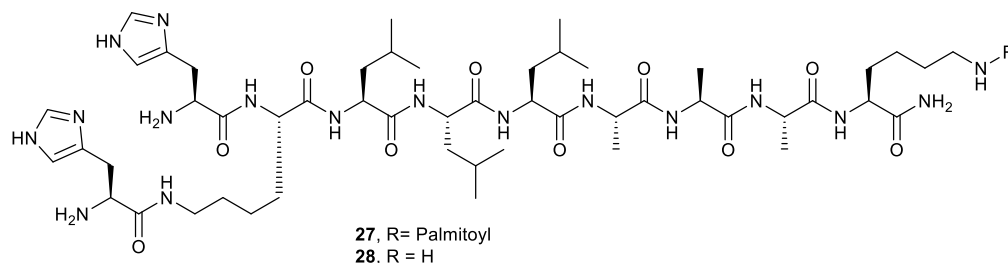
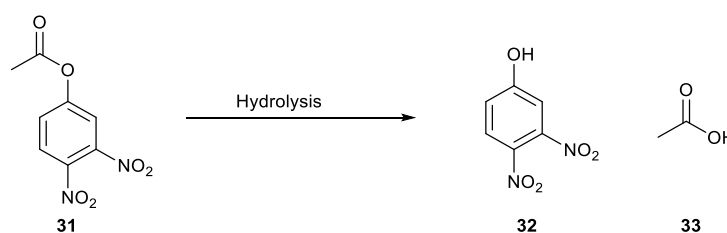


Figure 15: Histidine-functionalized self-assembling peptide amphiphiles studied by Stupp



Scheme 2: Ester hydrolysis being performed by nanostructures developed by Stupp

However, in 2008, Tu and co-workers⁴⁰ demonstrated a far more simplistic catalytic organogel (Figure 16). This organogel was able to maintain its supramolecular network as well as successfully performing phase-transfer catalysis for the alkylation of benzimidazole, which is described by the authors as a biphasic system of, solid and liquid (Scheme 3). It was thought that the large number of non-covalent interactions between gelators, were responsible for the stability of the supramolecular structure, even when catalysis was occurring.

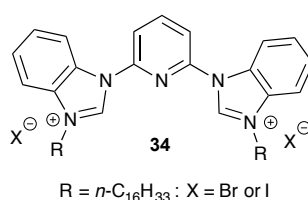
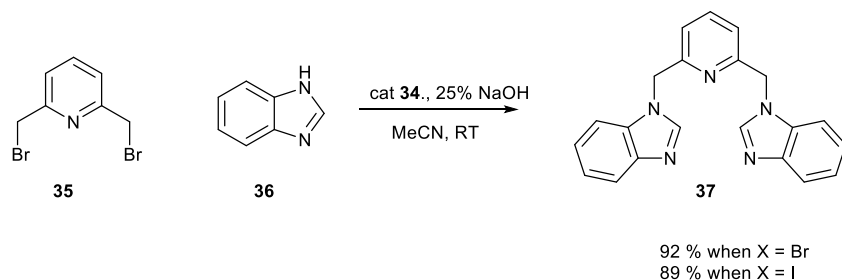


Figure 16: Organogelator developed by Tu and co-workers



Scheme 3: Phase-transfer catalysed N-alkylation of benzimidazole.

After this success, a number of other research groups such as those of Moretto,⁴¹ Miravet and Escuder⁴² began to produce organogels which were able to successfully catalyse reactions whilst maintaining the gel structure. These catalytic gelators all contained an L-proline moiety that has been widely shown to be an efficient asymmetric organocatalyst via the mechanism outlined in Scheme 4.⁴³

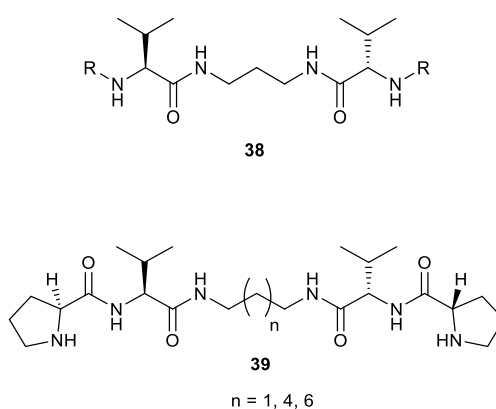
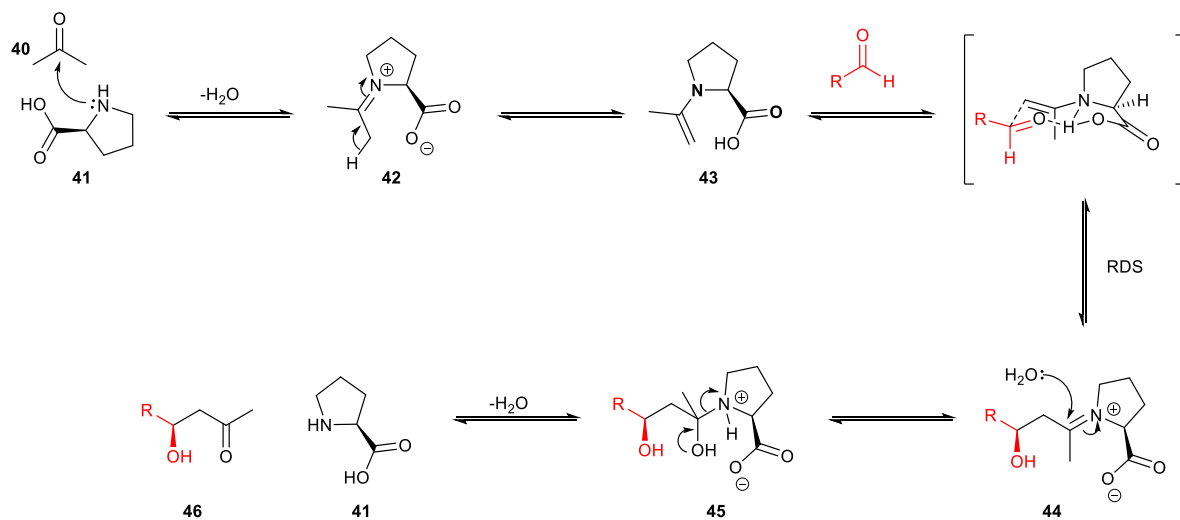
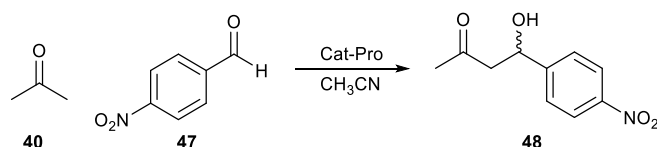


Figure 17: L-Valine bolaamphiphilic **36** scaffold used to design the L-proline derived bolaamphiphilic **39**

Influenced by the application of L-proline as an organocatalyst in asymmetric catalytic reactions, Miravet and Escuder designed gelators containing L-proline fragments. The new gelators were based upon a well-established assembling bolaamphiphilic backbone containing L-valine^{44,45} (Figure 17) and gelled in organic solvents such as acetonitrile, ethyl acetate or toluene. It was envisioned that the addition of the L-proline moiety would allow the gel to perform enamine-based catalysis (Scheme 4). As part of the gelator design, accessibility to the catalytic substrate was important, therefore the prolyl fragments were positioned at the termini of the bolaamphiphilic gelator as this should maximise their availability. The new gelators were tested for catalytic proficiency by performing an aldol condensation using acetone and 4-nitrobenzaldehyde (Scheme 5).



Scheme 4: Mechanism of L-proline as an organocatalyst for aldol condensation reactions



Scheme 5: Aldol condensation of acetone and 4-nitrobenzaldehyde

The reactions were performed using acetonitrile gels and also blank solutions. The blank solutions contained catalyst concentrations similar to that of the catalyst which remained in the sol-phase that is in equilibrium with the gel. It was found that the catalytic ability in both systems was the same. This showed that the reaction was probably taking place in the solution phase and not on the fibres. One reason for this is that aggregation inhibited catalysis. Further studies of this system showed that as time went on, the enantiomeric ratio decreased from 1:5 to a racemic mixture, whereas in solution this did not occur. It was concluded that the gel was acting as a base, yet the same compound under non-assembling conditions was not as basic. It was therefore proposed that self-assembly produced an enhancement of basicity, most probably due to a cooperation of neighbouring L-proline moieties organised as a charge relay system (Figure 18).

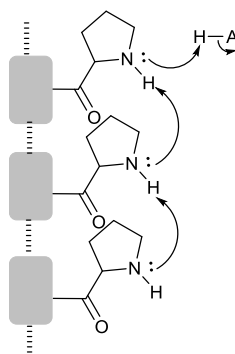
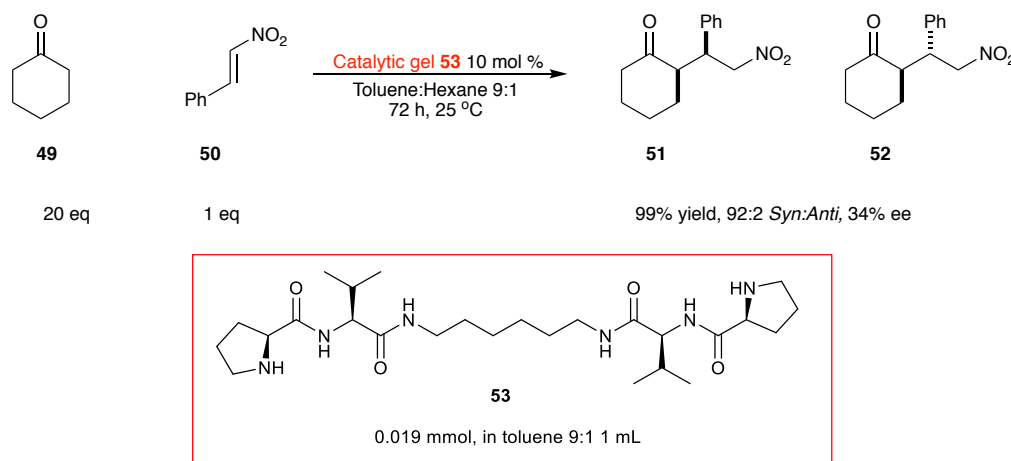


Figure 18: Cooperation of neighbouring proline moieties organised as a charge relay system

Escuder wanted to explore why gels formed in acetonitrile were active as a basic catalyst but were inactive in the direct aldol condensation. By exploring and having success with other reactions such as the Henry nitroaldol reaction (Scheme 6), it became apparent that the gel fibres were unable to form the required enamine. This was due to the nitrogen in the pyrrolidine ring being heavily involved in hydrogen bonding in the charge relay system shown in Figure 18. One of the factors which can influence the gel morphology and therefore the accessibility of catalytic substrates is the solvent. It is known that water is important in biocatalysis and many studies using L-proline have been performed in water. The work presented by Barbas⁴⁶ using an amphiphilic L-proline derivative, inspired Escuder to develop catalytic hydrogelators.^{38,47} The design of their new gelator was therefore amphiphilic (Figure 19).



Scheme 6: The 1,4-conjugate addition of cyclohexanone to trans- β -nitro-styrene

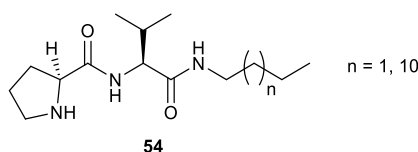


Figure 19: Amphiphilic hydrogelator with proline moiety

This amphiphilic molecule self-assembled to form transparent gels in water. Due to the design of the amphiphilic hydrogelator, van der Waals interactions and the hydrophobic effect positioned the long tail into a bilayer (Figure 20).

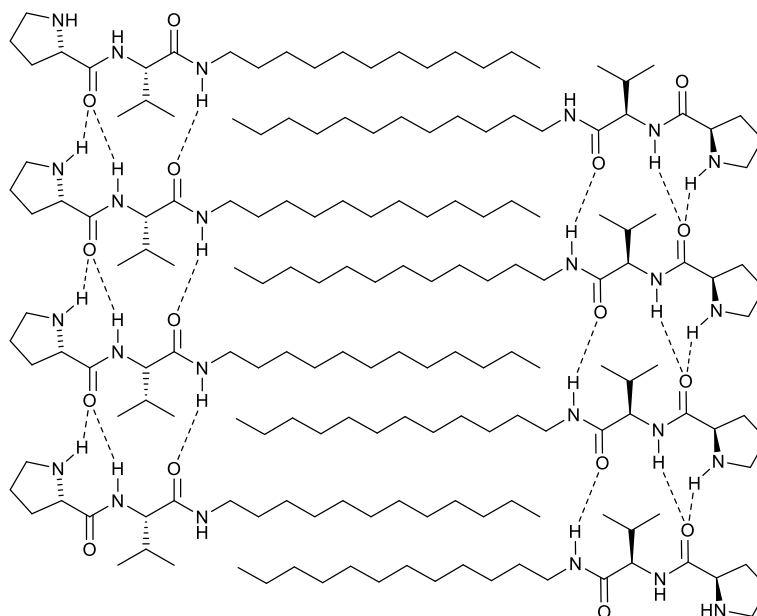


Figure 20: Sample spanning network structure showing hydrogen bonding interactions

The hydrogel was tested for catalysis by adding the reagents, 4-nitrobenzaldehyde and cyclohexanone, in toluene to the surface of the gel and the reaction was left for 24 h. The results of these reactions are shown in Table 2.

Table 2: Catalytic performance of amphiphilic hydrogel

Entry	Temperature (°C)	Time (h)	Yield (%)	<i>anti</i> : <i>syn</i>	ee (%)
1 ^a	25	36	> 99	75:25	12
2	25	16	> 99	91:9	18
3	5	24	98	92:8	88
4 ^b	5	24	> 99	93:7	87
5 ^c	5	24	> 99	92:8	90

^a Without toluene, ^b Entry 3 second run, ^c Entry 3 third run

The results from the aldol condensation with the hydrogel (Table 2) show that after 24 hours the reaction was complete with excellent stereoselectivity, however the % ee only became significant at low temperatures (5 °C) shown in Table 2 entries 3-5. Additionally, the hydrogel could be reused three more times, once the toluene layer had been decanted, with the same efficiency and stereoselectivity. It is however, somewhat difficult to understand how the reagents in toluene effectively diffuse into the hydrogel given the immiscibility of these two solvents.

In the process of getting the data shown in Table 2, it was noticed that randomly under what appeared to be similar conditions some samples failed to form

hydrogels leading to weak gels, dispersions or precipitates. The lack of gel formation did result in high yields of aldol condensation products after 24h. Studies into gel formation showed that different polymorphs occurred due to very slight modifications in the environmental parameters (temperature, aging time, ultrasounds), it was also shown that the precise polymorph formed can also affect the catalytic properties as the packing arrangements are subtly different.

In 2016 Escuder began studying short self-assembled peptide hydrogels.^{38,39,48} The short peptides synthesised contained three amino acid moieties and were all equipped with a catalytic functional group (Figure 21). It was shown that the peptides formed fibrillar network hydrogels and were catalytically active in their self-assembled form but were inactive in solution. This was an exciting observation as it indicated that enamine-based catalysis was occurring through self-assembly.

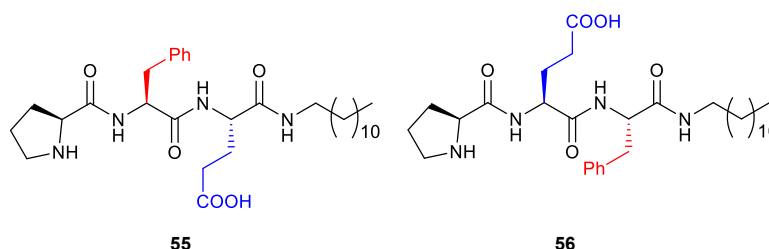
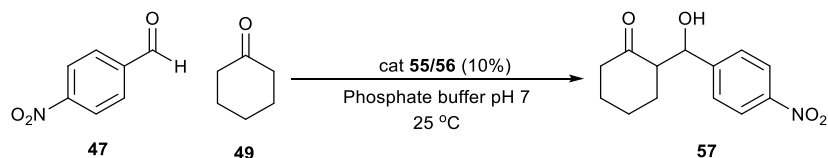


Figure 21: Short lipophilic peptide hydrogelator

Previous work discussed above revealed that these catalytic hydrogel systems were sensitive to small changes, therefore Escuder *et al.* explored how changing the peptide sequence affected both gelation and catalytic activity. Simply changing the order of phenylalanine and glutamic acid (Figure 21) produced two visually different gels, compound **55** formed a clear solution on heating that resulted in a clear hydrogel, while compound **56** formed a milky solution upon heating and an opaque hydrogel. When catalytic activity in an aldol condensation of cyclohexanone and 4-nitrobenzaldehyde was studied (Scheme 7), it was found that peptide sequence had an important role, thus suggesting that catalytic sites could be tailored. The results in Table 3 showed that only when the reaction time was shortened was there a difference in reaction rates between the two assemblies. After 2 h, catalyst **55** reached 93% conversion whereas catalyst **56** only reached 51% conversion. The formation of aggregates therefore played a role in the rate of catalysis, but had little impact on the diastereomeric ratio.



Scheme 7: Aldol condensation of 4-nitrobenzaldehyde and cyclohexanone

Table 3: Catalytic results for the aldol condensation reaction using compounds 55 and 56 as catalysts

Catalyst	Time (h)	Yield (%)	d.r (<i>syn/anti</i>)	e.r (<i>anti</i>)
55	72	>99	14:86	12:88
56	72	>99	20:80	12:88
55	15	>99	15:85	-
56	15	>99	9:91	-
55	2	93	8:92	-
56	2	51	15:85	-
55	1	83	10:90	-
56	1	32	14:86	-

What makes this work interesting is that the gelator itself is the catalyst and is a relatively simple molecule. In supramolecular gels, non-covalent interactions are responsible for the structure. Therefore, using the molecule for catalysis as well as the formation of the gel network can result in a loss of non-covalent interactions and weaken the gel network. However in Escuder's work, although some of these interactions will be removed during enamine catalysis, loss of the supramolecular network did not occur.

Escuder has also reported the use of supramolecular gels for the Huisgen 1,3-dipolar cycloaddition of alkynes and azides.⁴⁹ The gelator used was a derivative of the L-valine gelator functionalised with triazole fragments (Figure 22).

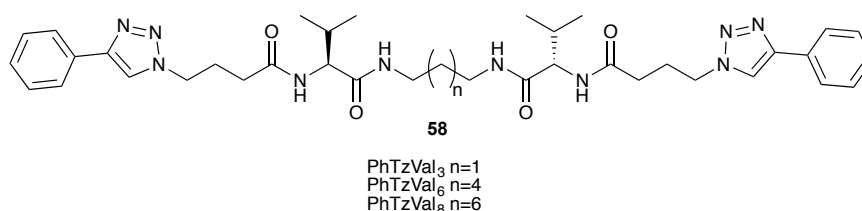
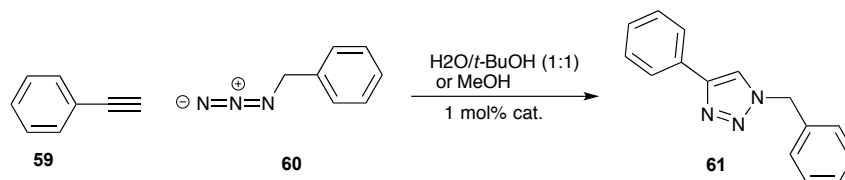


Figure 22: Structure of triazolyl functionalised gelator

Gelator (**58**), shown in Figure 22, was found to gel both alcohols (ethanol, 2-propanol and methanol) and water due to the amphiphilic nature of the molecule. It

was also found that the gelator could coordinate to copper which resulted in the formation of metallogels. The solvent used for the formation of metallogels was methanol. The metallogels were found to be capable of catalysing the Huisgen 1,3-dipolar cycloaddition of alkenes and azides (Scheme 8).



Scheme 8: Huisgen 1,3-dipolar cycloaddition between phenylacetylene and benzylazide

The metallogel successfully catalysed the Huisgen 1,3-dipolar cycloaddition with 50-60% conversion in the first 8 h. This was significantly higher than standard procedures where the copper salt $[\text{Cu}-(\text{MeCN})_4]\text{PF}_6$ was used. Indeed, in 72 h only 4% conversion was observed.^{50,51} The increase in conversion is thought to be due to coordination of Cu^{I} to the triazole functional group of the gelator, which results in the formation of hemiable copper complexes during catalysis. Aside from the bonding ability, the gel matrix itself may have an important role. It was suggested that the large fibres of the gel network generate a large surface area in contact with solution, therefore catalytic site availability is higher and in closer proximity to substrates. This in turn may enhance catalytic properties.

Since the success of the catalytic gels mentioned above, research groups are trying to further this field and explore the scope of catalytic gels. D'Anna and co-workers have recently reported the first use of gels for the study of asymmetric alcoholysis of anhydrides (Figure 23) in ionic liquid solutions.⁵² In this work it was shown that good yields of up to 99% and enantioselectivities of up to 81% were seen when using ionic liquid gels depending upon the conditions used.

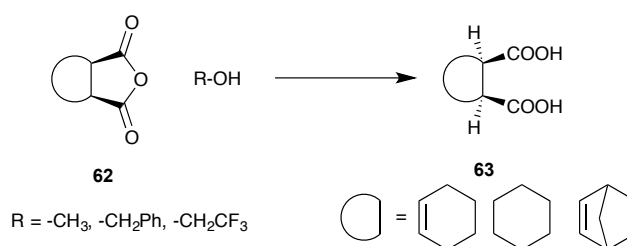


Figure 23: Asymmetric alcoholysis of anhydrides

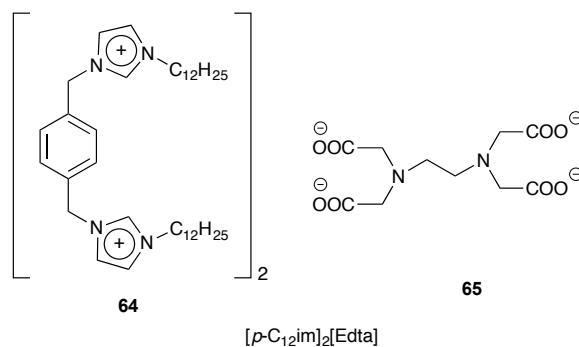


Figure 24: Gelator structure

It was found that the gelator shown in Figure 24, could gel ionic solvents such as **65-67** (Figure 25) forming ionogels, as well as forming gels in organic solvents such as 1-octanol. For this work ionogels were studied. Here the gel was used as a medium for the reaction and was not a catalyst as well. Instead a chiral catalyst (Figure 26) was added to the reagents once the ionogel had formed.

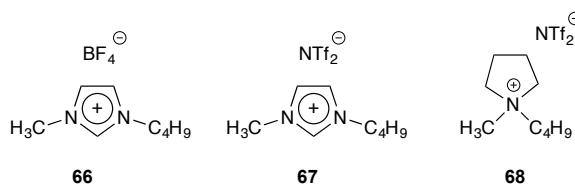


Figure 25: Ionic solvents used

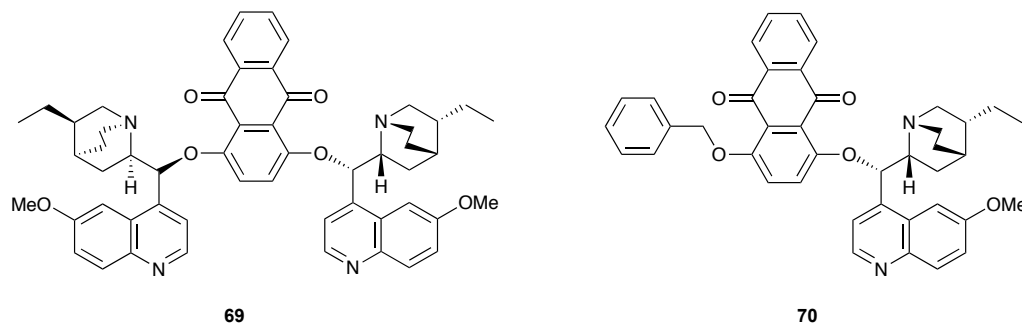


Figure 26: Chiral catalysts

In these studies both gel phase and solution phase were compared. There was a dramatic increase in both yield and enantioselectivity when the ionogel was used compared to solution-phase. Enantioselectivity changed from racemic in solution to 88% ee. In addition when the gel was made using 1-octanol, not only did the organogel degrade, no significant product formation was observed. It was reasoned that the general trend of reactivity and enantioselectivity was as a result of hydrogen bond donating or accepting ability in ionic liquids. The ionogel phase amplification of yield and ee% was due to the ability of the gel to act as a cage-like nano-reactor due to the gel matrix and non-covalent interactions playing an

important role in the performance of the catalyst both in terms of activity and stereoselectivity.

1.4 Supramolecular structures and the origins of life

The origin of life remains one of the biggest unanswered questions of our time. This is because there is little direct evidence surrounding the composition of the prebiotic atmosphere, temperature of the Earth or the initial building blocks required to develop life. It is for these reasons that scientists are inspired to take on such a challenging area of research. Origins of the universe are increasingly well understood; the biological evolution of life is also well understood but the chemical origins of the first simple cellular life form remain obscure.^{53–55}

There are a few things we already know, or can hypothesise, about the primordial Earth.^{56–58} However, when it comes to systems that we recognise as being living, it is instructive to consider the simplest cells, prokaryotes (Figure 27).

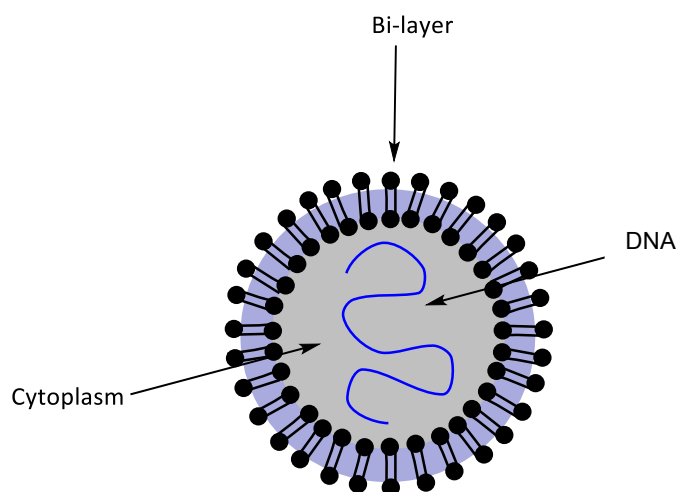
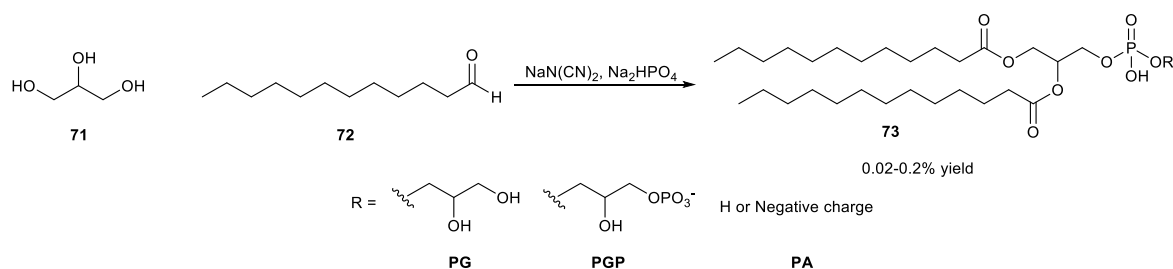


Figure 27: Prokaryotic cell

Prokaryotes are cells that consist of a plasma membrane, ribosomes, DNA and cytoplasm. From a chemistry point of view, a cell is a reaction vessel in which the interior is a gel. Researchers in the field of Origins of Life have different ideas on what defines a protocell from being membrane bound to being membrane free.^{59–61} Recent studies of vesicles composed of fatty-acid membranes have shed considerable light on pathways for protocell growth and division, as well as means by which protocells could take up nutrients from their environment. The supramolecular structure that dominates the area of protocells, is the vesicle. Vesicles consist of liquid or cytoplasm enclosed by a lipid bilayer and are a good

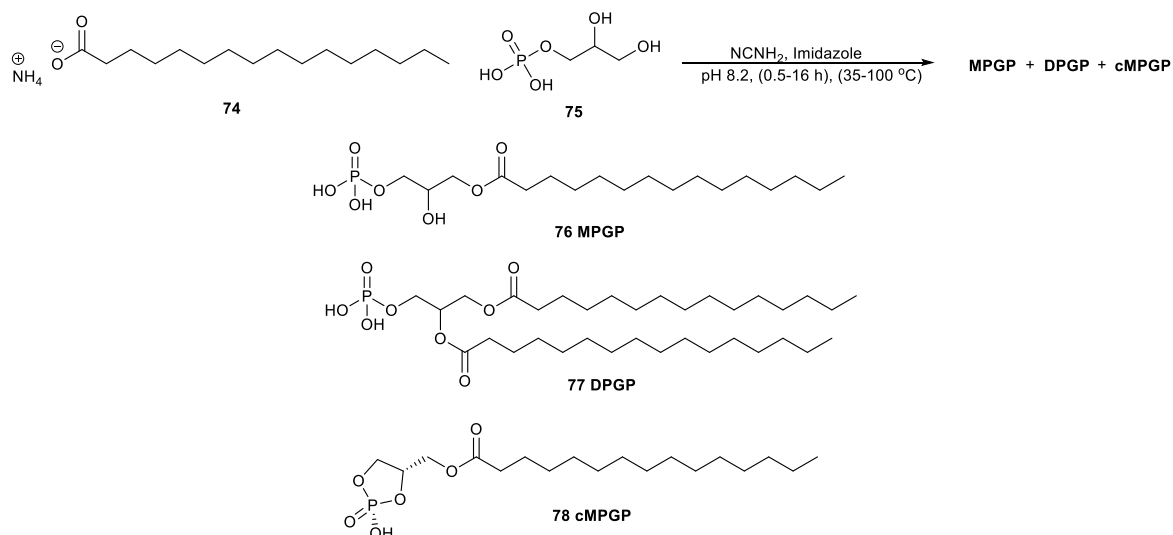
candidate for primitive cells as they resemble a structure similar to the modern day cell, yet are simple.

Deamer and co-workers were one of the first to synthesise lipids such as phosphatidic acids (PA) from glycerol, n-dodecylic acid (or aldehyde) in the presence of sodium dicyanamide and disodium hydrogen phosphate (Na_2HPO_4) yielded PA, phosphatidylglycerol (PG), and phosphatidyl glycerophosphate (PGP) in low amounts 0.02%–0.2% (Scheme 9).^{62–64}



Scheme 9: Synthesis of PG, PGP and PA from glycerol and n-dodecylic acid

Oro then further developed this work, demonstrating the synthesis of monopalmitoylglycerophosphate (MPGP), dipalmitoylglycerophosphate (DPGP) and monopalmitoyl cyclic glycerophosphate (cMPGP) (Scheme 10).^{63,65,66} However, it was thought that the complexity of these phospholipids was unlikely to be in the membrane for the first protocells. Therefore studies have progressed in the direction of fatty acid based lipids.



Scheme 10: Synthesis of further phospholipid MPGP, DPGP and cMPGP

The presence of fatty acids has been detected on extra-terrestrial meteorites.^{67,68} Fatty acids are amphiphilic monomers composed of a long hydrophobic tail-group and a hydrophilic head-group. When exposed to aqueous media, the amphiphilic

nature of the molecules results in the monomers arranging in such a way that unfavourable interactions (hydrocarbon chains and aqueous media) are minimised. It is only above a critical concentration, often referred to as the critical micellar concentration (CMC) or critical vesicle concentration (CVC), that the monomers self-assemble into supramolecular structures either micellar or vesicular in nature (Figure 28).⁶⁹⁻⁷¹

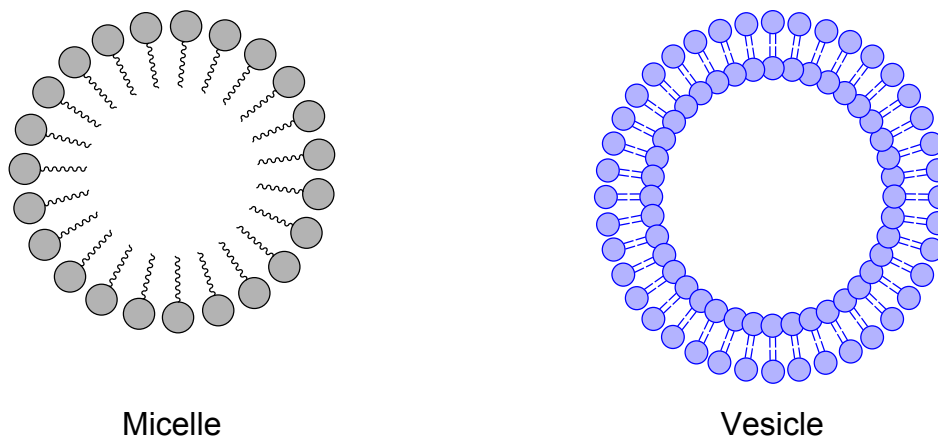


Figure 28: Structure of a micelle and a vesicle

Membranes that have been composed of fatty acids and have therefore been hypothesised to be a model for primitive membranes are only stable in a narrow pH range and at low ionic strength. As a result they are sensitive to aggregating effects of divalent cations (Mg^{2+} , Ca^{2+} , Fe^{2+}) that would have been present in Archaen sea water. Deamer and Namani reported that vesicles formed from a mixture of alkyl amines and fatty acid (Figure 29) at strongly basic and acid pH, and that they were resistant to the effects of divalent cations up to 0.1 M.⁷¹

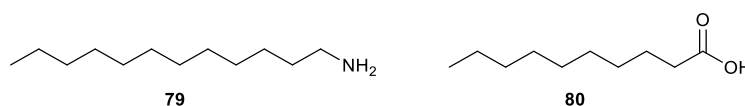


Figure 29: Structure of alkyl amine and fatty acid used to form stabilised vesicles

In addition, it was found that the permeability of the vesicles to pyranine, a fluorescent anionic dye, could be modified by changing the length of the amphiphilic chain or by addition of a polycyclic aromatic hydrocarbon such as pyrene. This work presented by Deamer *et al.*, implies that primitive cell membranes were likely to be composed of a mixture of both amphiphilic and hydrophobic molecules which would have risen due to an increased stability over membranes formed purely from fatty acids.

The Szostak lab presented a protocell model formed from oleic acid, which in the presence of glycerol monooleate can become stabilised, and permeable to

magnesium ions; which are required for ribozyme activity and RNA synthesis.^{72,73} Szostak progressed towards synthesis in vesicle protocells and demonstrated peptide bond formation of a dipeptide from lysine amide and phenylalanine amide ester where the dipeptide Ser-His (**82**) was the catalyst. In this model the product (**85**) formed would localise to the bilayer of the vesicle membrane and as a result, growth of the vesicle was observed. Vesicles that did not contain product tended to shrink (Figure 30).^{74,75}

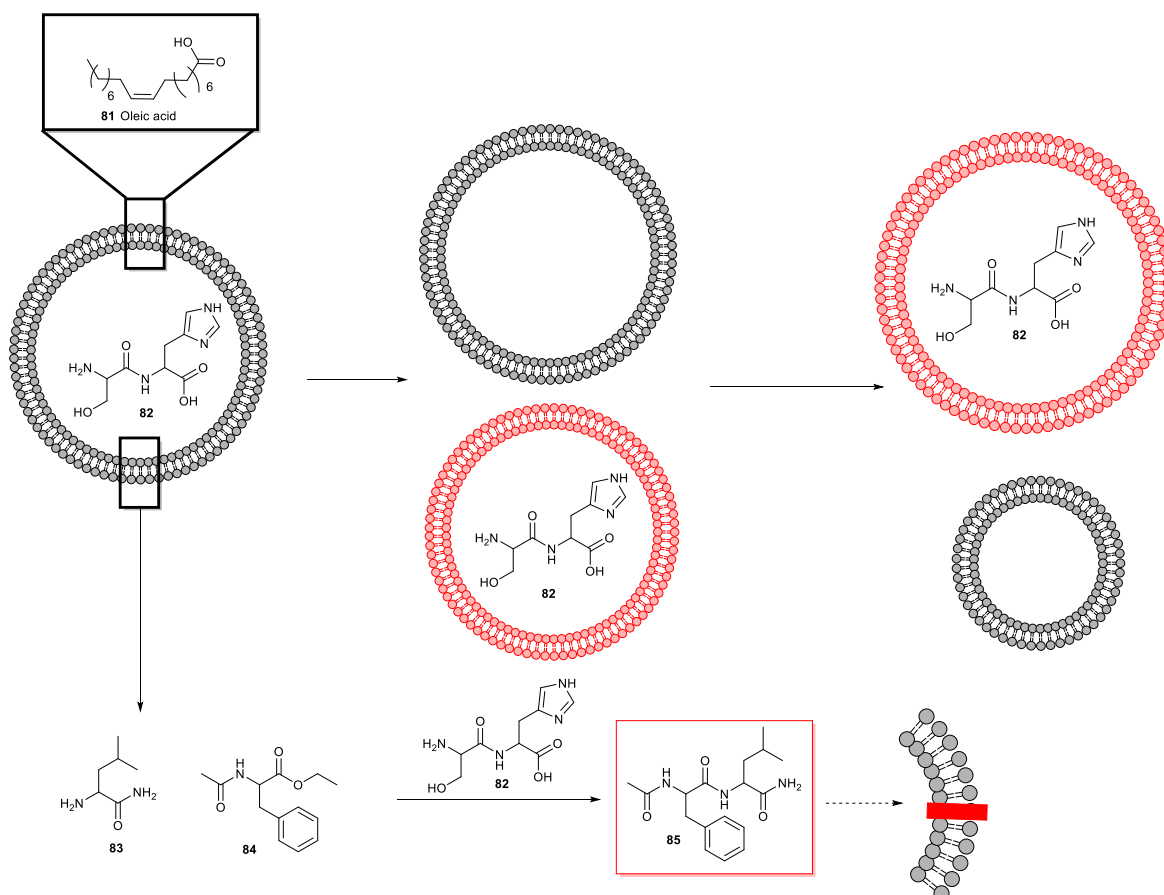


Figure 30: Synthesis of dipeptide derivative **85** inside a vesicle by the catalysis of Ser-His **82**. Once synthesised the product moved to the bilayer of the vesicle. The group found vesicles with the product would grow, where as those with-out would shrink

An alternative approach to a protocell mimic which avoids the initial need for vesicular membrane was presented by Pollack.⁷⁶ Pollack described the cell as being gel-like with the cell cytoplasm treated like a gel rather than an aqueous medium. In 2005, Trevors and Pollack⁷⁷ proposed that a primitive hydrogel was potentially a suitable environment for the assembly of pre-cells due to their ability to retain their integrity without a membrane. It was also suggested that the gel environment could also facilitate processes such as growth and division. This is due to the cohesive gel-like cytoplasm being an easier environment to partition

into two entities without cytoplasm freely flowing, acting similarly to a bacterial cell. In this model, membranes would develop later as a way to gain greater control over entry and exit to the primitive cellular environment.

Despite the strong correlation between hydrogel structure and cell cytoplasm and therefore the chance of such gel being reasonable protocell mimics, there are few examples of hydrogels as protocells without the presence of a membrane or support. As a result, agarose is often employed to demonstrate how a hydrogel could mimic a protocell. Sapara *et al.* showed that by using a firm hydrogel matrix, multiple compartments inside the same hydrogel unit could be formed by encapsulating aqueous droplets stabilized in an oil/lipid mixture. This method allowed stable encapsulation of the droplets. An aqueous droplet could be stabilized in an oil/lipid mixture, all encapsulated within an agarose hydrogel.⁷⁸ The stable encapsulation of these aqueous droplets in different oil compartments in a hydrogel allowed the formation of two bilayers close to each other. This is a step above a simplistic protocell but could be the first step towards engineering organelles and cell mimics for controlled electrical and chemical communication.

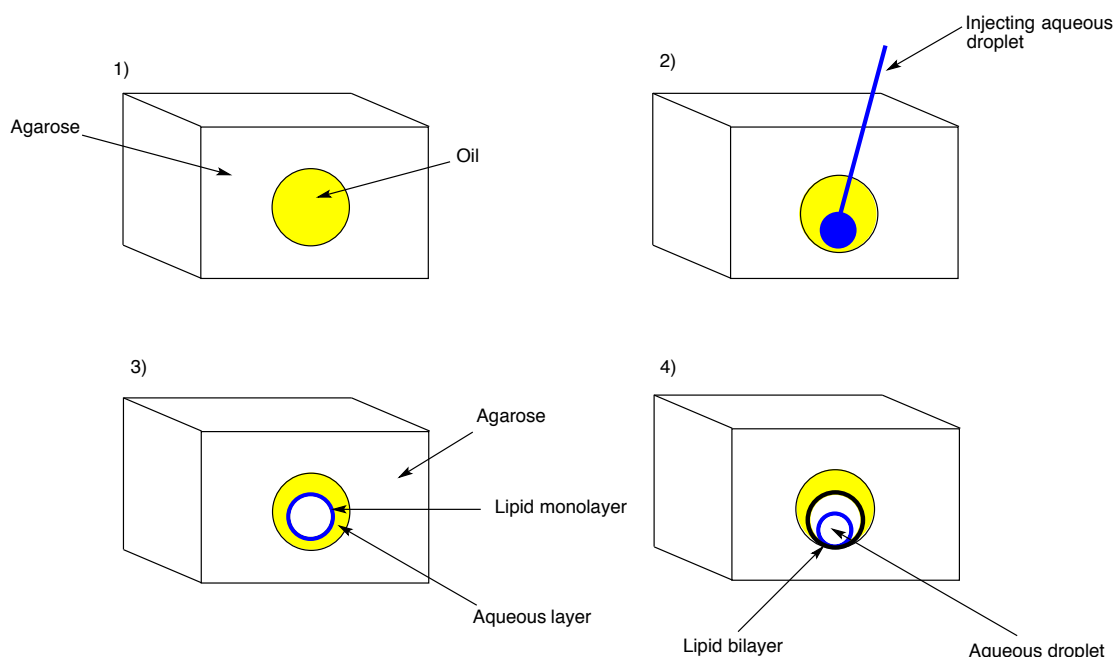
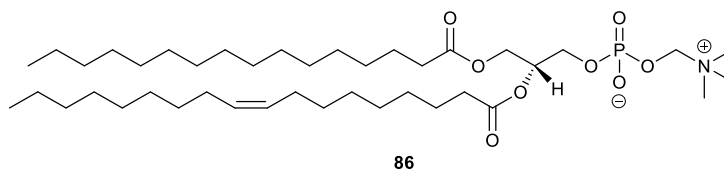


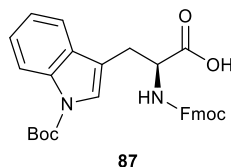
Figure 31: Droplet formation in a hydrogel

An alternative approach was reported by Mann; instead of using a hydrogel to encapsulate and as a result from multi-compartmentalised systems, Mann reported the self-assembly of hydrogelators within a vesicle.^{79,80} In this work it was found that the vesicles formed with hydrogels encapsulated were more robust and

did not aggregate compared to those without. This form of vesicle is proposed to be more cytoskeletal compared to vesicles without any gel.



Vesicle forming component



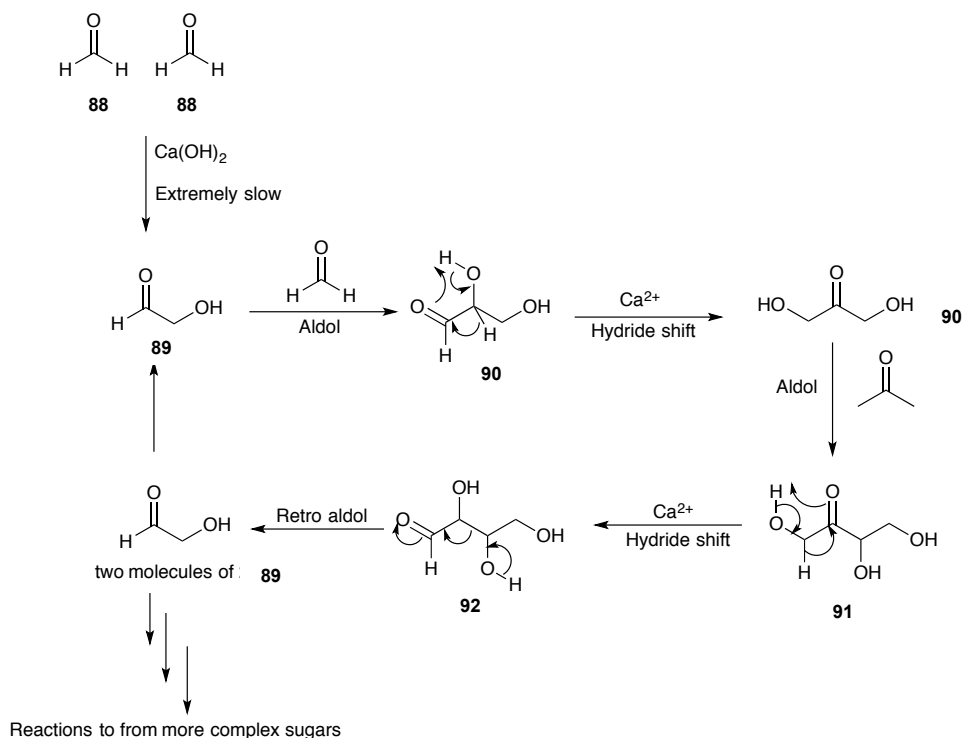
Hydrogel forming component

Figure 32: Compounds used to form vesicle with hydrogel encapsulated with in

Therefore there is considerable untapped potential for the exploration of LMWGs as primitive 'cell-like' media.

1.5 Origins of sugars

It is hypothesised that some of the dominant reactions of prebiotic chemistry are aldol condensation reactions, as these can result in the synthesis of many biologically important sugars and complex carbohydrates. It is widely believed that the first sugars arose from the formose reaction⁸¹ (first reported in 1891): an autocatalytic reaction of formaldehyde to form glycolaldehyde, with higher sugars forming as by products. As a result the formose reaction is conceptually one of the simplest syntheses of sugars. The mechanism proposed by Breslow⁸² (Scheme 11) shows that an unfavourable reaction is initially required. As a result this presents an interesting debate for the origins of sugars. In the proposed mechanism the initial step of the reaction, dimerization of formaldehyde, is slow because it requires "umpolung" chemistry to occur. Once the first step is performed the reaction then progresses more rapidly. The next stage results in the formation of glyceraldehyde (**90**) and after further hydride shifts, tetrose products can be formed. These molecules can undergo a retro aldol reaction to yield two molecules of glycolaldehyde (**89**). Therefore the cycle can begin again or alternatively the reaction can undergo further reactions to produce more complex carbohydrates.⁸³



Scheme 11: Reaction pathway for the formose reaction conceived by Breslow

Weiss *et al.* found that using a pure aqueous solution of formaldehyde did not result in the formation of glycolaldehyde (**89**).⁸⁴ It was therefore suggested that formaldehyde (**88**) contaminated with glycolaldehyde (**89**) was needed for the formose reaction. Lambert, however, reasoned that in the presence of naturally abundant species, such as silicates, formaldehyde would undergo fast oligomerization even in very alkaline conditions (pH 12).⁸⁵ Furthermore, there was a degree of control when synthesising prebiotically relevant sugars in this way. The reason for this control was due to silicates co-ordinating to the anomeric hydroxyl group and the adjacent hydroxylic group of monosaccharides (C4 and above). Based upon this work by Lambert, Banner suggested that another abundant species borate would be more likely to play this role.⁸⁶

There have also been some studies presented by Kopetzki and Antonietti⁸⁷ where hydrothermal conditions (up to 200°C and 100 bar) were used for the initiation step of the formose reaction. It was found that the formose reaction occurs at a greater rate in the presence of glycolaldehyde (**89**), but will interestingly also occur in the absence of glycolaldehyde, but in the presence of a dicationic species such as calcium acetate.

1.6 Prebiotic interest in phosphates

Phosphates are biologically relevant and important to modern biological systems. They provide structural robustness and solubility in an aqueous environment, for example the phospholipid bilayer required for mammalian cells. In addition phosphates are also required in DNA and RNA (**93**) and makeup the sugar phosphate back bone. Phosphate ester bonding is also commonly referred to as the biochemical energy currency in the form of ATP (**94**) which is required in many metabolic pathways (Figure 33).⁸⁸

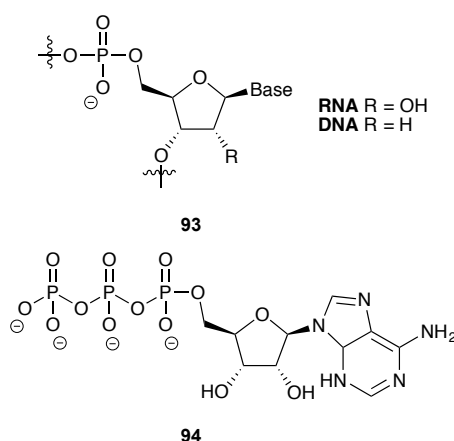
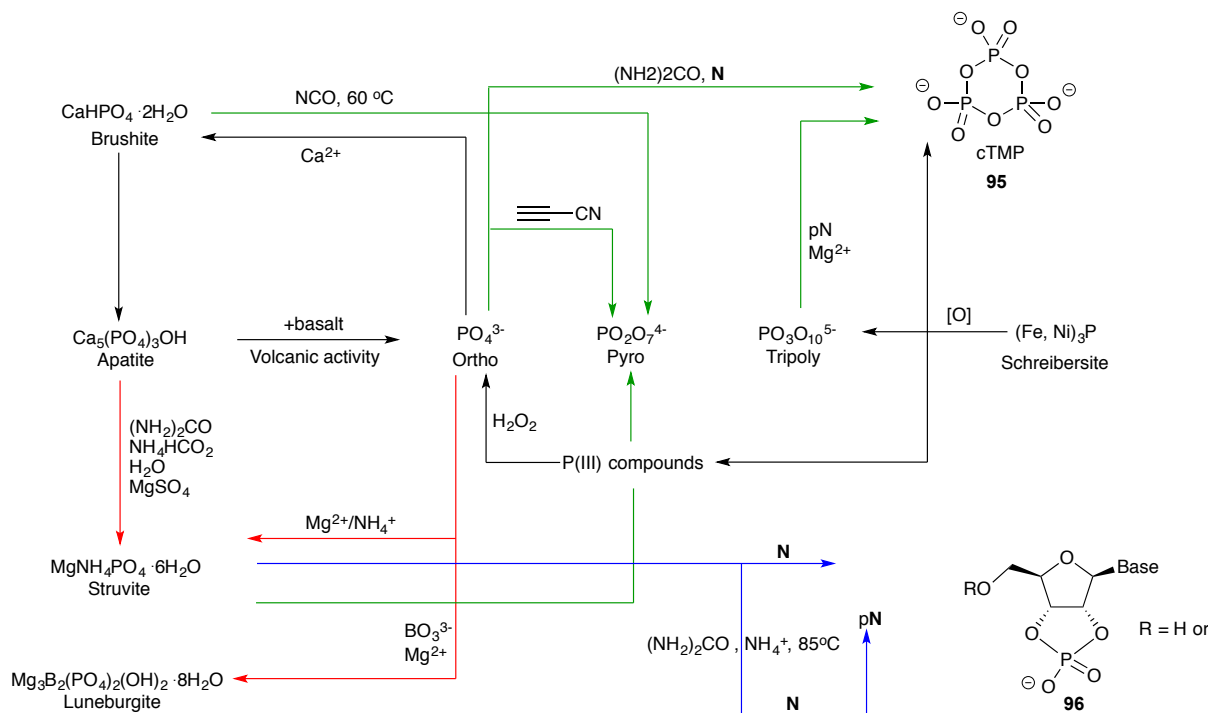


Figure 33: Biologically important phosphates

As phosphates have an important role in life's chemical processes, the origin and roles of phosphate must be studied. Currently theories such as the formose reaction and many other theories for the formation of other prebiotic building blocks reaction do not require the presence of phosphate.^{89–92} However this presents the question of how phosphate came to play an important role in biological systems? The origin of inorganic phosphate on the early Earth has been debated broadly. The most common form of phosphorus on the Earth is orthophosphate (PO_4^{3-}) found in apatite minerals and relatively insoluble, as this is found as the calcium salt. It is, however, possible that this source of phosphate could have played a role in prebiotic chemistry but with a different anion which might aid solubility especially in aqueous media. Other sources of phosphate have also been postulated (Figure 34).^{61,93–96}



Suggested prebiotic routes to orthophosphate and condensed phosphates production (black arrows), phosphate interconversion (green arrows), phosphate solubilisation (red arrows), and urea-mediated phosphorylation (blue arrows). **N** = nucleoside, **pN** = nucleotide, **cTMP** = cyclotriphosphate.^{61,93–96}

Figure 34: An overview of suggested prebiotic routes to phosphates

In the 1990's Eschenmoser *et al.* reported the dimerization of glycolaldehyde phosphate in aqueous NaOH solution.⁹⁷ At room temperature, in the absence of air, and after 7 days it was found that glycolaldehyde phosphate (**97**) dimerized in the presence of 2 M NaOH (Figure 35). A mixture containing the racemates for the two diastereomeric tetrose 2,4-diphosphates (**98**) and eight hexose 2,4,6-triphosphates (**99**) was obtained in 80% combined yield and a tetrose : hexose derivative ratio of ca 1:10.

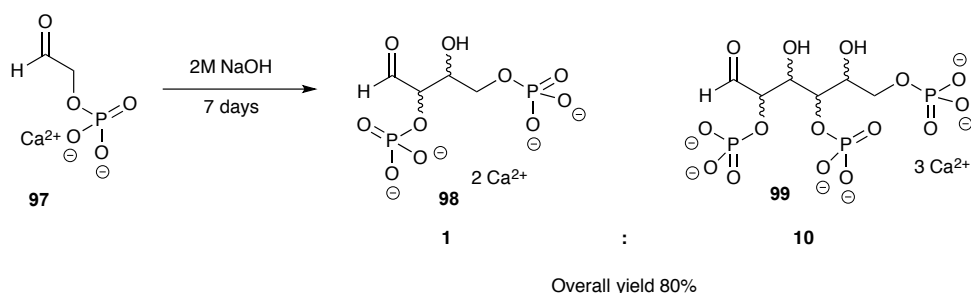


Figure 35: Dimerization of glycolaldehyde phosphate in aqueous sodium hydroxide

It was also noted that when the reaction was performed under the same conditions but in the presence of formaldehyde, racemic sugar phosphates are produced with an overall yield of 45%. The mixture contained glyceraldehyde-2-phosphate (**100**), aldotetrose- (**101**) and aldopentoses-2,4,-diphosphates (**102**) and aldohexose-2,4-6-triphosphates (**103**). In this scenario the aldophosphate sugars dominated.

Within these sugars ribose-2,4-diphosphate was the main component of the mixture. The results observed are reasoned to be due to electronics and steric hindrance. The aldol condensation of formaldehyde with glycolaldehydephosphate is preferred because formaldehyde is a good aldol electrophile. Whereas, in further aldol condensations, the product glyceraldehyde-2-phosphate is a worse aldol nucleophile compared to glycolaldehyde phosphate but is a better electrophile. Therefore crossed aldol reactions to give pentose products are observed.

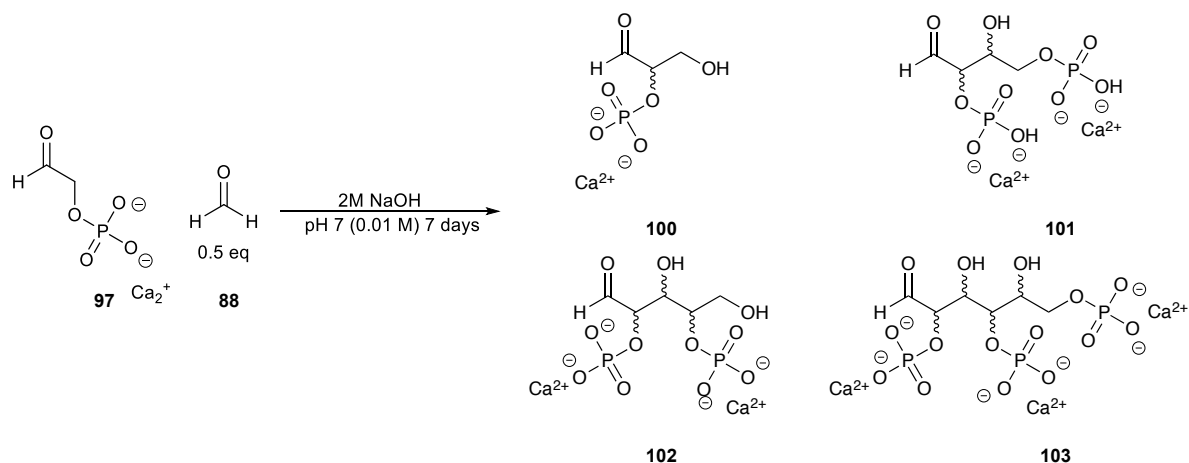
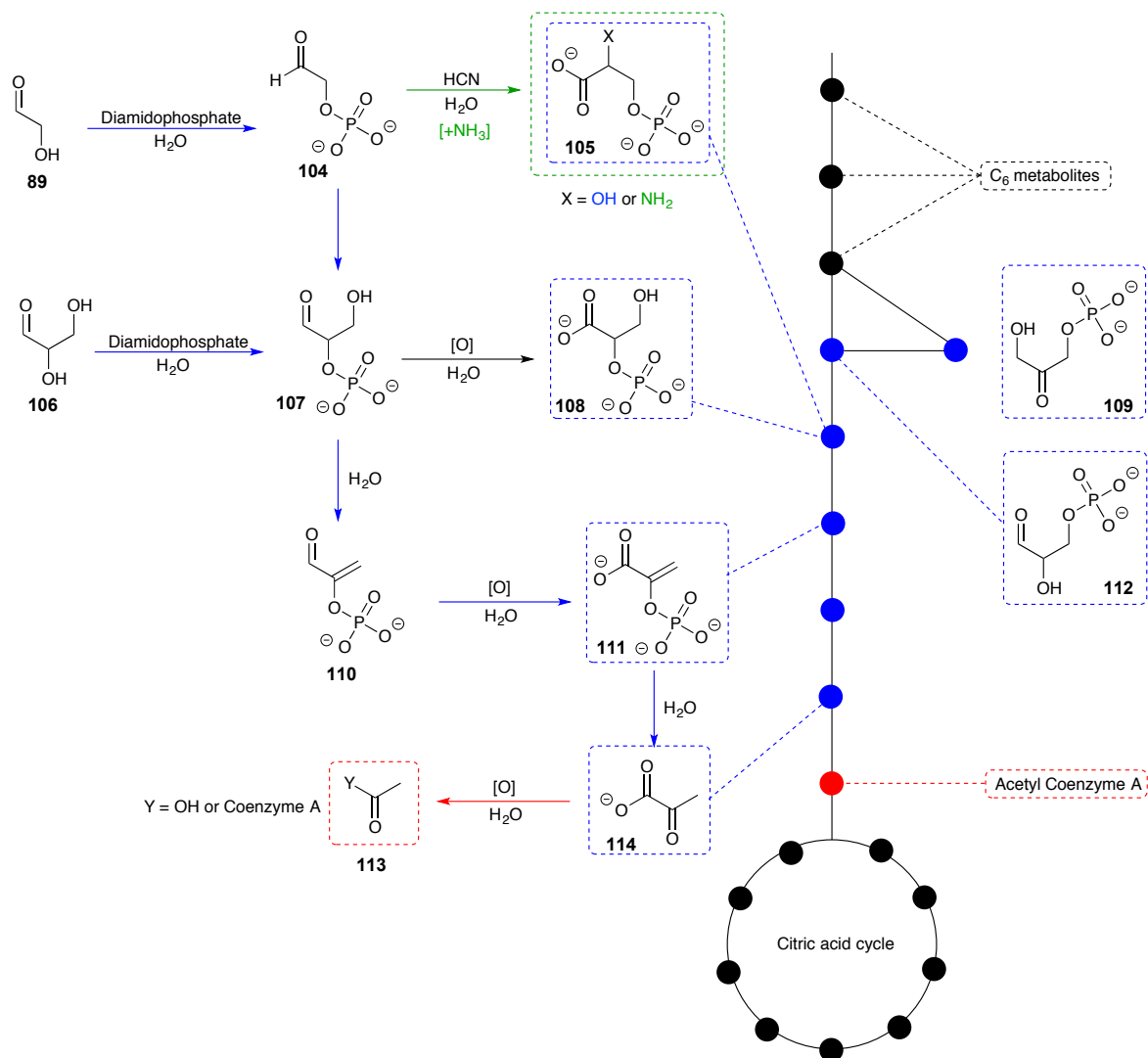


Figure 36: Dimerization of glycolaldehyde phosphate with formaldehyde in aqueous sodium hydroxide

Typically in the formose reaction, tars are observed when synthesising complex sugars due to the instability of the sugars, produced at high pH. This indicates that the phosphorylated sugars are significantly more stable compared to the non-phosphorylated parent sugars.

The work presented by Eschenmoser sparked interest as it showed the potential to be a plausible prebiotic route to the phosphoribose in prebiotic RNA. It is known that formaldehyde can be formed through ultraviolet irradiation of atmospheres containing carbon dioxide and carbon monoxide,⁹⁸ however, the source of short chain (C2, C3) sugars is not fully resolved.

In 2016 Powner *et al.* developed a network of prebiotically plausible reactions that synthesised all the intermediates of triose glycolysis.⁹⁹ It was shown that glyceraldehyde-2-phosphate can be oxidised to give glyceric acid 2-phosphate or dehydrated in pH 7 phosphate buffer to give phosphoenol pyruvaldehyde. The phosphoenol pyruvaldehyde can then undergo oxidation to produce one of biology's highest energy phosphates in excellent yield; phosphoenol pyruvate.



Blue arrows: prebiotic pathway to phosphoenol pyruvate (111) and pyruvate (114). Green arrow: divergent prebiotic synthesis of glyceric acid 2-phosphate (105 P x = CH) and phosphoserine (105 P x = NH₂) from glycolaldehyde-2-phosphate (104-P), which provides a generational link between glycolysis (blue) and serine metabolism (green). Red arrow: oxidative decarboxylation of pyruvate (114) to yield acetate (113). Black arrow: quantitative oxidation of glyceraldehyde 2-phosphate (107) to glyceric acid 2-phosphate (108). Structures boxed in blue highlight the alignment between the prebiotic network and the specific node on the metabolic triose glycolysis pathway. b, Enzymatically controlled pathway from C₆-metabolites to citric acid cycle via glyceraldehyde-3-phosphate (112) and dihydroacetone phosphate (109).⁹⁹

Figure 37: Potential prebiotic pathway to phosphorylate pyruvate

1.7 Prebiotic interest of amino acids

The world in which we live is a chiral world, predominantly making use of L-amino and D-sugars. Chirality must have been present on the prebiotic earth as it is important in life now. Amino acids are one of the more simplistic chiral building blocks responsible for life. As a result, the origins of amino acid homochirality is a key point of interest.

Miller and Urey carried out pioneering research into the origins of amino acids through an experiment, known as the electric discharge experiment (Figure 38).^{100,101} The aim of the research was to mimic conditions thought to be similar to that of early Earth and examine the chemistry of the products. A reductive atmosphere was created from boiling water that contained methane, ammonia and hydrogen. This reductive atmosphere was continuously circulated through an electrical discharge apparatus for one week. The researchers were able to identify amino acids (Figure 39) such as glycine (**115**), α -alanine (**116**) and β -alanine (**117**). In addition, further studies revealed other small molecules such as formic, acetic and lactic acids to be present.^{100,101}

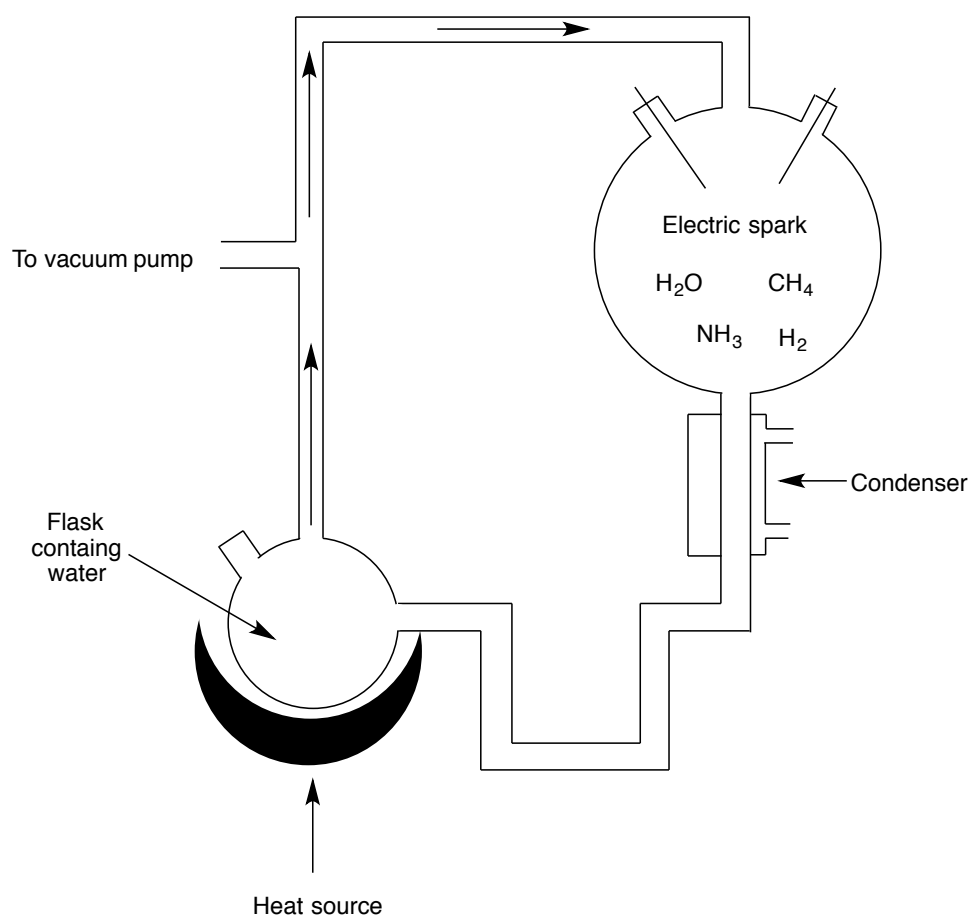
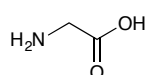
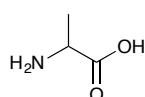


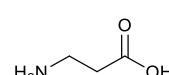
Figure 38: Miller-Urey electric discharge experiment set up



115



116



117

Figure 39: Amino acid structures identified in Miller-Urey electric discharge experiment.

This pioneering research into the formation of simple molecules such as amino acids in a prebiotic context was seminal in the field of prebiotic chemistry. It was the first experimental attempt to probe what would have happened on the early Earth and it also provided a pool of potential prebiotic materials. Since the early

experiment performed by Miller and Urey, knowledge and theories about the prebiotic Earth have grown. As a result, other hypotheses about how prebiotic chemicals, specifically amino acids, arrived on Earth have been explored such as meteorite bombardment, hydrothermal vents and more recently photo-redox reactions.

Around 3.5 billion years ago, the Earth underwent meteoritic bombardment. When meteorites impacted it is thought that amino acids and other essential building blocks may have been deposited on the Earth. Evidence for this scenario came from analysis of a number of meteorites that fell to Earth in recent years.^{102,103} The most significant of these was the Murchison meteorite which, on analysis, was found to contain a range of natural amino acids such as proline, valine, glycine and glutamic acid.¹⁰⁴ However, there has been some dispute with this analysis of the meteorites as the current Earth is abundant with amino acids and it has been suggested that the origin of these amino acids may be simple contamination.¹⁰⁵ Nevertheless, the high abundance of ¹³C and ¹⁵N present in the sample, in addition to small ee% in favour of L-amino acids, supports the hypothesis of an extraterrestrial origin.¹⁰⁶

Another scenario is that amino acids may have arisen from hydrothermal vents. In these systems, there are high temperatures (150°C) and carbon dioxide is reduced to methane when in contact with minerals such as pyrite or magnetite.¹⁰⁷ Conditions similar to those present at hydrothermal vents were replicated in a study. A one litre autoclave was heated to 150 °C with a pressure of 10 atmospheres (atm). The autoclave contained an aqueous phase consisting of potassium cyanide, formaldehyde, ammonium chloride and hydrochloric acid (HCl). In addition there was a mineral phase containing pyrite/magnetite or illite and a gaseous atmosphere of hydrogen and carbon dioxide (1:3). The reaction was left for 54 hours, after which the samples were acidified with HCl and analysed by gas chromatography (GC) and high-pressure liquid chromatography (HPLC).¹⁰⁸ The data indicated a number of L-amino acids with 100% ee (Figure 40): asparagine (Asp, **118**), serine (Ser, **119**), glutamic acid (Glu, **120**), glycine (Gly, **121**), alanine (Ala, **122**), cysteine (Cys, **123**), methionine (Met, **124**) and isoleucine (Ile, **125**) were present in milimolar concentrations. This was higher than the concentrations reported in the electric discharge experiment. However,

there was a lack of any D enantiomers of amino acids. This has again led to suggestions that there was contamination.¹⁰⁹

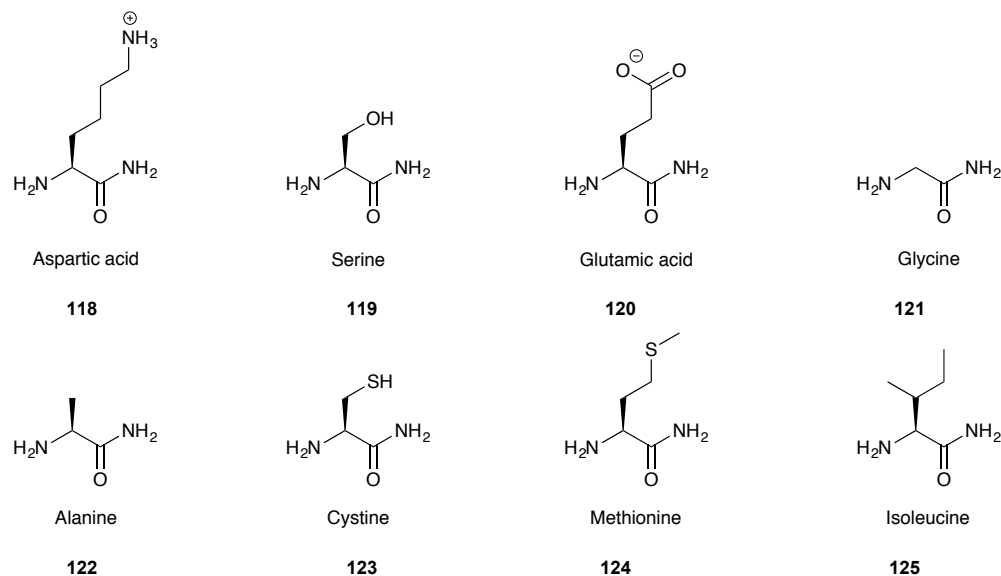
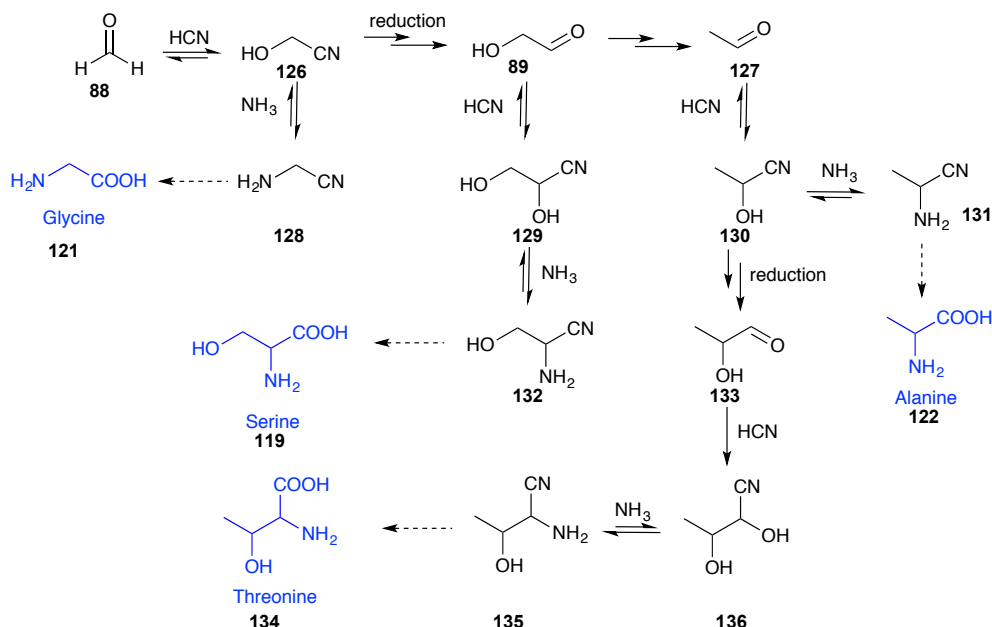


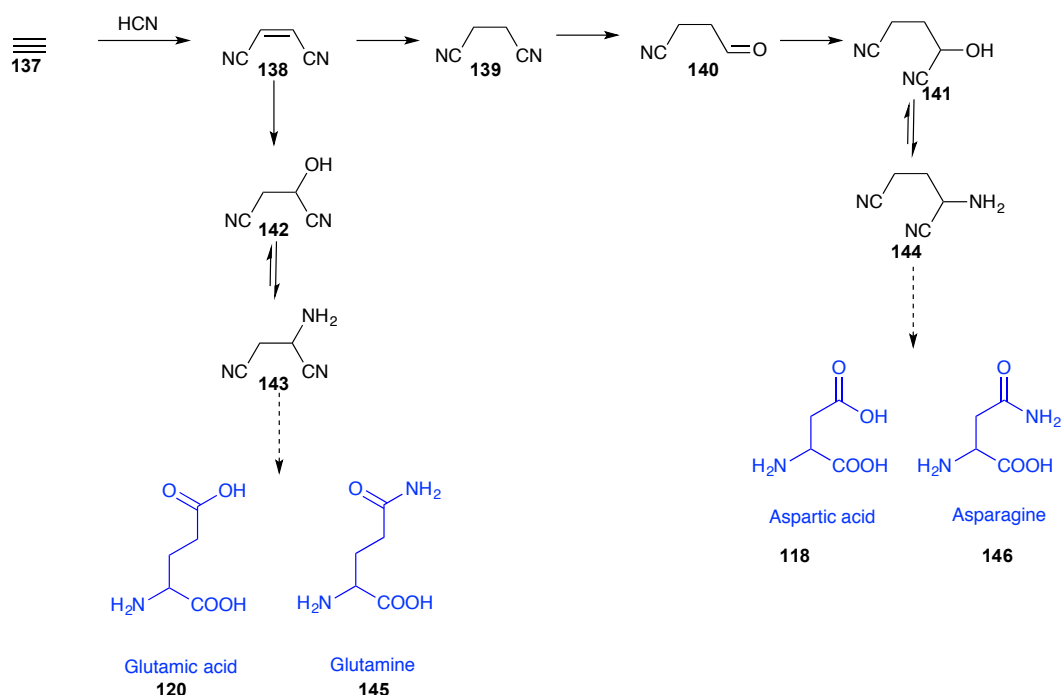
Figure 40: Amino acids identified in reaction replicating hydrothermal events

Another plausible scenario for the origins of amino acids involves using simple prebiotic building blocks such as ammonia and hydrogen cyanide and the photoredox reaction of copper salts. Sutherland and co-workers explored this scenario as part of their origins of life ‘systems’ chemistry.¹¹⁰ In this work they investigated the assembly of various biomolecular building blocks from potential prebiotic intermediates and one carbon feed stocks. In the experiments carried out by Sutherland and co-workers the key reactions are driven by UV light, use hydrogen sulfide as the reductant and can be accelerated by Cu(I)-Cu(II) photoredox cycles. It was thought that formaldehyde could be synthesised by oxidation of hydrogen cyanide (HCN) to cyanogen ((CN)₂) which would then reduce HCN to a formaldehyde imine, and after hydrolysis would generate formaldehyde. This unsurprisingly caused discussions that resulted in the possibility of amino nitriles being a plausible prebiotic precursor for amino acids. C2 and C3 sugars can be provided sequentially by a Kiliani-Fischer type homologation of HCN using Cu(I)-Cu(II) photoredox, with hydrogen sulfide as a reductant, resulting in the Strecker precursor amino nitriles being formed as by-products.



Scheme 12: Reaction pathway from formaldehyde to amino acids¹¹¹

It was also shown by Sutherland that even more amino acids could be formed by simple copper-catalysed cross-coupling of acetylene and HCN followed by addition of water and ammonia resulting in the amino nitriles which could then be converted into amino acids.¹¹⁰ The next question to be answered was ‘where could these types of reactions take place?’ it is hypothesised by Sutherland and co-workers that a geochemical scenario is the most likely location as there is evidence suggesting that shortly after meteoritic bombardment life started, and that processes involved with meteorite impact, may have been involved in the generation of HCN and phosphate on early Earth.



Scheme 13: Reaction pathway from acetylene to amino acids

This approach to the origins of amino acids is not too dissimilar to the theory provided by Miller and Stanley in their electric discharge experiment. However unlike the electric discharge experiment the work presented here is stepwise and mechanistic in nature, and could indicate that compartmentalised chemistries are required for life to begin, as the chemistries required often conflict, meaning that a one-pot approach may not be feasible.

1.8 Amino acids a prebiotic catalysts

As noted in Section 1.3, many organic syntheses benefit from catalysis. A catalyst cannot only increase the rate of reaction but also control stereochemistry. One of the most important reactions in chemistry is direct aldol condensation in which a C-C bond forms between two carbonyl compounds (Figure 41).^{112,113} Some gel-based catalysis of the aldol reaction were presented in section 1.3.

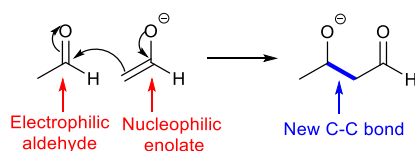


Figure 41: Carbon-carbon bond formation in direct aldol condensation

In 1957 Zimmerman and Traxler suggested that certain metal catalysed aldol reactions have six-membered cyclic transition states that would favour a chair conformation, due to this conformation being lowest in energy. This is commonly known as the Zimmerman-Traxler transition state model.¹¹⁴ In this model *E*-enolates give rise to *anti*-products and *Z*-enolates give rise to *syn*-products. This is because of the placement of substituents to minimise steric and electronic repulsions. The R substituent on the aldehyde however, has two choices; to go pseudoaxial or pseudoequatorial. Pseudoequatorial is favoured as there are fewer steric clashes (Figure 42) and as a result the product obtained is the *anti*-aldol product (Figure 43). Without a six-membered transition state there would be less steric control and stereo-selectivity would not be observed. This was an early example in which the impact of conformation on product configuration was elucidated, later becoming a key principle of organic chemistry.

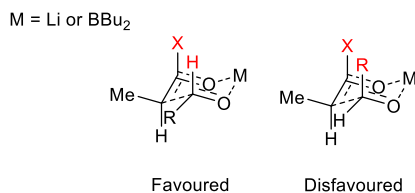


Figure 42: Zimmerman-Traxler model for the *E*-enolate

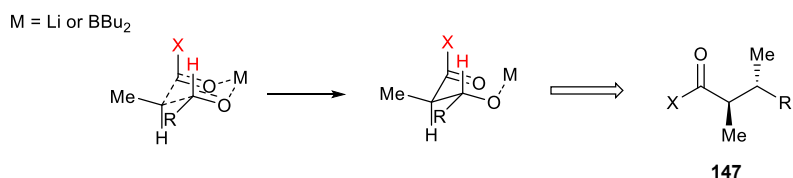
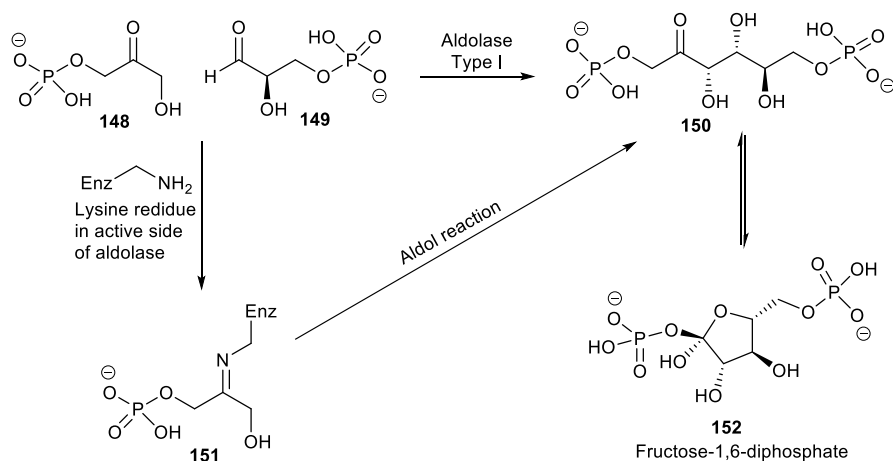


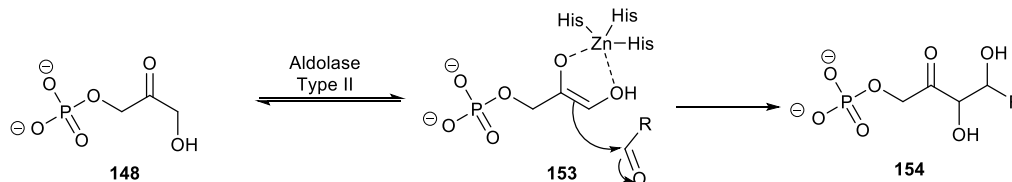
Figure 43: Product from favoured six-membered transition state using the Zimmerman-Traxler model

The Zimmerman-Traxler model often uses lithium or boron as the metal. However, lithium will not always give the best selectivity so boron and chiral auxiliaries are often favoured.^{115–120} When boron is used, the transition state is ‘tighter’ due to B-O bonds being shorter in length. The tighter transition state results in greater stereoselectivity. Although lithium and boron mediated C-C bond formation is well established, it is apparent that in nature, aldol reactions also occur to generate products containing β -hydroxyl carbonyl skeletons. These products often contain pharmacological activity, and are generated with stereocontrol. However, lithium or boron mediated transition states do not occur in biosynthesis, it is much more likely that enzymes catalyse type I aldolase reactions (Scheme 14). Type I aldolase enzymes contain a lysine residue in the active site of the enzyme that acts as a catalyst for the aldol reaction of hydroxyacetone phosphate **148** and glyceraldehyde phosphate **149** to form fructose,1,4-diphosphate **150** with two new stereocentres in a *syn* configuration.¹²¹



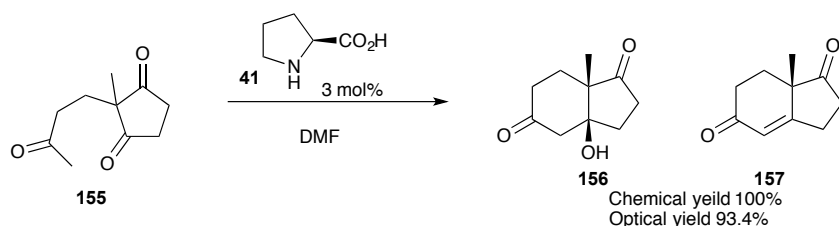
Scheme 14: Aldol reaction of the aldolase type I enzyme.

There is a second type of aldolase (Type II) that uses a zinc-cofactor bound to an enzyme active site. The zinc makes the α -proton more acidic by acting like a Lewis acid. This in turn activates the substrate allowing the zinc enolate to form. An example of this mechanism is shown in Scheme 15 using dihydroxyacetone phosphate (DAHP) **148** as the substrate.



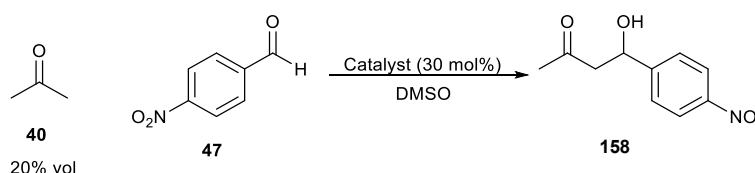
Scheme 15: Aldol type II reaction mechanism using a zinc-cofactor

However it is also plausible that small organic molecules will catalyse aldol condensation reaction with good stereoselectivity. The amino acid L-proline (**41**) was first used as an organo-catalyst in 1971.^{122,123} It was reported that catalytic amounts of amino acids were capable of promoting the intramolecular asymmetric aldol cyclisation reaction of a triketone. This occurred with excellent chemical yield and stereochemical selectivity, in an enantioselective version of a Robinson-like¹²⁴ annulation (Scheme 16).



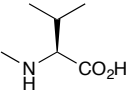
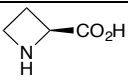
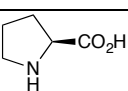
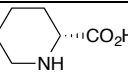
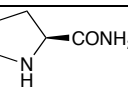
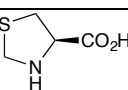
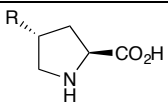
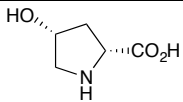
Scheme 16: The Eder-Sauer-Wiechert-Hajos-Parrish Reaction

In the early 2000s, Barbas and List studied proline (**41**) and other amino acids as an effective asymmetric catalyst for more general aldol reactions.¹²⁵ In this work, acetone was used in conjunction with 4-nitrobenzaldehyde in DMSO (Scheme 17), and later a variety of other aldehydes. Barbas and List proceeded to study different primary and acyclic secondary amino acids as catalysts. The results of this work are summarised in Table 4.



Scheme 17: Aldol condensation of acetone and 4-nitrobenzaldehyde in DMSO with 30 mol% catalytic loading

Table 4: Amino acid derivatives tested as catalysts for the asymmetric aldol reaction of acetone with 4-nitrobenzaldehyde

Entry	Catalyst structure	Yield	ee %
1	(L)-His, (L)-Val (L)-Try, (L)-Phe	< 10 %	Not determined
2	 159	< 10 %	Not determined
3	 160	55 %	40
4	 41	68 %	76
5	 161	< 10 %	Not determined
6	 162	< 10 %	Not determined
7	 162	67 %	73
8	 164	R 1 = 85 % R 2 = > 50 % R 3 = 70 %	78 62 74
9	 165	> 50%	62

The results show that the pyrrolidine ring has an important role in the efficiency of catalysis. Without a five membered ring, low yields are reported for entries 1, 2 and 5 in Table 4. In addition, having a carboxylate was imperative for enantioselectivity. When an amide unit (entry 6) was employed rather than a carboxylate (entry 4), enantioselectivity decreased dramatically. However, modifying the pyrrolidine ring was successful with varying degrees of selectivity and yield of product. This early work showed that proline and its derivatives allow a stable enamine intermediate to form, which then provides a 6-membered transition state required for enantio and diastereoselectivity in aldol catalysis.

In 2002, Barbas⁴² proposed a mechanism that indicates why proline gives both diastereoselectivity and enantioselectivity. In the mechanism it can be seen that there is an enamine six-membered non-metal Zimmerman-Traxler transition state. This transition state forms due to the carboxylate group participating in hydrogen bonding, and as a result, the transition state is organised in such a way that only one possible enantiomeric product can dominate.

When a hydroxylated ketone is used, the enamine which forms contains an *E* double bond. Due to the *E* double bond, the hydroxyl group must be equatorial on the six-membered transition state and therefore the *anti*-aldol product forms (Figure 44).

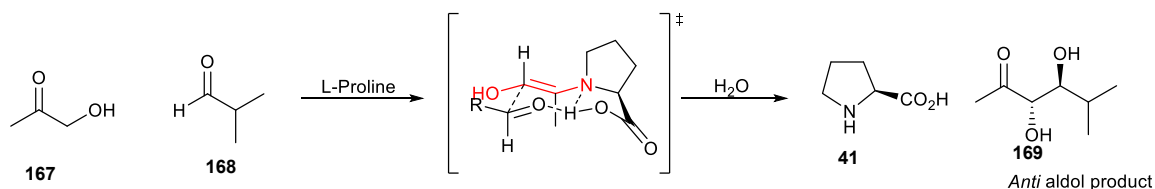


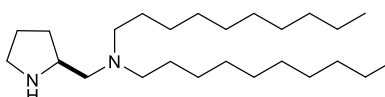
Figure 44: L-proline catalyst six-membered transition state involving a hydroxylated ketone

L-Proline and its derivatives have also been shown to catalyse many other reactions for example; asymmetric aldol,^{125–128} Mannich^{127,129} and Michael reactions.¹³⁰ The types of reactions and solvents L-proline and its derivatives can catalyse demonstrates the usefulness of organocatalysts of prebiotic nature. The main disadvantages of using amino acid catalysts such as L-proline, are that often a large catalytic loading (30 mol%) is required and the reactions can take up to 72 h before being complete. In some cases, however, yields and enantioselectivities can be poor.

The catalysis described above takes place in organic solvents, but, in pre-biotic chemistry performing reactions in water is of considerable importance given the dominance of this medium on Earth. However, using water as a solvent is not always practical for asymmetric catalytic reactions. Water can inhibit the activity of the catalyst or alter the enantioselectivity by disrupting the non-covalent interactions needed to stabilise the transition state.^{131,132} Hydrogen bond interactions are particularly sensitive to this type of disruption.

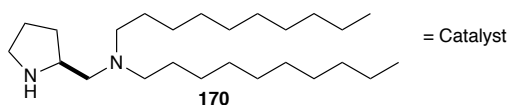
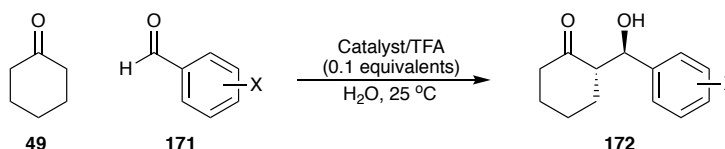
In 2006, Barbas reported an efficient enamine-based organocatalyst for direct asymmetric aldol reactions in water without the need for an organic co-solvent

such as DMSO.⁴⁶ It was reported that by synthesising a proline based catalyst with hydrophobic groups (Figure 45) catalysis of 4-nitrobenzaldehyde and cyclohexanone occurred; yet without the hydrophobic group no reaction took place (Scheme 18). Barbas suggested that this is due to the hydrophobic group increasing the surfactant-like nature of the catalyst. As a result the increase in hydrophobicity allows an organic environment to be formed within an aqueous environment, much like a micelle, therefore the reaction turns over as there is a region of 'higher' organic concentration.



170

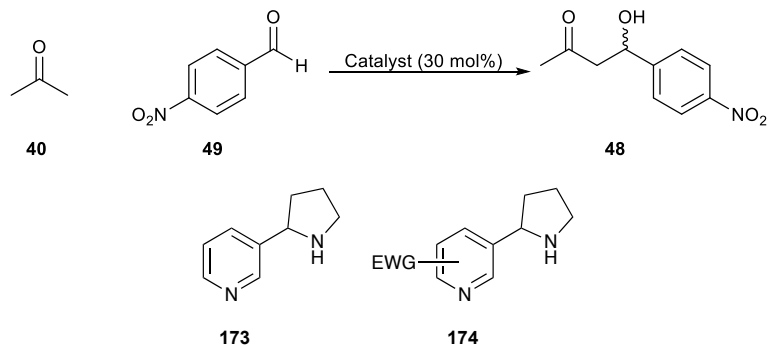
Figure 45: Bifunctional organocatalyst



Scheme 18: Organocatalysed aldol reaction in water

There is, however, a need for an additive in the reaction (Scheme 18). In water without any additive, the reaction with the same catalyst still gave good yield with high diastereoselectivity but almost no enantioselectivity. Whereas, on the addition of trifluoroacetic acid (TFA), enantioselectivity was achieved. It was revealed in work by Janda,¹³³ that TFA increases the amphiphilic character of the catalyst, which results in micelle formation, enantiomer enrichment and suppresses non-selective general base catalysis.

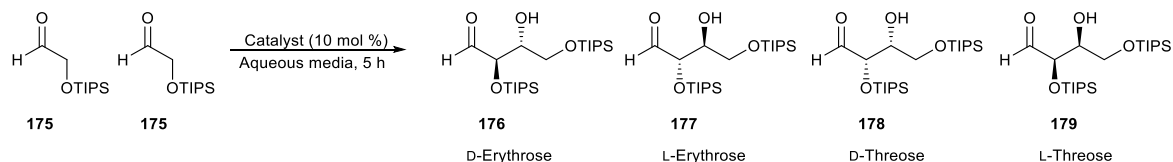
Janda and Dickerson¹³⁴ further explored the use of organocatalysts and studied nornicotine, a constituent of tobacco, as a catalyst for aldol condensation reactions in an aqueous environment (Scheme 19).



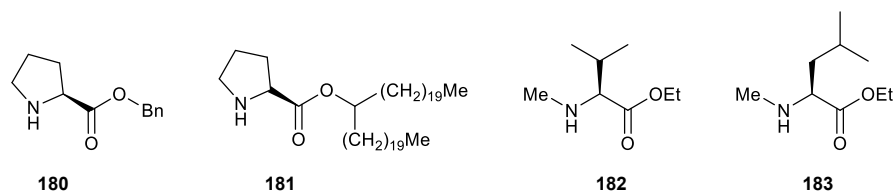
Scheme 19: The nor nicotine-catalysed aldol reaction investigated by Janda *et al.* ^{134,135}

In this study, acetone was used as the donor and 4-nitrobenzaldehyde as the acceptor. An interesting result was observed; in water there was no turnover of the reaction. However, at pH 7.4 in 12 h an 81% yield was observed in the same conditions. Without the catalyst only 6% conversion was seen. The reason for the change in reactivity at this controlled pH is thought to be due to eliminating hydrolysis of the enamine intermediate. Another finding by Janda *et al.*¹³⁵ was that by modifying the ring on the catalyst, the rate of reaction could be influenced. It was found that if an electron-donating group was incorporated then the rate of reaction would decrease, and if an electron-withdrawing group was used then the rate of reaction increased. Janda reasoned that the electron-withdrawing group decreased the pKa of the pyrrolidine nitrogen, which aids the formation of the reactive enamine intermediate as this makes the nitrogen more nucleophilic.

Janda's work inspired the Clarke group to study the prebiotic synthesis of sugars using simple amino acid derived organocatalysts. The Clarke group^{136–138} looked at the dimerization of triisopropyl (TIPS) protected glycolaldehyde with a variety of amino esters where the ester functionality is electron withdrawing. The key results of this early work are presented in Table 5.



Catalysts:



Scheme 20: TIPS protected glycolaldehyde dimerization with different amino ester catalysts

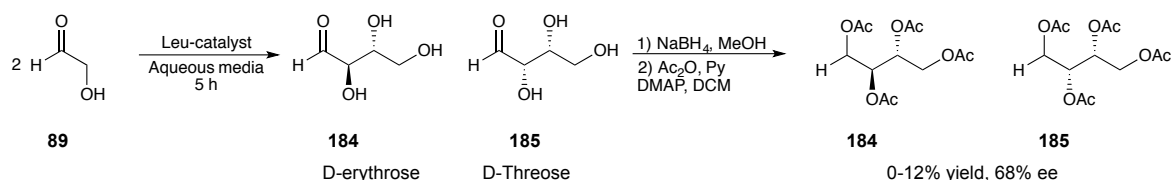
Table 5: TIPS protected glycolaldehyde dimerization using amino ester catalysts

Entry	Catalyst	Solvent	Major product	Combined yield %	d.r	ee % (<i>anti</i>)
1	180	Water	L-Erythrose	77	1.5:1.0	18
2	180	pH 7 buffer	L-Erythrose	70	1.5:1.0	47
3	181	Water	L-Erythrose	49	2.0:1.0	10
4	181	pH 7 buffer	L-Erythrose	52	5.5:1.0	46
5	182	Water	D-Erythrose	80	1.5:1.0	17
6	182	pH 7 buffer	D-Erythrose	79	1.5:1.0	57
7	183	Water	D-Erythrose	33	1.0:1.0	31
8	183	pH 7 buffer	D-Erythrose	40	1.5:1.0	79

The results from Clarke *et al.* showed that L-proline derived catalysts yielded L-erythrose as the major product (entries 1-5 Table 5), while the amino esters based on valine or leucine yielded D-erythrose as the major product (entries 6-8 Table 5). The reason for this selectivity was not given. The enhancement in enantiomeric excess of product upon buffering the system to pH 7, is understood to be due to eliminating general base catalysis which would otherwise result in products with no selective background reactions

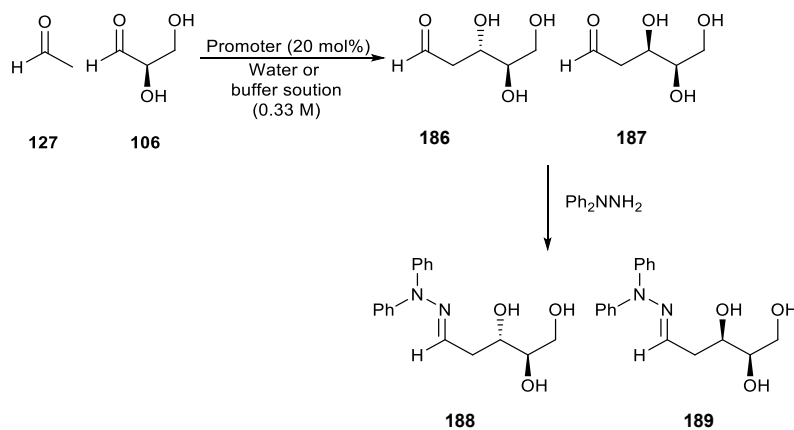
The next stage of this work was to understand the role of the TIPS protecting group. Clarke *et al.* therefore performed the same reactions but this time with unprotected glycolaldehyde (Scheme 21). The products from these reactions were

trapped with acetic anhydride to aid analysis. The results of this experiment showed that moving from TIPS protected to unprotected glycolaldehyde significantly reduced the yield of desired products (0-12%). In addition, the d.r. of the products also varied depending on pH; 1:1 at pH 6 and 7:1 at pH 7 with the same catalyst. It is important to note, that upon formation of the tetra-acetals a *meso* compound formed with erythrose therefore only an ee% can be determined for threose.

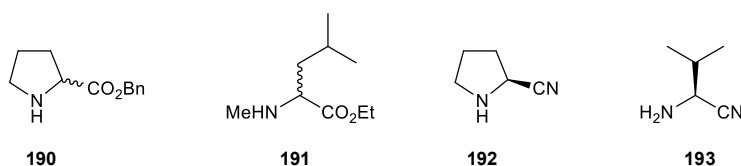


Scheme 21: Leu-catalyzed (**183**) direct asymmetric aldol reactions of unprotected glycolaldehyde

More recently Steer¹³⁶ *et al.* reported the synthesis of 2-deoxy-D-ribose from acetaldehyde and D-glyceraldehyde promoted by amino esters and also by amino nitriles (Scheme 22) therefore providing a potential route towards the key sugar building block of DNA based on this type of chemistry. In order to isolate the products, reaction mixtures were treated with *N,N*-diphenyl hydrazine to trap any carbohydrates formed and facilitate their isolation and characterisation as the hydrazone. The results in Table 6 show that amino esters **195** and **196** were able to catalyse the formation of 2-deoxy-D-ribose **186** and 2-deoxy-D-threopentose **187**, and had selectivity for 2-deoxy-D-ribose ca. 1:2 ratio respectively (entries 2-8 Table 6). In previous work, pH had an impact on the yield and selectivity of tetroses, therefore different pH values were tested but did not affect the yield or ratio of product. This result is important as it increased the possibility of the reaction proceeding in a prebiotic aqueous environment. Influenced by Sutherland's work¹³⁹ amino nitriles were explored. Amino nitriles are considered more likely early prebiotic species than amino acid esters. It was found that in the same reaction, similar yields and selectivities were obtained when using amino nitriles (entries 9 and 10 Table 6) as those reported for the use of amino esters (entries 2-8 Table 6).



Promoters:



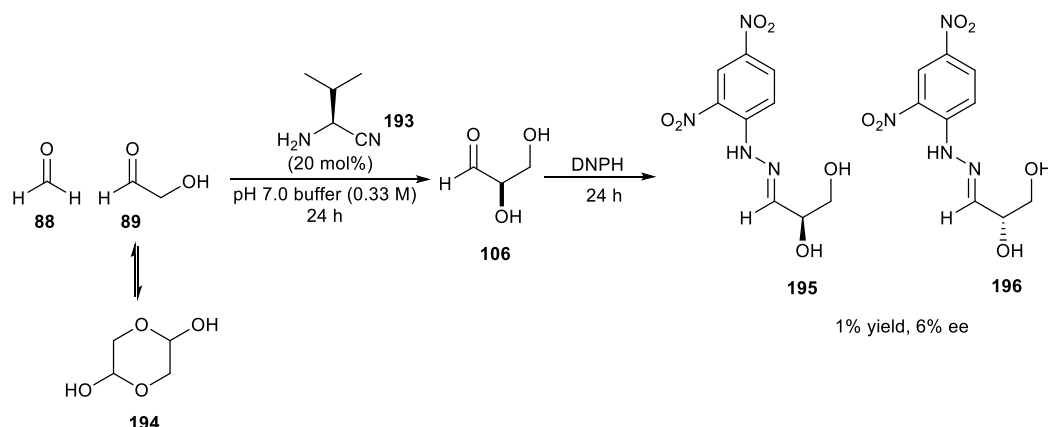
Scheme 22: Synthesis of diphenyl hydrazone protected 2-deoxy-D-ribose **186** and 2-deoxy-D-threopentose **187** by amino ester and amino nitrile promoters

Table 6: Result of the formation of 2-deoxy-D-ribose **186** and 2-deoxy-D-threopentose **187** in water

Entry	Catalyst	pH	Ratio	Combined yield %
1	None	7	-	0
2	L-190	Unbuffered	1.5:1.0	2
3	L-190	7	1.8:1.0	2
4	L-190	6	1.8:1.0	2
5	D-190	7	1.3:1.0	3
6	L-191	7	2.0:1.0	1.5
7	L-191	6	1.6:1.0	1.5
8	D-191	7	1.6:1.0	4
9	192	7	1.5:1.0	2
10	192	6	1.5:1.0	2
11	193	Unbuffered	1.7:1.0	2
12	193	7	1.7:1.0	5

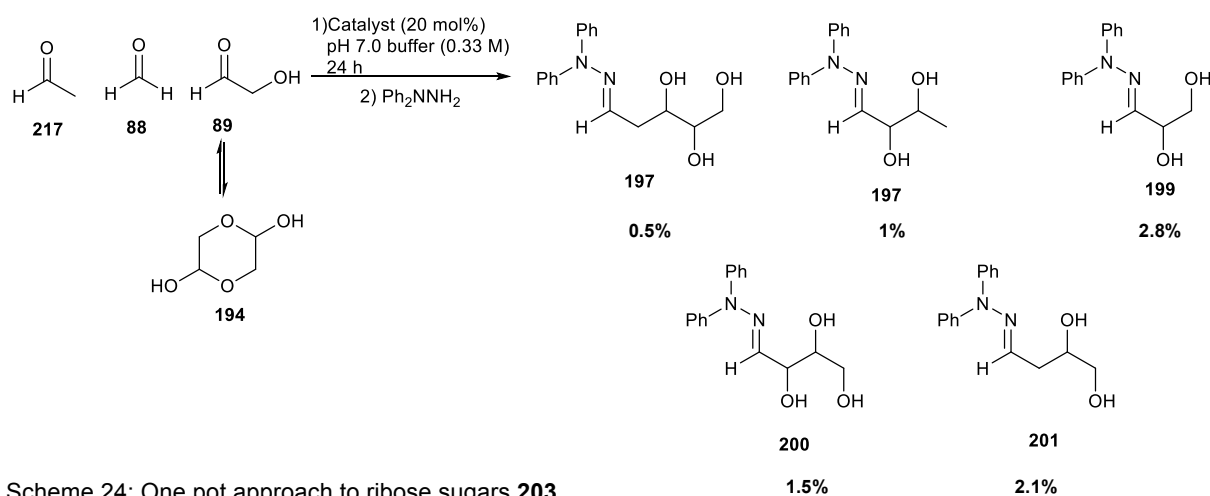
After showing that amino nitriles, **192** and **193**, can promote the D-deoxyribose-forming aldol reaction, the next challenge completing the prebiotic synthesis of 2-deoxy-D-ribose **186** from interstellar molecules, glycolaldehyde **89** and formaldehyde **88**, was attempted as it is postulated that these essential building blocks could be present in space.^{140–142} Using L-valine nitrile **193** as a catalyst, D-glyceraldehyde was successfully synthesised from glyceraldehyde dimer and 1

equivalent of formaldehyde at pH 7 (Scheme 23). Again to help analyse the product, 2,4-dinitrophenyl hydrazine was used as a trap.



Scheme 23: Formation of D-glyceraldehyde in pH 7.0 buffer, concentration of 0.33 M with respect to glycolaldehyde

With the ability to synthesise both D-glyceraldehyde 2-deoxy-D-ribose separately a one-pot approach from the three interstellar building blocks, formaldehyde, acetaldehyde and glycolaldehyde was attempted (Scheme 24). In this work both amino esters and amino nitriles were explored as catalysts. The results of the one pot approach showed that amino nitriles did catalyse the formation of trioses and tetroses (**197-200**) but not the formation of 2-deoxy-D-ribose (**197**). However, the amino ester (L-**190**) did synthesise 2-deoxy-D-ribose (**186**) over 2-deoxythreopentose (**187**).



Scheme 24: One pot approach to ribose sugars **203**

These specific reactions and catalysts are important because self-condensation aldol products such as 2-deoxy-D-ribose (**193**), which make up the sugar phosphate backbone in DNA, require specific chirality. In summary, therefore it is

possible to synthesise key amino acids and sugars in plausible prebiotic approaches using a range of methodologies

1.9 LMWGs as a catalytic media for prebiotic chemistry

As discussed in section 1.4, catalysis can take place using low molecular weight gels. Although this is dominated by organogels there are some examples of hydrogels used for catalysis.²⁹ It is also known that simple amino acids can catalyse aldol condensation reactions, and we can hypothesise that a protocell could be gel-like. As a result we can begin to ask the question “Can amino acids or simple peptides be used to create a catalytic hydrogel, to mimic a protocell?”

One relatively unstudied approach to the synthesis of a protocell, prior to the evolution of membranes, is the formation of a gel-like structure, which could arise from simple prebiotically available molecules like amino acids. Low molecular weight supramolecular gels are ideal for this because they are highly porous solvated materials and may have provided an appropriate medium for the organisation of simple components which could constitute early life; even if significantly more simplistic.

As discussed in chapter 1 section 1.3, Escuder developed self-assembled peptide hydrogels.^{42,143} The short peptides were shown to form fibrillar networks, hydrogels and were catalytically active in their self-assembled form for the aldol condensation of cyclohexanone and 4-nitrobenzaldehyde. Escuder saw the potential of this tri-peptide hydrogel (**55** or **56**) to be able to mimic a primitive cell. As a result explored further bio-inspired aldol condensation reactions (Scheme 19) to yield carbohydrate derivatives of prebiotic importance; threose and erythrose.^{121,144}

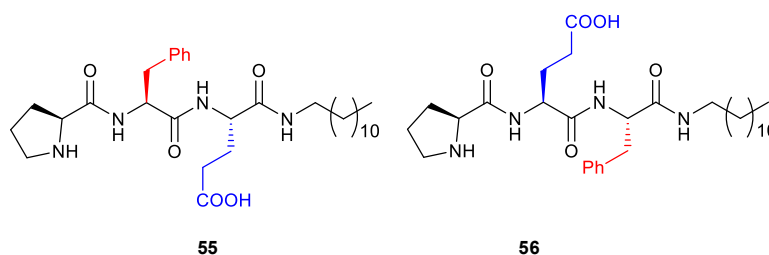
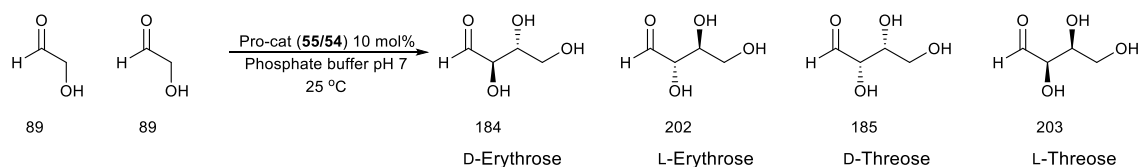
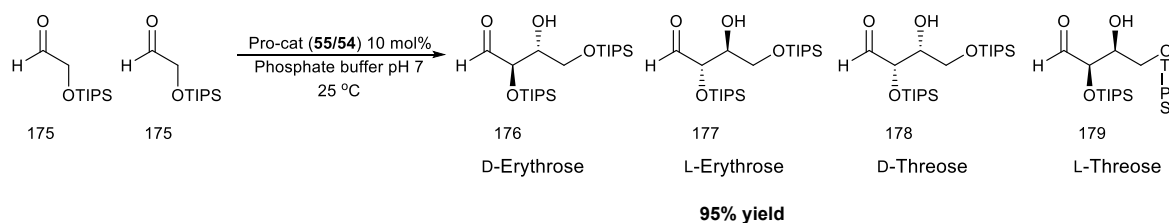


Figure 46: Short lipophilic peptide hydrogelator



Scheme 25: Aldol condensation of glycolaldehyde

Unfortunately, unprotected glycolaldehyde did not react in the presence of either self-assembled **54** or **55**. However, using TIPS-protected glycolaldehyde (Scheme 26) as described by Clarke *et al.*¹³⁸ resulted in the formation of a mixture (Figure 47) of the aldol product and the trimeric acetal.⁴⁸



Scheme 26: Aldol condensation of TIPS-protected glycolaldehyde

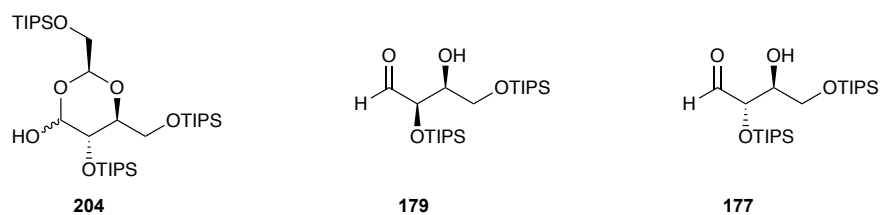
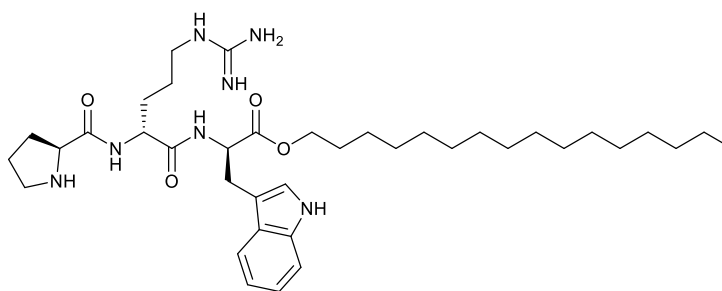


Figure 47: Products observed in the dimerization of TIPS protected glycolaldehyde

The work outlined by Escuder is of significance in prebiotic chemistry especially when considering a catalytic protocell. It demonstrated that established prebiotic catalysis can be introduced into LMWGs.

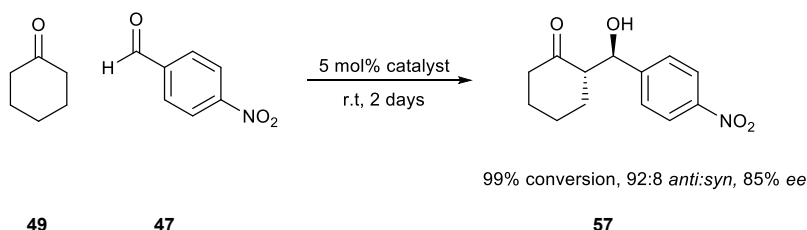
Recently, the self-assembly of lipopeptides in water has also been investigated by Alves and co-workers.¹⁴⁵ The tripeptide containing L-proline, L-arginine and L-tryptophan (Figure 48: Structure of the lipopeptide) where the proline residue is the catalytic site. To this tripeptide sequence C₁₆ hydrocarbon chain is added, making the molecule surfactant-like. It was found that the lipopeptide molecules self-assembled to form spherical micelles with a diameter of about 6 nm at a cmc of 0.19 mM. In addition the amphiphilic nature of the peptide allowed aldol condensation reactions to be performed in water with excellent yields >99% as

well as excellent diastereoselectivities (92:8) and enantioselectivities (85%) (Scheme 27).



205

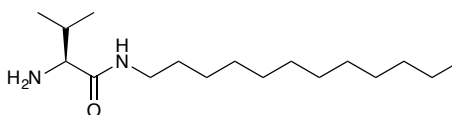
Figure 48: Structure of the lipopeptide



Scheme 27: Aldol condensation of 4-nitrobenzaldehyde and cyclohexanone with tripeptide

Interestingly, only when self-assembled structures were present, were these results observed. As mentioned earlier, vesicles/micelles could also be potential protocell structures. This is therefore exciting in the field of prebiotic chemistry and suggests another potential path to the design of a protocell.

In the Clarke research group, a simplified amino acid amide hydrogelator (**206**) (Figure 49) was recently developed.¹⁴⁶ The amino acid amide gelator is similar to those synthesised by Escuder, however, it is more prebiotic as it contains only a long carbon chain and a valine amino acid head group which could enable enamine based catalysis. This is a similar structure to fatty acids which could form membrane or bi-layer structure required for a cell like structure.



206

Figure 49: Valine amide hydrogelator

1.10 Conclusions and project aims

This literature review has highlighted some of the research that has taken place in organocatalysis. Amino acids have been shown to overcome the challenge of performing enamine catalysis in water. This work has been successful in terms of high yields and good selectivities. In addition to solution phase organocatalysis, catalysis using supramolecular structures such as gels has been discussed. This area of research is fairly new but is showing promising result with a wide variety of applications, with such gels having the potential to be used in biological systems or to mimic, in a simple way, biological environments such as protocells.

The review also explored how organocatalysis using amino acids and supramolecular structures can be linked to prebiotic chemistry. This section of the review discussed recent research into the origins of amino acids, sugars and protocell mimics. Many theories have been put forward to explain the origins of amino acids some of these include meteorite bombardment, electric discharge experiments and photoredox chemistry. There has also been a considerable amount of research into the formation of sugars. The most popular theories of the origins of sugars are based upon the formose reaction. Several groups have shown that simple sugars such as threose and erythrose as well as pentose sugars can be synthesised by amino acids and prebiotically relevant amino esters and nitriles. The area of research in prebiotic chemistry has also expanded into supramolecular chemistry. Supramolecular structures such as vesicles and gels have been hypothesised to be plausible cell-like mimics. As a result many research groups have studied the origins of lipids required for the formation of vesicles as well as utilising the knowledge of amino acids as organocatalysts to synthesise simple peptides which form hydrogels and catalyses simple aldol condensation reactions. However of these supramolecular structures simple hydrogels have not been shown to synthesis prebiotically relevant sugars.

The main aims of this research project were to:

- i) Synthesis a family of amino acid amides, of potential prebiotic origin, to be tested for their ability to form gels and be catalytically proficient.
- ii) Synthesise erythrose and threose in a potential prebiotic supramolecular environment or "protocell".
- iii) Progress the potential prebiotic environment to the formation of phosphorylated sugars.

Building on the work of Steer, it was proposed to synthesise some amino acid amides (Figure 50) and test their gelation potential. The key target was to explore their potential in prebiotically relevant reactions. It was reasoned that model aldol reactions (Scheme 28) would be useful in assessing catalytic potential.

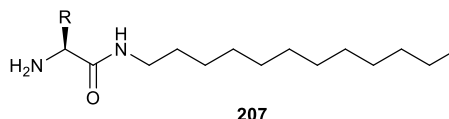
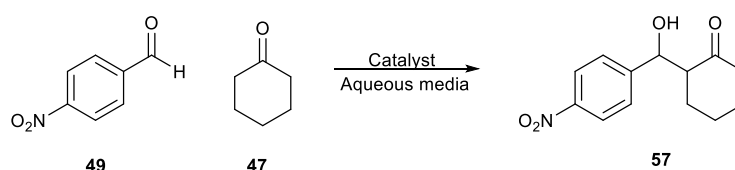
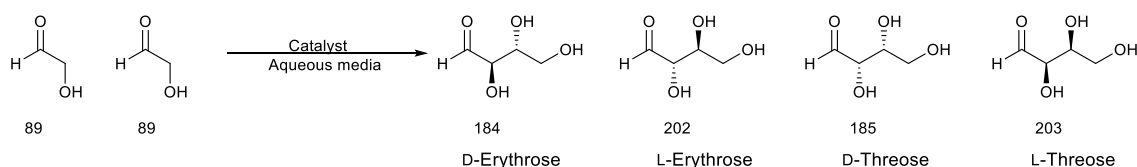


Figure 50: Proposed structure of amino acid amide

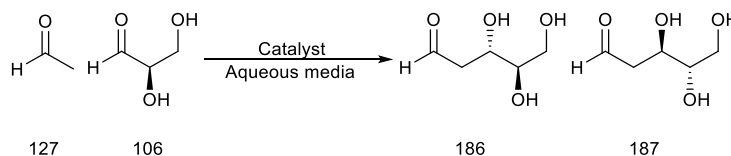


Scheme 28: Model aldol condensation reaction of 4-nitrobenzaldehyde (**49**) and cyclohexanone (**47**)

It was then intended that more prebiotically relevant aldol reactions such as the dimerization of glycolaldehyde (**89**) for the formation of threose (**185-203**) and erythrose (**184-202**) (Scheme 29), and also the aldol condensation of acetaldehyde (**127**) and D-glyceraldehyde (**106**) for the formation of ribose sugars (Scheme 30) were to be studied.



Scheme 29: Dimerization of glycolaldehyde



Scheme 30: Aldol condensation of acetaldehyde (**127**) and D-glyceraldehyde (**106**)

In this way, the potential of simple and minimal gelation systems of potentially prebiotic reactions to operate in catalytic processes was to be explored. It was reasoned that key challenges would be:

- Maintaining gel integrity during catalysis

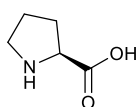
- Achieving good levels of conversion in heterogeneous reaction systems
- Demonstrating selectivity in terms of product synthesis for diastereomeric ratio and enantioselectivity

During this project the goal was to address and find solutions for these problems.

2.0 Amino acid amides as catalysts and hydrogelators

2.1 Aims:

Amino acids are known to have been present on the early Earth, and as explained in Chapter 1, it is also known that amino acids, such as L-proline (**41**) (Figure 51), can catalyse aldol condensation reactions and influence the chirality of reaction products. Amino acids such as L-proline (**41**) have the ability to arrange reagents into a six-membered transition states as shown in scheme 4, Chapter 1.^{126,147} It is this transition state which dictates the stereochemistry of the product. There has been a lot of work on amino acid based catalysis using L-proline in the solution phase in both organic solvents and water.^{128,138,147-149} This has begun to unlock the potential of using a catalyst such as L-proline in prebiotic chemistry. We therefore proposed expanding the use of amino acids by synthesising LMWGs containing L-valine (**208**), L-serine (**119**) or L-glutamine (**145**) (Figure 52), which may have been present on primordial Earth,^{57,100} to combine prebiotic catalysis with soft gel materials. These amino acids were selected as they are the natural form of amino acid (L) and have different side chains, which could play an important role either as catalysts and/or in modifying gelation.



41

Figure 51: L-Proline

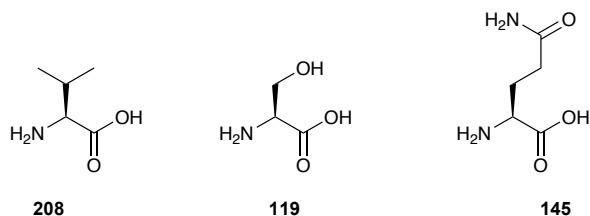


Figure 52: L-Valine (**208**), L-serine (**119**) and L-glutamine (**145**)

We proposed to convert these amino acids into amides which could be tested for catalytic proficiency in a model aldol condensation reaction in a prebiotic environment and have the potential to self-assemble into a sample spanning network. The data collected would give insight into selectivity and efficiency of these systems and whether they are plausible pre-biotic catalysts. This would further the area of enamine-based catalysis with implications for prebiotic chemistry, using molecules that also have the ability to self-assemble into supramolecular structures. It was hoped that supramolecular assembly may influence the catalytic outcome both in terms of diastereoselectivity and enantioselectivity. In particular, we were interested in ultimately developing systems that operate in water; the most likely prebiotic solvent.

Three amino acid amides were selected for synthesis; L-valine amide (**206**), L-serine amide and L-glutamine amide (**208**) (Figure 53). L-Valine amide (**206**) was chosen as it has a non-polar aliphatic side chain. In addition, previous work in the Clarke group¹⁴⁶ suggested that L-valine amide (**206**) with a 12 carbon chain, was a hydrogelator but lacked structural integrity when performing catalysis in the gel phase. The other two amino acid amides were chosen as they have different side chains, that of serine is often found in many important enzyme active sites and glutamine (**145**) has a more polar side chain with hydrogen bonding potential. It is reasoned that these features could have an impact on catalytic ability and/or supramolecular assembly. In addition the same chain length 12 carbon chain was retained as in valine amide (**206**) the 12 carbon chain allowed a hydrogel to form.

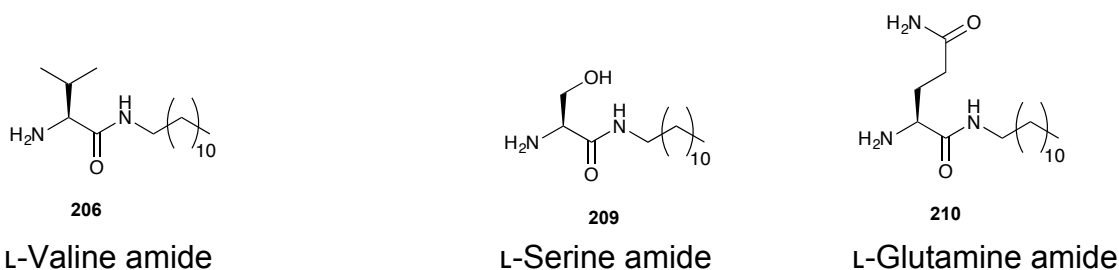
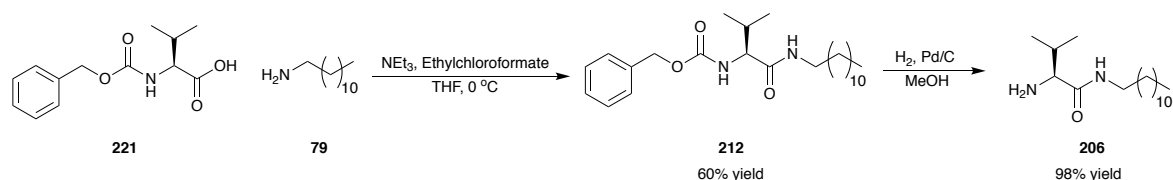


Figure 53: Amino acid amide targets to be synthesised

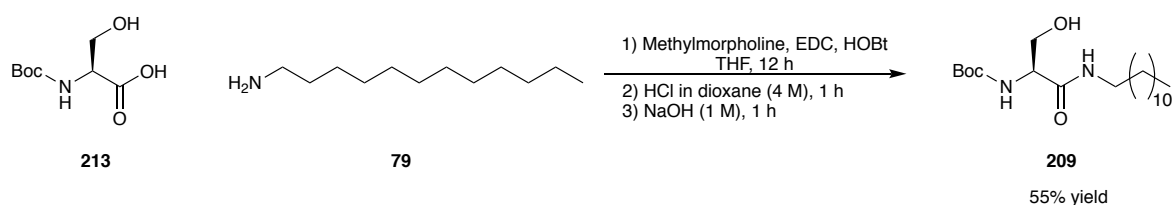
2.2 Results and discussion

2.2.1 Synthesis of valine (206), serine (209) and glutamine amide (210)

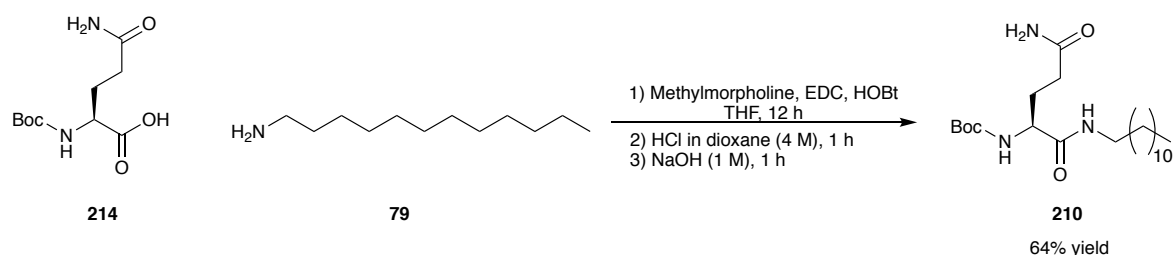
The synthesis of L-valine amide (**206**) was carried out by Andrew Steer, a PhD student in the Clarke group (Scheme 31).¹⁴⁶ The synthesis involved the amide coupling of L-valine (**208**) to dodecylamine (**79**) followed by hydrogenation of the Cbz group. The synthesis of serine amide (**209**) and glutamine amide (**210**) was performed as part of this thesis work and used a simple coupling reaction of dodecylamine and Boc-protected amino acid. Once coupled and purified by column chromatography (DCM: MeOH 90:10), the Boc protecting group was removed with 4 M HCl in dioxane. The final products were analysed by ¹H NMR and yielded white solids with a 55% yield for L-serine amide and a 64% yield for L-glutamine amide (**210**).



Scheme 31: Synthesis of L-valine amide (**206**)



Scheme 32: Synthesis of L-serine amide (**209**)



Scheme 33: Synthesis of L-glutamine amide (**210**)

Using the synthesis described in Scheme 32 and Scheme 33, both serine amide (**207**) and glutamine amide (**210**) were synthesised successfully. However, there were problems with being able to reproduce clean product due to solvent

occlusion and minor impurities. Optimisation of the coupling reactions will be described in a later chapter.

2.2.2 Solvent screening for valine (206), serine (209) and glutamine (210) amides for gelation:

A variety of solvent with different polarities were tested to determine the gelation potential of valine amide (206), serine amide (209) and glutamine amide (210). The initial outcome of this process was to simply observe whether or not a visual gel formed (Table 7). Relatively high concentrations of gelator valine amide (206), serine amide (209), and glutamine amide (210) (3 % wt/v) were tested to give a good chance of observing gelation (Figure 54). The results Table 7 in show that the amides form gels in different solvents. Valine amide (206) only gels in water and will not form a gel in organic solvents, whereas serine amide (209) and glutamine amide (210) form gels mainly in organic solvents.

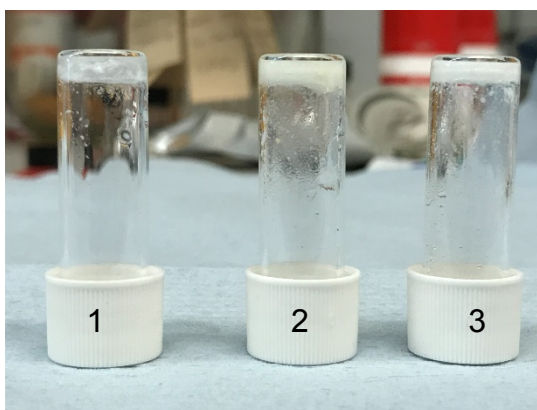


Figure 54: Hydrogel formed: 1= L-valine amide (206), 2= L-serine amide (209), 3= L-glutamine amide (210)

Table 7: Solvent screening for gelation with amides, 3 mg gelator in 0.1 mL solvent

Solvent	Hansen parameters			Did it gel?		
	δ_d	δ_p	δ_h	Valine amide (206)	Serine amide (209)	Glutamine amide (210)
Acetone	15.5	10.4	7	Clear solution	Clear solution	White precipitate
Acetonitrile	15.3	18	6.1	Clear solution	Yes opaque	Semi-gel
Chloroform	17.8	3.1	5.7	Clear solution	Clear solution	Clear solution
Cyclohexane	16.8	0	0.2	Clear solution	Yes, white gel	Yes, white gel
Diethyl ether	14.5	2.9	5.1	Clear solution	White precipitate	White precipitate
DMF	17.4	13.7	11.3	Clear solution	Clear solution	Clear solution
DMSO	18.4	16.4	10.2	Clear solution	Clear solution	Clear solution
Ethyl acetate	15.8	5.3	7.2	Clear solution	White precipitate	White precipitate
Methanol	15.1	12.3	22.3	Clear solution	Clear solution	Clear solution
THF	16.8	5.7	8	Clear solution	Clear solution	Semi-gel
Toluene	18	1.4	2	Clear solution	Yes, transparent	Semi-gel
Water	15.6	16	42.3	Yes, white gel (Fig 17)	Yes, white gel (Fig 17)	Yes, white gel not consistent (Fig 17)

Hansen parameters for solvents δ_d : Dispersion forces, δ_p : Polar forces, δ_h : Hydrogen bonding

The solvent screen results (Table 7) show that serine amide (**209**) and glutamine amide (**210**) are both hydrogelators and organogelators to some degree. In particular, serine amide forms gels in acetonitrile, cyclohexane and toluene, and glutamine amide (**210**) forms gels in cyclohexane and THF. We suggest that the greater water solubility of the OH side chain of serine enhances the aqueous solubility, therefore the gelator is dispersed more evenly though the solution and aggregates are not visible unlike the valine system (Figure 54). It is clear that as the side chain becomes more polar (serine amide (**209**) and glutamine amide (**210**)), the solubility in organic solvent decreases – especially so for the less polar solvent. This provides these two compounds with greater capacity to form organogels than valine amide (**206**), which with an apolar side chain is much more soluble in organic solvents and hence less likely to self-assemble. As a polar system, we note that glutamine amide (**210**) did not always form consistent gels in water. This is probably because it is more soluble in this medium, somewhat limiting its ability to assemble into a ‘solid-like’ network.

The opacity of the gels that formed is most likely due to the morphology of the aggregates. Opaque gels are more crystalline and microscale whereas, transparent gels are more nanoscale in terms of morphology.^{150,151} This reflects the ability of the self-assembled aggregates to scatter light, which depends on their size.

Furthermore, the formation of a gel itself is delicate. There needs to be a balance in the gelator molecule’s solubility and insolubility in the solvent of interest. If the gelator is too soluble it will simply dissolve and if it is too insoluble it will just undergo uncontrolled precipitation. It can be predicted which solvents will be gelled by a set of three parameters known as Hansen parameters¹⁵². The Hansen parameters are:

- Dispersion parameter, δ_d
- Polarity parameter, δ_p
- Hydrogen bonding parameter, δ_h

These three parameters can be treated as co-ordinates for a point in three dimensions also known as ‘Hansen space’. The closer two molecules are in this three-dimensional space, the more likely they are to dissolve into each other. For gelation, it is usually observed that there is a zone in Hansen space in which the

molecule is neither too soluble nor too insoluble and for which gelation can be expected (Figure 55).

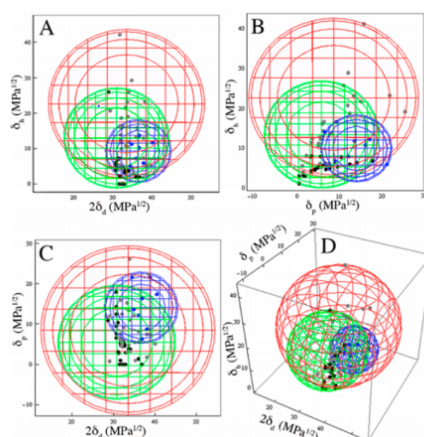


Figure 55: Two-dimensional projection (A-C) and a 3D rendering (D) of the Hansen space using minimal enclosing spheres and appearance at the CGC. The blue sphere encloses DBS solutions, the green sphere encloses opaque gels, and the red sphere encloses clear gels¹⁵²

Hansen solubility parameters¹⁵², in theory, the prediction of the solubility of a material in solvents by looking at three parameters of the solvent, dispersion force (δ_d) polar forces (δ_p) and hydrogen bonding (δ_h). These parameters were used to determine if more detailed conclusions could be drawn about the solvents in which gelation occurred. Firstly the Hansen parameters were considered individually to see if there was a common theme with one parameter then 3-D plots (Figure 56, Figure 57 and Figure 58) were produced where all parameters of the solvents could be considered and simultaneously cross-referenced with the ability to form a gel. However, there was no clear pattern to explain why gelation occurred in some solvents but not all in others. This lack of correlation is very apparent in the 3-D plot for valine (**206**) and serine amide (**209**) solvent screen (Figure 56 and Figure 57) where there are very few points where gels occur this makes it hard to understand any patterns as to which solvents form gels and which do not.

The solvent screen for glutamine amide (**210**) however, has a broader variety of solvents, which form gels, partial gels and no gels (Figure 58). Glutamine amide (**210**) formed organogels in cyclohexane. Using the Hansen parameters of the solvent, we might have predicted that chloroform or toluene would also form gels too, as these two solvents have similar parameters to cyclohexane. However, this was not the case no gel formed in chloroform but a semi-gel was observed in toluene. This could suggest that toluene is at the borders of the gelation region for

solvents of this type, where there is a low δ_h , δ_p and high δ_d . Equally acetonitrile only forms semi gels this again implies that we are at the edge of another gelation border. However it is important to note that although water formed gels it was not consistent.

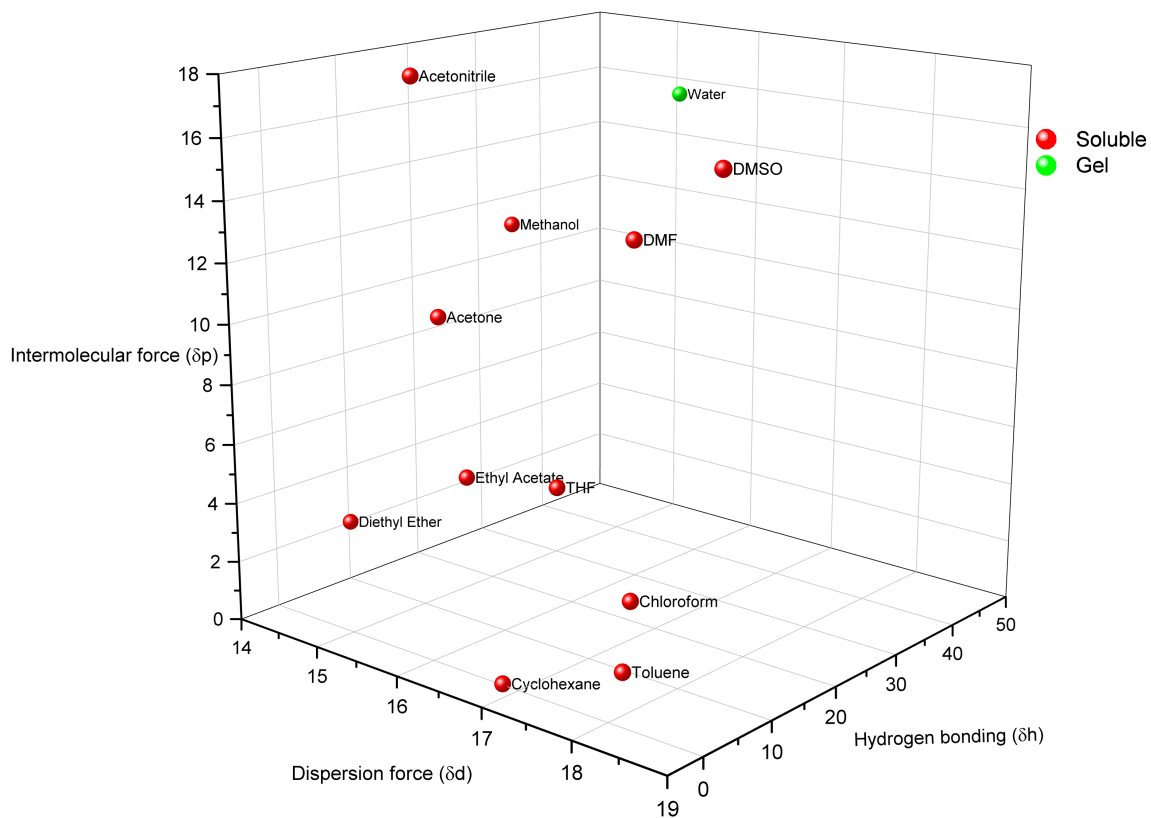


Figure 56: Valine amide (206) 3-D Hansen parameter plot

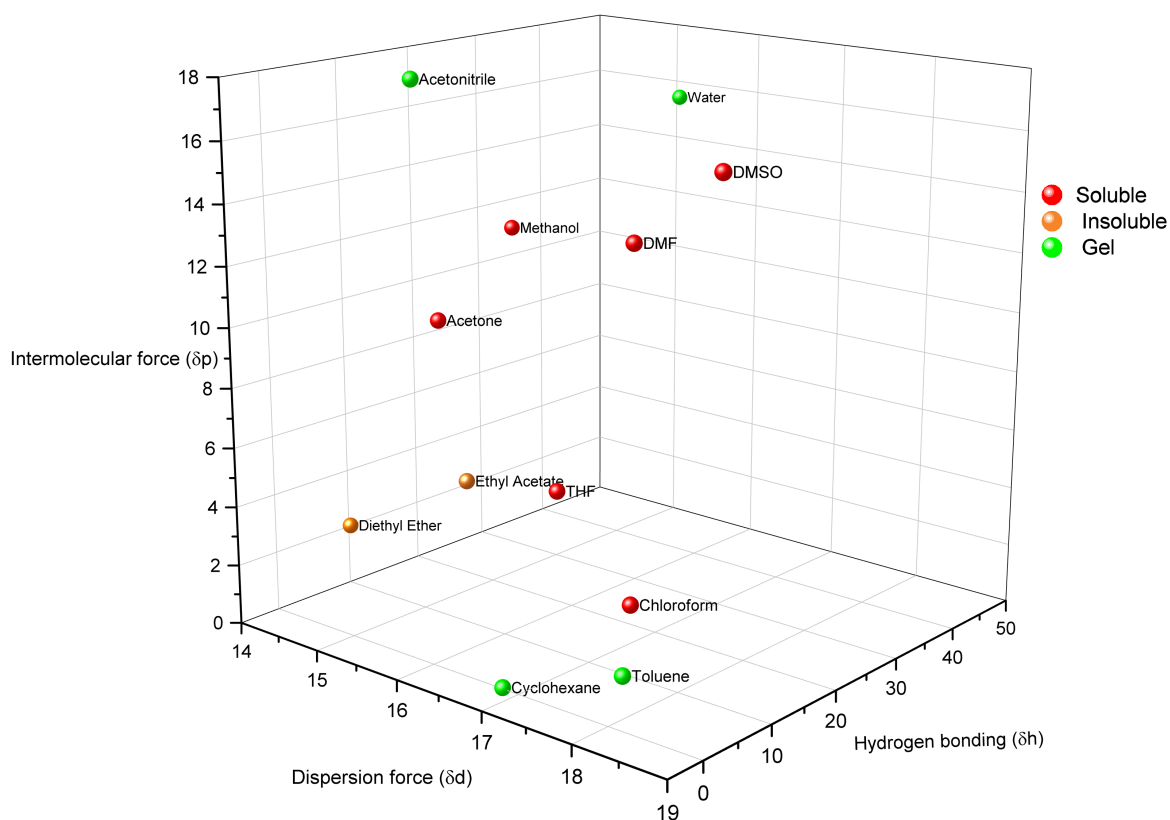


Figure 57: Serine amide (209) 3-D Hansen parameter plot

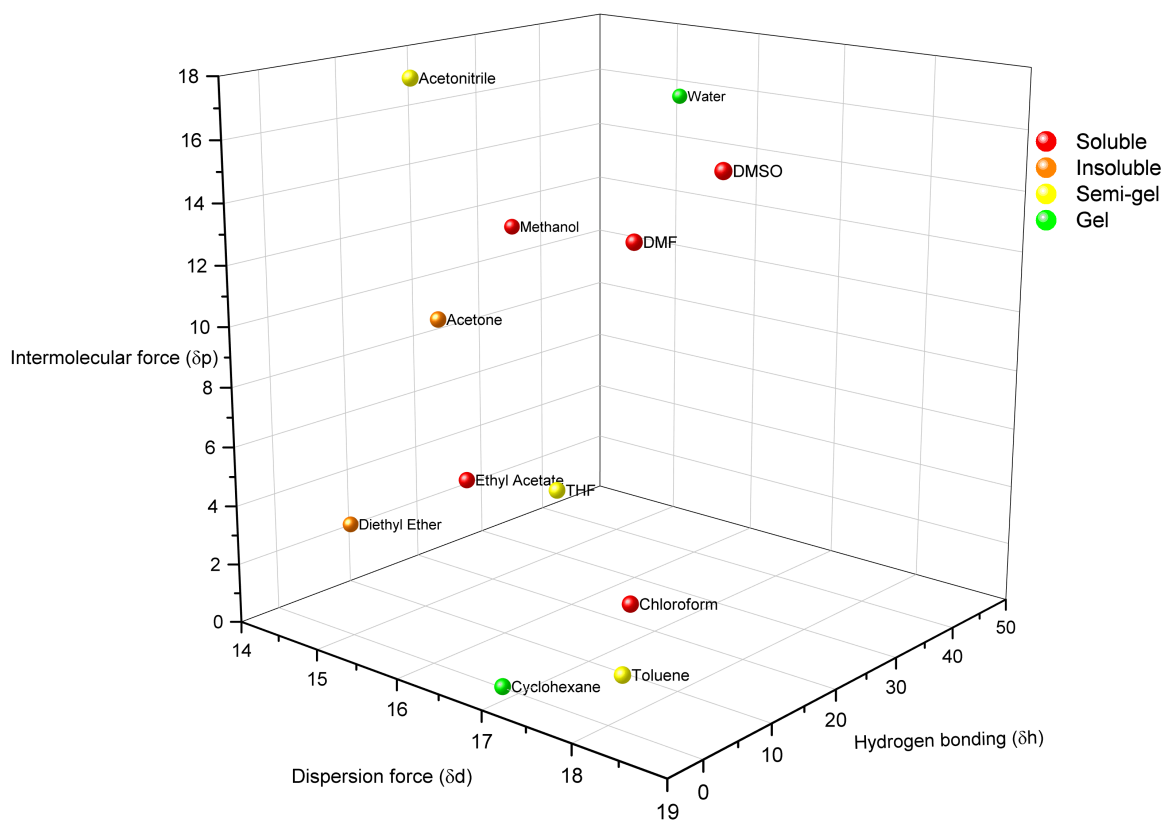
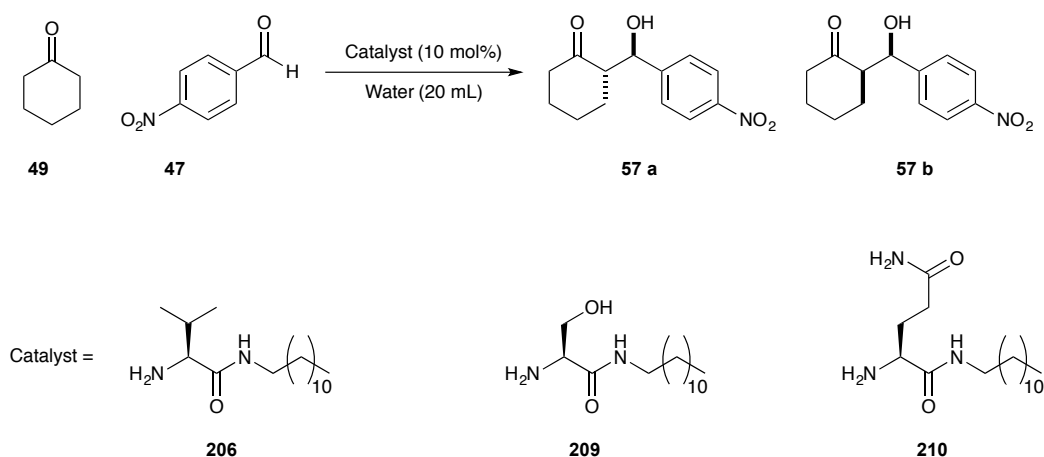


Figure 58: Glutamine amide (210) 3-D Hansen parameter plot

2.2.3 Simple catalysis of 4-nitrobenzaldehyde (**47**) and cyclohexanone (**49**) in a direct aldol reaction:

Although the gelation was solvent limited and inconsistent, the catalytic ability of the compounds was investigated. These amino acid amides, have the potential to not only form sample-spanning networks, but also to be catalytic by virtue of the amine terminus allowing enamine based catalysis. Therefore, each amino acid amide was tested for catalysis in the aldol condensation of 4-nitrobenzaldehyde (**47**) and cyclohexanone (**49**) (Scheme 34). This reaction was chosen not because it is prebiotic, but because the components have good reactivity and the inclusion of an aromatic ring ensures the reaction is easy to monitor. Although we are ultimately interested in performing catalytic reactions on the hydrogel we wanted to initially perform the reaction in the solution phase in water, as this is a medium of interest. Due to the nature of these reagents, the reaction itself is heterogeneous.



Scheme 34: Direct Aldol condensation of 4-nitrobenzaldehyde (**47**) and cyclohexanone (**49**) in water catalysed by simple amino acid amides

A solution of 4-nitrobenzaldehyde (**47**) (1 eq) in cyclohexanone (**49**) (10 eq) was added to an aqueous solution of the amide (0.1 eq) in water (20 mL) and a heterogeneous mixture formed. The reaction was left stirring for 24 h, 48 h and 72 h. In reality each time-point was a separate reaction, because the heterogeneous nature of the reaction meant that aliquot sampling did not give accurate representation of reaction progress. After the allotted time, the reaction mixture was extracted with dichloromethane (DCM) then the solvent was removed in *vacuo*. ^1H NMR analysis of the crude product in deuterated chloroform (CDCl_3)

was performed to calculate conversion and diastereomeric ratio (d.r) (Figure 59 and Figure 60). The result of these reactions are shown in Table 9 and Table 10.

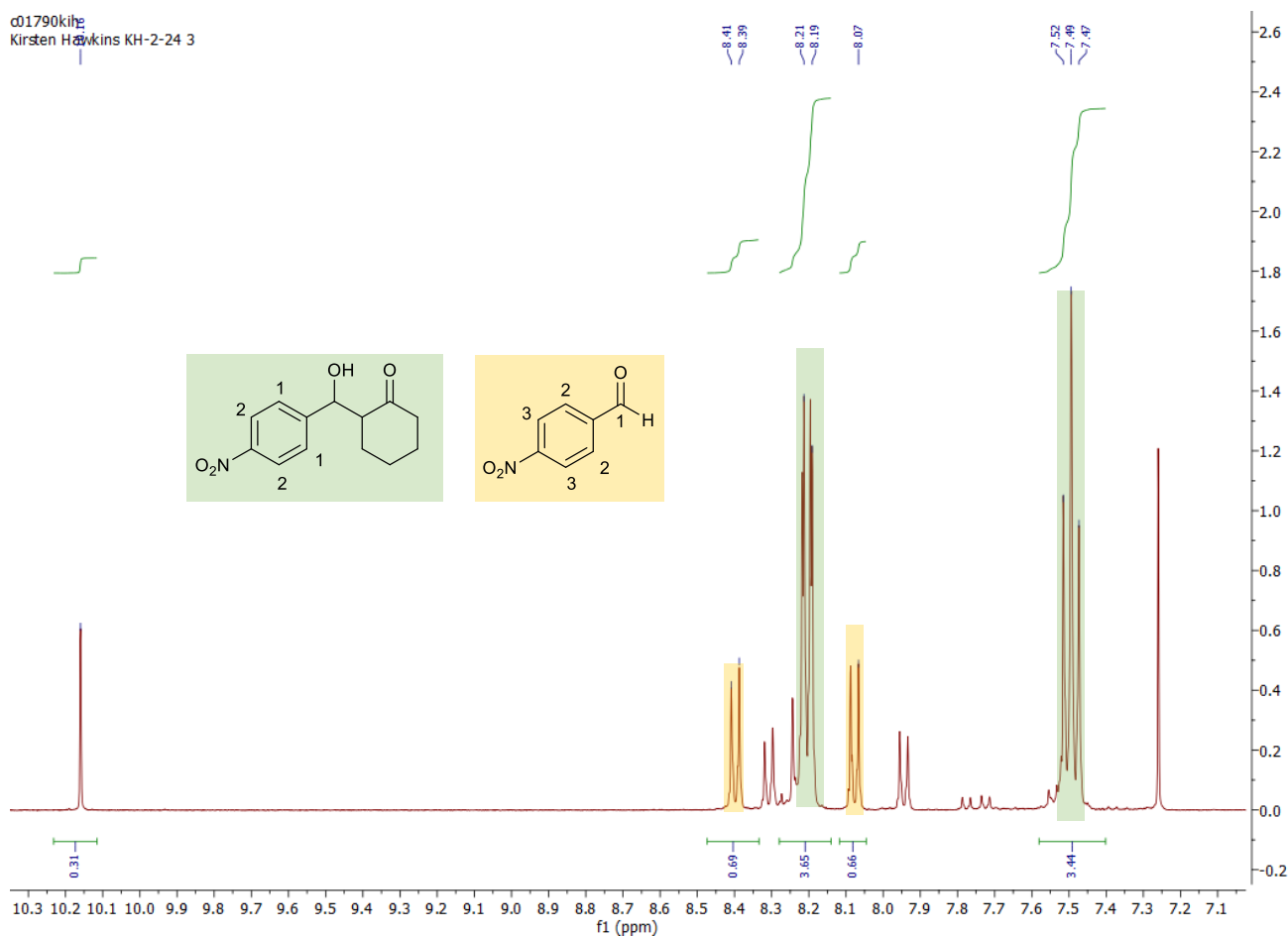
To determine percentage conversion from starting material the total integration of the aromatic protons of 4-nitrobenzaldehyde was calculated. The signal which correspond to the starting material are the singlet at 10.16 ppm, and the two doublets at 8.41 ppm and 8.07 ppm respectively. The aromatic signals which correspond to the product are the two overlapping doublets at 8.21 ppm and 8.20 ppm, as well as the overlapping doublets at 7.41 ppm 7.48 ppm. These peaks in the product overlaps due to the two diastereomers produced in the reaction.

$$\text{total intergration of aromatic protons} = 0.69 + 3.65 + 0.66 + 3.44 = 8.44$$

Then the integrations of aromatic product peaks were totalled and divided by the total integration of aromatic protons

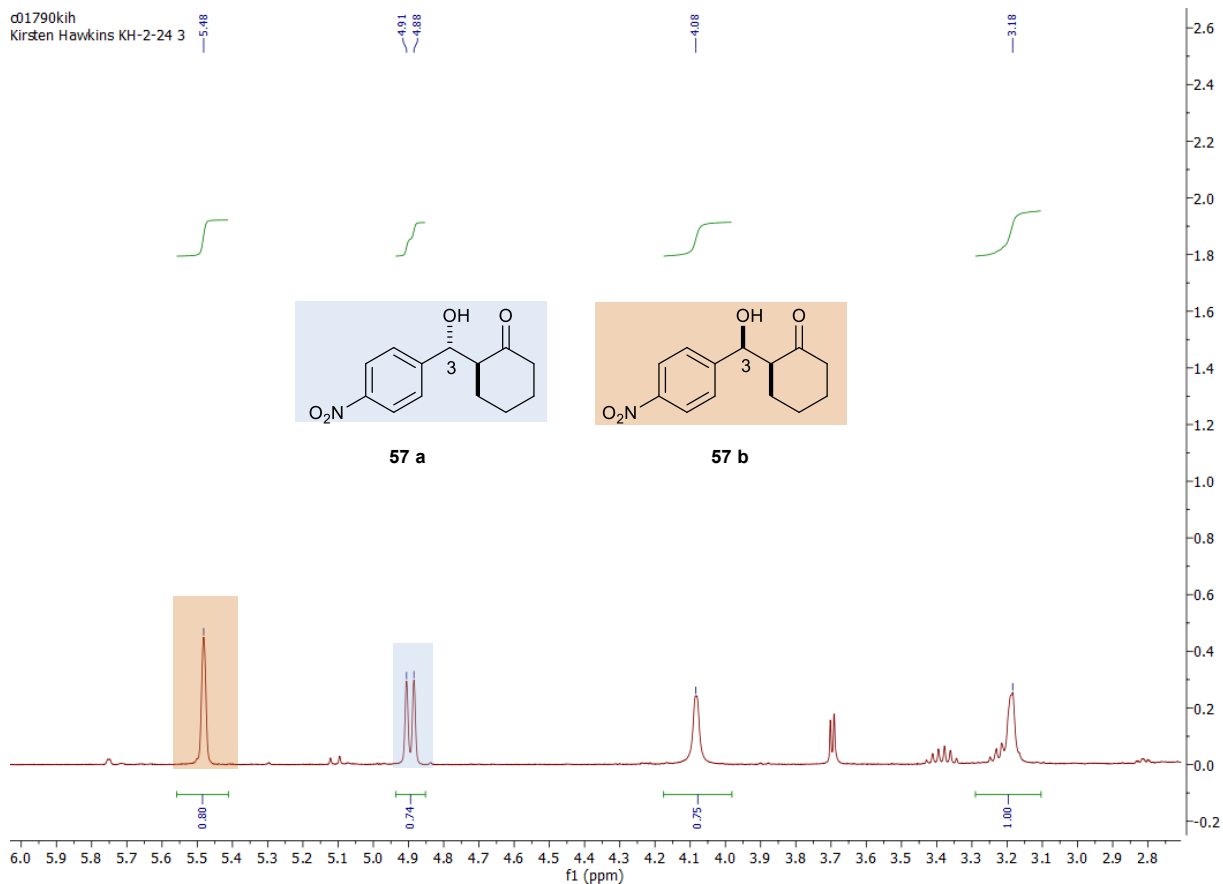
$$\frac{3.56 + 3.44}{8.44} \times 100 = 83\%$$

To determine the *syn: anti* Diastereomeric ratio by ¹H NMR the signals in the lower end of the spectrum are required. For the *syn* product there are two signals a broad singlet at 5.49 ppm and a second broad singlet at 3.18 ppm. For the *anti*-product there are also two signals a double doublet at 4.89 ppm and a broad singlet at 4.08 ppm. By using the integrals of the distinct signals at 5.49 ppm and 4.89 ppm the diastereomeric ration can be determined. It is also important to note that there were also aromatic peaks at 8.3 and 7.9 ppm the origin of these signals will be discussed in detail later on. However in results reported the integration of these peaks was also taken into consideration when determining the conversion.



Starting material key peak of 4-nitrobenzaldehyde (**49**) ¹H NMR (400 MHz, CDCl₃): 10.16 (1H, s, H₁), 8.41 (2H, d, *J* = 8.6 Hz, H₃), 8.07 (2H, d, *J* = 8.6 Hz, H₂) Product key peaks ¹H NMR (400 MHz, CDCl₃): 8.21 (1H, d, *J*=8.8 Hz, H₂), 8.20 (1H, d, *J* = 8.9 Hz, H₂) 7.41 (1H, d, *J*=8.5 Hz, H₁) 7.48 (1H, d, *J* = 8.4 Hz, H₁)

Figure 59: ¹H NMR of crude reaction material for the aldol condensation of 4-nitrobenzaldehyde (**47**) and cyclohexanone (**49**) in CDCl₃. Showing the aromatic region only used for conversion calculations



Syn product key peaks (**57 b**) ^1H NMR (400 MHz, CDCl_3): 5.49 (1 H, br. s, H_3), 3.18 (1 H, br. s, OH), Anti product (**57 a**) key peaks ^1H NMR (400 MHz, CDCl_3): 4.89 (1H, dd, $J=3.2$ Hz, 8.35 Hz, H_3), 4.08 (1 H, d, $J=3.2$ Hz, OH)

Figure 60: ^1H NMR of crude reaction material for the aldol condensation of 4-nitrobenzaldehyde (**47**) and cyclohexanone (**49**) in CDCl_3 . Showing the aliphatic region only used for diastereoselectivity calculations

Table 8 Valine amide (**206**) catalysed aldol condensation of 4-nitrobenzaldehyde (**47**) and cyclohexanone (**49**) in water

Solvent	Time h	Conversion %	Crude NMR d.r anti:syn	Gel?
Water	24	34 (± 7)	1.23:1.00 (± 0.12)	No
Water	48	42 (± 10)	1.28:1.00 (± 0.08)	No
Water	72	82 (± 8)	0.96:1.00 (± 0.02)	No

Table 9: Serine amide (**209**) catalysed aldol condensation of 4-nitrobenzaldehyde (**47**) and cyclohexanone (**49**) in water

Solvent	Time h	Conversion %	Crude NMR d.r anti:syn	Gel?
Water	24	12 (± 0.4)	1.21:1.00 (± 0.02)	No
Water	48	30 (± 9)	1.68:1.00 (± 0.28)	No
Water	72	50 (± 7)	1.86:1.00 (± 0.17)	No

Table 10: Glutamine amide (**210**) catalysed aldol condensation of 4-nitrobenzaldehyde (**47**) and cyclohexanone (**49**) in water

Solvent	Time h	Conversion %	Crude NMR d.r anti:syn	Gel?
Water	24	38 (± 8)	2.14:1.0 (± 0.10)	In-situ
Water	48	87 (± 17)	1.44:1.00 (± 0.24)	In-situ
Water	72	98 (± 0.9)	1.30:1.00 (± 0.32)	In-situ

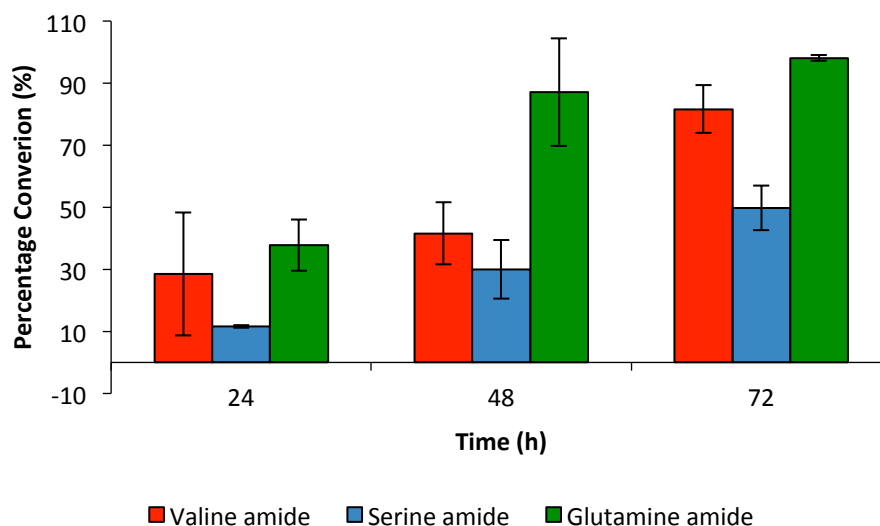


Figure 61: Graph showing the percentage of conversion at time intervals of 24 h, 48 h and 72 h with different amino acid amides. Data reported here is an average of three experiments, error bars show the deviation in the data repeats

Figure 61 shows that at less than 48 h, the percentage conversions are low, however at 48 h and above, the rate of conversion to product starts to increase. There is a notable difference in percentage conversion depending upon the catalyst used. Serine amide (**209**) has the lowest conversion at both 48 h and 72 h ca. 30% and 50% respectively whereas glutamine amide (**210**) has a very high conversion ca. 87% and 98% respectively and valine amide (**206**) is intermediate ca. 41% and 81% respectively. One of the reasons for this could simply be the poor homogeneity of the reaction.

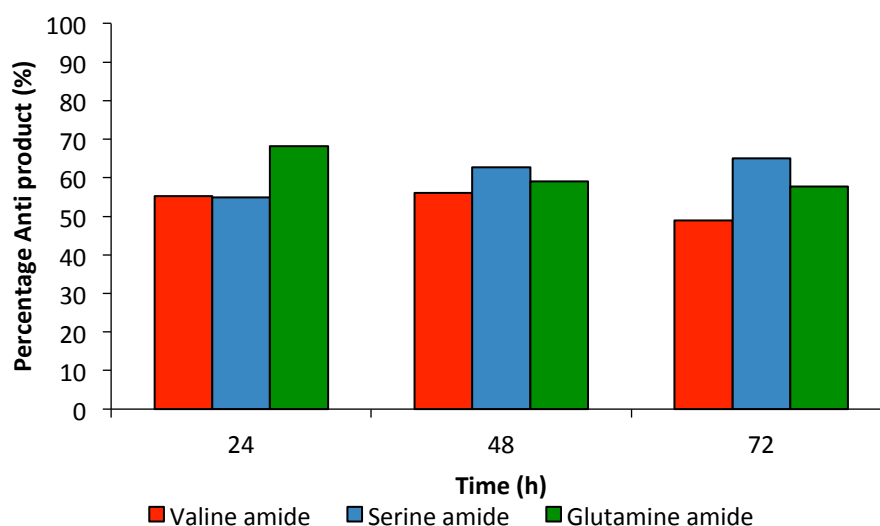


Figure 62: Graph showing percentage *anti* product for different catalysts

The graph in Figure 62, shows that the diastereoselectivity of the aldol product (taken as an average of three reactions) does not change with the amino acid amide used. However, the large variation associated with each reaction suggests that these amides are not particularly selective for this reaction when presented as an average. This is most likely a result of the heterogeneous nature of the reaction. There is limited stereoselectivity with all catalysts and as time increases there tends to be a loss in initial selectivity. This could potentially be due to retro-aldol reactions. Further NMR analysis indicates that there is also another aromatic product being formed (Figure 63). The nature of this will be discussed in later chapters.

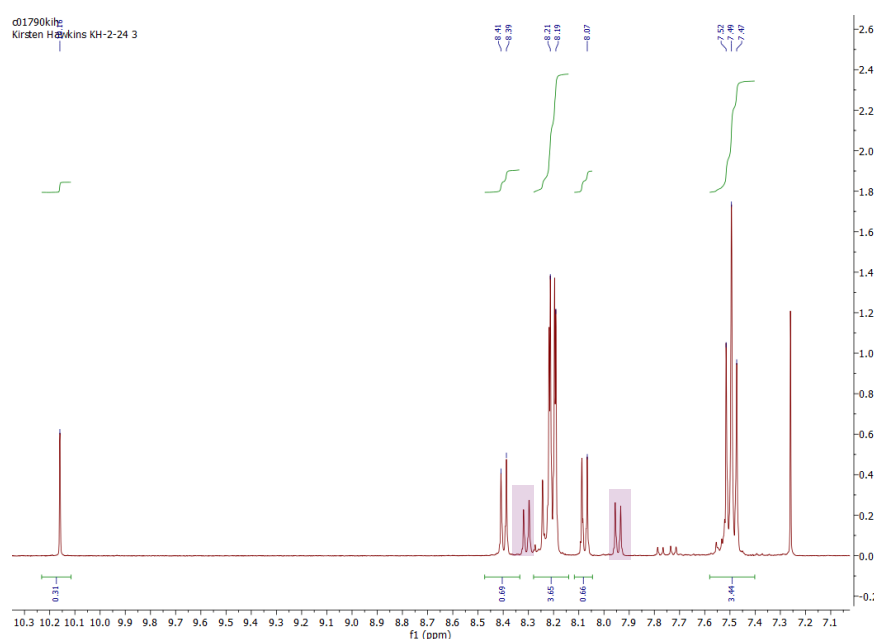


Figure 63: Suspected new compound formed in situ due to appearance of new aromatic peaks in ^1H NMR

Typically when using an organocatalyst such as L-proline there is selectivity for the anti-product as a result of the Zimmerman-Traxler like transition state (Figure 64).¹²⁶ However the results obtained here and the erratic nature of the data suggest that no such transition state is forming therefore any selectivity observed is due to facial attack, the homogeneity of the reaction is limiting selectivity or there is general base catalysis taking place.

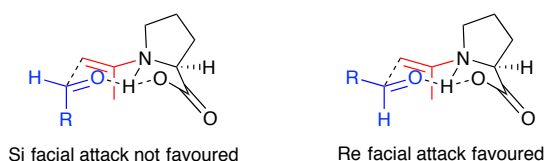
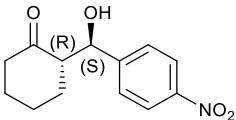
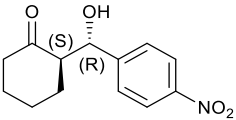
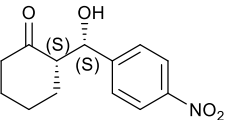
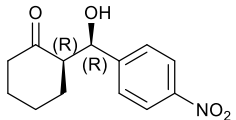


Figure 64: Zimmerman-Traxler like transition state of L-proline

In the aldol condensation of 4-nitrobenzaldehyde (**47**) and cyclohexanone (**49**) there are four possible isomers. We therefore used chiral HPLC analysis of the crude reaction mixture to understand the system further, and determine if there was any enantioselectivity within the *syn* and *anti*-products. A method reported by Rolando and co-workers was used.¹⁵³ In this method enantiomers were separated using an immobilised cellulose chiralpak column, IB, as the stationary phase and a solution of Hexane:IPA 97:3 was used for the mobile phase with a flow rate of 1 mL/min. The four isomers with their retention times reported are shown in Table 11.

Table 11: Retention times of enantiomers from HPLC traces reported by Rolando and co-workers¹⁵³

	<i>Anti</i> -major	<i>Anti</i> -minor	<i>Syn</i> major	<i>Syn</i> minor
Retention time (min)	28.8	34.8	23.6	26.7
				
	215	216	217	218

The conditions provided a clean separation of the 4 aldol stereoisomers. There is a shift between our retention times and the retention times reported in the literature. This is possibly due to column properties or the difference in the temperature of the HPLC instrument, however, the relative times were consistent. As a result we are able to assign the enantiomers to the peaks (Figure 65).

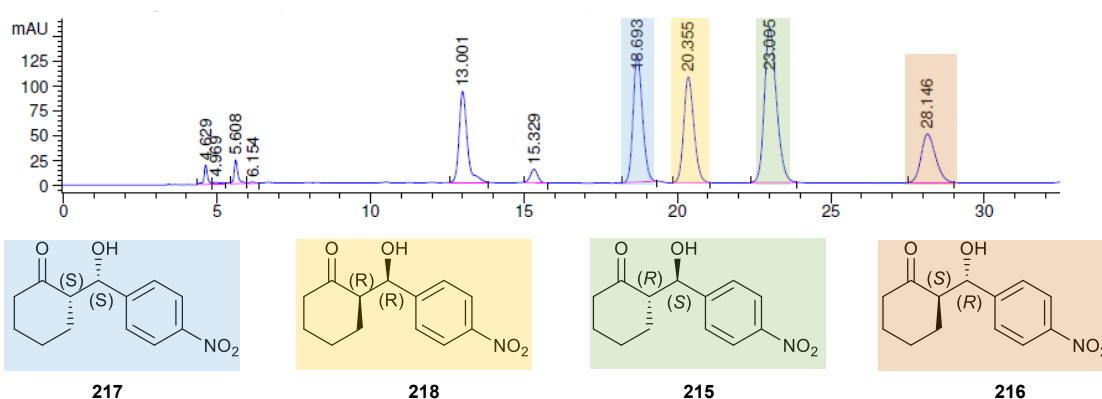


Figure 65: HPLC trace of crude aldol condensation of 4-nitrobenzaldehyde (**47**) and cyclohexanone (**49**). IB Chiral Pak, 1 mL/min, 97:3 Hexane.

However, the ee% obtained from the HPLC (Table 12 -Table 14) indicated limited enantio stereoselectivity with any of the catalysts (Figure 66).

Table 12: L-valine amide (**206**) catalysis HPLC ee%

Solvent	Time h	Crude HPLC ee%	In situ gel?
Water	72	Syn 10% Anti 4%	No
Water	72	Syn 13% Anti 60%	No
Water	72	Syn 6% Anti 9%	No

Table 13: L-serine amide (**209**) catalysed HPLC data

Solvent	Time h	Crude HPLC ee%	In situ gel?
Water	72	Syn 6% Anti 13%	No
Water	72	Syn 2% Anti 21%	No
Water	72	-	No

Table 14: L-glutamine amide (**210**) catalysis HPLC data

Solvent	Time h	Crude HPLC ee%	In situ gel?
Water	72	Syn 5% Anti 45%	Yes
Water	72	Syn 18% Anti 27%	Yes
Water	72	Syn 10% Anti 24%	Yes

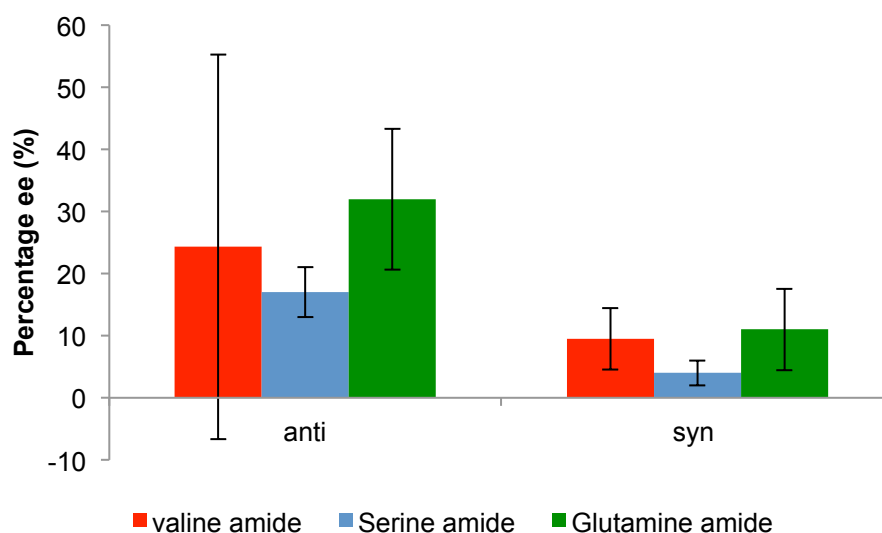
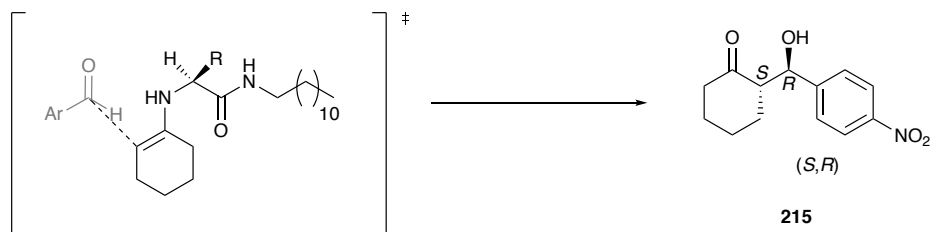


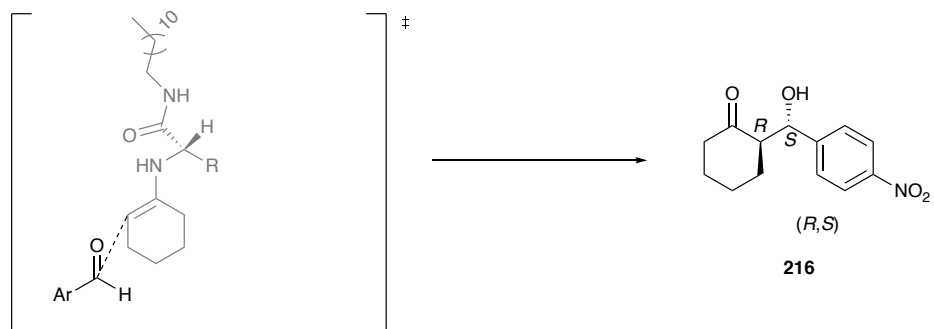
Figure 66: Graph showing HPLC ee% of crude material after 72 h with different catalysts

4-Nitrobenzaldehyde (**47**) is a non-chiral molecule, and as a result, attack of the Re face or Si face of the molecule is equally likely. The only factor that can determine the stereochemistry is the steric hindrance of the side chain of the amino acid amide assuming that the catalyst is intimately involved in directing the reaction. We therefore propose the transition states in Figure 67 and Figure 68 to account for any diastereoselectivity that we have observed.

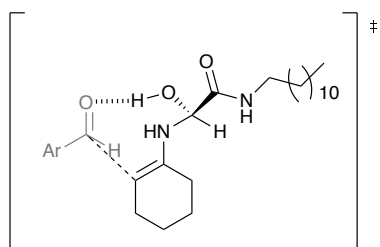
Much like when L-proline is used as a catalyst, in the aldol condensation reaction of 4-nitrobenzaldehyde (**47**) and cyclohexanone (**49**), an enamine intermediate is formed from the L-amino acid amide reacting with the ketone, cyclohexanone (**49**). Once the enamine has formed, facial attack on the aldehyde can occur. ¹H NMR data indicates that we are getting a slight increase in the *anti*-product over the *syn*-product however the diastereoselectivity is small. In addition enantioselectivity is also only minor. This indicates that we are going *via* a transition state where there is a minimal difference in energy of intermediates. We therefore hypothesise that for *anti*-product the aldehyde approaches in such a way that the oxygen can hydrogen bond with the R-branch of the catalyst, in the case of glutamine amide (**210**) this would be the NH₂ and for serine amide (**209**) this would be the alcohol and in valine amide (**206**) we would see no such interaction (Figure 67). Mahrwald reported evidence for this type of interaction that allows some control in transition states using Histidine.¹⁵⁴ However computational studies show that this interaction is very weak.¹⁵⁴ To obtain the *syn*-product we see the aldehyde inverted so the aldehyde group is orientated away from the catalyst (Figure 68). Due to the fact that we observe ca. 2:1 *Anti:Syn* diastereoselectivity the energy differences between these conformations must be small.



Enamine transitionstate with aldehyde
approaching from the back



Enamine transitionstate with aldehyde
approaching from the front



Possible hydrogen bonding, with R branch

R = amino acid R branch

Figure 67: Transition state required to give the stereochemistry observed when *anti*-favours

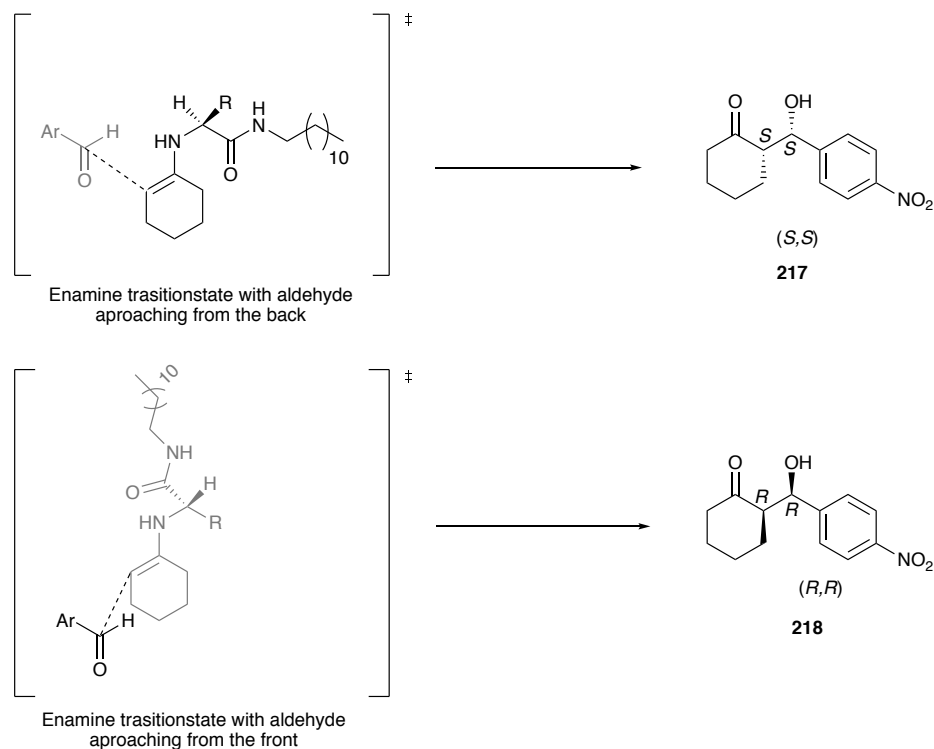


Figure 68: Transition state required to give the stereoselectivity observed when *syn* favours

Furthermore, we can begin to explain the lack of enantioselectivity in a similar manner. For the *anti*-product there is a slight ee%. This again can be justified by the approach of the aldehyde. For the major enantiomer we are observing aldehyde approach from the back of the enamine. One reason for this is to avoid steric clash with the R branch of the catalyst, as H-H steric restriction is lower than H-R_{branch}. Whereas for the minor product the aldehyde approaches the enamine from the front therefore passing the R_{branch} where H-R_{branch} steric restriction would be larger. In the *syn* product there is significantly less enantioselectivity, again any selectivity seen here will also be most likely due to the approach from the back face of the enamine being more sterically favoured compared to the front approach. It is thought that the selectivity for the *syn* product is poorer due to the lack of interaction of the R_{branch} with the aldehyde by hydrogen bonding.

The data obtained indicates there is little control sterically or covalently with any of the catalysts to truly dictate relative and absolute stereochemistry. We suggest that one of the reasons for this is the heterogeneous nature of the reaction, meaning the interaction of catalyst and reagents will not be consistent. Other research groups have often opted to add a small quantity of DMSO to homogenise

the reaction mixtures, however we decided against this, as we felt it was important that the reactions were performed in water to mimic prebiotic conditions.

Overall, glutamine amide (**210**) gave the best conversion rates (Table 10). ^1H NMR analysis of the crude product showed excellent yields with nearly 100% conversion after 72 h. In addition, when the reaction was essentially complete after 48 h it shows some evidence of reaction control under these highly heterogeneous conditions. Furthermore, aside from the catalysis of the reaction itself, it was noticed that a gel had formed after the 48 h time period (Figure 69). The fact that a gel had formed but the percentage conversion had reached near completion is very interesting and will be discussed later in further detail.

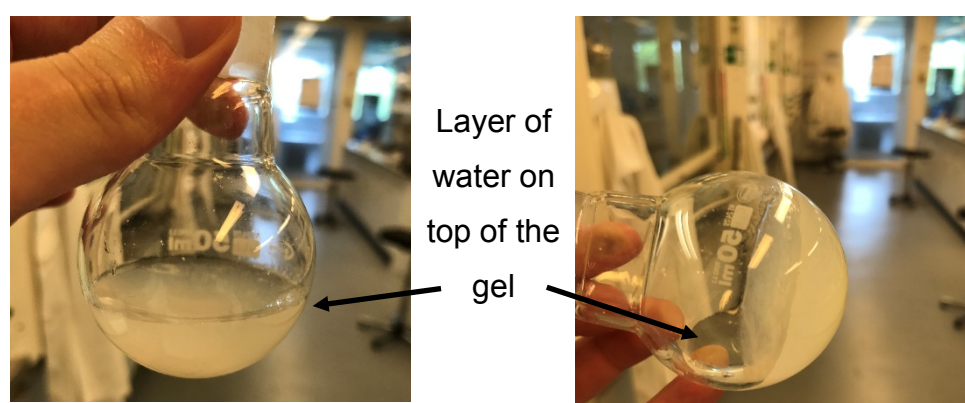


Figure 69: Aldol reaction containing glutamine amide (**210**), cyclohexanone and 4-nitrobenzaldehyde (**47**) in water (20 mL) that resulted in gelation of most of the reaction mixture

2.3 Conclusions

Initially we tested the ability of these three amino acid amides to form gels. The least polar valine amide (**206**) formed gels in water but not in organic solvents. More polar serine amide (**209**) formed gels in some organic solvents, while the most polar glutamine amide (**210**) formed gels in some organic solvents but was less reproducible at forming gels in water. The appearances of the gels most likely indicate that different aggregates are forming.

It was then shown that valine (**206**), serine (**209**) and glutamine amides (**210**) are all catalytically active in the solution phase for the heterogeneous aldol reaction between cyclohexanone (**49**) and 4-nitrobenzaldehyde (**47**). ^1H NMR data indicated good conversions and some limited selectivity. The diastereoselectivity of the *syn* or *anti*-product appears to be dictated by the steric interactions rather

than the formation of a six-membered transition state and as a result HPLC shows that enantioselectivity is poor. The literature discussed in Chapter 1 shows that good enantioselectivities can be observed, however this is when in solution-phase but with the addition of DMSO.¹²⁷ In the case presented here, the reactions being performed here are heterogeneous. It is believed that the heterogeneous nature of the reaction results in ee% being inconsistent. However through this catalysis work, a new gel was identified when using glutamine amide (**210**) (0.1 eq) in the presence of 4-nitrobenzaldehyde (**47**) (1 eq) and cyclohexanone (**49**) (10 eq) in low concentrations. This is very interesting and we therefore targeted its understanding in further detail (see Chapter 3).

3.0 A novel Two-component hydrogel

3.1 Aims:

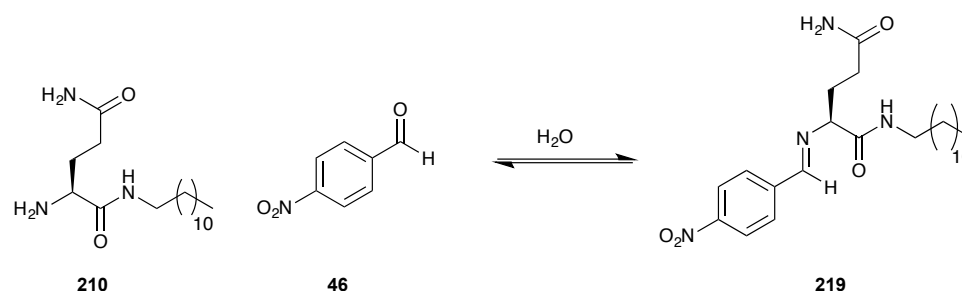
Two-component gels remain rare and two-component hydrogels are even rarer. However, they have a vast array of interesting properties and potential applications as described in Chapter 1. With two-component systems, new gelators can be identified that may have beneficial and tuneable properties due to the way in which each component can be independently modified. It was found (Chapter 2) that a hydrogel formed *in situ* during a glutamine amide (**210**) catalysed aldol reaction between 4-nitrobenzaldehyde (**47**) and cyclohexanone (**49**) in water. We therefore, began to investigate the formation of the hydrogel. This novel system still needed to be understood and fully characterised. Therefore the following research aims were identified:

- Uncover the species responsible for gelation.
- Discover the stoichiometric relationship between the required molecular components.
- Identify how much of the components are being incorporated into the gel network.
- Characterise the gel across multiple length scales using a range of techniques; for example, SEM/TEM, minimum gelation concentration and T_{gel} .
- Carry out an aldehyde screen to see if other similar components form gels.
- Explore any special properties of these hydrogels, and hence determine the generality of this approach to hydrogel formation.

3.2 Results and discussion:

3.2.1 Evidence for Schiff base formation

We suspected that the two-component gel was due to the formation of a Schiff base (**219**) between aldehyde and amide (Scheme 35) presented in the reaction described in Chapter 2. We had seen some evidence of this product during the analysis of these catalytic reactions.



Scheme 35: The proposed two-component hydrogelation system

In an attempt to determine if the hypothesis of the Schiff base (**219**) formation resulting in gelation was correct, three systems were set up to explore the possible direct combinations that might result in gelation.

- 1) Glutamine amide (**210**) (20 mg 6.4 μ mol) in 20 mL water
- 2) Glutamine amide (**210**) (20 mg 6.4 μ mol) and 4-nitrobenzaldehyde (**47**) (98.8 mg, 0.64 mmol) in 20 mL water
- 3) Glutamine amide (**210**) (20 mg 6.4 μ mol) and cyclohexanone (**49**) (0.67 mL 6.4 mmol) in 20 mL water

In each case the suspension of was left to stand in a 50 mL round bottomed flask with no external stimuli applied as the initial gel formed with no external stimuli. Out of these three systems, number **2** formed a gel as identified by tube inversion after 24 hours only.

Analysis of the 1:1 gel by electron ionisation mass spectroscopy (Figure 70) showed that a Schiff base (**219**) was indeed formed *in situ*. It is proposed that the Schiff base (**219**) is responsible for gelation. Furthermore, when the 1:1 gel was dehydrated in *vacuo* and analysed by ¹H NMR an imine peak could be identified (singlet at 8.47 ppm), along with other signals corresponding to the Schiff base

(219) formed between glutamine amide (210) and 4-nitrobenzaldehyde (47) (Figure 71).

Analysis Filename dks64937kh_P1-D-7_01_5343.d
 Method 800p_lcms_2c1s.m
 Submission Name dks64937kh
 Instrument micrOTOF
 ESI Positive

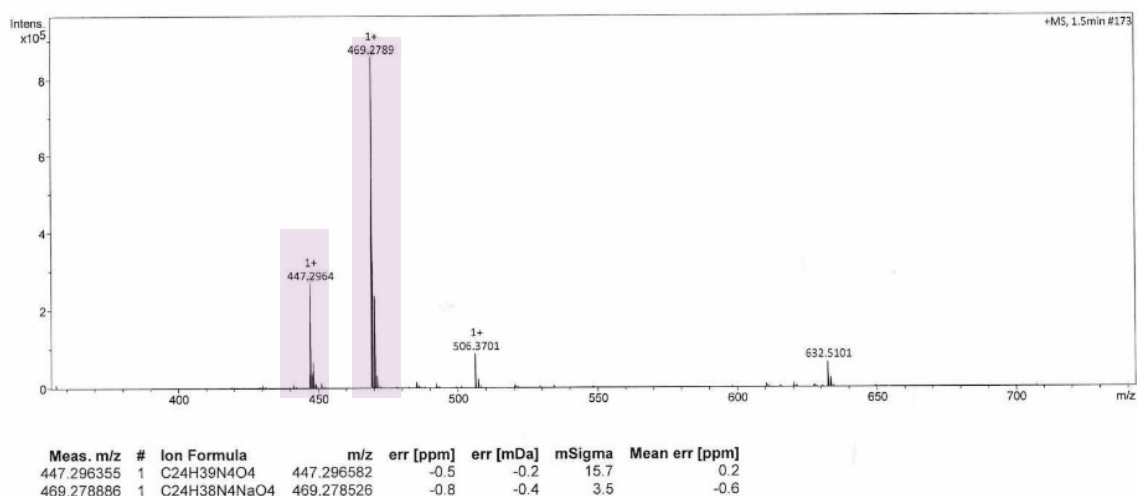
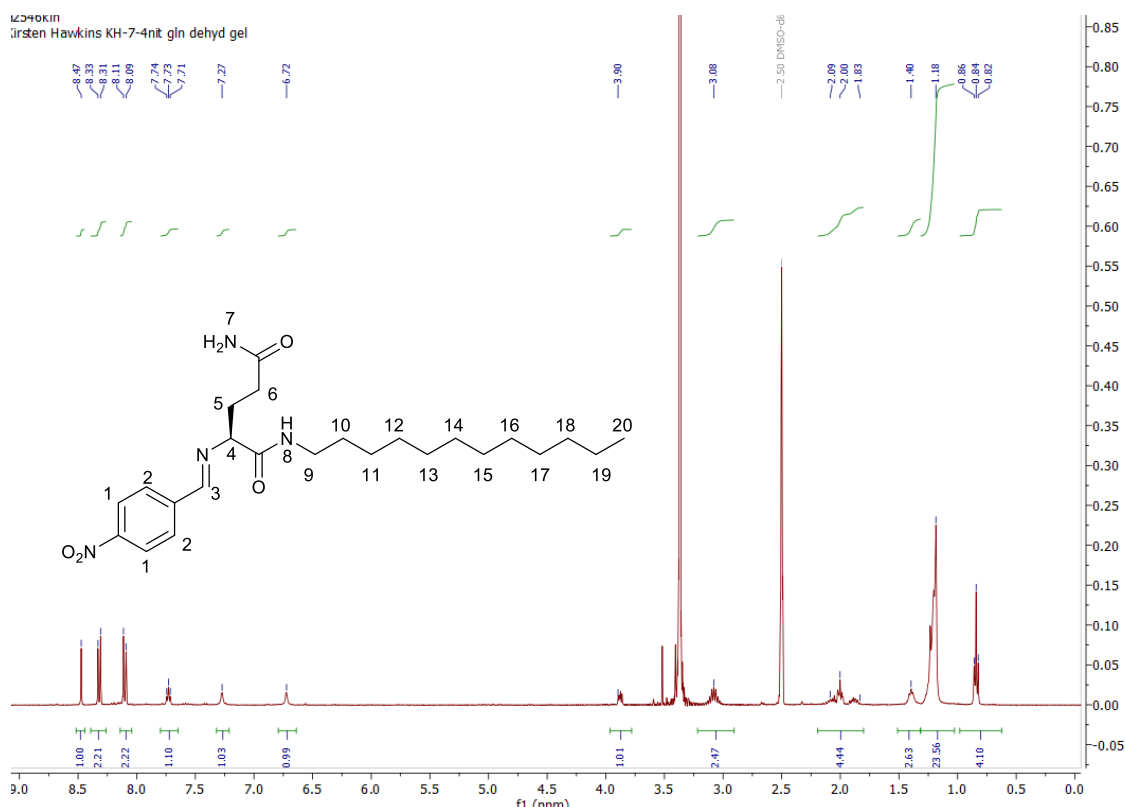


Figure 70: Mass spectroscopy of sample proposed to be a Schiff base formed from glutamine amide (210) and 4-nitrobenzaldehyde (47)



¹H NMR (400 MHz, DMSO-*d*₆) δ ppm: 8.47 (s, 1H, H₃), 8.33 (d, 2H, *J* = 8.9 Hz, H₁), 8.31 (d, 2H, *J* = 9.0 Hz, H₂), 7.73 (t, 1H, *J* = 5.9 Hz, H₈), 7.27 (s broad, 1H H₇), 6.72 (s broad, 1H H₇), 3.98-3.76 (m, 1H, H₄), 3.31-3.02 (m, 2H, H₉), 2.21-1.85 (m, 2H, H₅), 1.44-1.36 (m, 2H, H₆), 1.46-1.32 (m, 2H, H₁₀), 1.28-1.15 (m, 20H, H₁₁₋₁₉), 0.84 (t, 3H, *J* = 7.2 Hz, H₂₀)

Figure 71: ¹H NMR of dehydrated two-component gel system

3.2.2 Two-component gel system

The optimal ratio of glutamine amide (**210**) and 4-nitrobenzaldehyde (**47**) required for gel formation was then investigated. Initially a stock solution of glutamine amide (**210**) (1 mg mL^{-1}) was made: to make the stock solution, glutamine amide (**210**) was added to water and heated to dissolve it. The stock solution was then added to the 4-nitrobenzaldehyde (**47**) whilst it was still hot. The mixture was either sonicated or left to stand at room temperature. Unfortunately using a stock solution of either 1 mg mL^{-1} or 2 mg mL^{-1} did not result in effective gelation at glutamine amide (**210**): aldehyde ratios of 1:0.5, 1:1 and 1:10. However, this method introduced a new element that could affect gelation. Heat puts energy into the system, which could result in aggregation prior to aldehyde addition. As in the original system discussed in section 3.2.1 no heating was required.

In our second approach, the individual components were weighed out, mixed as solids and water was added to form a suspension. The suspension was subsequently treated in two ways:

1. Sonicated (1 minute) and then left to stand at room temperature, or,
2. No sonication but left to stand at room temperature

When sonicated, gel formation was much more effective (Table 15 entries 4-6).

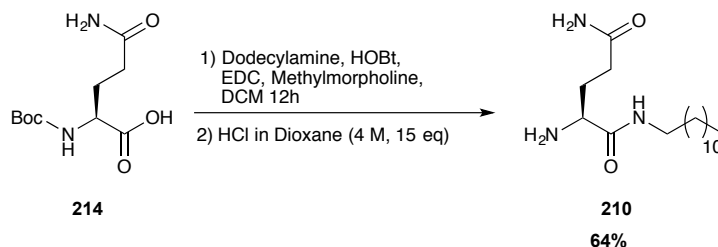
Gels were formed at 1:1 molar ratios of the two components 4-nitrobenzaldehyde (**47**) and glutamine amide (**210**) (1 mg , 3.19 mmol of glutamine amide (**210**)). Gels were also formed in the presence of excess aldehyde, but if only 0.5 eq of aldehyde were used then only very weak gels were formed. The use of sonication to initiate gelation is a well-known phenomenon in supramolecular gel science.¹⁵⁵

Table 15: Method to initiate gelation with varying concentrations of 4-nitrobenzaldehyde (**47**). Gelation determined by tube inversion.

Entry	Equivalents of 4-nitrobenzaldehyde	Treatment to initiate gelation	Did it gel?
1	10	Leave	Very weak gel
2	1	Leave	Semi gel
3	0.5	Leave	No gel
4	10	Sonicate	Gel
5	1	Sonicate	Gel
6	0.5	Sonicate	Very weak gel

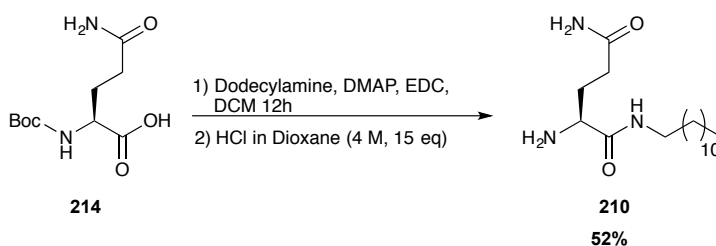
3.2.3 Optimising synthesis of glutamine amide

Although it was evident that a gel could form, a second synthesised batch of glutamine amide (**210**) did not form gels. Analysis by ^1H NMR showed that there were batch-to-batch variations with purity of glutamine amide (**210**) from solvent occlusion to trace amounts of coupling agents, both of which could be inhibiting gelation. Therefore, the synthesis was optimised to ensure that the glutamine amide (**210**) could be readily synthesised with no impurities. The most common cause of impurities was from solvent occluding in the material. In the original synthesis, ethyl acetate was used in the organic aqueous work up. However, using ethyl acetate was found to cause emulsions to form, and upon standing would result in gel formation. To resolve this problem dichloromethane (DCM) was used in both the coupling reaction and also the aqueous work up. Using DCM (Scheme 36) did improve the reaction as solvent occluding no longer occurred. The synthesis was optimised further due to minor impurities believed to be due to 1-hydroxybenzotriazole hydrate or by-products, which resulted in a brown sticky solid rather than a fine white powder. In addition, 1-hydroxybenzotriazole hydrate (HOBt) is not ideal because it has increased hazards compared to other coupling agents.



Scheme 36: Initial synthesis of glutamine amide (**210**)

The synthesis was therefore changed so that 4-dimethylaminopyridine (DMAP) was used instead of HOBt and methylmorpholine (Scheme 37). If required, the crude material was purified by column chromatography in DCM:MeOH (9:1). The deprotection step used 4 M HCl in dioxane followed by free basing with 1 M NaOH for 2-12 hours to yield the free amine. The glutamine amide (**210**) produced using the optimised synthesis formed effective and reproducible gels using a heat cool cycle where the suspension was heated until boiling (ca 100 °C) and left to cool at room temperature for at least 5 hours. Therefore, all further results in this chapter used this approach to generate gels.



Scheme 37: Optimised synthesis of glutamine amide

3.2.4 Identifying the minimum ratio of aldehyde to amide required to form a gel

With optimisation of the synthetic methods and the gelation protocol, experiments were performed to identify the minimum molar ratio of the two components required for effective gelation.

Table 16: Identifying the minimum ratio of 4-nitrobenzaldehyde (**47**) to glutamine amide (**210**) (1mg, 3.16 mmol) required to form a hydrogel in 1 mL water. Gelation determined by tube inversion.

Entry	Equivalents of 4-nitrobenzaldehyde	Quantity of 4-nitrobenzaldehyde	Did it gel?
1	0.0	0 μg	No gel
2	0.1	50 $\mu\text{g} \pm 5 \mu\text{g}$	No gel
3	0.2	100 $\mu\text{g} \pm 5 \mu\text{g}$	No gel
4	0.3	140 $\mu\text{g} \pm 5 \mu\text{g}$	No gel
5	0.4	190 $\mu\text{g} \pm 5 \mu\text{g}$	No gel
6	0.5	240 $\mu\text{g} \pm 5 \mu\text{g}$	No gel
7	0.6	290 $\mu\text{g} \pm 5 \mu\text{g}$	Weak gel
8	0.7	340 $\mu\text{g} \pm 5 \mu\text{g}$	Gel
9	0.8	390 $\mu\text{g} \pm 5 \mu\text{g}$	Gel
10	0.9	440 $\mu\text{g} \pm 5 \mu\text{g}$	Gel
11	1.0	480 $\mu\text{g} \pm 5 \mu\text{g}$	Gel

The results in Table 16 show that 0.6 equivalents of 4-nitrobenzaldehyde (**47**) is the minimum amount required to form a weak gel (entry 7). For the two-component system containing 1 mg glutamine amide (**210**), 0.7 equivalents of 4-nitrobenzaldehyde (**47**) can be considered as the true minimum (entry 8) as gels formed, whereas 0.6 equivalents of aldehyde only yields a weak gel (entry 7).

Analysis of the 1:1 gel by ^1H NMR was then carried out. By performing ^1H NMR spectroscopy on a gel, only those components that are soluble in the liquid-like phase, and hence mobile on the NMR timescale, can be observed. Compounds that are within the self-assembled ‘solid-like’ network have broad peaks.^{156–158} The use of a mobile internal standard allowed quantification of the system. For this system chloroform (2 μL , 2.9 mg) was used as a solvent spike as chloroform is soluble in water up at this quantity and would have a signal in a region on the ^1H NMR free from aldehyde and glutamine amide (**210**) resonance. The ^1H NMR of the gel showed that a small proportion, ca. 0.4 equivalents, of the 4-nitrobenzaldehyde (**47**) was still mobile on the NMR timescale, which suggests that 0.6 eq of aldehyde are sufficient to support a gel-forming network. The remainder of the aldehyde is either mobile within the gel, or in fast equilibrium with

the self-assembled gel network. This is an interesting result as it implies that not all the glutamine amide (**210**) needs to form a Schiff base (**219**) with the aldehyde (**47**), and thus some free amide (**210**) could be available within the gel fibres for catalysis. The fact that 4-nitrobenzaldehyde (**47**) is needed in the gel is noteworthy, and could explain why in previous work (in the glutamine amide (**210**) catalysed aldol reaction of 4-nitrobenzaldehyde (**47**) and cyclohexanone (**49**), chapter 2), a gel was still observed even though there was conversion of starting material to product.

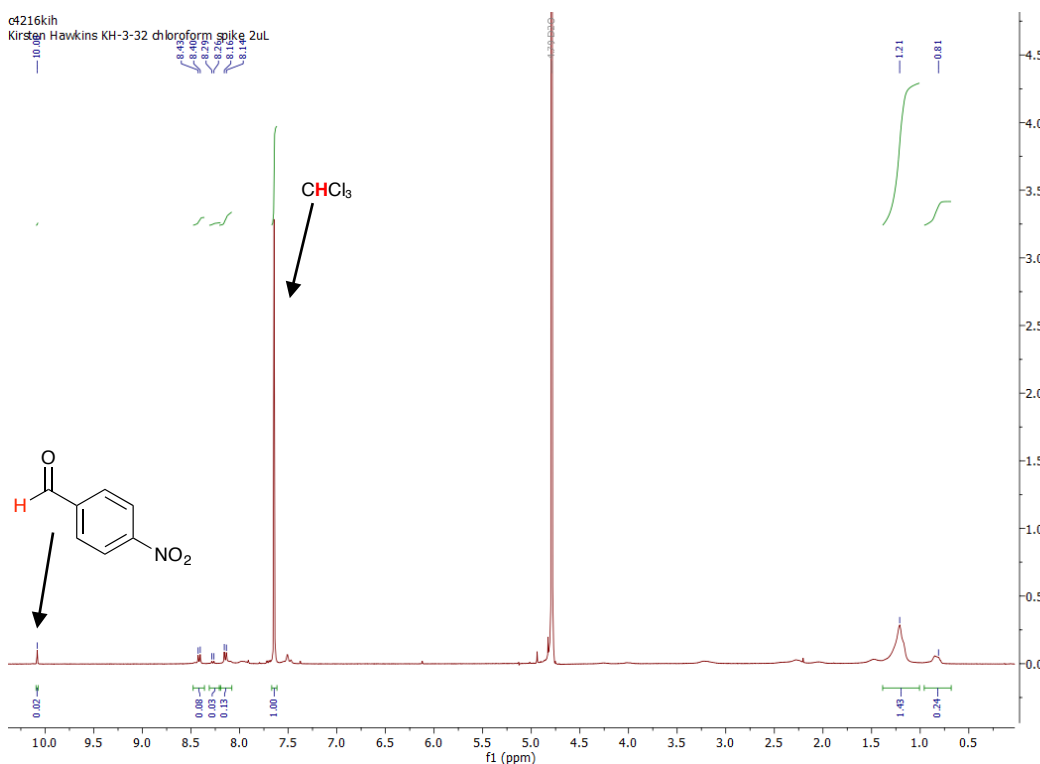


Figure 72: ^1H NMR of 4-nitrobenzaldehyde (**47**) (670 μg) and glutamine amide (**210**) (1.5mg) hydrogel with chloroform spike (2 μL). Obtained in D_2O (0.7 mL) 400 MHz

In order to calculate the amount of mobile aldehyde, first the number of moles of the standard used (chloroform, 2 μL) need to be calculated:

$$m = \rho \times v = 1.48 \times 2 \times 10^{-3} = 2.96 \times 10^{-3} \text{ g}$$

$$\text{Moles of chloroform used} = \frac{2.96 \times 10^{-3}}{119.38} = 24.79 \times 10^{-6} \text{ mole}$$

$$\text{Moles for 1 H} = 24.79 \times 10^{-6} \text{ moles}$$

Next the number of moles of mobile aldehyde seen in the NMR are determined

$$\text{Integral for mobile aldehyde} = 0.02$$

$$\text{Therefore moles of mobile aldehyde} = 24.79 \times 10^{-6} \times 0.02 = 0.497 \times 10^{-7} \text{ moles}$$

With the moles of mobile aldehyde the concentration of mobile aldehyde can be calculated:

0.497×10^{-7} moles of mobile aldehyde (RMM = 151) are free in 0.7 mL D_2O .

$$0.497 \times 10^{-7} \times 151 = 7.48 \times 10^{-6} \text{ g in } 0.7 \text{ mL}$$

$$7.48 \times 10^{-6} \times 1.42 = 1.06 \times 10^{-5} \text{ g/mL} = 1.06 \times 10^{-2} \text{ g/L}$$

Finally to calculate the % mobile aldehyde the concentration of aldehyde added must be calculated:

concentration of aldehyde added = 670 μg in 0.7 mL

$$670 \times 10^{-3} \times 1.42 = 0.95 \times 10^{-3} \text{ g/mL} = 0.95 \text{ g/L}$$

$$\frac{1.06 \times 10^{-2}}{0.95} \times 100 = 1\% \text{ mobile aldehyde}$$

Ideally, the internal standard used should be miscible with the deuterated solvent as this will ensure that the solvent spike signal corresponds to the entire solvent spike added. Although the concentration of chloroform should be soluble in water we repeated the experiment with fully miscible solvents. We therefore trialled some water miscible solvents, DMSO and methanol. When using DMSO or methanol as a solvent spike it became apparent that it was disrupting the gel network as a precipitate was visible down the centre of the NMR tube. Analysis of the data showed that when using DMSO as a spike 8%, of the aldehyde (**47**) was mobile. When using methanol, 31% aldehyde (**47**) was mobile. In addition NMR data obtained using the methanol spike showed the presence of the Schiff base (**219**). In total only 50% of the aldehyde (**47**) was involved in the gel network the rest was either involved in the gel network or had reacted to form the Schiff base (**219**).

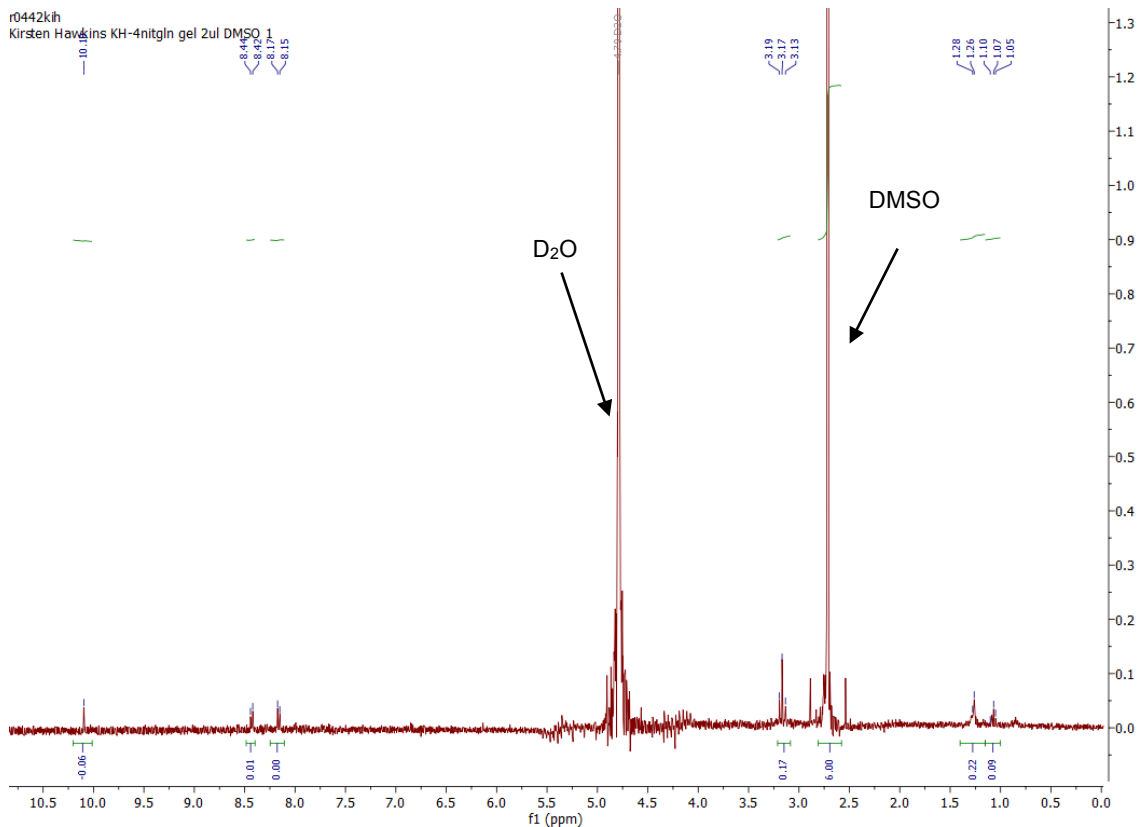


Figure 73: Gel NMR of 4-nitrobenzaldehyde (**47**) and glutamine amide (**210**) (1:1, 1.48 mg mL⁻¹) with DMSO solvent spike (2 μL)

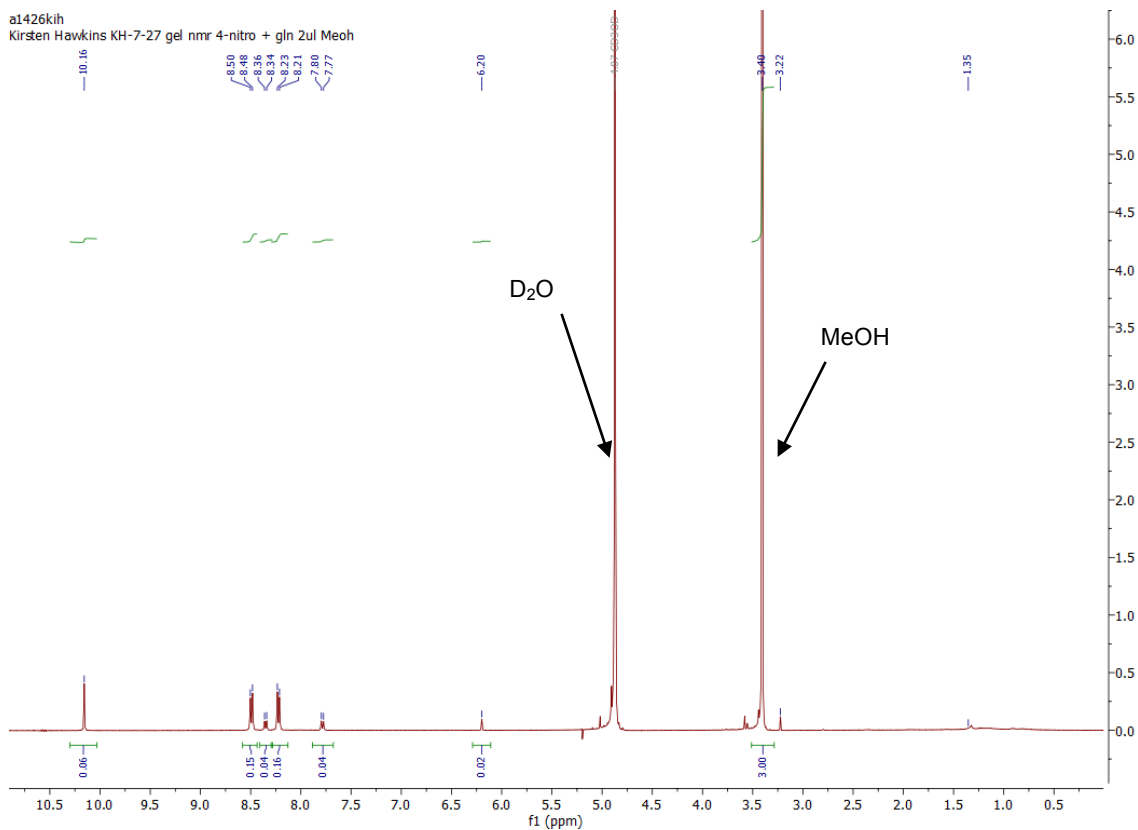


Figure 74: Gel NMR of 4-nitrobenzaldehyde (**47**) and glutamine amide (**210**) (1:1, 1.48 mg mL⁻¹) with MeOH solvent spike (2 μL)

3.2.5 Identifying the minimum gelation concentration of a 1:1 aldehyde: amide system

With the preferred 1:1 molar equivalents of 4-nitrobenzaldehyde (**47**) and glutamine amide (**210**) established (and a minimum of 0.7:1.0 ratio), we turned our attention to the minimum gelator concentration (MGC). The system examined above was at a very low concentration, just 0.1% wt/vol with respect to glutamine amide (**210**). This system was initially selected to study because the quantity of glutamine amide (**210**) present is the same as that in the original reaction where the *in situ* gelation was first discovered (Chapter 2). Although the system is already at a low concentration, a minimum gelation concentration still needs to be identified. In addition, using higher concentrations could potentially give more robust gels, so higher concentrations were also investigated.

Table 17: Varying the concentration of the 1:1 system to find the minimum gelation concentration (MGC) and most robust gel, 1 mL water

Entry	Mass of glutamine amide	Equivalents of 4-nitrobenzaldehyde	Mass of 4-nitrobenzaldehyde	Did it gel?
1	0.50 mg	1.0	240 $\mu\text{g} \pm 5 \mu\text{g}$	Very weak gel
2	1.00 mg	1.0	480 $\mu\text{g} \pm 5 \mu\text{g}$	Gel
3	2.00 mg	1.0	960 $\mu\text{g} \pm 5 \mu\text{g}$	Gel
4	3.00 mg	1.0	1.44 mg $\pm 5 \mu\text{g}$	Gel
5	4.00 mg	1.0	1.92 mg $\pm 5 \mu\text{g}$	Gel
6	5.00 mg	1.0	2.40 mg $\pm 5 \mu\text{g}$	Gel

The results in Table 17 show that the minimum gelation concentration of the 1:1 system is greater than 0.5 mg glutamine amide (**210**) (entry 2-6). Above 0.5 mg, gelation occurred more consistently. However, there is a maximum limit to the concentration, due to the insolubility of 4-nitrobenzaldehyde (**47**) in water. In the gels formed above 5 mg of glutamine amide (**210**) and 1 eq of 4-nitrobenzaldehyde (**47**), visible needles of aldehyde could be seen as above 2.34 mg/mL 4-nitrobenzaldehyde is not soluble in water. In addition, solid particulate

could be observed on the bottom of the vial this could be insoluble Schiff base of unreacted glutamine amide, which may affect the gel properties. Therefore the highest concentration for gelation is 5 mg/ mL with respect to glutamine amide (**210**). It is reasonable to state that a total gelator loading of 0.74 mg (0.5 mg + 0.24 mg = 0.74 mg) can achieve gelation in 1 mL of water is just 0.074% (w/v %). This makes the glutamine amide and 4-nitrobenzaldehyde hydrogel one of the most efficient hydrogelators reported to date. Given the rarity of two-component hydrogels the low gelator loading is therefore significant. The maximum gelation concentration is 7.4 mg (5 mg + 2.4 mg) in 1 mL of water, which is 0.74% (w/v %).

3.2.6 Physical properties and characteristics of the two component system

Another property of the two-component gel system that was investigated was the temperature at which the gel broke down into a sol, the T_{gel} . This is a valuable property because it gives useful information about the thermal stability of the gel. The T_{gel} was determined by heating the gel at 1 °C per minute in an oil bath. At each degree of temperature increase the sample was removed and inverted to determine if the gel was still self-supporting. The temperature at which the gel did not self-support was recorded as the T_{gel} .

Table 18: T_{gel} of glutamine amide (**210**) and 4-nitrobenzaldehyde (**47**) hydrogel 1:1 (1 mL water)

Entry	Mass of glutamine amide	Equivalents of 4-nitrobenzaldehyde	T_{gel} / °C
1	1.00 mg	1.0	61 ± 0.5
2	2.00 mg	1.0	69 ± 0.5
3	3.00 mg	1.0	70 ± 0.5
4	4.00 mg	1.0	72 ± 0.5
5	5.00 mg	1.0	83 ± 0.5

Table 19: T_{gel} of glutamine amide (**210**) (1 mg, 3.16 mmol) and 4-nitrbenzaldehyde (**210**) hydrogel with varying equivalents of 4-nitrobenzaldehyde (**47**) (1mL water)

Entry	Equivalents of 4-nitrobenzaldehyde	T _{gel} / °C
1	0.6	26 ± 0.5
2	0.7	76 ± 0.5
3	9.0	76 ± 0.5
4	10	62 ± 0.5

The T_{gel} values presented in Table 18 show that as the concentration of the two-components in the 1:1 system increases the T_{gel} also increases. The increase in T_{gel} is not surprising as it is expected that as the concentration of the components that make up the sample-spanning network increases, there will be more fibres present and therefore a more thermally stable gel.¹⁵⁹

Due to the fact that there are two components required for the hydrogel it was important to also see how the T_{gel} is affected by changing the ratio of glutamine amide (**210**) to 4-nitrobenzaldehyde (**47**) (Table 19). It was already established in Table 16 that the minimum number of equivalents of 4-nitrobenzaldehyde (**47**) required for gelation was 0.6. However Table 19 shows that the minimum equivalents of 4-nitrobenzaldehyde (**47**) required to make a thermally stable gel was 0.7, below this the T_{gel} was close to room temperature. Conversely once the number of equivalents of 4-nitrobenzaldehyde (**47**) increases to above 9, there was a decrease in the T_{gel}. This was most likely due to the presence of material that is not fully incorporated into the gel disrupting the gel network, for example a significant amount of undissolved aldehyde as the maximum solubility of 4-nitrobenzaldehyde (2.34 mg) in 1 mL water has been exceeded.

The morphology of the gel was characterised by transmission electron microscopy (TEM) (Figure 75) and scanning electron microscopy (SEM) (Figure 76). The images produced from TEM and SEM show that the 1:1 two-component gel (1 mg / mL with respect to glutamine amide (**210**)), is web-like with nano-fibres that are of mixed widths (55-110 nm). As the T_{gel} changed with concentration SEM images of the two-component systems were recorded for the 2 mg / mL, 3 mg / mL and 5 mg / mL (with respect to glutamine amide (**210**)) 1:1 gel system. It was found that as the concentration increased, nodular aggregates appear to be formed on the fibres themselves (Figure 77, Figure 78 and Figure 79). The aggregation observed has

not been fully explored but is an interesting result, and it seems plausible that excess material has a secondary aggregation mode. Alternatively, the nodules may be associated with the less soluble material as the concentration of gelator in increased.

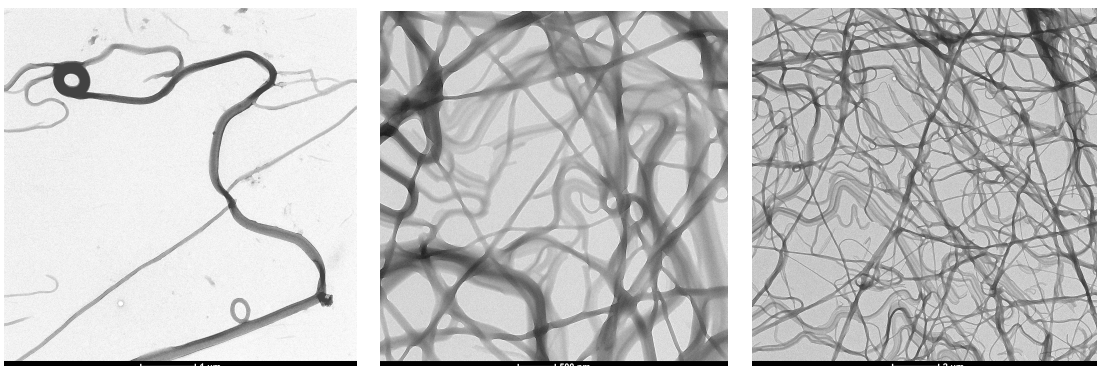


Figure 75: TEM image 1 mg / mL glutamine amide (**210**) and 480 μg 4-nitrobenzaldehyde (**47**) (1:1)

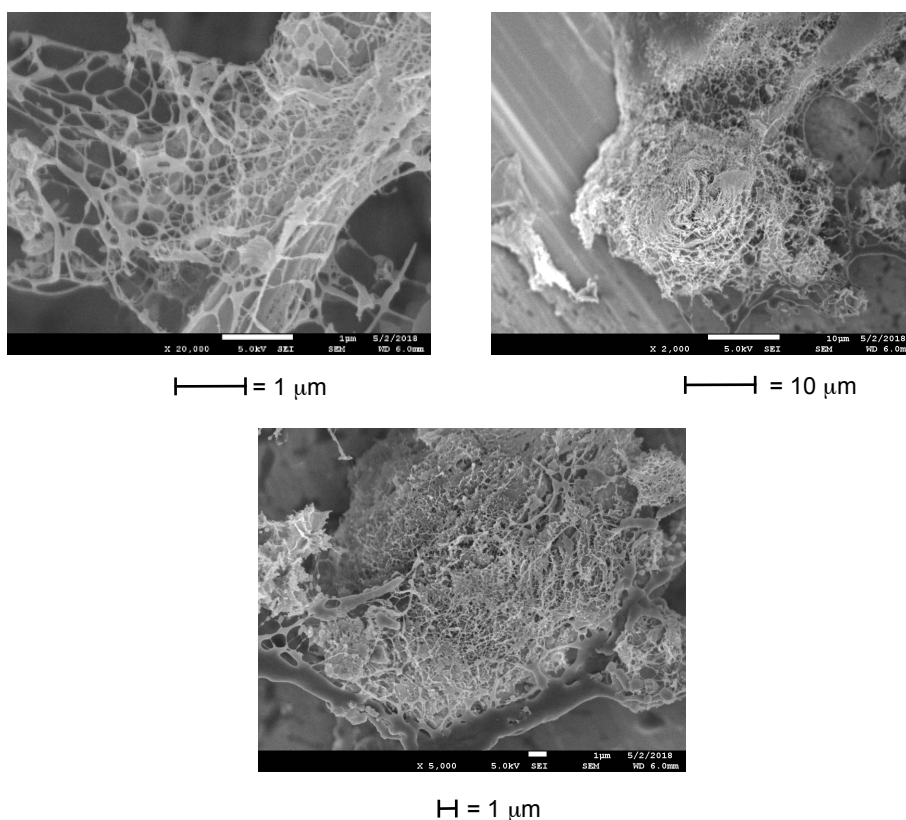


Figure 76: SEM image 1 mg / mL glutamine amide (**210**) and 480 μg 4-nitrobenzaldehyde (**47**) (1:1)

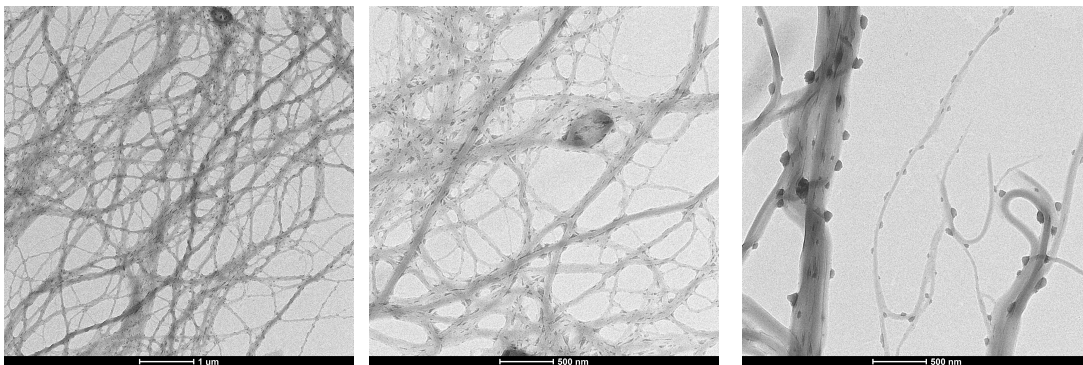


Figure 77: TEM image 2 mg / mL glutamine amide (**210**) and 960 μg 4-nitrobenzaldehyde (**47**) (1:1)

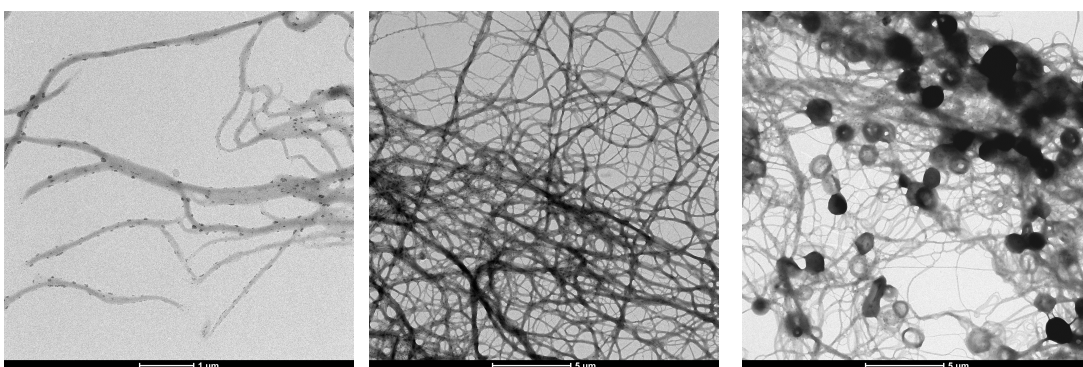


Figure 78: TEM image 3 mg / mL glutamine amide (**210**) and 1.44 mg 4-nitrobenzaldehyde (**47**) (1:1)

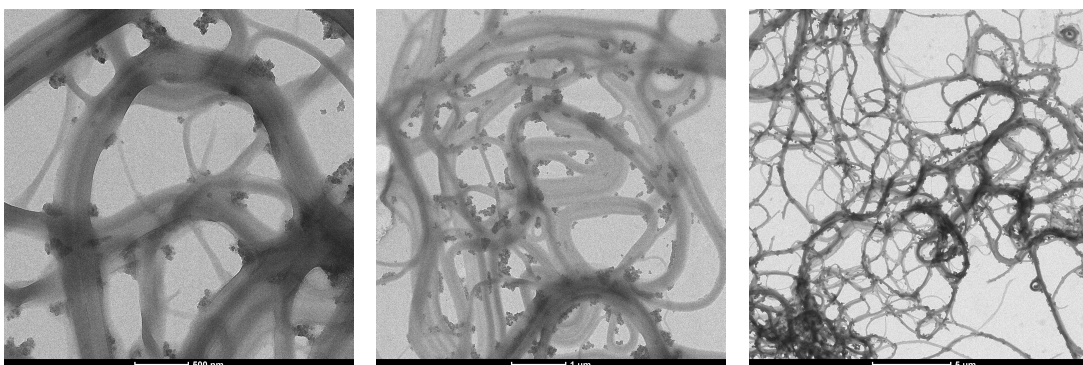


Figure 79: TEM image 5 mg / mL glutamine amide (**210**) 2.4 mg 4-nitrobenzaldehyde (**47**) (1:1)

3.2.7 Dynamic light scattering (DLS)

It was suspected that the glutamine amide (**210**) might aggregate on its own in the absence of aldehyde although without forming a gel due to the presence of a polar head group and a long alkyl chain. For this reason, dynamic light scattering (DLS) was used both on the glutamine amide (**210**) on its own and on the two-component system with 4-nitrobenzaldehyde (**47**) as it goes through the heat cool

cycle. The data collected showed that the glutamine amide (**210**) on its own was indeed aggregating (Figure 80) with a peak at ca 1000 nm. DLS assumes all objects as spherical, which would be highly unlikely in this case it is more likely that there is just aggregation; therefore no special significance should be read into the number. However, clearly some aggregation is occurring giving rise to light scattering. When the two-component system was monitored over time, initially there was one peak (corresponding to glutamine amide (**210**) on its own) but as the sample began to cool a second peak at a larger diameter started to appear as the gel started to form (Figure 82). We suggest that the glutamine amide (**210**) initially aggregates, but does not support a sample spanning gel. Modification by reaction with the aldehyde then encourages the formation of a spanning gel network perhaps due to a change in solubility of the aggregates induced by Schiff base (**219**) formation.

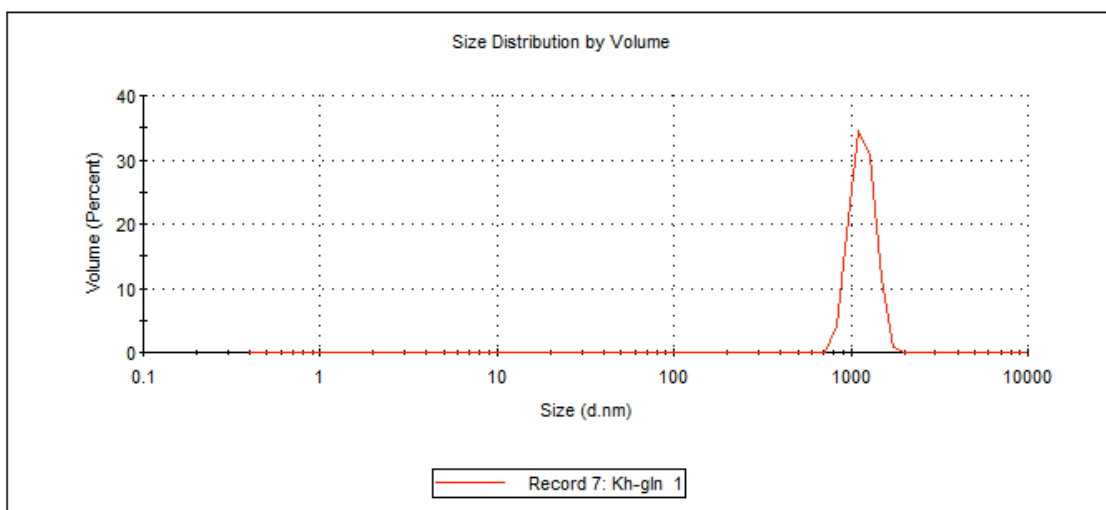


Figure 80: DLS data of glutamine amide (**210**) 1 mg/ mL

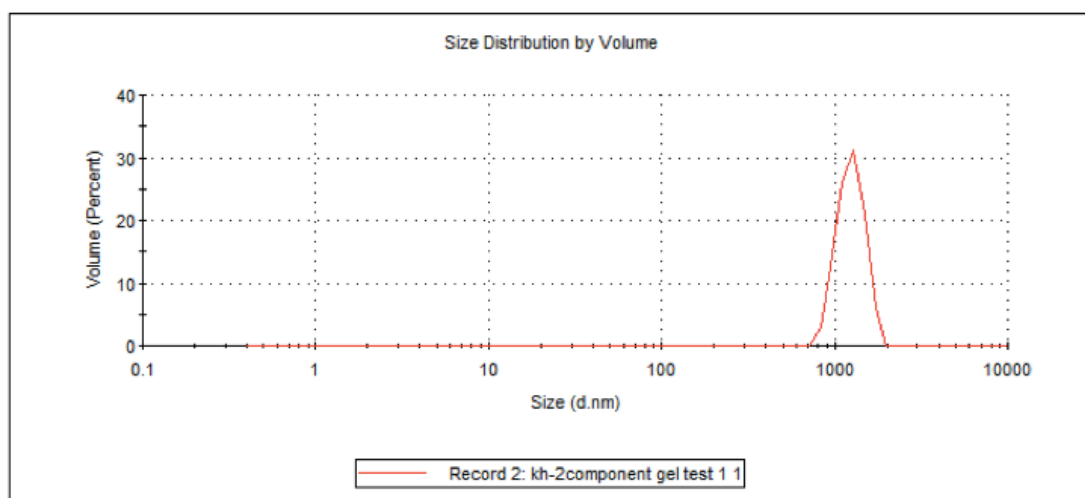


Figure 81: a) Initial DLS of 1:1 glutamine amide (**210**) and 4-nitrobenzaldehyde (**47**) in 1 mL water (ca 100 °C)

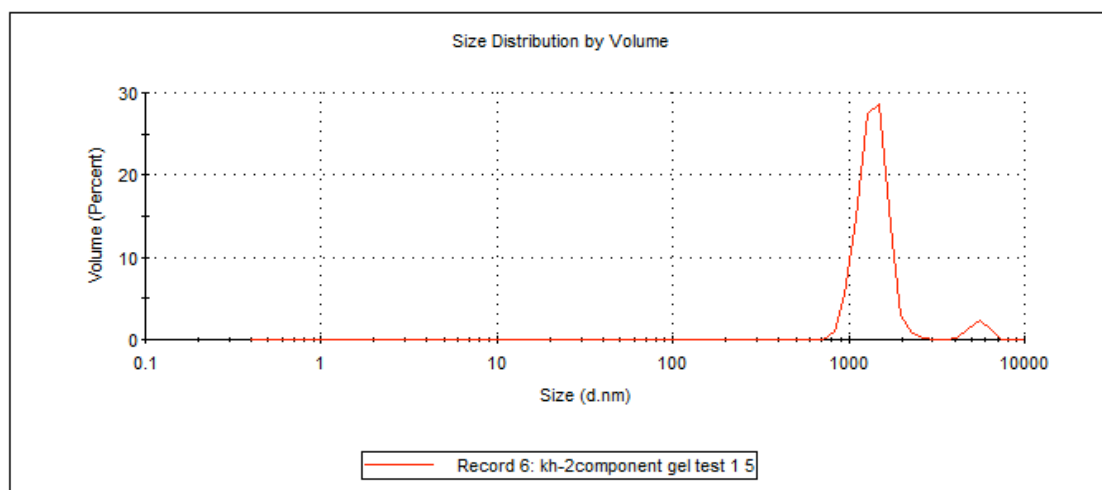


Figure 82: DLS of 1:1 glutamine amide (**210**) and 4-nitrobenzaldehyde (**47**) in 1 mL water after standing for 5 h

3.2.8 Circular Dichroism spectroscopy:

Circular dichroism (CD) spectroscopy is a solution-phase technique that is effectively UV-Vis spectroscopy using circularly polarised light, and can be thought of as “chiral spectroscopy”.¹⁶⁰ Circular dichroism can be used to determine if chirality of the monomers is also present in self-assembled systems and can provide detailed information about the solvated gel. If the molecule is achiral then there will, of course, be no bands in the CD spectrum as the difference in absorbance of right- and left-circularly polarized light is equal. Whereas a chiral molecule may show CD bands either positive or negative because there will be a difference in the absorbance of right- and left-circularly polarized light. The bands observed appear at the same wavelength as those observed by UV-Vis spectroscopy.

Self-assembled nanostructures with chirality usually significantly increase the CD band intensity due to superchiral organisation of the chromophores in the nanostructure compared to the system where aggregates have not formed. Variable temperature (VT) CD can be used to show that the CD bands present in the self-assembled nanostructure at room temperature decrease in intensity on elevation of temperature, as the self-assembly breaks down. Variable temperature CD was performed on the two-component gel at a total loading of 1.48 mg/mL (1.00 mg glutamine amide (**210**) + 480 μ g aldehyde (**47**)) in 1 mL water in a

cuvette with a path length of 1 cm. However, the CD spectra produced were not usable due to the HT (High tension) parameter exceeding the ideal values (600 V). If the HT voltage is equal to or above 600 V (on the Jasco J810), there are not enough photons being sampled by the photomultiplier tube to measure a reliable or valid CD signal. There are two reasons for large HT value:

- 1) The gel that formed is opaque, light needs to pass through the gel for CD spectroscopy
- 2) The concentration of the gel was too low

Therefore a second method was used where CD spectra recorded were taken below the minimum gelation concentration and at elevated temperature, to keep all the components in solution. Again the HT parameter was too high and there was a significant amount of noise in the spectra until the concentration was 0.25 mM or below. A CD spectrum of the sample both in solution phase, below the minimum gelation concentration, (Figure 83 and Figure 84) was recorded.

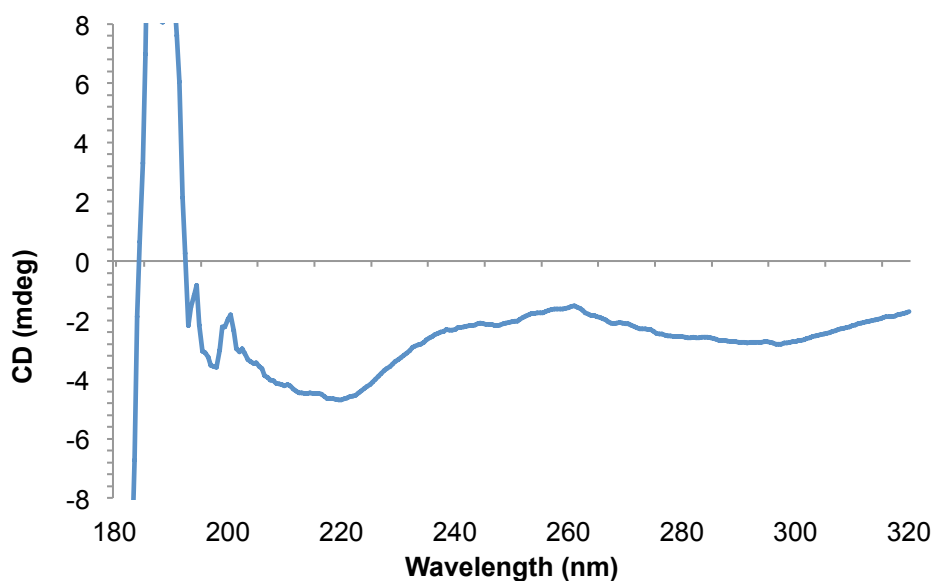


Figure 83: CD spectrum of 1:1 glutamine amide (**210**), 4-nitrobenzaldehyde (**47**) (solution 0.0625 mM)

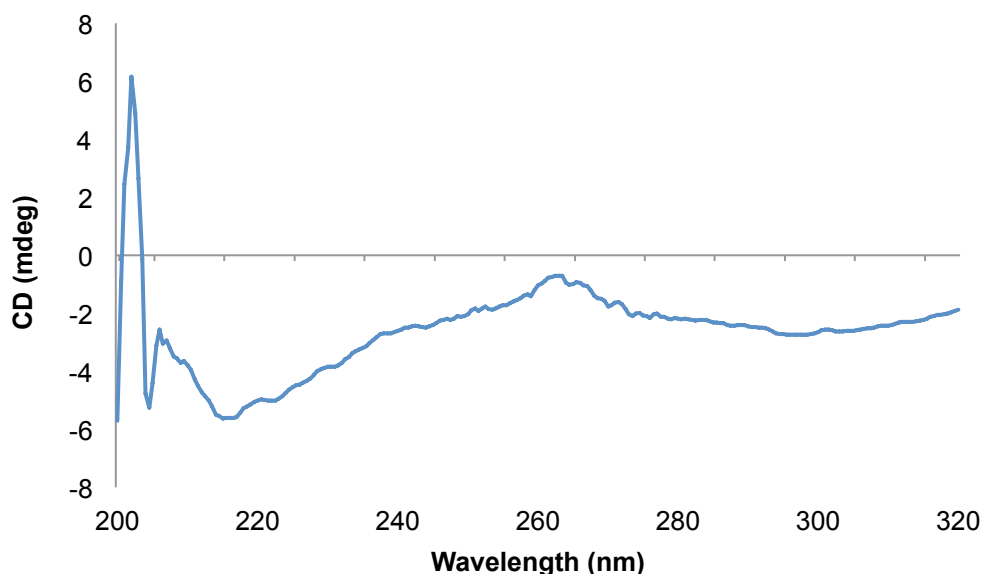


Figure 84: CD spectrum of 1:1 glutamine amide (**210**) 4-nitrobenzaldehyde (**47**) solution 0.25 mM

The spectra show that below minimum gelation concentration we are able to record a CD trace as a dilute solution. The spectrum shows that there is chirality in the system being analysed as in both Figure 83 and Figure 84 there are peaks in the spectrum. The peak at 300 nm corresponds to the 4-nitrobenzaldehyde (**47**) and 220 nm corresponds to the amide most likely as the Schiff base (**219**). In Figure 83 we observed slightly less defined peaks compared to in Figure 84 due to the concentration of the sample.

As it has been shown that a CD spectrum can be recorded at concentrations below gelation CD spectrum of the gel was attempted once more but this time using a cuvette with a shorter path length (1 mm) was used. The sample was prepared with a total loading of 1.48 mg in 1 mL of water was heated then an aliquot of 450 μL was transferred to the cuvette and left to cool at room temperature for 12 h. Using the cuvette with a shorter path length a VT CD spectrum of the gel was successfully recorded (Figure 85).

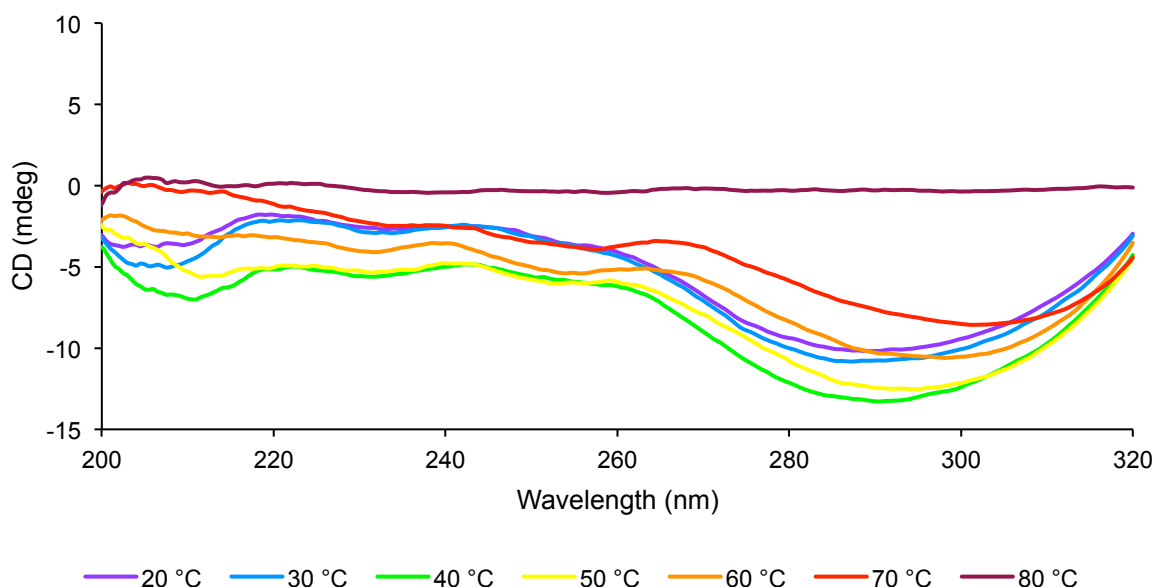


Figure 85: Variable temperature of 1:1 glutamine amide (**210**) 4-nitrobenzaldehyde (**47**) gel CD spectra 1.48 mg total loading in 1 mL. 450 μ L sample taken and transferred to 1 mm quartz cuvette for analysis

The spectra produced with variable temperature CD (Figure 85) shows that at 20 – 40 $^{\circ}$ C there is an increase in CD intensity. This could be due to the opacity of the gel changing as the temperature increased as the gel network begins break and therefore becomes more translucent. As a result, the light passes through the sample with less scattering. However after 40 $^{\circ}$ C, ca. T_{gel} , the gel behaves as expected as temperature increases the CD bands decrease with intensity. This is evidence of a nano-structure as when the nanostructure breaks down superchiral organisation of the chromophores is lost.

3.2.9 pH screening

Another aspect to consider regarding the two-component gelation event is pH. In prebiotic chemistry, pH has been found to play an important role when performing aldol condensation reaction in water. Often when a buffered solution (pH 7) there is an amplified enantiomeric excess in aqueous conditions compared to non-buffered systems. This is due to the elimination of base and acid catalysis, only the catalyst will be involved in the reaction.

As these gels are being studied to gain an understanding of simple cells present on primordial Earth the ability to form gels at different pH is of interest. Furthermore, the ability of gels to operate in applications such as drug delivery will

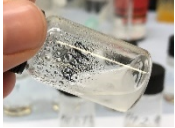

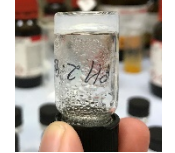

depend on their pH response. Therefore the ability of the two-component system to gel in buffer solutions with different pH values was tested.

Table 20: pH buffer solution screen for a 1:1 two-component system with glutamine amide (**210**) (1mg, 3.19 mmol) and 4-nitrobenzaldehyde (**47**) in 1 mL

Entry	pH	Did it gel?
1	4 (citrate)	No gel, precipitate
2	6.4 (phosphate, citrate)	Very weak gel
3	7 (phosphate)	No gel, precipitate
4	7.4 (tris)	No gel, precipitate
5	10	No gel, precipitate

As can be seen in Table 20, gelation did not occur in buffers. The presence of salts in the buffer might be responsible for inhibiting self-assembly. To explore this further, pH studies were carried out by simply modifying the pH of water by using HCl or NaOH to determine whether gels would form at different pH values in the absence of salts.

Table 21: HCl or NaOH adjusted solution pH screen for a 1:1 two-component system using glutamine amide (**210**) (1 mg, 3.19 mmol) and 4-nitrobenzaldehyde (**47**) 1mL

Entry	Aldehyde equivalents used	pH	Result	
1	1	1.19	No gel	
2	1	1.92	No gel	
3	1	2.90	Gel	
4	1	3.98	Semi-gel	



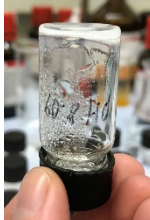


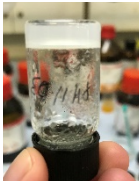

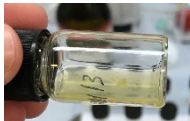
5	1	5.16	Semi-gel	
6	1	5.80	Gel	
7	1	8.09	No gel	
8	1	9.00	No gel	
9	1	10.03	Gel	
10	1	11.03	Gel	
11	1	11.90	No gel	
12	1	13	No gel	

Table 21 shows hydrogels can be formed in pHs above and below that of deionised water. It can therefore be reasoned that the salts in the buffered solutions were inhibiting gelation. Gelation does not occur at the extremes of the

pH scale (pH 13 or pH 1 entries 1 and 12) but does take place in the pH ranges 3-6 (entry 3-6) and 10-11 (entry 9 and 10). At pH 13, although no gel formed, the solution turned orange/brown upon heating. Another interesting factor to notice is the appearance of the hydrogel at different pH. The hydrogel which formed at pH 2.90 (entry 3) looked visually different. A very clear gel formed, unlike the usual opaque gel formed in deionised water. The reason for this needs to be analysed further but it is most likely due to solubility of the components at pH 2.90 and the direction in which the equilibrium of the reaction is pushed. Typically for imine formation an acid catalyst is required and a method of water removal such as Dean-Stark apparatus is used due to imines being easily hydrolysed (Figure 86). In addition, careful balance of pH is required in the formation of the imine. Imine formation can be thought of in two-steps. In the first step a hemiaminal is formed, this occurs fastest at a pH 4-6, at a lower pH too much amine is protonated therefore is less likely to react with the aldehyde, which will also be protonated. However, once the hemiaminal is formed acidic conditions (above pH 6) are favoured, as this will protonate the OH and make a good leaving group resulting in dehydration and the formation of the desired imine.



Figure 86: Acid catalysed imine formation

The pH screening has shown some interesting information about the gelation and shows that it could have potential for us in biological systems.

3.2.10 Self-healing properties

We were interested to determine whether the novel two-component gel could reform due to the reversible nature of the Schiff base. To learn about the thixotropic potential of the gel several investigations were carried out. Three methods of breaking the gel network down were tested, manually shaking, injecting (Figure 87) and de-hydrating. Once broken down the system was allowed to heal in different ways (Table 22).

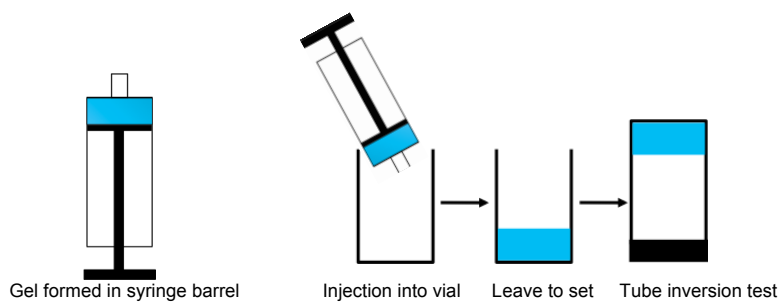


Figure 87: Injection gel method

Table 22: Self-healing test 1:1 4-nitrobenzaldehyde (**47**) glutamine amide (**210**) gel 3.16 μmol in 1 mL water

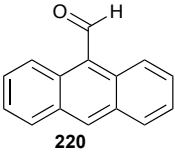
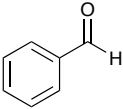
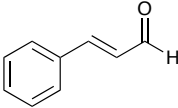
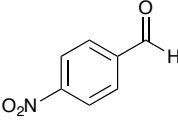
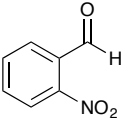
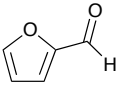
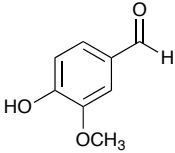
Method of breaking gel network	Method of re-healing gel	Did it form a gel? (1:1 gel system)	Time taken
Shaking	Re-applying external stimuli (heat cool)	Yes	4-12 h
Shaking	Left to rest no external stimuli	Yes	12 h
Injecting	Left to rest no external stimuli	Yes	4-12 h
De-hydrating	Re-hydrating and external stimuli applied	No gel	N/A

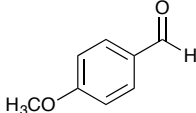
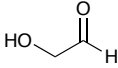
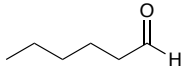
The results in Table 22 are exciting, especially the ability to self-heal after injection through a syringe. This means the gel system could potentially be used as a medium for the application of drugs *in vivo* with the gel forming in the delivered location. The ability of the gel to reform is worth investigating further by performing detailed rheological studies. The self-healing ability of the two-component gel system is most likely due to the dynamic equilibrium of the amide (**210**) and Schiff base (**219**). The reversible reaction in principle assists the system in retaining solubility as the gel is broken down and hence being able to reform *in situ*. The fact that gelation does not occur once the gel is dehydrated then rehydrated with external stimuli applied, indicates that the kinetics of the reaction control the gelation process.

3.2.11 Aldehyde screening

A variety of aldehydes were then investigated to determine the generality of the established two-component gelation system. Therefore an aldehyde screen was carried out using a 1:1 aldehyde to glutamine amide (**210**) molar ratio. The aldehyde screen was performed at a loading of 5 mg mL⁻¹ to give the best possible chance of finding additional new gels.

Table 23: Aldehyde screen of the 1:1 two-component system glutamine amide (**210**) (5 mg, 15.97 mmol) 1mL

Entry	Aldehyde	Structure	Result
1	9-Anthraldehyde	 220	Gel
2	Benzaldehyde	 221	Gel
3	Cinnamaldehyde	 222	Gel
4	4-Nitrobenzaldehyde	 47	Gel
5	2-Nitrobenzaldehyde	 223	Gel
6	Furfural	 224	Inconsistent gel
7	Vanillin	 225	No gel

8	4-Methoxybenzaldehyde		No gel
		226	
9	Glycolaldehyde		No gel
		227	
10	Hexanal		No gel
		228	

The aldehyde screen in Table 23 indicated that a number of other aldehydes also form gels in the presence of glutamine amide (**210**) (entries 1, 2, 3, 4 and 5). The aldehydes that result in gelation contain aromatic functional groups (entries 1, 2, 3, 4 and 5). When the aromatic group contains electron-poor substituents gelation occurs more frequently (entries 4 and 5). Conversely, electron-donating aromatic aldehydes do not form gels with glutamine amide (**210**) (entries 7 and 8). We believe that the reason for gelation is due to the formation of the Schiff base being slow, and once Schiff base begins to form there is a change in solubility that results in self-assembly which is observed as a gel.

In the two-component gel there is no acid to catalyse the formation of the Schiff base therefore the reaction is driven by nucleophilicity. As a result electron-poor aromatic aldehydes will be favoured as nucleophilic addition favours electron-poor substrates. For the gel formation we see this pattern with the aromatic aldehydes. When an electron-withdrawing group is present on the aromatic aldehyde gelation occurs. We even observe gel formation when there is a neutral aromatic aldehyde such as benzaldehyde (**221**) (entry 2). Whereas, when the aromatic aldehyde contained an electron-donating functional group gelation did not take place (entry 7 and 8).

The results in Table 23 also show the importance of the aromatic ring on the aldehyde. We believe that the aromaticity plays an important role in self-assembly which results in the gels observed (entries 1, 2, 3, 4 and 5). The aromatic interactions are known as π - π stacking interactions. These interactions can occur in either a 'face-to-face' or 'edge-to-face' manner (Figure 88). The first of these,

face-to-face, generally occurs between aromatic rings that have $\delta+$ and $\delta-$ carbon atoms. As a result interactions between electron-rich aromatic systems and electron-poor rings are the strongest. The other interaction, edge-to-edge, is a type of hydrogen bonding between very weak $H^{\delta+}$ and electron-rich aromatic ring donors. By having an aromatic ring there is now a $\pi-\pi$ stacking interaction in addition to hydrogen bonding (Figure 89 and Figure 90). This could be more favourable in aqueous solvents as water is both a hydrogen bond-donor and acceptor and may disrupt hydrogen-bonding interactions between molecules. Aromatic rings tend to increase the hydrophobicity of the molecule therefore allowing non-covalent interactions that result in self-assembly.

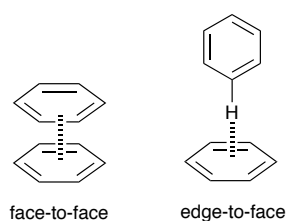


Figure 88: $\pi-\pi$ stacking interactions

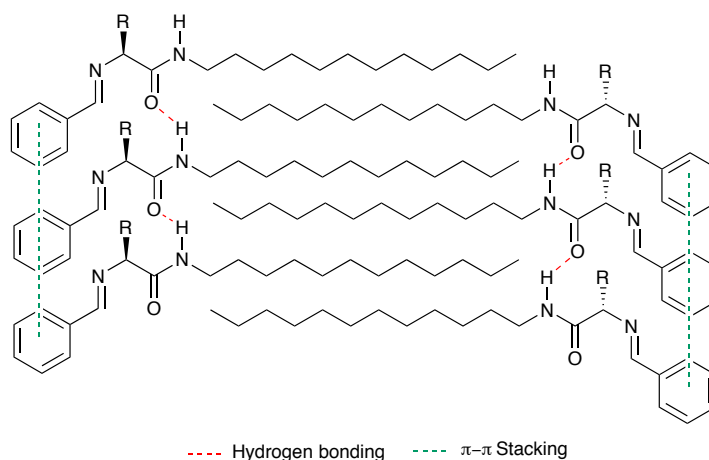


Figure 89: Non-covalent interactions involved with self-assembly when aromatic ring is present

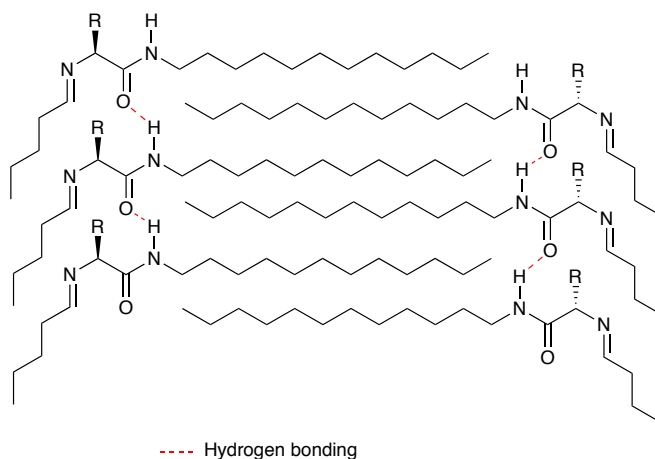
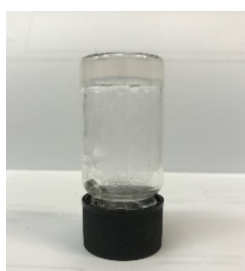
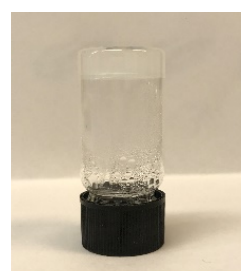


Figure 90: Non-covalent interactions involved with self-assembly when aliphatic chain is present

Furthermore, when the nitro group moves from the 4-position to the 2-position gelation still occurs but the appearance of the gel is different; a transparent gel forms (Figure 91).



2- Nitrobenzaldehyde gel



4- Nitrobenzaldehyde

Figure 91: 2-Nitrobenzaldehyde glutamine amide gel compared to 4-Nitrobenzaldehyde (**47**) glutamine gel

To understand the two-component gel further we wanted to see if the imine had been formed with all aldehydes mixed with glutamine amide (**210**) or only those which formed gels. Therefore, ESI mass spectroscopy was used on sample of either the hydrogel or the residue of those that did not form hydrogels. It was found that both aldehydes that formed hydrogels with glutamine amide (**210**), and those that did not formed imines as shown for example in Figure 92 - Figure 96. This implies that the resulting imine was forming a product which was even more insoluble than the starting components in water. Evidence for insolubility is the presence of a precipitate in solution.

Analysis Information

Analysis Filename: dks69823kh_P1-F-3_01_4898.d
 Method: ESI_low mass_2c1s.m
 Submission Name: dks69823kh
 Acquisition Date: 17/04/2018 09:39:24
 Instrument: compact
 ESI
 Positive

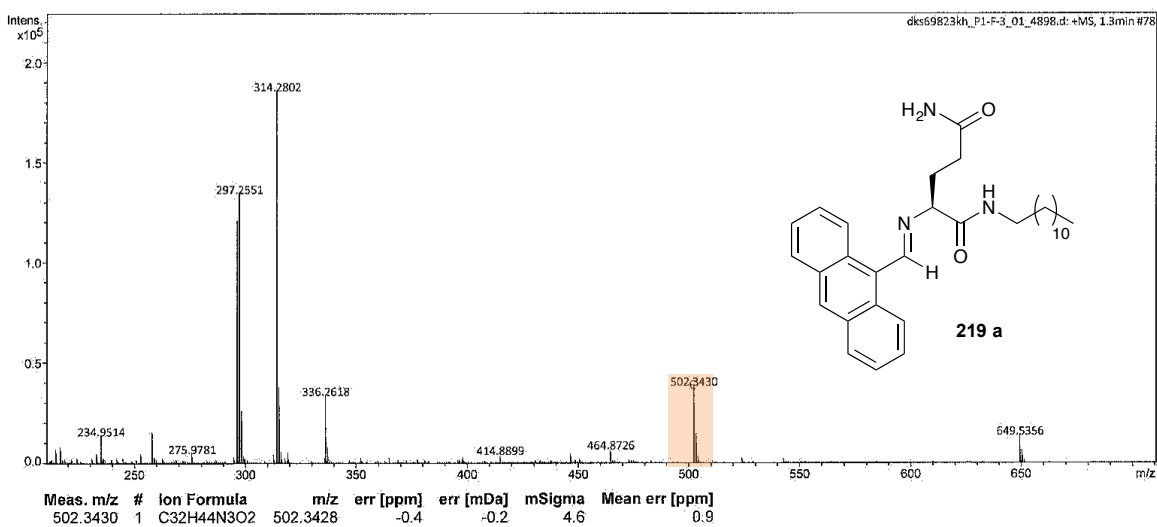


Figure 92: Mass spectrum of 9-anthraldehyde (**220**) and glutamine amide (**210**) imine formed in gelation. RMM = 503.34

Analysis Information

Analysis Filename: dks68647kh_P1-F-4_01_3922.d
 Method: ESI_low mass_2c1s.m
 Submission Name: dks68647kh
 Acquisition Date: 26/02/2018 09:45:46
 Instrument: compact
 ESI
 Positive

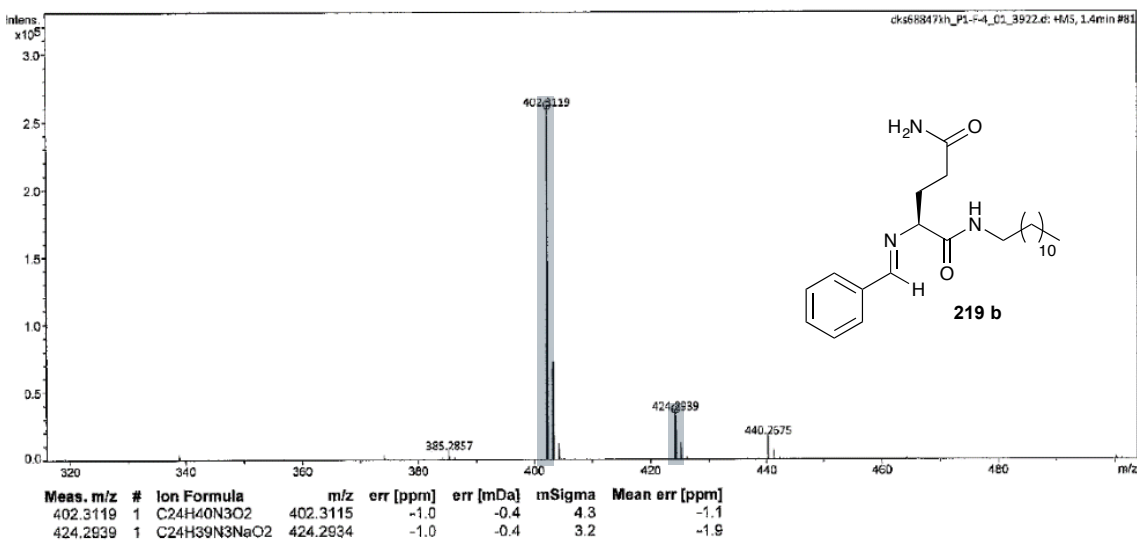


Figure 93: Mass spectrum of benzaldehyde (**221**) and glutamine amide (**210**) imine formed in gelation. RMM = 402.31, 424.29

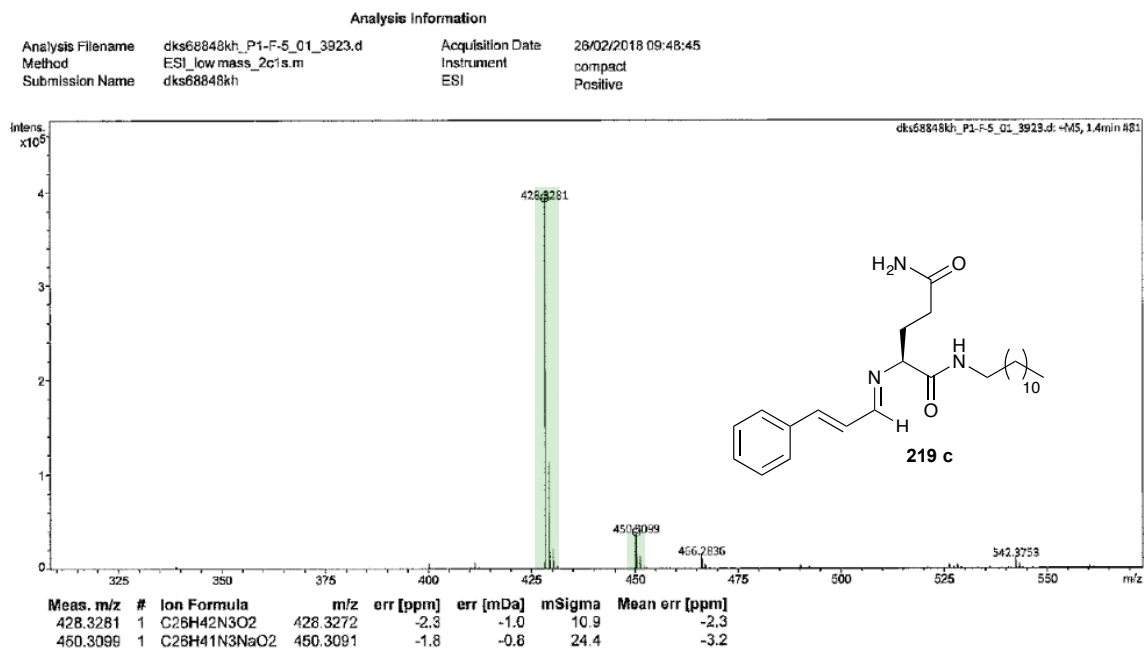


Figure 94: Mass spectrum of cinnamaldehyde (**222**) and glutamine amide (**210**) imine formed in gelation. RMM = 427.32, 450.80

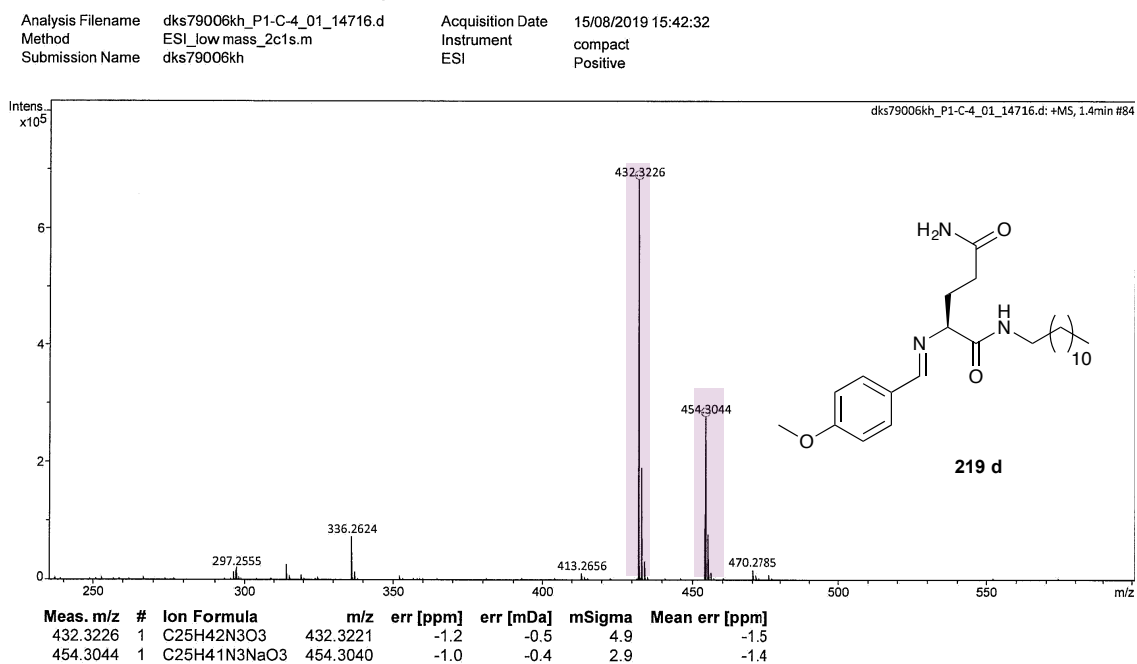


Figure 95: Mass spectrum of 4-methoxybenzaldehyde (**226**) and glutamine amide (**210**) imine formed in solution. RMM = 432.22, 454.30

Analysis Filename dks79007kh_P1-C-5_01_14717.d Acquisition Date 15/08/2019 15:45:29
 Method ESI_low mass_2c1s.m Instrument compact
 Submission Name dks79007kh ESI Positive

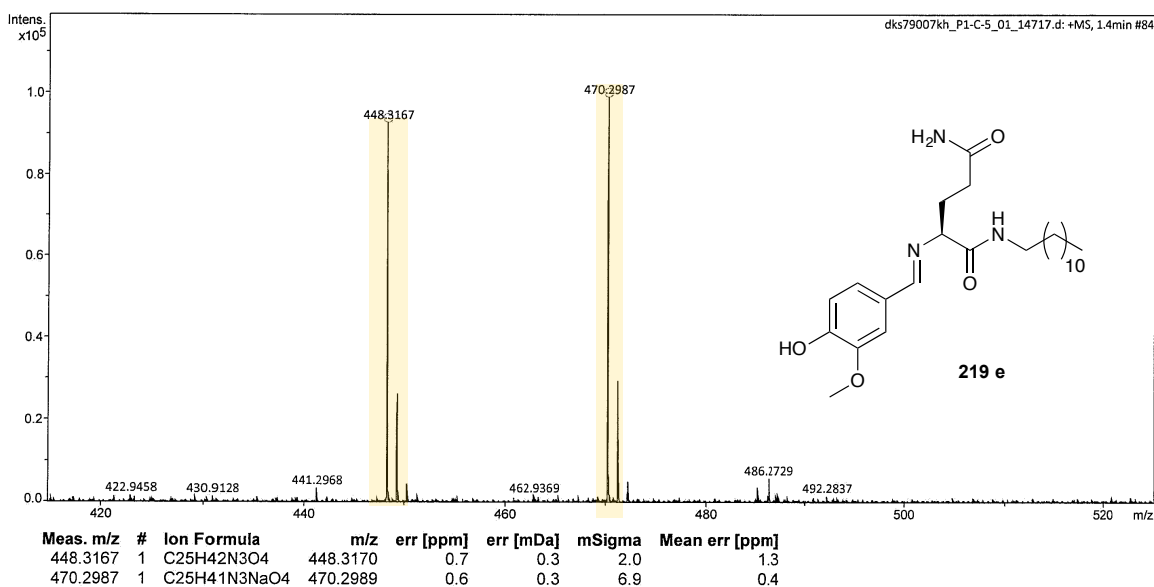


Figure 96: Mass spectrum of vanillin (**225**) and glutamine amide (**210**) imine formed in solution. RMM = 448.31, 470.29

In addition to the ESI MS analysis of the system, ^1H NMR was used to try and determine if there was any correlation between the quantity of Schiff base formed and gelation. The results showed that there was no-correlation, both samples which formed gels and those which did not showed good conversion to imine > 50%. However to analyse the sample that did not form gels water was removed *in vacuo* then the deuterated organic solvent is added to dissolve the residue without this procedure signals in NMR would be poor due to insolubility. In the process of removing the water it is possible that the imine forming reaction is being driven forward as removal of excess water is often required for imine formation. As a result the data obtained cannot be used to identify if there is relationship between imine formation and gelation.

None-the-less the aldehyde screen also showed the potential for the two-component system to be tuned and used for other applications. It is particularly noteworthy that furfural (**224**) can be used, as furfural is a bio-renewable feedstock.

Furthermore, aldehydes can play important roles as fragrance molecules, and some gels have potential for controlled fragrance release. More significantly with regards to this project, however, the ability of aldehydes to form gels is of interest

because they have been suggested as prebiotic molecules.¹⁶¹ In particular benzaldehyde (**221**) is a very simple plausible prebiotic aromatic aldehyde.^{162,163}

3.2.12 Physical properties and characterising different aldehyde gels

The physical properties of the hydrogels formed by different aldehydes were then determined. Figure 97 shows that the choice of aldehyde involved in the gel and therefore formation of the imine can significantly change the T_{gel} . The variation in T_{gel} shows that the two-component hydrogel is tuneable as by varying the aldehyde the temperature at which the gel becomes solution changes.

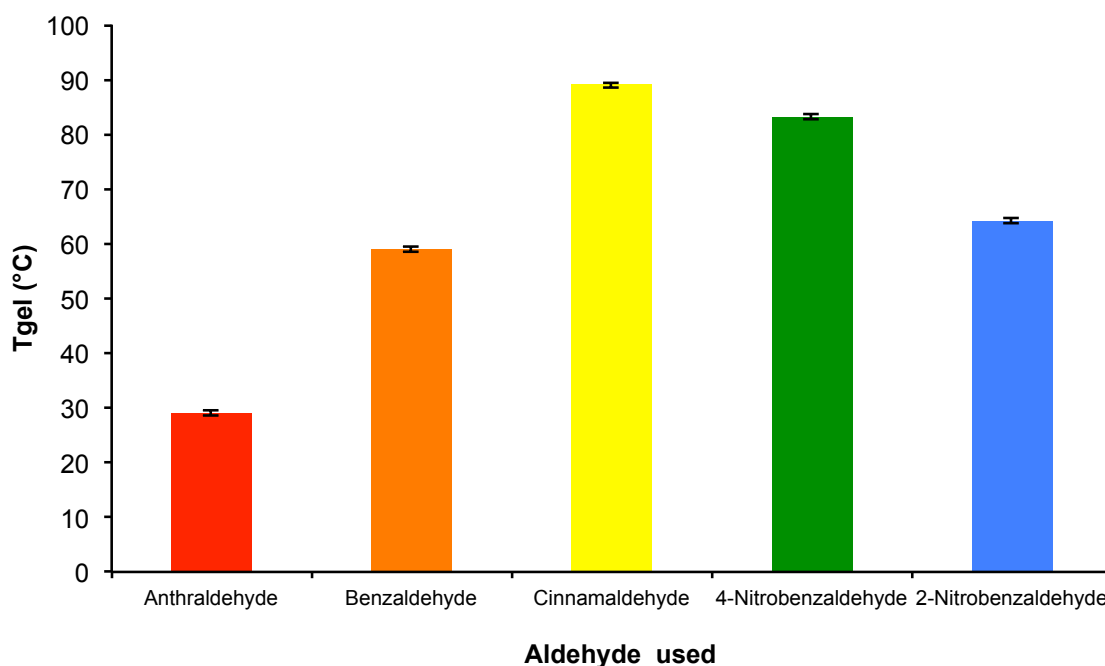


Figure 97: Graph of T_{gels} for different aldehyde derivatives of the aldehyde : glutamine amide (**210**) hydrogel 1:1 5 mg of glutamine amide in 1 mL water

It is also interesting that the gel network itself appears very different by SEM depending upon the aldehyde used. When using 9-anthraldehyde (**220**) the gel network is more web-like with thick nano-fibres with a width of 0.4 - 0.6 μm (Figure 98), the benzaldehyde (**221**) derivative is more fibrous and irregular with a fibre width of 0.6 - 1.5 μm with more branching (Figure 99). Cinnamaldehyde (**222**) has a very distinct and uniform gel-network, the fibres have a width of 0.4 μm and are more linear and are more densely packed (Figure 100) whereas the 2-nitrobenzaldehyde (**223**) derivative is more web-like with nanofibres between 0.2 - 0.3 μm but less well defined (Figure 101) compared to the 9-anthraldehyde (**220**) derivative.

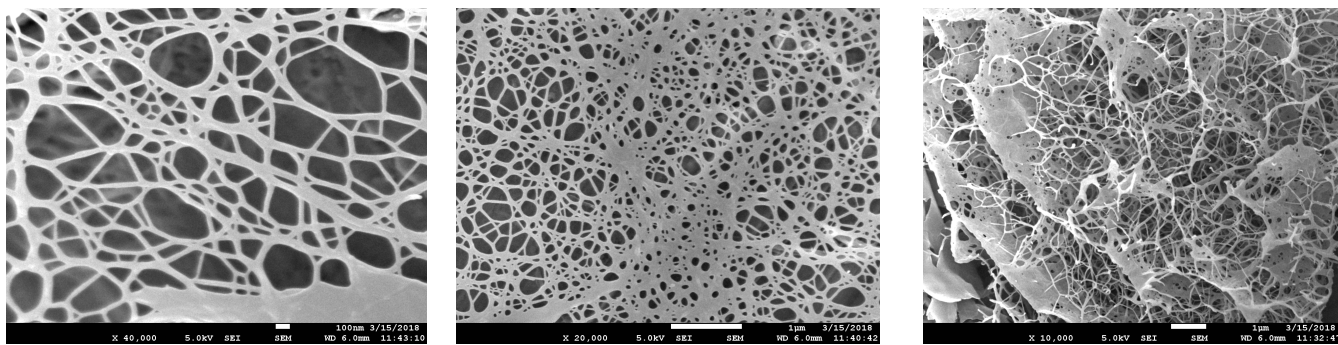


Figure 98: SEM of 9-anthraldehyde (**220**) two-component hydrogel with glutamine amide (**210**)

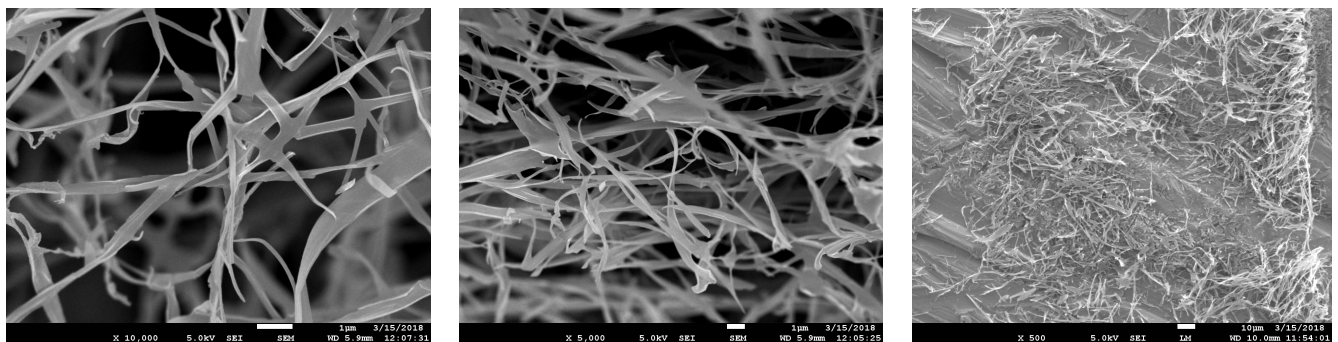


Figure 99: SEM of benzaldehyde (**221**) two-component hydrogel with glutamine amide (**210**)

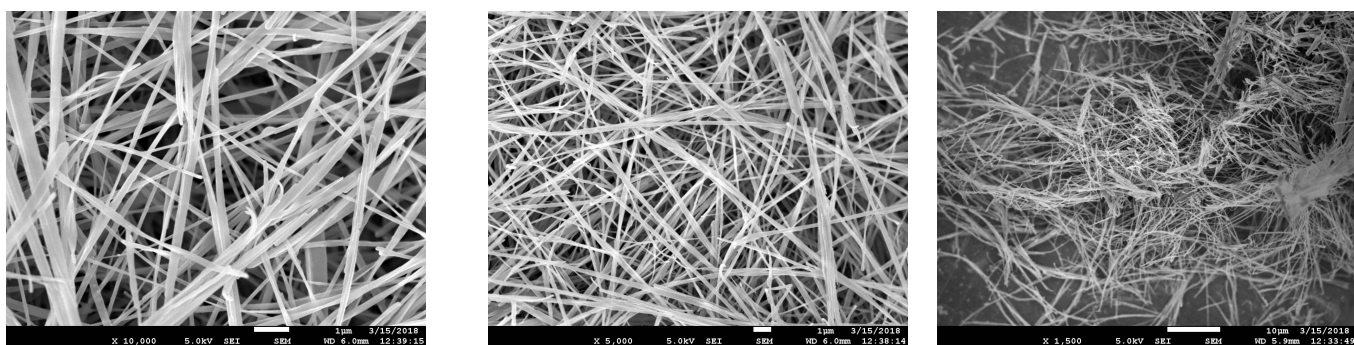


Figure 100: SEM of Cinnamaldehyde (**222**) two-component hydrogel with glutamine amide (**210**)

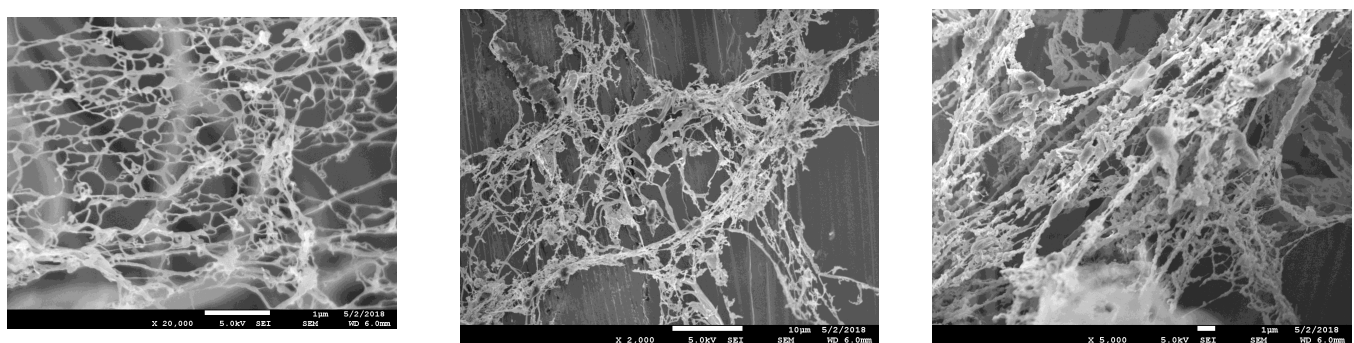


Figure 101: SEM of 2-nitrobenzaldehyde (**223**) two-component hydrogel with glutamine amide (**210**)

3.2.13 Rheology

As mentioned above, the rheological properties of the gel need to be studied, as this will provide insight into the physical properties of the gel. To do this a sample of the gel needs to be prepared. It can be difficult to transfer such gels onto a rheometer stage and therefore there are various ways in which samples can be prepared:

1. Bottomless vial attached to a glass plate with sealant (Figure 102). Removal of gel is relatively easy as it comes out the bottom of the vial.

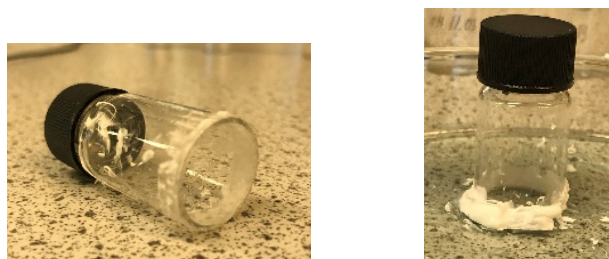


Figure 102: Bottomless vial, and bottomless vial attached to glass plate with sealant

2. Bottomless vial in a suba-seal (Figure 103)



Figure 103: Bottomless vial in suba-seal

3. Made in situ on the rheometer plate

Sample preparation began initially using a bottomless vial attached to a glass plate with sealant. The gel used was formed of 4-nitrobenzaldehyde (**47**) and glutamine amide (**210**) (1:1) at 1.48 mg in 1 mL and a higher concentration of 7.4 mg in 1 mL. The solution was heated before being transferred to the bottomless vial attached to the glass plate and left to cool. After 12 h the gels had formed, however, removal of the vial resulted in the gel breaking down. Therefore a second method was trialled using a bottomless vial and a suba-seal. Using a

bottomless vial in a suba-seal the gel should be less likely to break as removal of the suba-seal should be easier than removing sealant. Unfortunately, the gel did not form. This is most likely due to the rubber preventing the gel network from forming. To allow gelation to take place in using the suba-seal, a small glass disc was placed in the bottom of the suba-seal (Figure 104) and the bottomless vial placed on top, after 12 h the gel had formed. However, when the vial was removed the gel collapsed.



Figure 104: Left bottomless vial in suba-seal, no glass bottom, Right suba-seal with glass bottom

Before moving to the final method of forming the gel on the rheometer plate, forming the gel in pH 2.9 was trialed to see if pH would improve stability of the gel sample allowing transfer to the rheometer plate. The gel that formed at pH 2.9 was chosen, as this gel appeared more homogenous compared to samples prepared with deionised water. However forming successful samples suitable for rheology was still problematic as transfer to the plate often broke the gel.



Figure 105: Rheology sample made with 4-nitrobenzaldehyde (**47**) and glutamine amide (**210**) (1.48 mg 1 mL) with pH 2.90 solution.

The hydrogel formed from 4-nitrobenzaldehyde (**47**) and glutamine amide (**210**) (1:1) at pH 2.9 was first tested by increasing the shear strain but with a constant frequency of 1 Hz. In rheological terms the robustness of the gel is defined as the strain which can be applied before the gel network is broken down, and is characterised by the crossover point between G' and G'' . For the gel formed from

4-nitrobenzaldehyde and glutamine amide (**210**), the strain applied before the gel network is broken down is relatively low ca. 12% and indicates a weak gel (Figure 106). This is however a parameter which can be increased with concentration as the sample used was formed at a total gelator loading of 1.48 mg / mL.

Following this, a shear strain in the linear viscoelastic region (LVE) is selected as a constant shear strain applied to the gels whilst varying the oscillation frequency of the plates. The linear viscoelastic region is the region over which little to no change in the properties of the gel are seen with changes in strain. This ensures that any small deviations in the strain the materials subjected to will not adversely affect the results of the experiment. The two key properties of the material that can be determined from the rheological data are the stiffness and robustness of the gel. Stiffness is a measure of the amount of force needed to deform the material and is characterised by using the storage modulus (G') and loss modulus (G'').

From the results of the frequency sweep (Figure 107), shows that the gels formed with 4-nitrobenzaldehyde (**47**) and glutamine amide (**210**) (1:1) are weak as we observe break down of the gel at about 2 Hz. The storage and loss moduli of elastic materials show no change with increasing frequency. In contrast, viscous liquids respond linearly to these changes. Therefore, the point at which the gradient of the plot increases can be considered the point at which these materials behave more like a liquid than a gel.

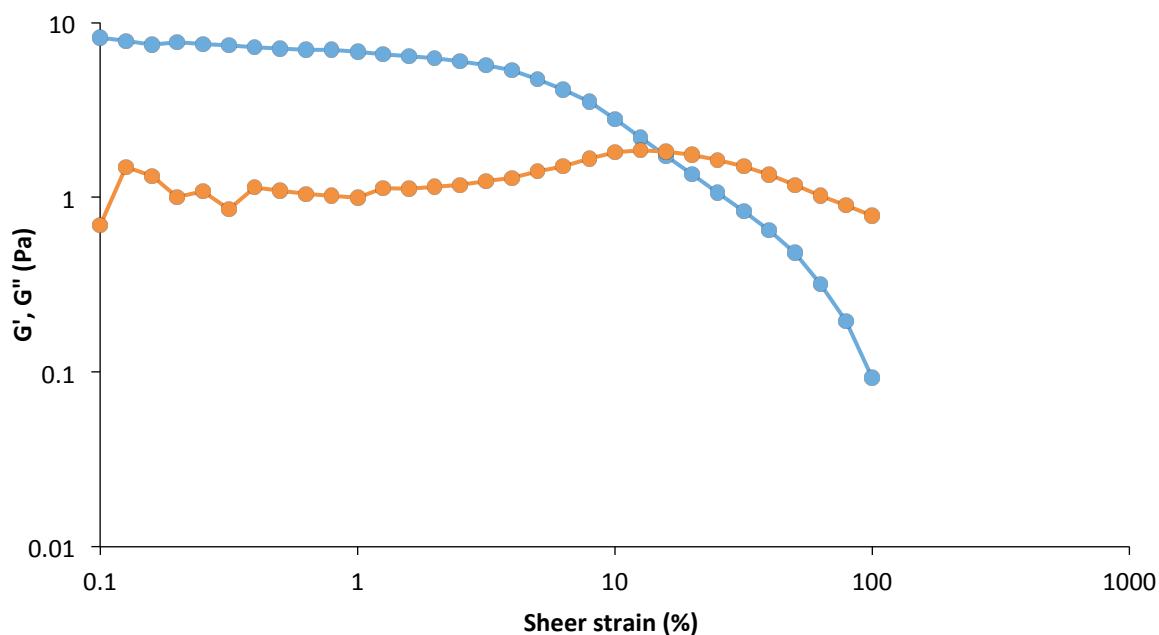


Figure 106: 4-Nitrobenzaldehyde (**47**) (480 μg) and glutamine amide (**210**) (1 mg) Gel 1:1 in 1 mL pH 2.9. Elastic (G' , blue circles) and loss (G'' , orange circles) moduli of hydrogels with varying shear strain (frequency = 1 Hz).

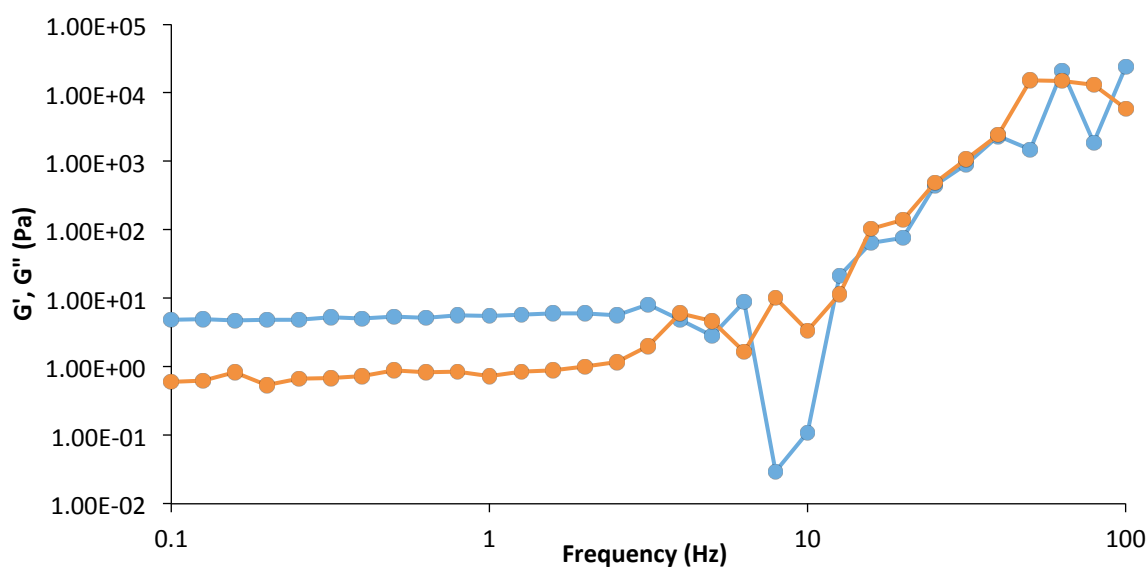


Figure 107: 4-Nitrobenzaldehyde (**47**) and glutamine amide (**210**) gel 1:1 pH 2.9. Elastic (G' , blue circles) and loss (G'' , orange circles) moduli of hydrogels with varying frequency

It was then decided to see if a change in aldehyde improved the ability to form rheology samples. The first aldehyde trailed was benzaldehyde (**221**) with deionised water. The hydrogels formed using benzaldehyde (**221**) did work better with the bottomless vial and sealant method compared to when 4-

nitrobenzaldehyde (**47**) was used in deionised water, but the sample did not come out in a form that would be able to be used for rheology (Figure 108).



Figure 108: Benzaldehyde and glutamine amide (**210**) (5 mg) 1:1 rheology sample prepared using a bottomless vial and sealant.

2-Nitrobenzaldehyde (**223**) was investigated as the gel produced is visually different compared to the 4-nitrobenzaldehyde (**47**) gel. It was therefore proposed that the 2-nitrobenzaldehyde (**223**) gel may also be easier to work with for making rheology samples. Method 1, sealant and a bottomless vial, was employed for sample preparation using 2.4 mg of glutamine amide (**210**) and 1.2 mg of 2-nitrobenzaldehyde in 1 mL water. The gel formed and removal of the glass vial was successful (Figure 109), as was transfer of the sample to the rheology plate.



Figure 109: Rheology sample made with 2-nitrobenzaldehyde (**223**) and glutamine amide (**210**)

The rheological data obtained show that the gel formed with 2-nitrobenzaldehyde and glutamine amide (**210**) is a very weak gel, slightly stronger than the gel formed with 4-nitrobenzaldehyde (**47**) in pH 2.9, although a higher total loading was used. The hydrogel formed was first tested by increasing the shear strain but with a constant frequency of 1 Hz. Figure 110 shows that the point the gel breaks down is at a shear strain of ca. 15%, which is only slightly higher than when using 4-nitrobenzaldehyde (**47**) at a pH 2.9, again indicating a weak gel.

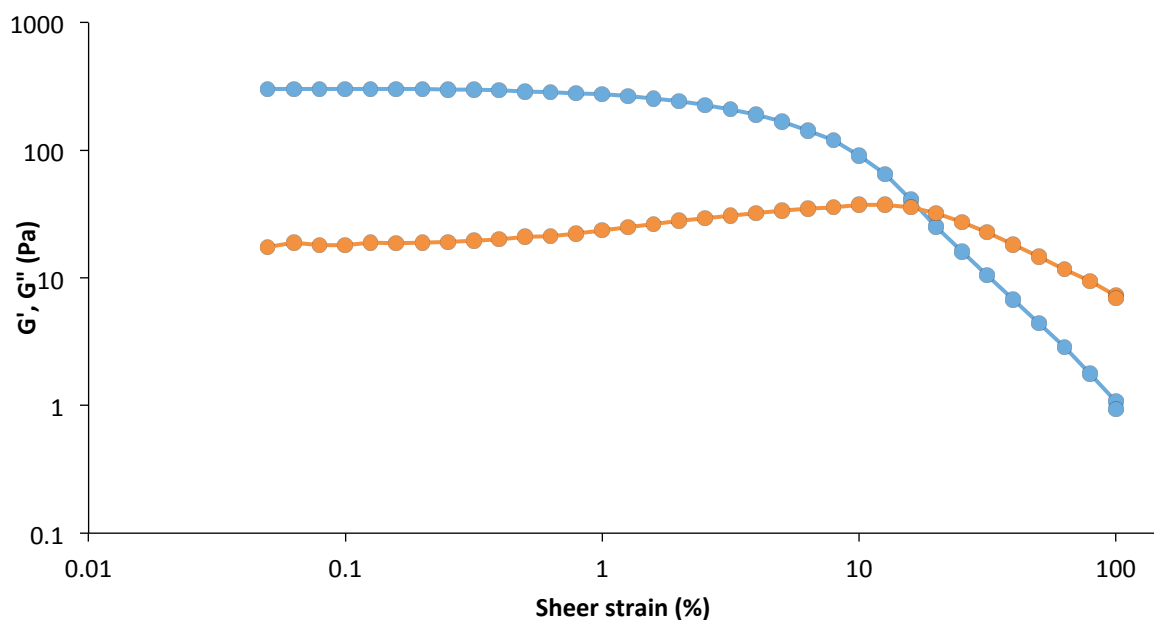


Figure 110: 2-Nitrobenzaldehyde (**223**) (1.2 mg) and glutamine amide (**210**) (2.4 mg) Gel 1:1 in 1 mL water Elastic (G' , blue circles) and loss (G'' , orange circles) moduli of hydrogels with varying shear strain (frequency = 1 Hz).

The results of the frequency sweep (Figure 111), shows that the gels formed with 2-nitrobenzaldehyde (**223**) and glutamine amide (**210**) (1:1) are weak as the gel breaks down at ca. 10 Hz again this is larger than that observed when using 4-nitrobenzaldehyde (**47**).

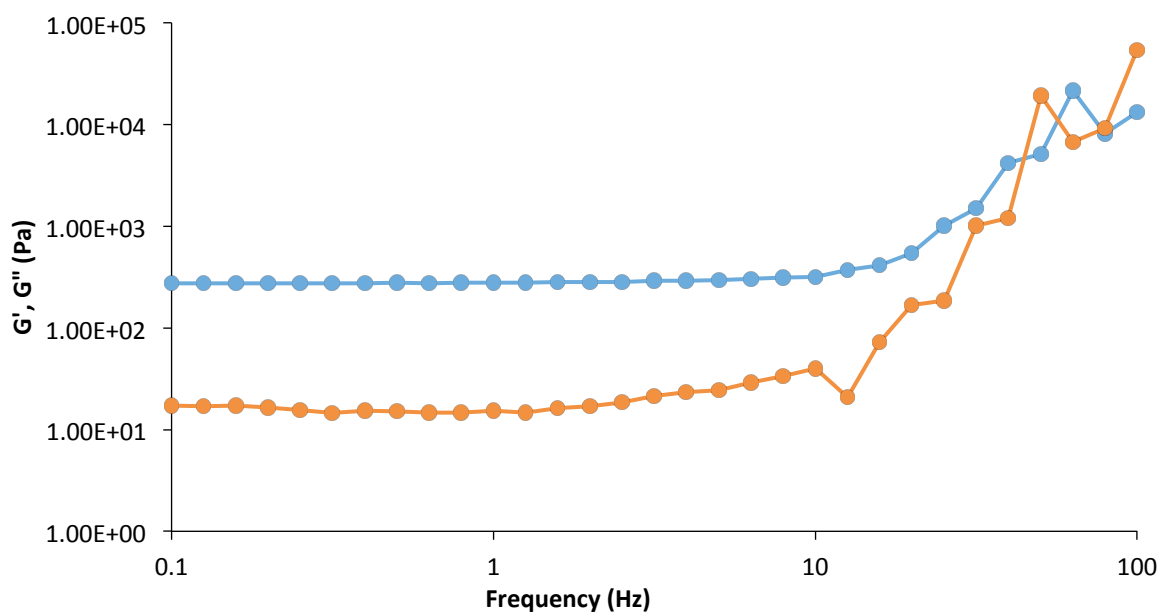


Figure 111: 2-Nitrobenzaldehyde (**223**) (1.2 mg) and glutamine amide (**210**) (2.4 mg) hydrogel (1:1) in 1 mL water. Elastic (G' , blue circles) and loss (G'' , orange circles) moduli of hydrogels with varying frequency

3.3 Conclusions

In this work, a new two-component hydrogelator has been established. The two-component system's physical properties have been identified showing that the thermal stability is dependent upon the quantity of 4-nitrobenzaldehyde (**47**): if there is too little 4-nitrobenzaldehyde (**47**) then the T_{gel} is around room temperature, but if there is too much 4-nitrobenzaldehyde (**46**) the T_{gel} is reduced due to crystallinity.

Imaging of the gel structure of a 1:1 amide (**218**): 4-nitrobenzaldehyde (**46**) gel in 1 mL of water by SEM showed a nanofibrillar morphology consistent with the self-assembly of a supramolecular gel. As the concentration of both components increased, there was a change in the structure of the gel network. Aggregates increasingly form on the sides of the fibres. This is interesting and could give more insight into the supramolecular properties of the system.

The two-component system with 4-nitrobenzaldehyde (**47**) and glutamine amide (**210**) is self-healing. The gel can self-heal if there is external intervention (heat-cool) or if left on its own. It can even re-heal if injected into another vial from a syringe. This particular property is most likely due to the system being in dynamic equilibrium based on a reaction between two components. However, if the gel is dried and then re-hydrated it does not reform. Gelation must therefore depend on the kinetics of the dynamic equilibrium, which gives rise to the gelator and causes gelation. It is thought that gelation is due to slow formation of the Schiff base enabling the assembly of gel nanofibres without the system becoming too insoluble.

It was also identified that the aldehyde played an important role in gelation. In general the aldehydes that interact with the glutamine amide (**210**) and caused gelation are electron poor and contain an aromatic ring. This is indicative of π - π interactions as well as hydrogen bonding in the gel network, as well as a better ability to form the Schiff base derivative. It is important to note that the position of the substituent can also have an effect on gelation as 2-nitrobenzaldehyde (**223**) does result in the formation of a clear gel whereas 4-nitrobenzaldehyde (**47**) forms an opaque gel.

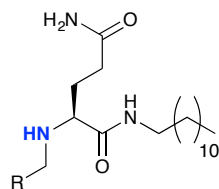
Rheological data on the gel systems showed that the two-component hydrogel is very weak compared to other hydrogel systems such as DBS hydrazide.⁵ However the samples produced are at very low concentrations. By increasing the overall concentration rheological samples should be produced more easily and could allow analysis of all the combinations of aldehyde and amide that form hydrogels. Nonetheless, there will be a limit in this system as to how high the concentration will go as we have seen evidence in the 4-nitrobenzaldehyde (**47**) glutamine amide (**210**) system that as concentrations of aldehyde increase we begin to get precipitate of the aldehyde which would give false rheological data.

This new hydrogel system is a rare example of a two-component hydrogel, which functions at very low concentrations, and has significant potential for technological applications. In particular, the self-healing characteristics give the gel potential in biotechnology applications such as drug delivery and tissue engineering.

4.0 Developing a prebiotic protocell

4.1 Aims

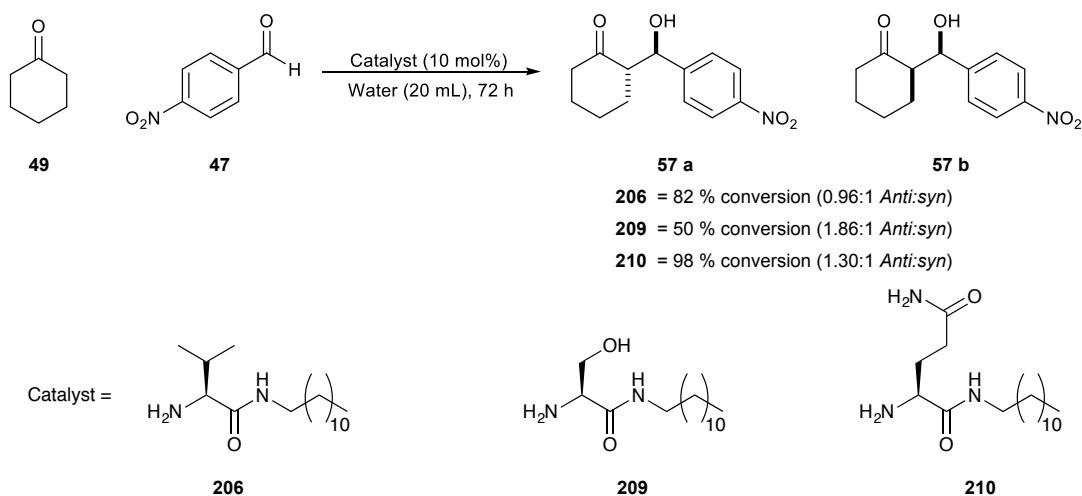
Building on the findings of the previous chapters, we wanted to combine supramolecular gels and prebiotic catalytic chemistry with the long term goal of synthesising sugars in a potentially prebiotic setting that could mimic an early cell, a protocell. Conceptually, a protocell is a primitive ancestor of the complex biological cell.^{59–61} A protocell can be described as a self-assembled compartmentalised system wherein a chemical reaction can occur using energy from the environment and containing some type of information system. Supramolecular chemistry enables very simple molecules to self-assemble to form hydrogels and can be modified to contain units such as amino acids which are capable of catalysis. As a result we propose that simple hydrogel systems could be used to mimic some aspects of a protocell namely compartmentalisation and the potential for a chemical reaction to occur.



229

Figure 112: Amine target molecule with catalytic site (in blue) available

It has already been shown in Chapter 2 that single amino acid amides are capable of catalysing simple aldol condensation (Scheme 38) reactions in heterogeneous solution phase, although reproducibility was problematic due to the heterogeneous nature of the system. In addition, some of the catalysts formed hydrogels, while others formed organogels. If a reaction was applied to the surface of the hydrogel, structural maintenance during catalysis did not occur, with gels being destroyed. It was also discovered, in Chapter 3, that glutamine amide in the presence of an aldehyde resulted in a hydrogel. The hydrogel assembled as a result of the formation of an imine (**231**) *in situ* (Figure 114), which acts as a low-molecular-weight-gelator.



Scheme 38: Direct aldol condensation in water catalysed by valine (**206**), serine (**209**) and glutamine (**210**) amides as hydrogels or organogels

The novel two-component hydrogel system was versatile with respect to the aldehyde used, however gelation occurred predominantly when the aldehyde contained an aromatic group. We therefore reasoned that by modifying the imine (**231**) formed in the two-component system that we could very simply develop a new hydrogelator (Figure 113) that is also catalytically active and may maintain the

gel structure throughout catalysis. A straightforward way of doing this is to reduce the imine (**231**) to an amine. Amines are potentially catalytic in aldol condensations, and there is only a small structural change from the imine (**231**), which led us to believe that gelation properties may be conserved. The work presented by Tu⁴⁰ in 2008 highlighted that an increase in non-covalent interactions within a gel is imperative to the structural maintenance during catalysis. We believe, in our case, that the presence of the aromatic ring may help maintain gelation during catalysis as a result of π - π stacking and hydrophobicity.

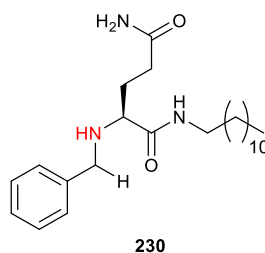
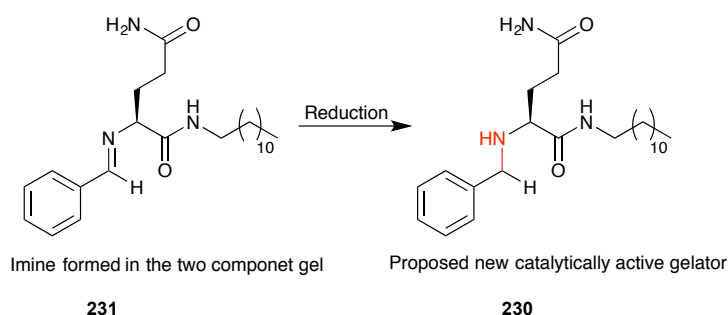


Figure 113: Proposed new hydrogelator with catalytic activity (shown in red)

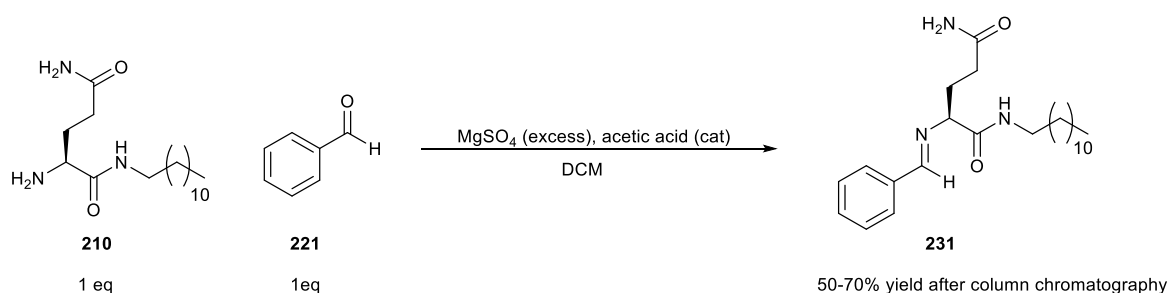
During the studies of the two-component hydrogelator system, in chapter 2, we discovered that aromaticity was important for self-assembly to take place. However for a plausible prebiotic concept we want to keep the aromaticity as simple as possible. Therefore from the aldehydes which formed gels, we want to explore the potential of benzaldehyde (**221**). Benzaldehyde (**221**) was selected as this was the simplest aromatic aldehyde that was screened and was therefore more plausible as a prebiotic aromatic moiety to incorporate into the new motif for catalytic and gelation studies. (Figure 114). It is worth noting that, at least in principle, under reductive conditions the target amine can be produced in one step from the glutamine amide and benzaldehyde (**221**) making it a plausible prebiotic system.



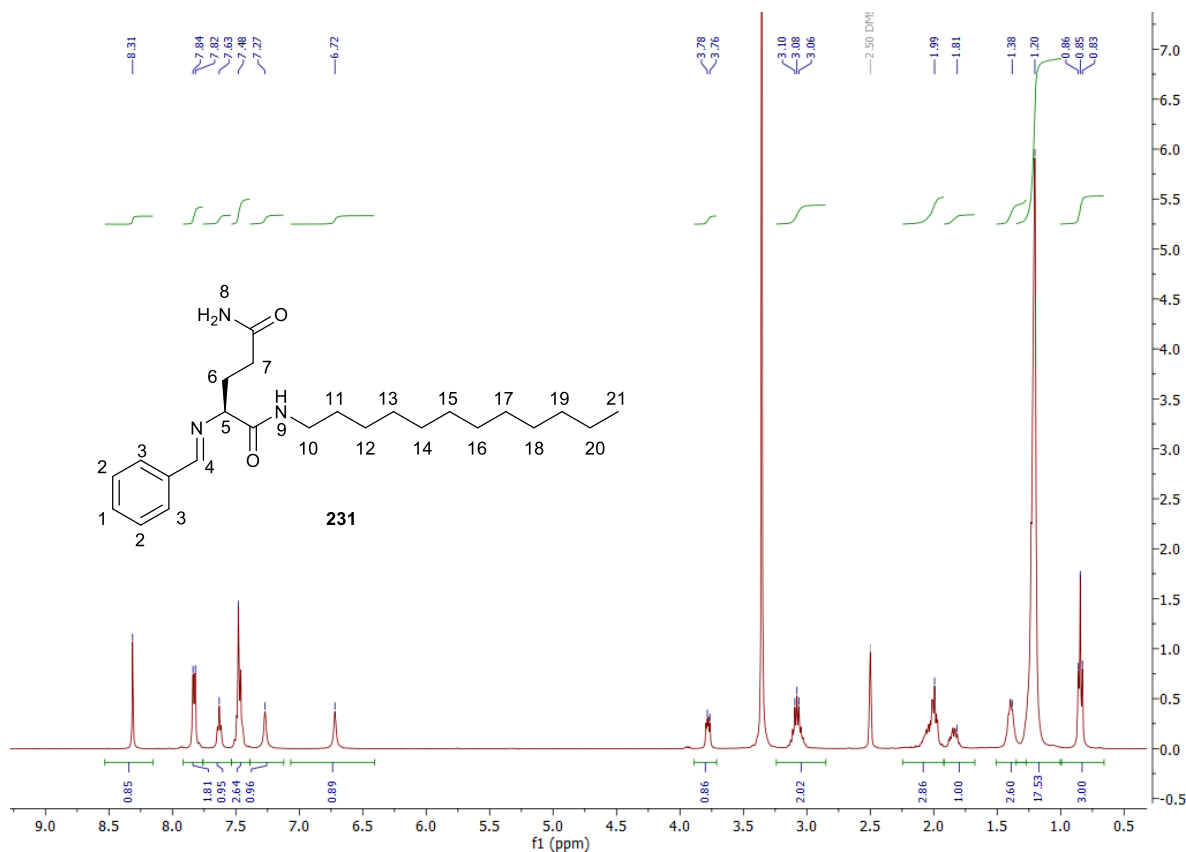
4.2 Results and discussion:

4.2.1 Synthesis of benzylglutamine amide (**230**)

The first stage of the synthesis was formation of the imine (**231**). To a dichloromethane (DCM) solution of glutamine amide was added benzaldehyde (**221**) and an excess of MgSO_4 as a drying agent (Scheme 39). The reaction was left to stir overnight or until complete. The MgSO_4 was filtered off and solvent was removed *in vacuo* to yield white solid of the imine (**231**).



Scheme 39: Synthesis of the imine (**231**)

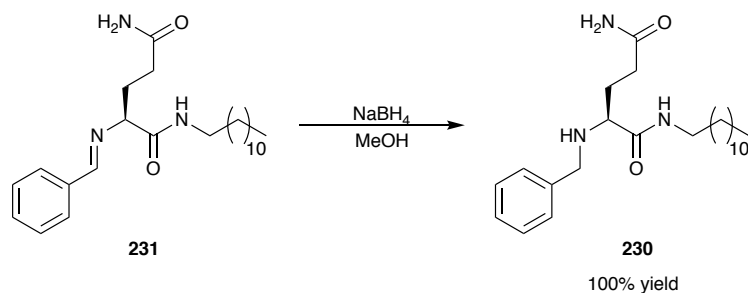


¹H NMR (400 MHz, DMSO-*d*₆) δ ppm: 8.31 (s, 1H, H₄), 8.33 (d, 2H, *J* = 8.9 Hz, H₃), 7.63 (t, 1H, *J* = 5.9 Hz, H₉), 7.56-7.37 (m, 3H, H₁₋₂), 7.27 (s broad, 1H, H₈), 6.72 (s broad, 1H, H₈), 3.98-3.76 (m, 1H, H₅), 3.31-3.02 (m, 2H, H₁₀), 2.21-1.85 (m, 2H, H₆), 1.44-1.36 (m, 2H, H₇), 1.46-1.32 (m, 2H, H₁₁), 1.28-1.15 (m, 20H, H₁₂₋₂₀), 0.84 (t, 3H, *J* = 7.2 Hz, H₂₁.)

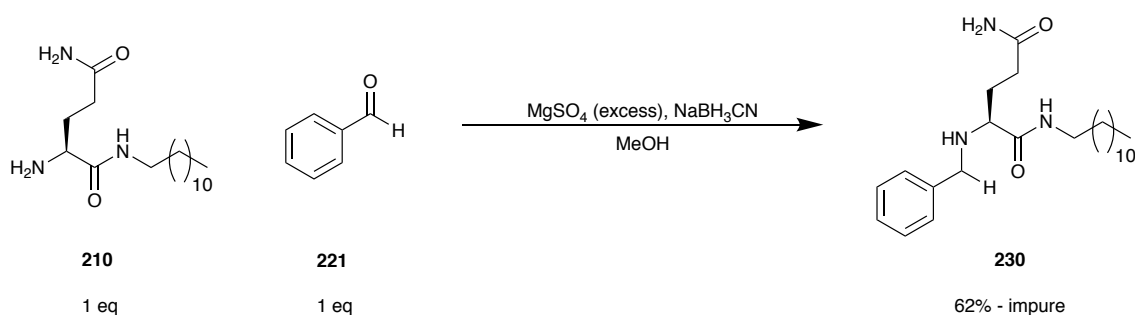
Figure 115: ¹H NMR of benzylglutamine imine (**231**) in deuterated DMSO. 400 MHz

From here, two methods were used to reduce the imine (**231**) to the amine. The first method was addition of sodium borohydride (NaBH₄) once the imine had formed (Scheme 40). However, this method was slow at producing the reduced species taking 6-7 days. As a result, a second approach was taken, using sodium cyanoborohydride (Scheme 41). In this approach we hoped that we would drive the reaction forward as when imine was formed it would be reduced, therefore disturbing the equilibrium of imine and amine and allowing a greater proportion of imine to be converted to the desired product. Sodium cyanoborohydride was much more effective in reducing the imine (**231**) to give the desired product with a shorter reaction time. The advantage of this method is that a 'one-pot' approach can also be used, as the reducing agent will not reduce the benzaldehyde (**221**) to the alcohol. Using a one-pot approach is also beneficial as there would only be one purification step required. However, using this method resulted in the final material being contaminated with unreacted aldehyde even after aqueous work up.

In addition, column chromatography was not possible to carry out as the reduced species streaked making it hard to separate aldehyde and obtain product in a good yield.



Scheme 40: Reduction of imine (**231**) to amine using sodium borohydride



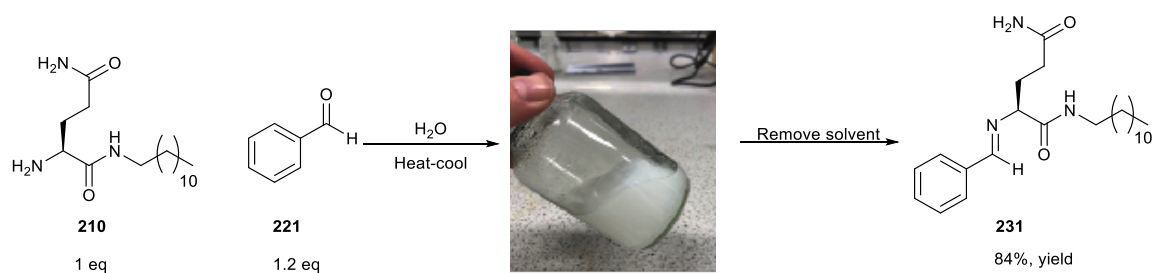
Scheme 41: Reduction of imine (**231**) to amide using sodium cyanoborohydride

The reactions described above therefore required significant optimisation to improve reaction time and also purity of the final product.

Typically to form an imine (**231**), organic solvent, drying agent and an acid (to lower the pH to 4) are required. However in this scenario these did not yield the quantities of imine (**231**) required to then take forward to the next stage of the synthesis. It is already known that the imine (**231**) is present during gelation. It was therefore decided that the imine (**231**) could be synthesised via gelation.

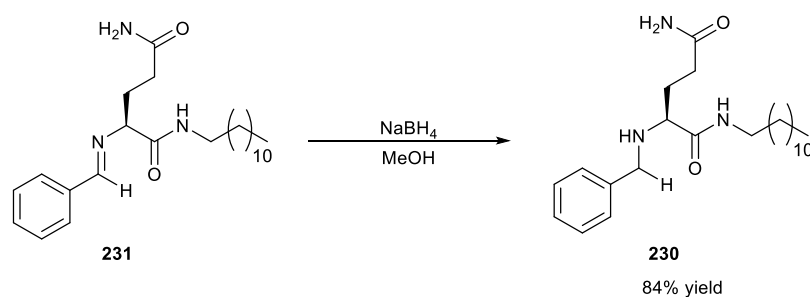
To synthesise the imine (**231**) via gelation, glutamine amide was added to benzaldehyde (**221**) (1.2 eq) followed by water. The suspension was then sonicated, heated and left to cool, forming the self-assembled gel. The gel was then dissolved into DCM and solvent removed *in vacuo* to yield a white solid. This is an unusual method to synthesise imine (**231**) as water is present, which typically results in the hydrolysis of the imine (**231**) although there are some example of imine (**231**) formation in the presence of water.^{164,165} However the procedure successfully yielded the desired imine (**231**) with good yield. We reason that one of the reasons for the imine (**231**) not being hydrolysed here, is the fact that the

formation of the gel network is energetically favoured; as a result the imine (**231**) remains stable towards hydrolysis to avoid breakdown of the gel. Assembly of the gel may also produce steric hindrance limiting the access of water, therefore preventing the chance of hydrolysis of the imine. Furthermore, we reason that gel assembly, as a favoured process, maximises imine (**231**) yield on thermodynamic grounds.

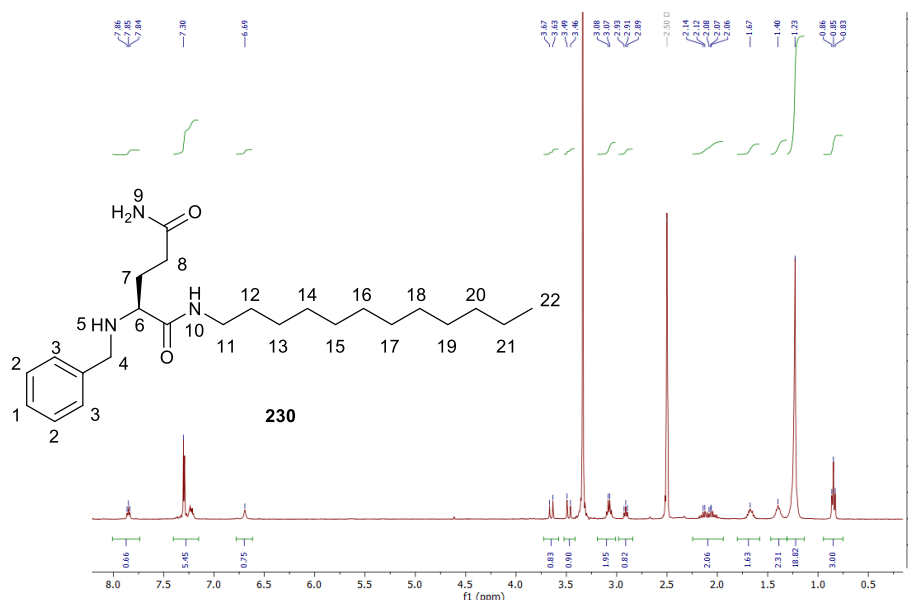


Scheme 42: Synthesis of the imine (**231**)

With the formation of the imine (**231**) established, the next stage of the synthesis was reduction. When sodium cyanoborohydride had been used in the methods above purity of the final product was an issue. Therefore we decided to increase the equivalents of sodium borohydride to see if the reduction was more efficient. To do this the imine (**231**) was added to a methanol solution of excess sodium borohydride (Scheme 43). This reaction was significantly faster and we were able to obtain a clean product in high yield for both steps.



Scheme 43: Reduction of imine (**231**) with sodium borohydride to yield benzylglutamine amide (**230**)

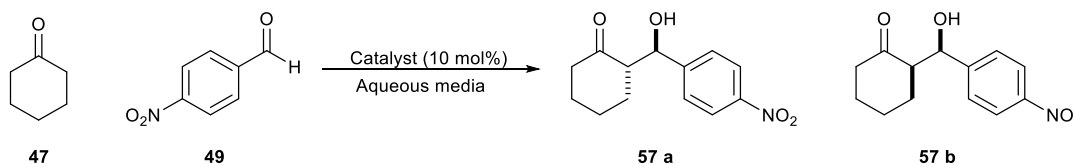


¹H NMR (400 MHz, DMSO-*d*₆) δ ppm: 7.85 (1H, t, *J* = 5.7 Hz, H₁₀), 7.30 (2 H, d, H₃), 7.19 - 7.26 (3 H, m, H_{1,2}), 6.70 (2 H, s, H₉), 3.65 (1 H, d, *J* = 13.28 Hz, H₄), 3.48 (1 H, d, *J* = 13.74 Hz, H₄), 3.08 (2 H, q, *J* = 6.41 Hz, H₁₁), 2.91 (1 H, t, *J* = 6.64 Hz, H₆), 2.22- 1.99 (2 H, m, H₈), 1.77 - 1.58 (1 H, m, H₇), 1.48-1.36 (2 H, m, H₁₂), 1.23 (20 H, m, H₁₃₋₂₁), 0.85 (3 H, t, *J* = 6.64 Hz, H₂₂)

Figure 116: ¹H NMR of benzylglutamine amide (**230**) in deuterated DMSO

4.2.2 Solution phase catalysis of 4-nitrobenzaldehyde and cyclohexanone

With the synthesis of benzylglutamine amide (**230**) achieved, our attention turned to the next aim of the project, to investigate the catalytic potential of benzylglutamine amide (**230**) in water. Therefore, this molecule was tested for catalysis in the same aldol condensation as the single amino acid amides, between 4-nitrobenzaldehyde and cyclohexanone in water.



Scheme 44: Aldol condensation of 4-nitrobenzaldehyde (**49**) and cyclohexanone (**47**) in water

Initially the catalysis was carried out in solution. A solution of 4-nitrobenzaldehyde (**47**) (1 eq) in cyclohexanone (**49**) (10 eq) was added to an aqueous solution of the benzylglutamine amide (**230**) (0.1 eq) in water (10 mL) and a heterogeneous system formed. The reaction was left for 24 h, 48 h and 72 h, with each time frame

representing a new reaction because the reaction is heterogeneous, and therefore analysis by aliquots did not give an accurate representation of the system. After the allotted time, the reaction mixture was extracted with chloroform, then the solvent was removed *in vacuo*. ¹H NMR analysis of the crude product was obtained to calculate conversions and diastereomeric ratios (dr) (Table 24) using the approach described in more detail in Chapter 2. To identify if there was any enantioselectivity HPLC was performed using the same conditions as reported in Chapter 2 in conjunction with retention times reported by Rolando and co-workers (Table 11).¹⁵³

Table 24: Benzylglutamine amide catalysed aldol condensation of 4-nitrobenzaldehyde and cyclohexanone in solution in water

Amide catalyst	Entry	Time h	Conversion %	NMR dr of crude anti:syn	HPLC of crude ee%
Benzyl glutamine amide	1	24	24	1.99 : 1.00	<i>Anti</i> : 16 % <i>Syn</i> : 11%
	2	24	21	1.95 : 1.00	<i>Anti</i> : 17 % <i>Syn</i> : 7 %
	3	24	25	2.10 : 1.00	<i>Anti</i> : 16 % <i>Syn</i> : 10%
	4	48	24	2.14 : 1.00	<i>Anti</i> : 22 % <i>Syn</i> : 8 %
	5	48	46	2.20 : 1.00	<i>Anti</i> : 15 % <i>Syn</i> : 7 %
	6	48	31	2.10 : 1.00	<i>Anti</i> : 23 % <i>Syn</i> : 12 %
	7	72	42	1.98 : 1.00	<i>Anti</i> : 15 % <i>Syn</i> : 8 %
	8	72	53	2.11 : 1.00	<i>Anti</i> : 16 % <i>Syn</i> : 6 %
	9	72	36	1.93 : 1.00	<i>Anti</i> : 16% <i>Syn</i> : 7%

The results in Table 24 show that this new amide is a moderate catalyst in water. At 24 h (entries 1-3) there is a consistent conversion of start material to product of ca. 25 % (Figure 117). In addition, there is good selectivity of ca. 2:1 *Anti*: *Syn*

diastereomeric ratio (Figure 118) as measured by ^1H NMR. In addition, HPLC indicated that there is an enantioselectivity (ee %) of ca. 15% for the *anti*-product and ca. 10% for the *syn*-product when using this catalyst (Figure 119). This exciting result indicates shows that this catalyst is more selective and reproducible than the simple amides described in Chapter 2, where there were fluctuations in conversion (50-98%) and an ee% of ca. 1.3 for the anti product depending upon the catalyst used.

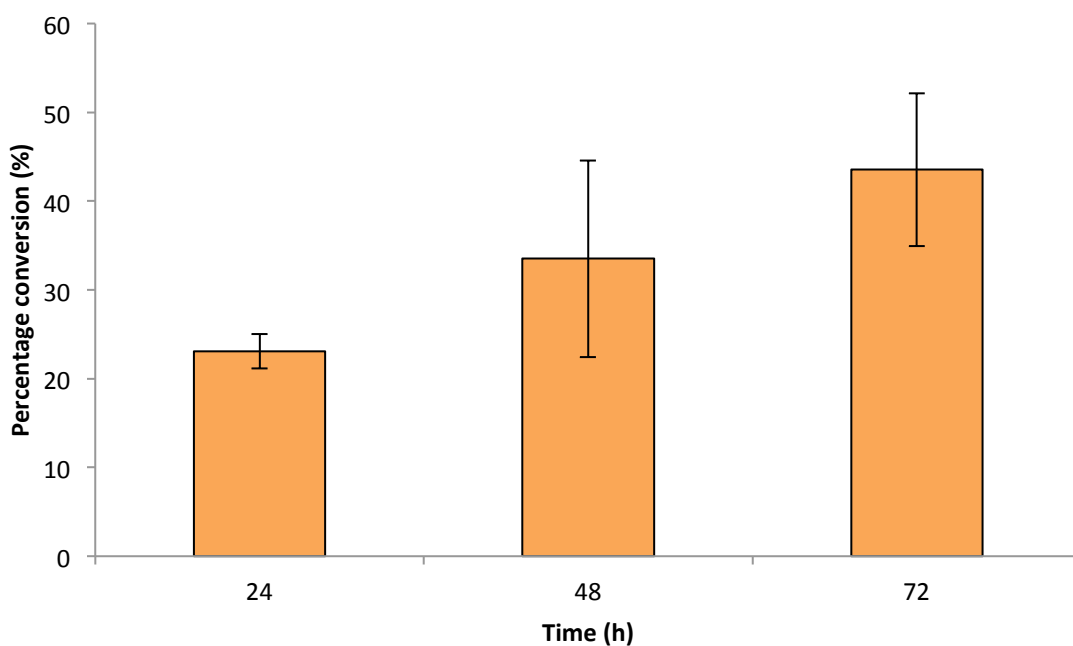


Figure 117: Percentage conversion of start material to product over time using benzylglutamine amide (**230**) 10 mol% in water

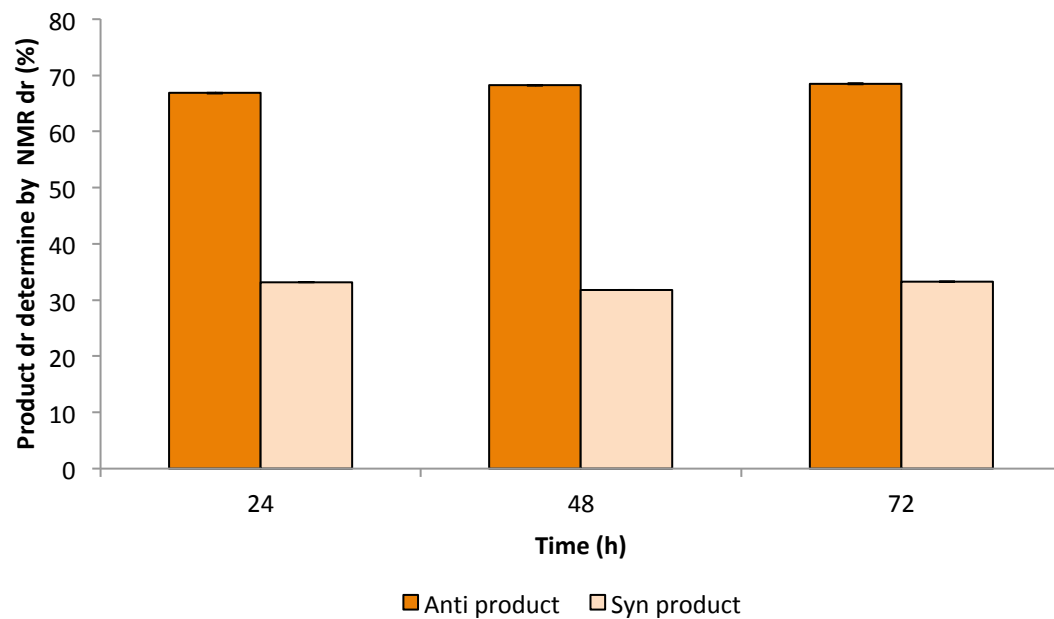


Figure 118: NMR dr % for Anti product using 10 mol% benzylglutamine amide (**230**) in water

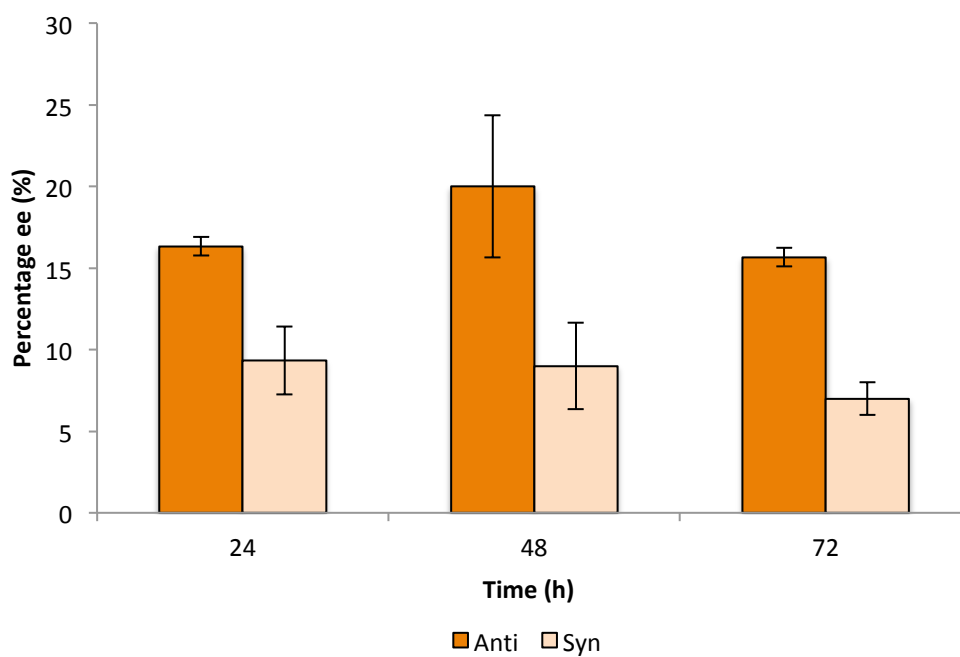


Figure 119: HPLC *Syn Anti* ee% with benzylglutamine amide (**230**) in water

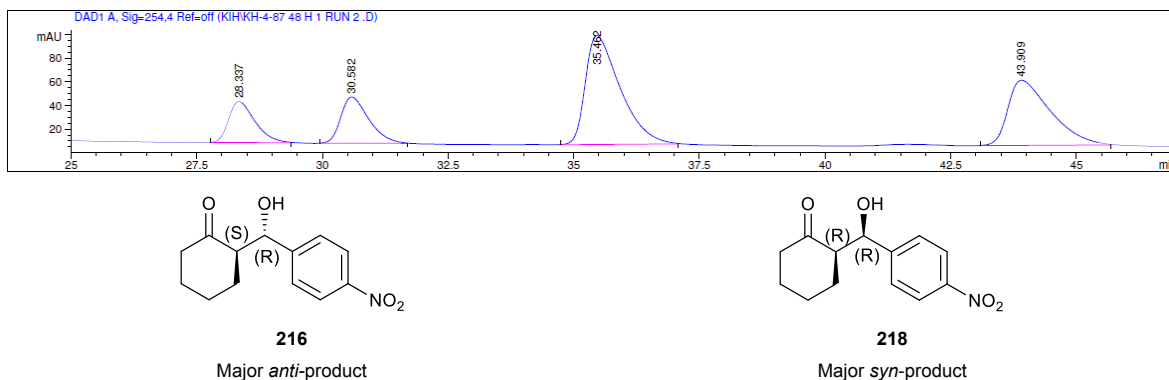


Figure 120: Example of HPLC trace of 4-nitrobenzaldehyde (**47**) and cyclohexanone (**49**) aldol condensation in water catalysed by benzylglutamine amide (**230**) at 48 h crude reaction

Now that a more selective catalyst, than the catalysts presented in chapter 2, has been identified, it was important to ensure that the reaction taking place is primarily due to the catalyst rather than acid or base mediated catalysis. Therefore, the pH of the reaction was recorded and found to be pH 8.6. A buffer solution was made at this pH and the reaction was run again for 72 h but without catalyst. The results of this experiment showed that general base catalysis was also taking place, giving 50% conversion with a 2:1 *Anti*: *Syn* d.r. However, as expected, no ee% was present. This showed that the catalyst is responsible for the enantioselectivity seen.

To further the investigation of the system, reactions were also carried out at pH 4 and pH 7 both with and without catalyst present. The results of the controlled reactions (Table 25, Figure 121 and Figure 122) are very exciting, showing that at pH 7 and pH 4 there is a significant enhancement of ee% (Figure 123). At these pH values without the catalyst, the conversions are much lower due to the absence of general base catalysis. Furthermore, the presence of catalyst therefore significantly increases conversion. At pH 7, the catalysed reaction also showed a greater diastereo selectivity for the *anti*-product, and at pH 4 there is an increase in the enantioselectivity of both *syn* and *anti* products.

Table 25: Controlled pH reactions * D.R ratio approximate due to poor conversion therefore peaks unclear

Entry	Catalyst present	Time h	pH	Conversion %	NMR dr of <i>Anti:Syn</i>	HPLC of crude ee %
1	No	72	8.6	50	2.00:1.00	<i>Anti</i> :1 <i>Syn</i> : 1
2	Yes	24	7	11 %	1.88:1.00	<i>Anti</i> : 51 <i>Syn</i> : 16 <i>Anti</i> : 59 <i>Syn</i> : 19 <i>Anti</i> : 58 <i>Syn</i> : 18
3	Yes	24	4	5 %	1.94:1.00	<i>Anti</i> : 72 <i>Syn</i> : 34 <i>Anti</i> : 73 <i>Syn</i> : 35 <i>Anti</i> : 74 <i>Syn</i> : 34
4	No	24	7	4%	1.98:1.00*	<i>Anti</i> : 1 <i>Syn</i> : 1
5	No	24	4	0.3 %	0.84: 1.00*	<i>Anti</i> : 1 <i>Syn</i> : 1

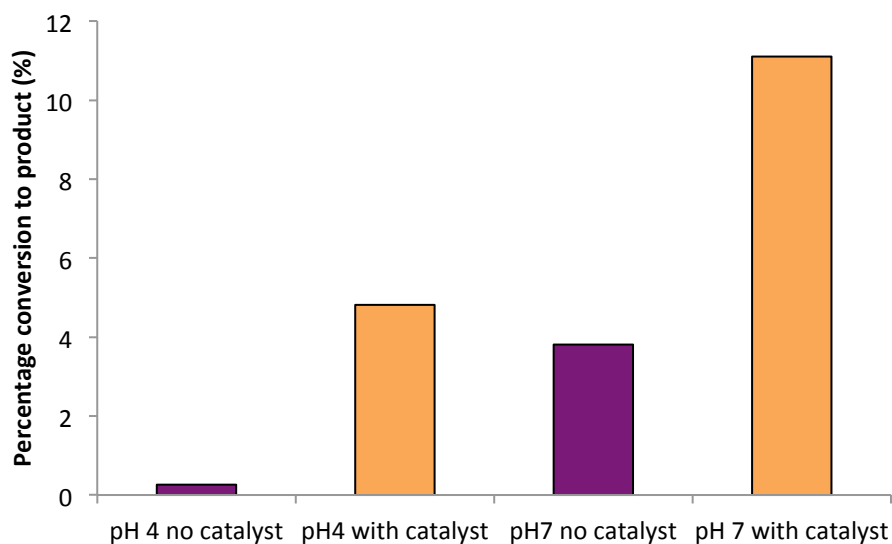


Figure 121: Graph showing percentage conversion of start material to product in 24 h at different pH and with or without catalyst (231)

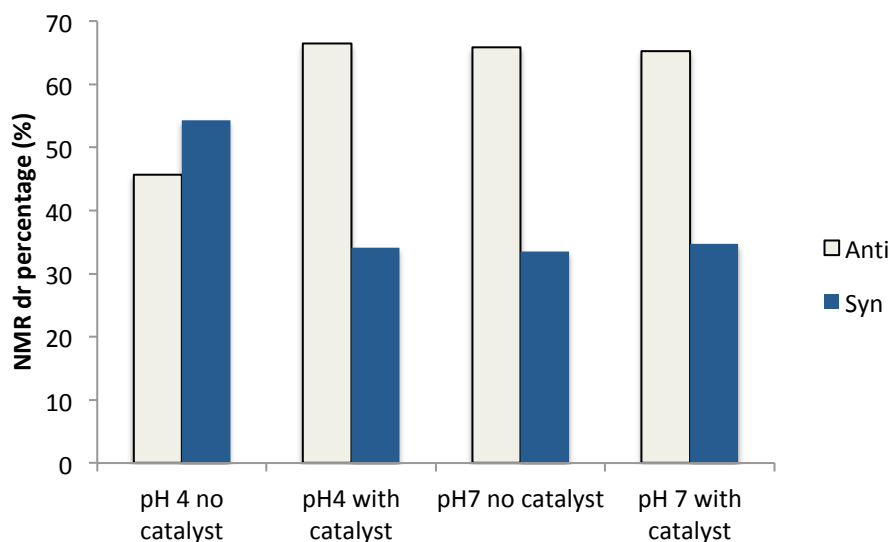


Figure 122: Graph showing percentage *anti* product at different pH in 24 h with and without catalyst (**231**)

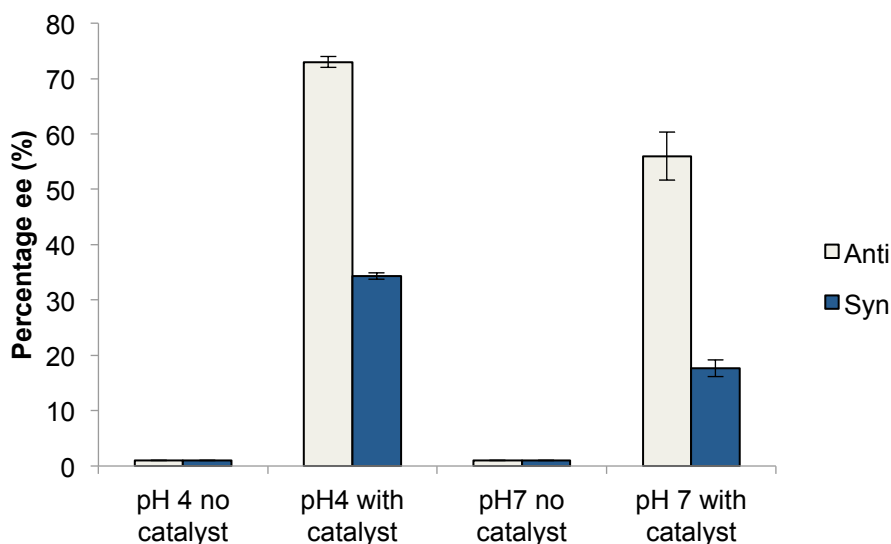


Figure 123: Graph showing *syn* and *anti* ee% at different pH with catalyst (**231**) in 24 h

As in Chapter 2, for the aldol condensation reaction of 4-nitrobenzaldehyde (**47**) and cyclohexanone (**49**), it was proposed that an enamine intermediate is formed from the L-amino acid amide reacting with the ketone, cyclohexanone (**47**). Once the enamine has formed facial selective attack on the aldehyde can occur. ^1H NMR data indicate that we are getting a slight increase in the *anti*-product over the *syn*-product, in addition we are also getting enantioselectivity. In this case, much like the simple amide reported in chapter 2 it is thought that there is no six-membered transition state forming as there is no carboxylic acid group present, but we are seeing a small ee%. This indicates that there steric bulk of the aromatic ring is playing a role in the transition state. When using benzylglutamine amide

(**230**) as the catalyst one side of the amine is blocked by the aromatic ring. Therefore, there are additional steric constraints and also the ability for hydrogen bonding for enamine formation. As a result, it is believed that for this reason, diastereo and enantioselectivity are observed. We therefore hypothesise that for the *anti*-product, the aldehyde approaches with the carbonyl pointing down (Figure 124). In this orientation there could be hydrogen bonding with the benzylic protons. Whereas for the *syn*-product the aldehyde will approach with the carbonyl point upwards where hydrogen bonds of this sort cannot be formed (Figure 125). However, this bonding interaction will have a small energetic value and is most likely the reason why we obtain a small diastereoselectivity of *anti*: *syn*. To obtain the major *anti*-product the aldehyde will preferentially approach from behind the enamine as this avoids the steric clash with the side chain. The minor enantiomer is obtained due to the aldehyde approaching from the front of the enamine. This is the minor product as the steric interaction of H with the R branch of the glutamine moiety is greater than the H-H interaction caused by attack from behind the enamine. The same rationale can also be used to explain the major *syn* enantiomer observed.

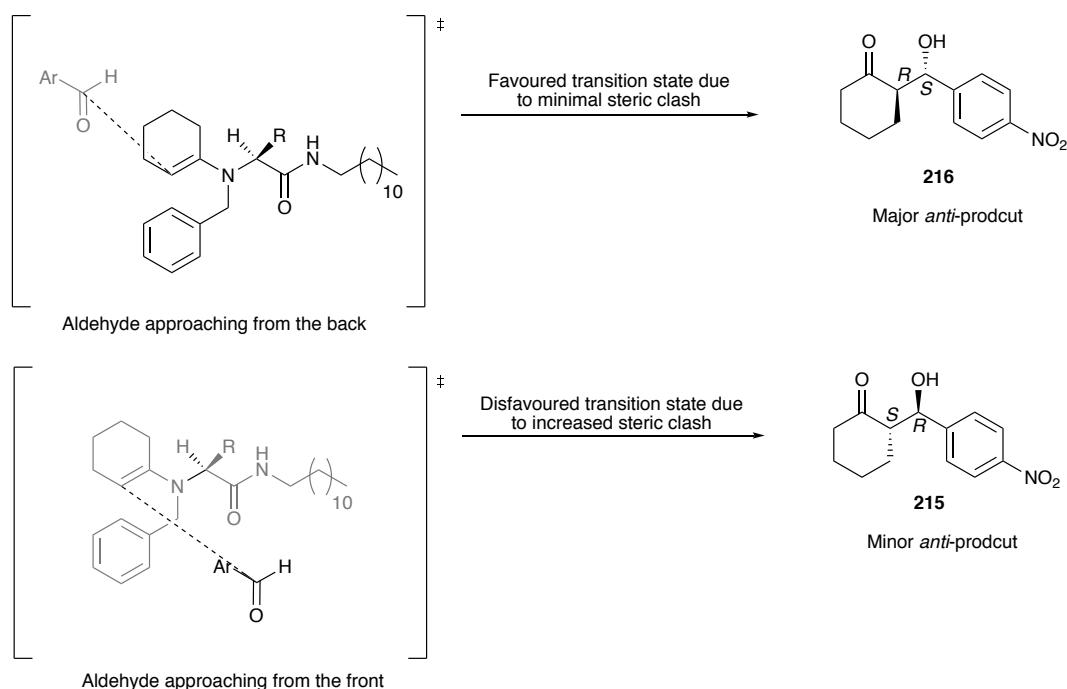


Figure 124: Proposed transition state for the major and minor *anti* products

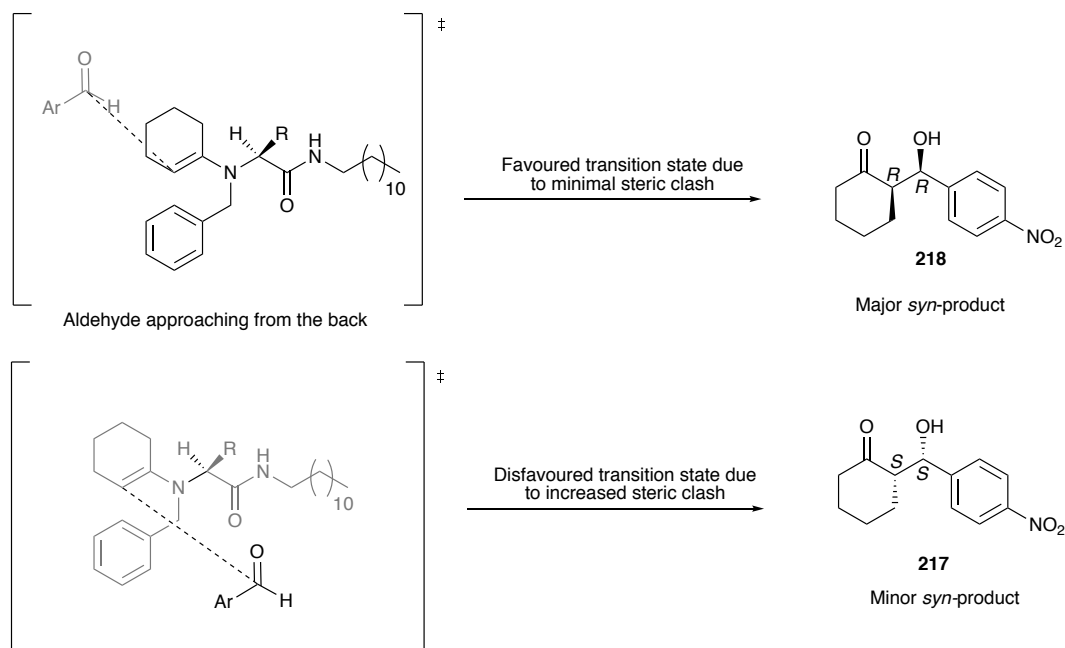


Figure 125: Proposed transition states for the major *syn* products

4.2.3 Gelation and characterisation

Aside from its catalytic ability, the other property that we were interested in with this new compound was its supramolecular potential. Therefore we carried out a simple gelation test where a high concentration (30 mg mL^{-1}) was used to establish if a gel could indeed form.

Benzylglutamine amide (**230**) (3 mg) was added to water (0.1 mL) then heated and left to cool overnight (ca. 8-12 h). The highly concentrated test showed that the molecule is capable of forming a gel (Figure 126). Although heat cool cycles did result in gelation, it was found that heating followed sonication (30 seconds) before cooling was a more effective way to induce gelation with gels forming more consistently and faster (ca. 2 h) (Figure 127). This means there is potential for benzylglutamine amide (**230**) to be a useful catalytic hydrogel.

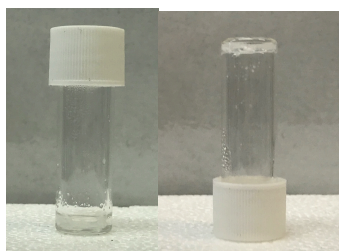


Figure 126: Results of the highly concentrated gelation of benzylglutamine amide (**230**) (3 mg) water (0.1 mL) using tube inversion test. Heat cool induced

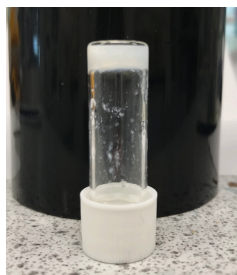


Figure 127: Result of highly concentrated gelation on benzylglutamine amide (**230**) (6 mg) in water (0.2 mL) using tube inversion test. Heat then sonicate induced gelation.

With a method to initiate gelation established, our attention turned to characterising the gel. Scanning electron microscopy (SEM) imaging shows that the sample-spanning network is highly fibrous with nano-fibres of ca. 37 nm wide which is more nanoscale than those found in the two-component gel discussed in Chapter 3 (Figure 128). It was found that the new hydrogelator (**230**) has a minimum gelation concentration (MGC) of 0.3 mg mL^{-1} (0.03 %wt/Vol) and can therefore be considered as a super-gelator (Figure 129). This is a lower gelator loading than the previous two-component system presented in Chapter 3. This suggests that the addition of the aromatic functional group has indeed provided additional robustness. The T_{gel} of this new gelator is $50 \text{ }^{\circ}\text{C}$ at a gelator loading of 1 mg/mL . This T_{gel} value is similar to the two-component system, albeit at a lower concentration than the two-component system studied previously in Chapter 3. Variable temperature circular dichroism spectroscopy (VT CD) was also carried out on the gel using the same method as in Chapter 3. The spectrum (Figure 130) of the variable temperature CD showed that there is chirality present in the gel that when the temperature is increased the CD signal becomes weaker, which is characteristic of a supramolecular assembly. Analysis of the gel by ^1H NMR shows that there was >95% incorporation of gelator into the gel network with no NMR resonance associated with the gelator being observed (Figure 131). A small solvent screen and pH screen was also carried out to understand more about the gelation conditions of this system (Table 26 and Table 27). The results of this are interesting, as the gelator is also an organo-gelator, and does appear to have some pH sensitivity. However, the concentration of gelator is high therefore effectiveness of the buffer is lessened repeating this experiment at a lower gelator loading would be give more insight into the pH sensitivity of this gelator. It is also important to note that the visual appearance of the gel is very different to those observed in the two-component system discussed in Chapter 3 the hydrogel produced with benzylglutamine amide (**230**) is more transparent compared to the

two-component hydrogel. This implies that there is less scattering of light and the network is most likely more nano-scale.

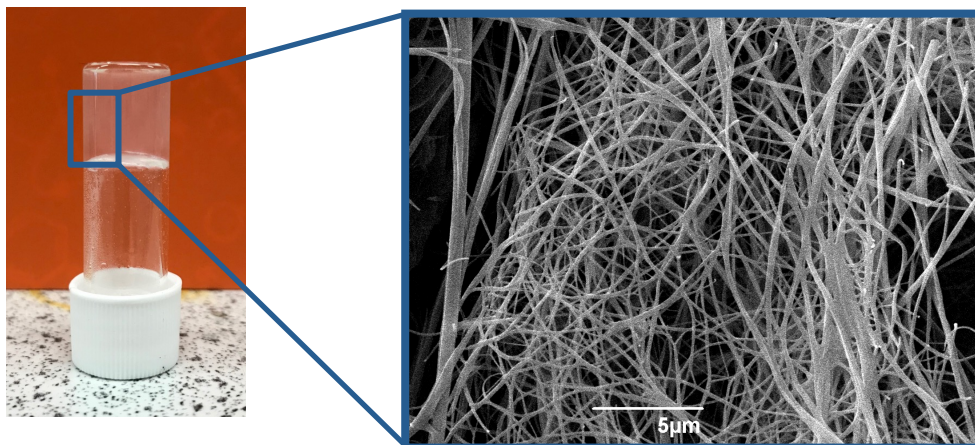


Figure 128: 1 mg mL^{-1} benzylglutamine amide (**230**) gel and SEM image of the gel network

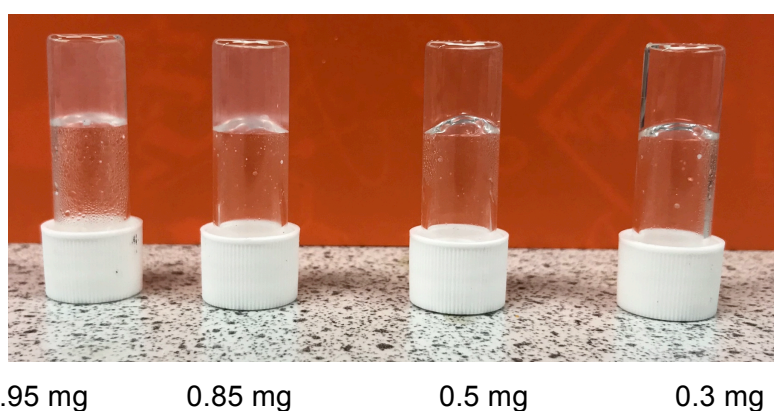


Figure 129: Minimum gelation concentration mg mL^{-1}

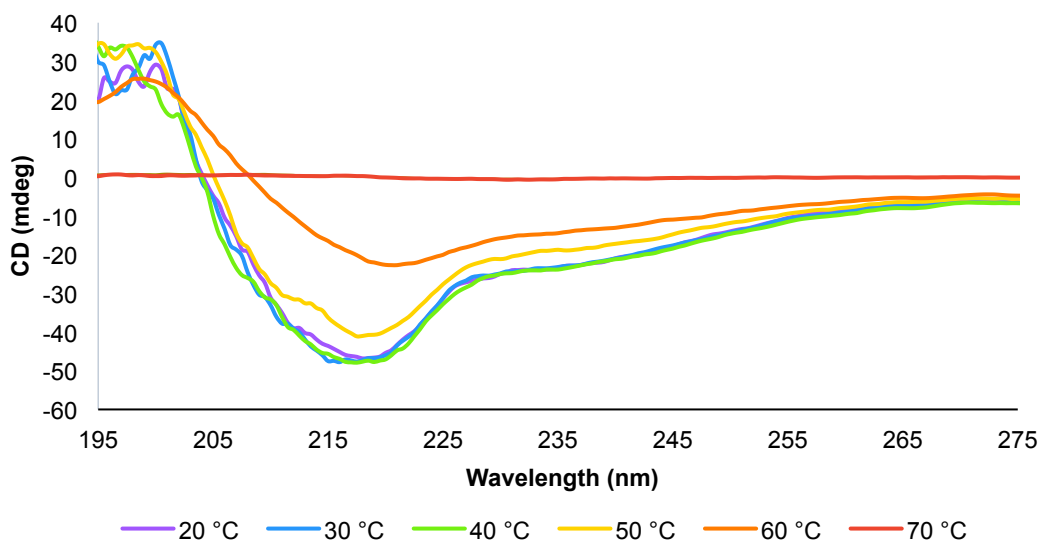


Figure 130: Variable temperature of CD spectrum of benzylglutamine amide (**230**) gel 1 mg in 1 mL transferred $450 \text{ }\mu\text{L}$ 1 mm quartz cuvette

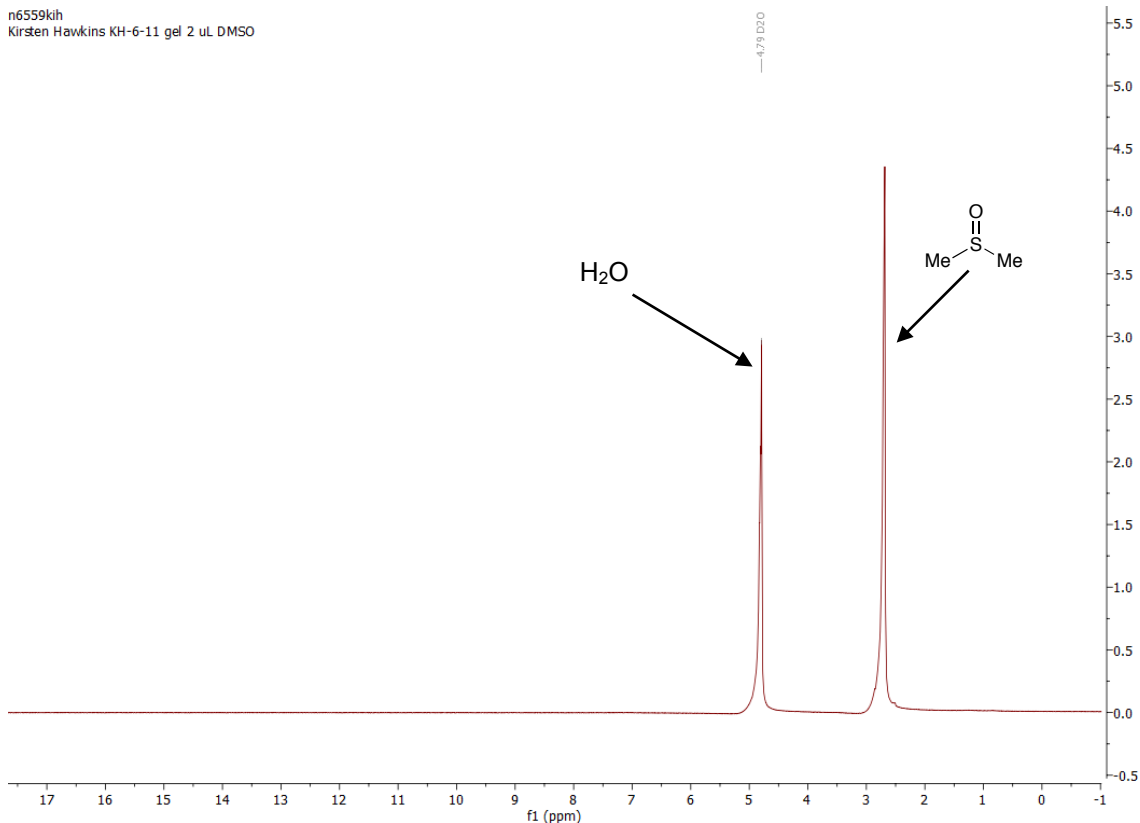


Table 26: pH screen (0.01 M buffer) of benzylglutamine amide (**230**) (3 mg / 0.1 mL, 0.1 M)

pH	Did it gel?
1	Yes
4	No
7	Yes
10	No

Table 27: Solvent screen of benzylglutamine amide (**230**) (3 mg / 0.1 mL, 0.1 M)

Solvent	Did it gel?
Acetonitrile	Yes
Toluene	No
Cyclohexane	Yes
Ethyl acetate	No
THF	No

The rheology of the gel was also studied. The samples were prepared as normal, heat, sonicate then allow the gel to form on the rheology plate itself. To do this the rheology plate was heated to 70°C, and the gel solution was transferred to a

bottomless vial that was on the rheology plate. Once the solution was in the vial it was held firmly until a seal had formed and the gel could be left to set with the rheology plate cooling back to 20°C. This method of sample formation could be used with this system as gel formation is significantly faster than the two component hydrogel discussed in Chapter 3. In addition, this method was the most consistent way of forming samples as transfer from one surface to another didn't take place therefore less chance of the gel breaking. Rheology measurements were then carried out in the same way as described in Chapter 3.

As explained in Chapter 3, the robustness is characterised by the crossover point between G' and G'' . The data of this shown in Figure 132 show that the gel is stiff but has a smaller resistance to strain in comparison to the two-component gel reported in chapter 3. For the gel benzylglutamine amide (**230**), the shear strain is relatively low at ca. 1.9%, and indicates a weak gel.

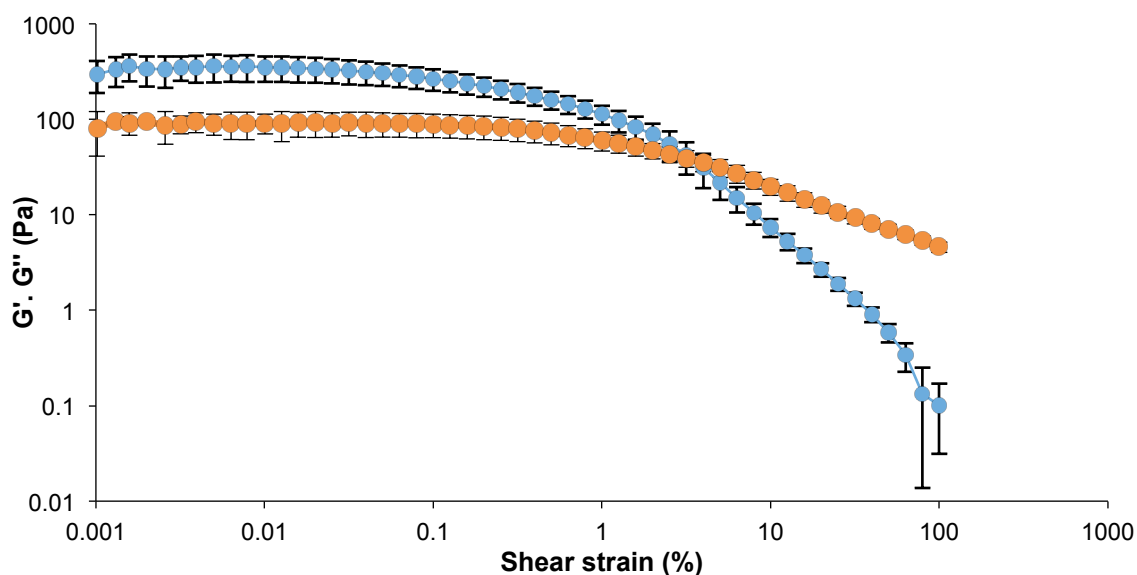


Figure 132: Benzylglutamine amide (**230**) Gel 4 mg in 1 mL water. Elastic (G' , blue circles) and loss (G'' , orange circles) moduli of hydrogels with varying shear strain (frequency = 1 Hz).

The results of the frequency sweep (Figure 133) show that the gels formed with benzylglutamine amide (**230**) are weak as we observe breakdown of the gel at about 15 Hz, however, this is stronger than the two component gel reported in Chapter 3. The storage and loss moduli of elastic materials show no change with increasing frequency. In contrast, viscous liquids respond linearly to these

changes. Therefore, the point at which the gradient of the plot increases can be considered the point at which these materials behave more like a liquid than a gel.

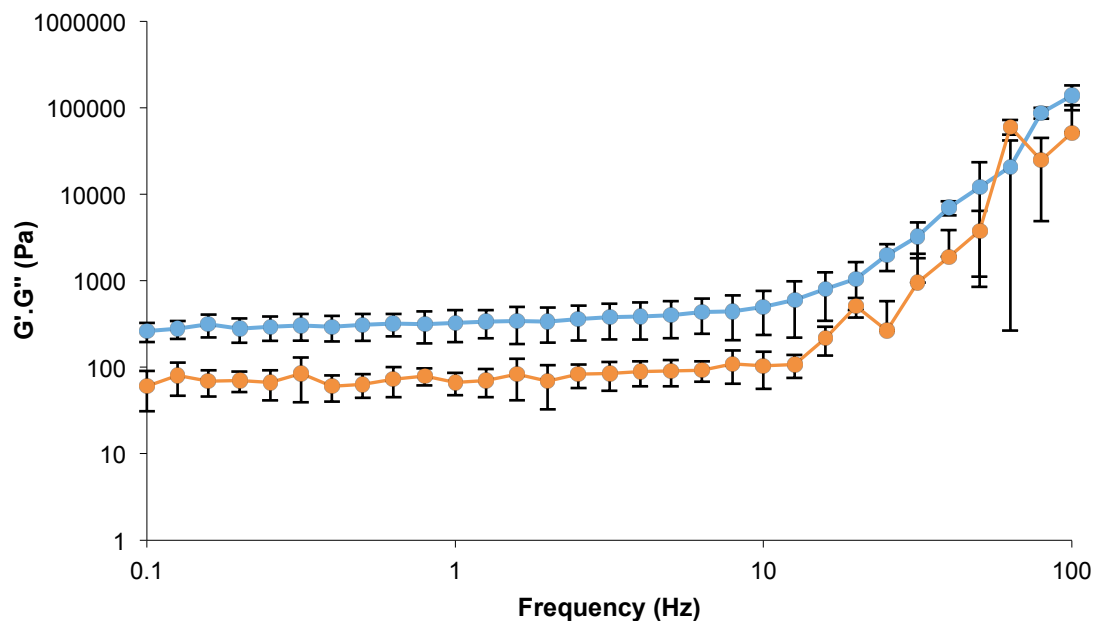


Figure 133: Benzylglutamine amide (**230**) Gel 4 mg in 1 mL water. Elastic (G' , blue circles) and loss (G'' , orange circles) moduli of hydrogels with varying frequency

4.2.4 Catalysis on the gel

Earlier it was shown that the catalyst, benzylglutamine amide (**230**), could turn-over a simple aldol condensation reaction between 4-nitrobenzaldehyde (**47**) and cyclohexanone (**49**) in a heterogeneous solution. We therefore decided that the next stage was to test the catalytic ability of the intact hydrogel.

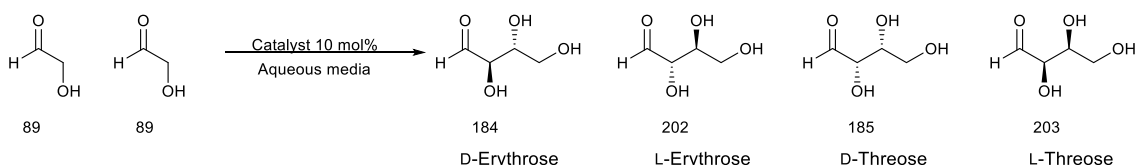
Initially, studies were carried out on the surface of the gel with a neat mixture of 4-nitrobenzaldehyde (**47**) and glutamine amide (**210**), and the gel structure was retained. However this system was very sensitive to vial size. On scaling up the size of the gel to obtain quantifiable evidence of turnover of starting material to product, the gel collapsed instantaneously when the reaction mixture was pipetted on top of the surface of the gel (Figure 134). It is well known that the mechanical properties of gels depend on vials in which they are made¹⁶⁶ and we suggest that the gel in the larger vial is weaker as a result of its greater surface area. It is believed that the gel breaks down because it dissolves in the cyclohexanone (**49**) pipetted onto the top of the sample.



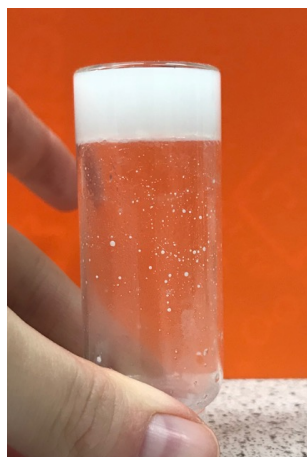
Figure 134: a) Benzylglutamine amide (**230**) gel before reagents pipetted on top of the surface. b) Once reagents added to the surface of the gel

As a result we changed the aldol condensation reaction of interest to the dimerization of glycolaldehyde: a prebiotic reaction (Scheme 45). Aside from this reaction being important from a prebiotic point of study, this aldol condensation reaction is water soluble unlike that between 4-nitrobenzaldehyde (**47**) and cyclohexanone (**49**). Therefore, we reasoned that the gel should remain as a gel as there is no organic component, such as cyclohexanone (**49**), to dissolve the gelator.

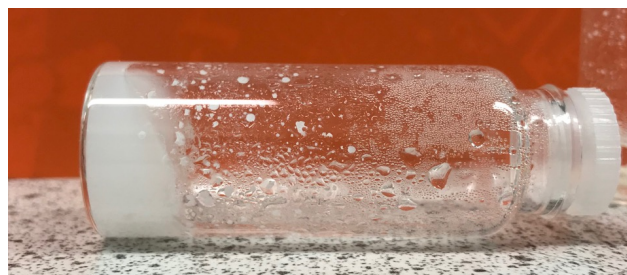
The gel was prepared by a heat, sonicate and cool cycle. Once the gel was formed two equivalents of glycolaldehyde (**89**) was dissolved in water (200 μ L) then added in small aliquots (twenty 10 μ L additions) to the surface of the gel. The reason for these small additions is to ensure the glycolaldehyde (**89**) is dispersed over the gel surface rather than being localised. The gel reaction was then monitored for the next 24 h to see if the gel structure remains. These initial studies looked promising, as the gel remained intact even after 48 h.



Scheme 45: Dimerization of glycolaldehyde (**89**)



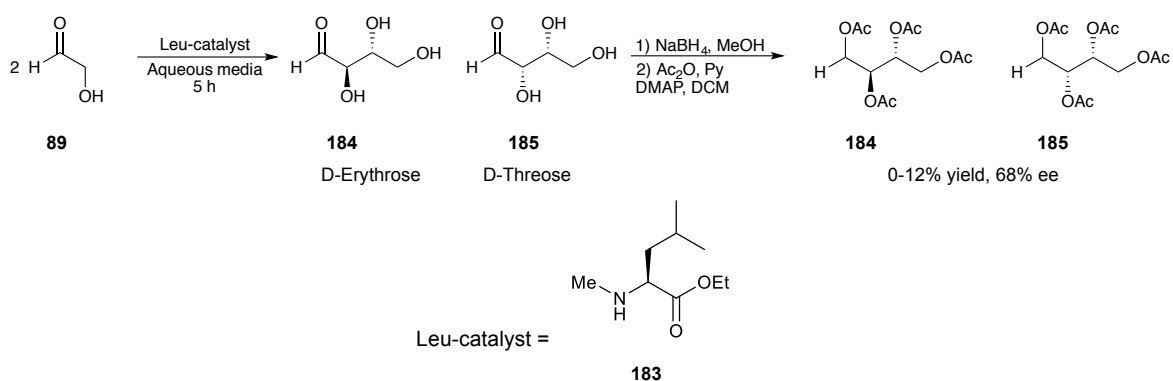
c



d

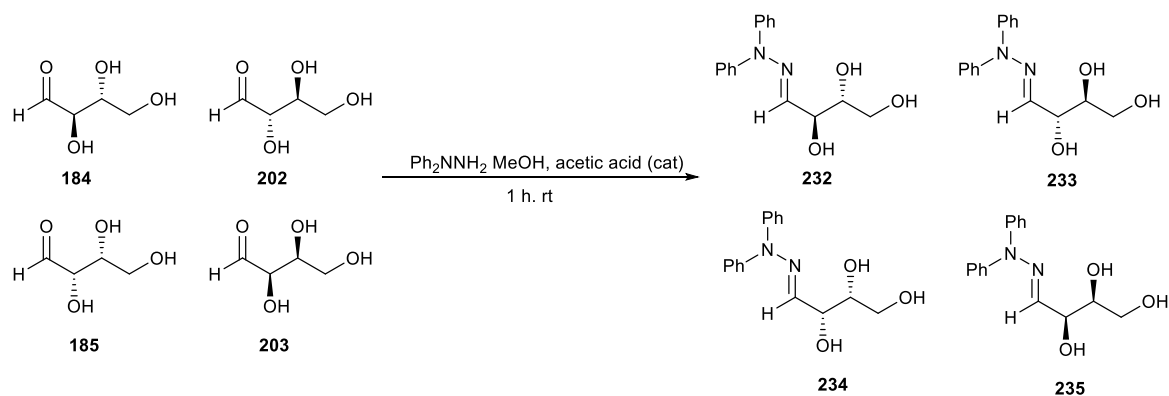
Figure 135: c) Benzylglutamine amide (**230**) gel before reaction. d) Benzylglutamine amide (**230**) gel after aldol reaction has been on the gel for 48 h

There was however, a difficulty with analysing the products of this reaction. Both the product of dimerization, threose and erythrose and the glycolaldehyde dimer have the same formula mass ($m/z = 120$) we also wanted to determine an ee% for all the products. Previously in the Clarke group, reduction followed by acylation protection (Scheme 46) of the crude material has been used and derivatives analysed using ^1H NMR and Chiral GC.¹⁶⁷ However using this method only the ee% of the threose can be determined as acetyl protecting of erythrose results in a *meso* compound as a result no ee% can be determined.



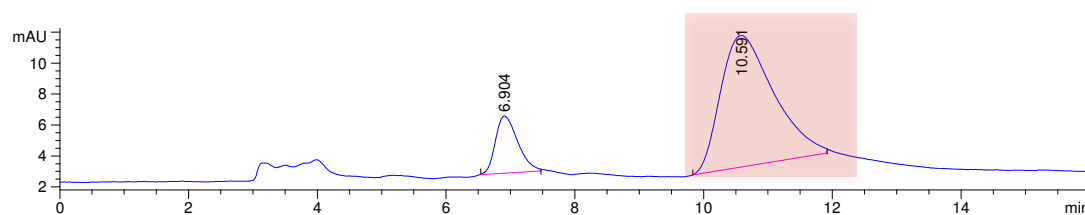
Scheme 46: Acylation of threose and erythrose for analysis of dimerization of glycolaldehyde by chiral GC

An alternative method was to convert the products with diphenyl hydrazine to yield hydrazone derivatives (Scheme 47). The advantage of this method is that chiral HPLC can be employed and there is retention of all four enantiomers. In the Clarke group¹⁴⁶ this method had been briefly explored previously but no HPLC conditions had been developed.

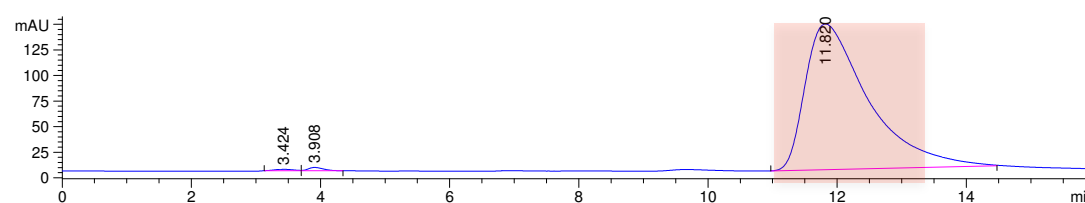


Scheme 47: Synthesis of diphenyl hydrazone

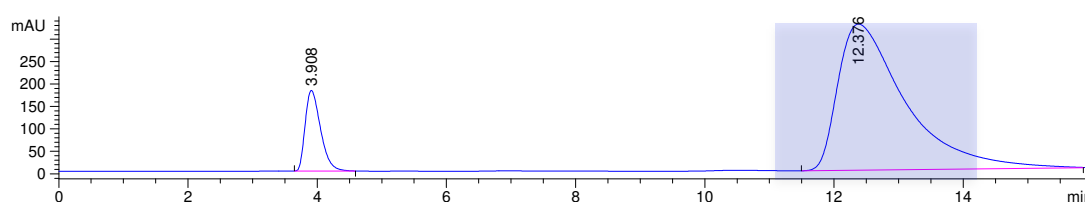
We therefore prepared standards of the four enantiomers. L-threose (**235**), D-threose (**234**), L-erythrose (**233**) and D-erythrose (**232**) were converted into the hydrazone, by adding diphenyl hydrazide in methanol with acetic acid and stirring for 1 h. The products were purified by column chromatography (gradient starting from 98:2 DCM: MeOH to 100% methanol). The standards were then analysed by ^1H NMR and Chiral HPLC. Chiral HPLC of the individual standards was performed on the Chiral-pak AD-H column (85:15 *n*-Hexane :IPA) (Figure 136).



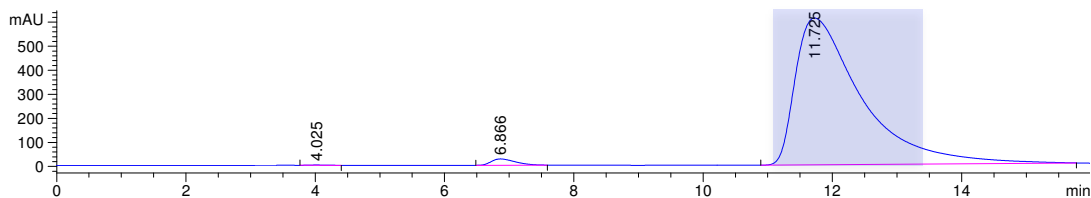
L-Erythrose hydrazone (**233**) retention time 10.591 min



D-Erythrose hydrazone (**232**) retention time 11.820 min



L-Threose hydrazone (**234**) retention time 12.376 min



D-Threose hydrazone (**235**) retention time 11.725 min

Figure 136: Erythrose and Threose Hydrazone HPLC traces Chiralpak AD column (85:15 *n*-hexane: IPA)

Although HPLC traces of the standards had different retention times, when a standard containing all D/L erythrose and threose hydrazones was analysed, only the L-erythrose hydrazone (10.416) was distinguishable. The peak at 12.304 is as a result of L-threose, D-threose and D-erythrose co-eluting.

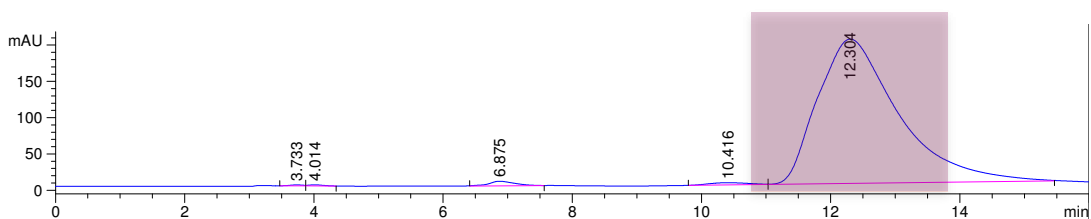
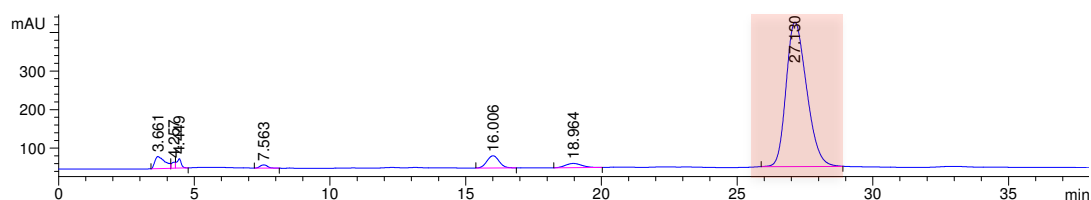
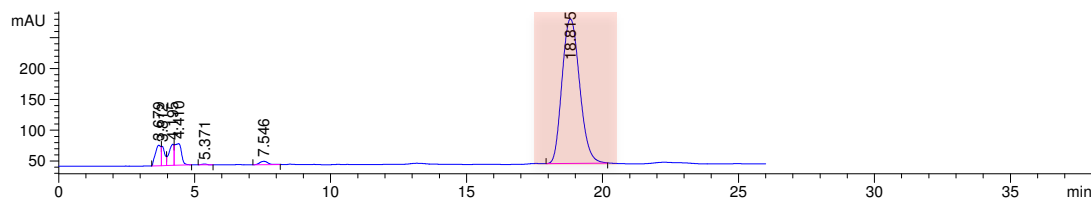


Figure 137: Mixed hydrazone HPLC trace Chiralpak AD column (85:15 *n*-hexane: IPA)

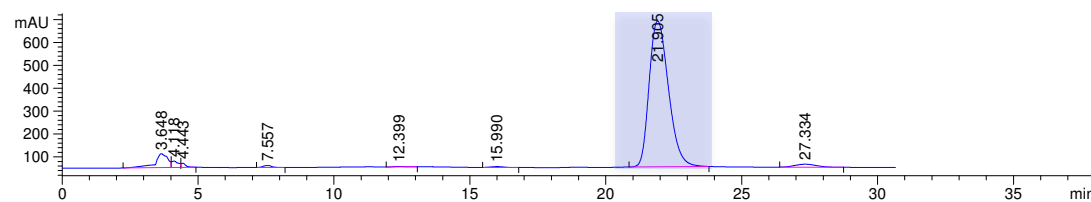
A number of chiral HPLC columns and solvent systems were then tested to achieve separation of all four enantiomers. It was found that the four enantiomers could be separated using an IC Chiral-pak column with a 90:10 ratio of Hexane: IPA at 40°C.



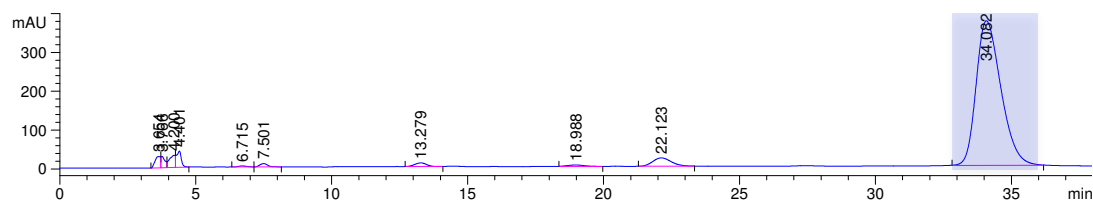
D-Erythrose (**232**) hydrazone retention time 27.130 min



L-Erythrose (**233**) hydrazone retention time 18.815 min



D-Threose (**234**) hydrazone retention time 21.905 min



L-Threose hydrazone (**235**) retention time 34.082 min

Figure 138: Erythrose and Threose Hydrazone HPLC traces Chiralpak IC column (90:10 *n*-hexane: IPA) 40 °C

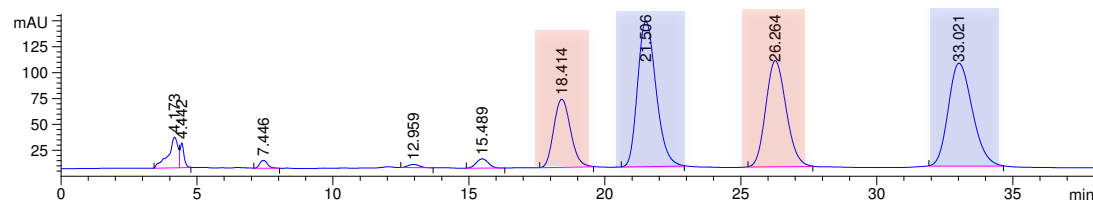


Figure 139: Mixed Hydrazone HPLC trace Chiralpak IC column (90:10 *n*-hexane: IPA) 40 °C. L-erythrose hydrazone = 18.414 min, D-threose Hydrazone = 21.506 min, D-erythrose = 26.264 min, L-threose = 33.021 min

With chiral HPLC conditions established, analysis of the dimerization of glycolaldehyde on the catalytic hydrogel could be carried out by converting products to the diphenylhydrazones with purification by column chromatography. To do this, the hydrogel was dehydrated under vacuum. To the residue diphenylhydrazine in methanol was added followed by 1-2 drops of acetic acid and left to stir at room temperature for 1 h. After stirring for 1 h the solvent was removed. ^1H NMR analysis was then carried out on the crude hydrazone mixture to obtain a conversion of glycolaldehyde to the desired erythrose and threose. Before chiral HPLC, column chromatography (98:2 DCM: MeOH) was carried out to remove excess diphenyl hydrazine and minimise the excess glycolaldehyde present. Chiral HPLC was then performed on the mix of threose and erythrose hydrazone products.

In the crude ^1H NMR there is a triplet at 6.46 ppm which corresponds to the hydrazone proton of glycolaldehyde (**236**), the doublets at 6.49 ppm and 6.52 ppm correspond to the hydrazone proton of threose (6.49 ppm) and erythrose (6.52 ppm). As these peaks all correspond to one proton, we can simply use the integration of the peaks to calculate the conversion.

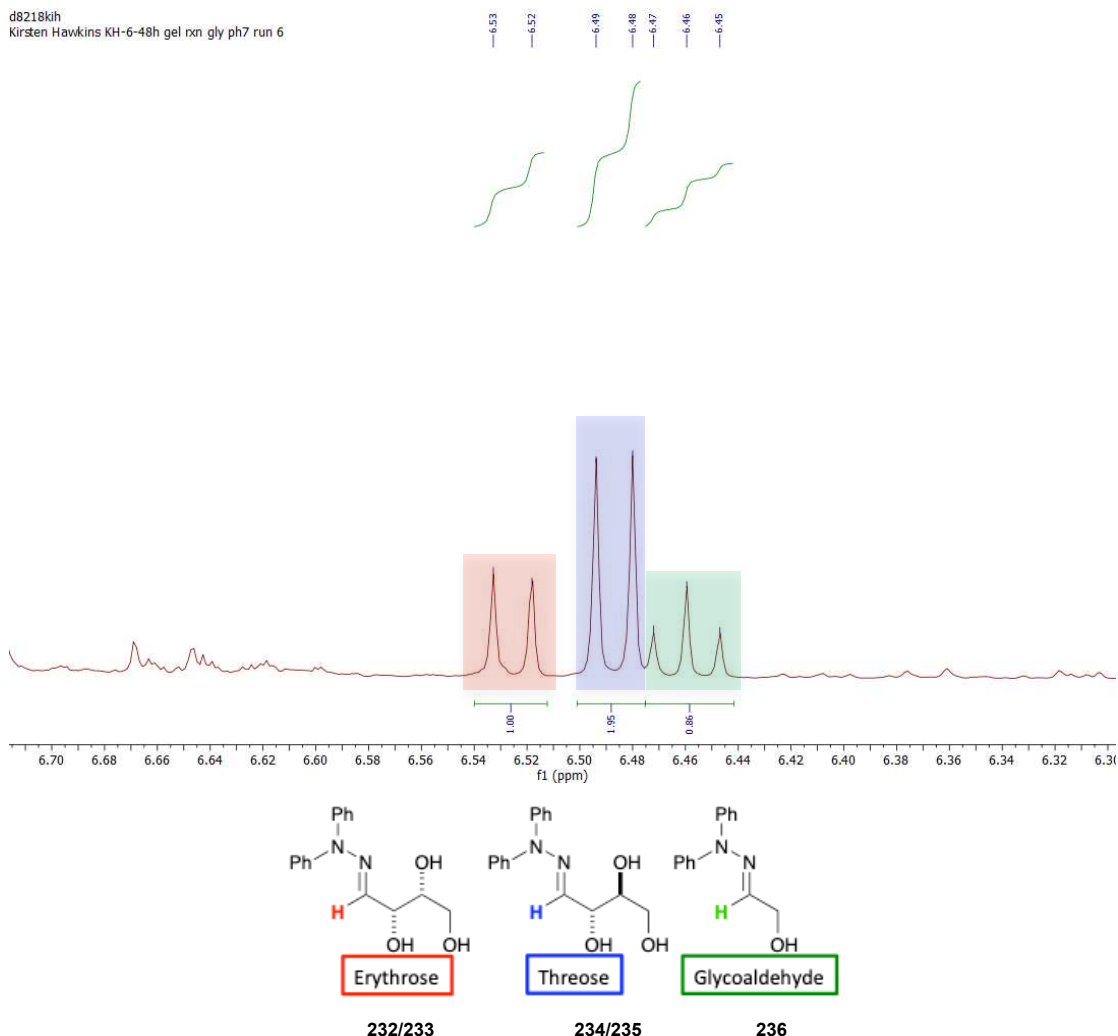


Figure 140: An authentic crude ^1H NMR of the dimerization of glycolaldehyde (**89**) on the benzylglutamine amide (**230**) gel. Protected as the hydrazone

From the ^1H NMR shown in Figure 140 Integral for glycolaldehyde hydrazone = 0.86, integral for threose hydrazone = 1.95, and integral for erythrose = 1.00.

$$\text{Summation of integrals} = 0.86 + 1.95 + 1.00 = 3.81$$

From here we then sum the threose and erythrose integral and divide by the total number of proton integrals to get a percentage

$$\text{Threose and erythrose intergral sum} = 1.95 + 1.00 = 2.95$$

$$\text{percentage of threose and erythrose} = \frac{2.95}{3.81} \times 100 = 77\%$$

The results shows that when using deionised water as the solvent for the hydrogel, there is conversion of glycolaldehyde (**89**) into erythrose and threose ca. 10%, with a diastereoselectivity for threose (**185/203**) over erythrose (**184/202**) ca. 2.5:1 as determined by ^1H NMR. The results from these NMR studies are significant as there is selectivity for threose (**185/203**) over erythrose (**184/202**) (Figure 140).

Conversely, previous work in the Clarke group, discussed in chapter 1, showed selectivity for erythrose over threose.^{136–138}

Moreover, chiral HPLC studies of the hydrazones demonstrated that there is a slight enantiomeric excess for L-threose (**235**) ca. 2-7% and D-erythrose (**232**) ca. 3%. When using pH 7 (0.01 M Phosphate) buffer as solvent to form the gel there was a dramatic increase in conversion of glycolaldehyde to threose and erythrose (68%) (entry 4). In addition, there was still a selectivity for threose over erythrose (2.28:1). The chiral HPLC traces show that there is a slight enantiomeric enhancement of the L-threose (**235**) (6.5%) but a complete change in the favoured enantiomer of the erythrose, with slight enrichment of L-erythrose (**232**) (2.5%). It is therefore clear that the self-assembled gel is catalysing this prebiotically relevant reaction and influencing the stereochemical outcome *via* intimate involvement in the reaction event. Furthermore, when the monomer was tested as a catalyst in solution phase at both pH 7 and in water there was limited conversion ca. 5% (entry 7 and 8). Due to the low conversion a D.R could not be reliably determined. This is a very interesting result and suggests that the presence of the gel network is important for catalysis to occur effectively.

Table 28: Dimerization of glycolaldehyde (**89**) with benzylglutamine amide (**230**) data on the hydrogel over 48h

Amide catalyst	Entry	Solvent	Conversion %	Crude NMR dr Erythrose to Threose	HPLC ee%
Benzyl glutamine amide gel	1	Water	12	1.00 : 2.77	Ery: 2 % Thr: 2 %
	2	Water	10	1.00 : 2.90	Ery: 2 % Thr: 3 %
	3	Water	7	1.00 : 1.38	Ery: 2 % Thr: 7 %
	4	pH 7	68	1.00 : 2.28	Ery: 3 % Thr: 7 %
	5	pH 7	43	1.00 : 1.94	Ery: 1 % Thr: 6%
	6	pH 7	76	1.00 : 1.95	Ery: 4 % Thr: 10 %
Benzyl glutamine amide	7	pH7	5 %	N/A	N/A
monomer	8	water	5 %	N/A	N/A

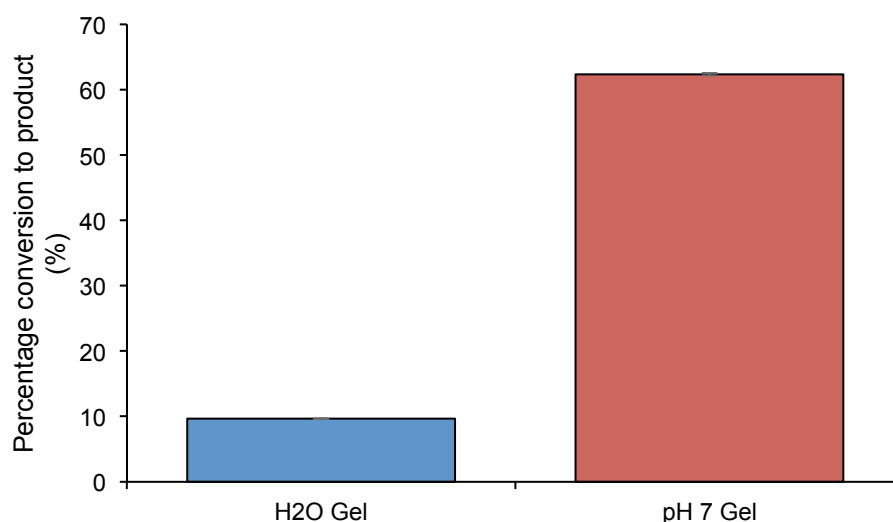


Figure 141: Percentage conversion to threose (**234/235**) and erythrose (**232/233**) in water and pH7 analysed as the hydrazone

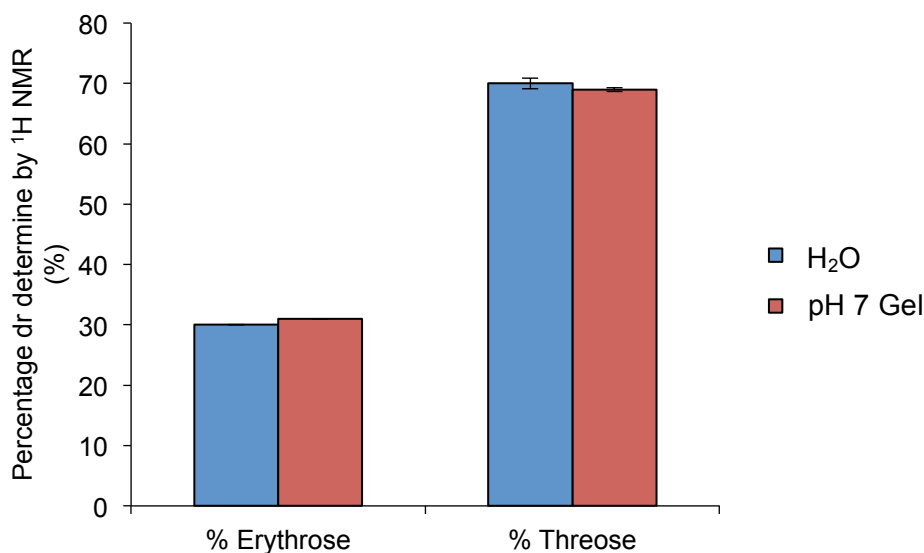


Figure 142: Diastereomeric ratio of erythrose (**232/233**) to threose (**234/235**) in pH7 and water analysed as the hydrazone

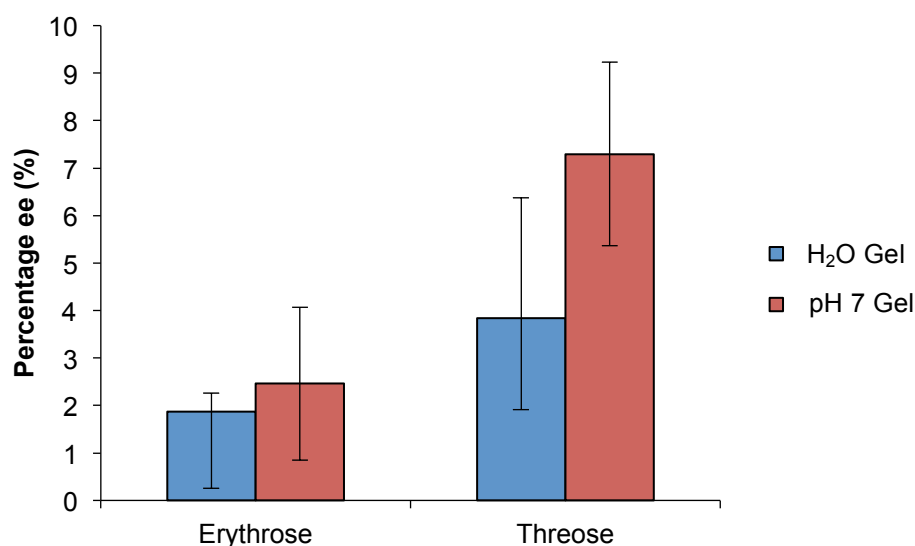


Figure 143: Enantioselectivity of erythrose (**232/233**) and threose (**234/235**) in water and pH7 analysed at the hydrazone

If we compare our findings to others in the literature, we find that the results are similar with respect to diastereoselectivity of tetrose product, where threose (**203/185**) is reported to be higher than erythrose (**184/202**). The yields are harder to compare as not all literature presents yields of products, possibly due to problems isolating without protection such as that presented by Pizarello and Webber^{168,169}. Pizarello and Webber reported two catalytic systems for the formation of threose and erythrose in the first instance single amino acids were used and ee% of 2-5% were reported. After this a significantly higher ee% was reported of > 80% ee for D-erythrose (**184**) when using a dipeptide which would

have more chirality in the catalyst and therefore increased the chiral control of products yielded. When yields of threose and erythrose are presented there is loss of the ee% of erythrose (**184/202**). Nonetheless reported yields for reactions over a duration of 7 days are reported at ca.50%¹⁷⁰. This is not too dissimilar to the overall conversions that we report. It is important to note that the duration of the reactions we present are only 48 h not 7 days.

When reactions take place in a gel environment there are also other aspects that could be responsible for the selectivity aside from the chirality of the molecule itself. The gel network can play an important role, as there are pockets similar to the active site of an enzyme, which could affect the stereochemistry of the product. Gelator assembly can potentially amplify chiral effects. These other aspects do not usually have to be considered in simple solution phase catalysis, as the isolated catalyst molecule alone will determine the stereochemistry.

4.3 Conclusion:

In this report, we have presented a successful synthesis of both imine (**231**) and desired amine (**230**) using gelation as a means of obtaining the imine (**231**) product in good yield. With the new catalyst in hand we then demonstrated the catalytic ability of the amine (**230**) in water as a heterogeneous system for the reaction between cyclohexanone (**49**) and 4-nitrobenzaldehyde (**47**). Here it was shown that the amine was capable of catalysis with good conversion and ee. It was also shown that pH played an important role in catalysis, when reactions were performed at pH 4 and 7, conversion to product was lower due to the removal or acid base catalysis. However, in the absence of catalyst the percentage conversion to product was even lower. Furthermore, at both pH 7 and 4 there was a significant increase in enantioselectivity for the *anti*-product compared to the unbuffered system, indicative of intimate involvement of the catalyst in the absence of base.

Our attention then turned to understanding the supramolecular properties of the amide-based system. It was identified that both organogels and hydrogels form. The hydrogelator is thermally stable and can be considered as a super-gelator forming gels at 0.03 %wt/vol. This is a lower gelator loading than the previous two-component system presented in Chapter 3. It therefore follows that our

hypotheses about this new gelator were correct; the addition of the aromatic functional group has indeed provided additional robustness. Furthermore, we have used the gel as a medium to perform catalysis on. The results demonstrated that the reagents used are important, as when performing the standardised cyclohexane (**49**) and 4-nitrobenzaldehyde (**47**) aldol condensation reaction the gel collapsed. However, when we pursued a prebiotic reaction, the dimerization of glycolaldehyde, we had success in both conversion to threose and erythrose and maintenance of the gel structure. When performed at pH 7 there was a dramatic increase in conversion and also some increase in enantioselectivity was seen. It was also interesting to see that the major enantiomer of the erythrose changed from the D-form to the L-form upon changing pH.

5.0 A prebiotic route to 2-deoxy-D-ribose and phosphorylated sugars

5.1 Aims

Having designed a successful system for the formation of threose and erythrose from glycolaldehyde using a catalytic hydrogel, the next step was to test the scope of this catalytic gel further. Work presented earlier (Chapter 1) by Steer *et al* showed that amino nitriles catalysed the formation of 2-deoxy-D-ribose in aqueous media.^{136,140–142} We therefore wanted to investigate the potential prebiotic formation of 2-deoxy-D-ribose and 2-deoxythreopentose (Figure 144) in the gel environment.

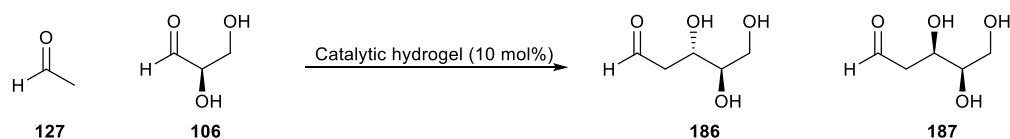


Figure 144: Formation of 2-deoxy-D-ribose (**186**) and 2-deoxythreopentose (**187**)

In addition, we have shown in Chapter 4 that the benzyl glutamine amide hydrogel is able to catalyse the dimerization of glycolaldehyde to yield threose and erythrose with moderate diastereoselectivity and enantioselectivity. Eschenmoser⁹⁷ reported the more challenging formation of the phosphate derivatives of threose and erythrose from glycolaldehyde phosphate in aqueous

sodium hydroxide media (Figure 145). This inspired us to see if our much milder hydrogel system could also produce these evolutionary important phosphate sugars.

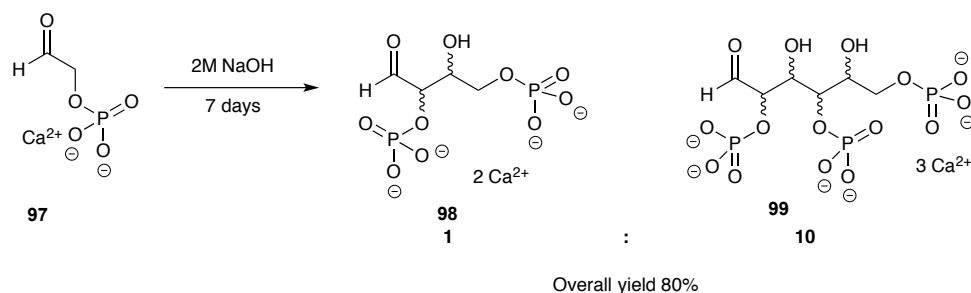


Figure 145: Formation of 2,4-threosephosphate and 2,4-erythrosephosphate (**98**) from the dimerization of glycolaldehyde phosphate (**97**)

5.1 Results and Discussion

In Chapter 4 the ability of benzylglutamine amide (**230**) hydrogelator as a catalyst for the dimerization of glycolaldehyde was presented. As a result, investigations into the synthesis of 2-deoxy-D-ribose (**186**) and 2-deoxy-threopentose (**187**) using the catalytic hydrogel began. To do this, the same procedure that was developed for gel-based reactions of glycolaldehyde was used. The reactions were carried out on a gel prepared *via* a heat-sonicate-cool cycle and at pH 7 (0.01 M phosphate buffer). These conditions were used as they were shown previously, in the dimerization of glycolaldehyde, to give the best conversions and selectivities. Due to the volatility of acetaldehyde (**127**) a stock solution in pH 7 (0.01 M, phosphate buffer) was prepared. This was then added to D-glyceraldehyde (**106**) and the solution was added to the surface of the gel and left for 48 h. When the reagents were added to the surface of the gel part of the gel, initially broke down, however after a period of time this reformed as shown in Figure 146 photo b.

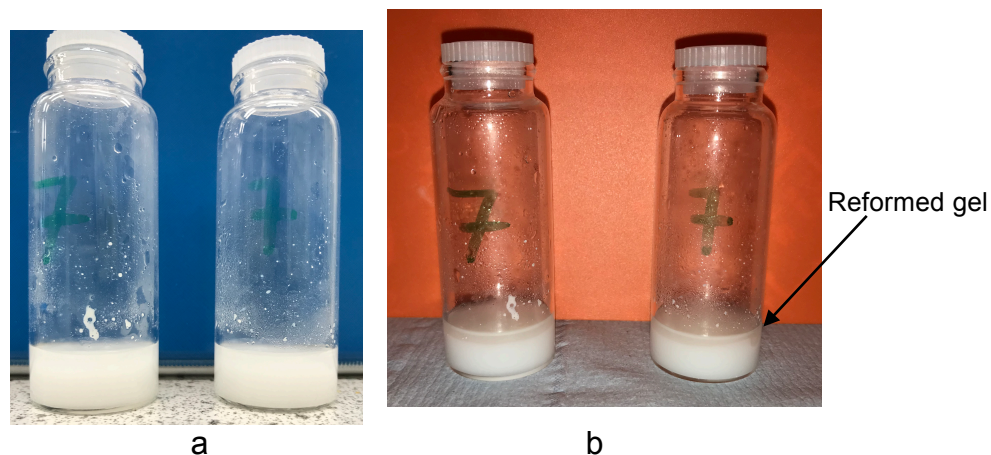
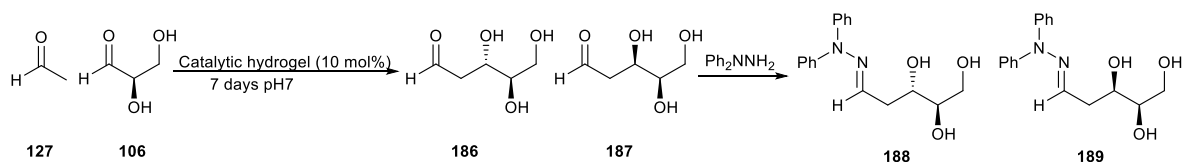


Figure 146: Image a gel with reagents on the surface. Image b shows the layer of reagents on the gel

After 48 h the gel structure survived. Solvent was removed in *vacuo* then diphenyl hydrazine was added to produce the hydrazine protected sugars (Scheme 48) following the same procedure as that described in Chapter 4. The resulting crude mixture was purified by column chromatography and then analysed by electrospray mass spectroscopy (ESI) and ^1H NMR spectroscopy. However, we were unable to detect the formation of any trapped pentose which should be seen in ^1H NMR as a triplet at 6.65 ppm (Figure 147). Only trapped starting material (**236**) which appears in the ^1H NMR as a doublet at 6.44 ppm was observed (Figure 148).



Scheme 48: *N,N*-Diphenyl hydrazine trapping of reaction mixture

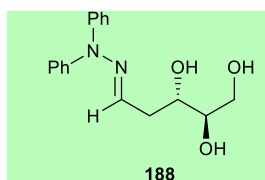
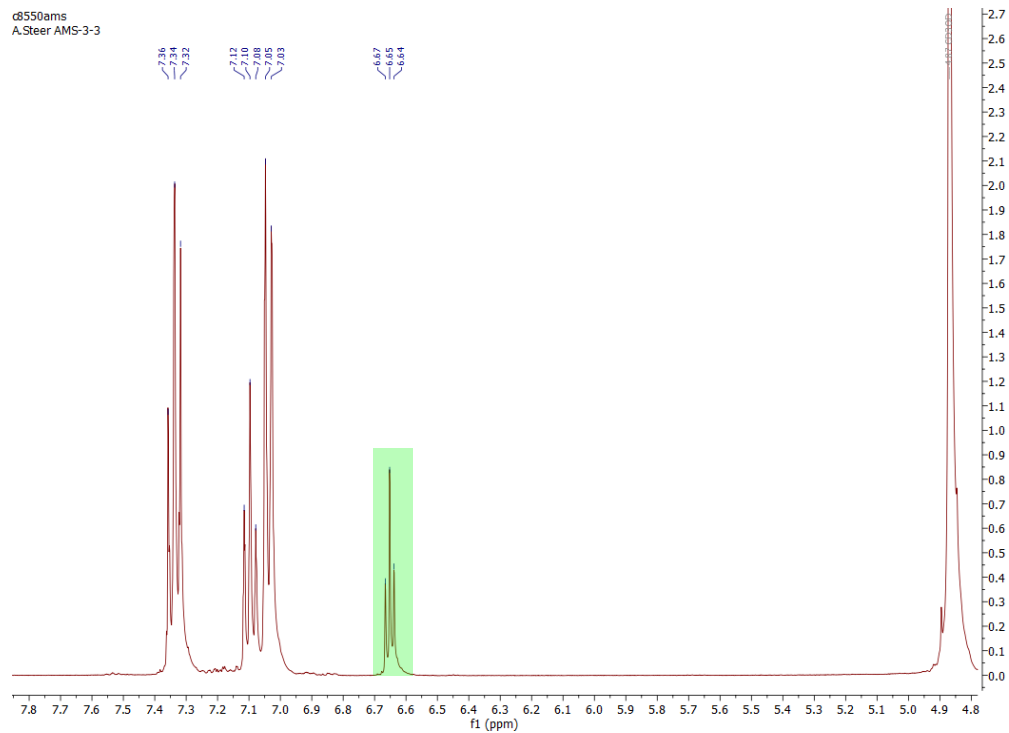
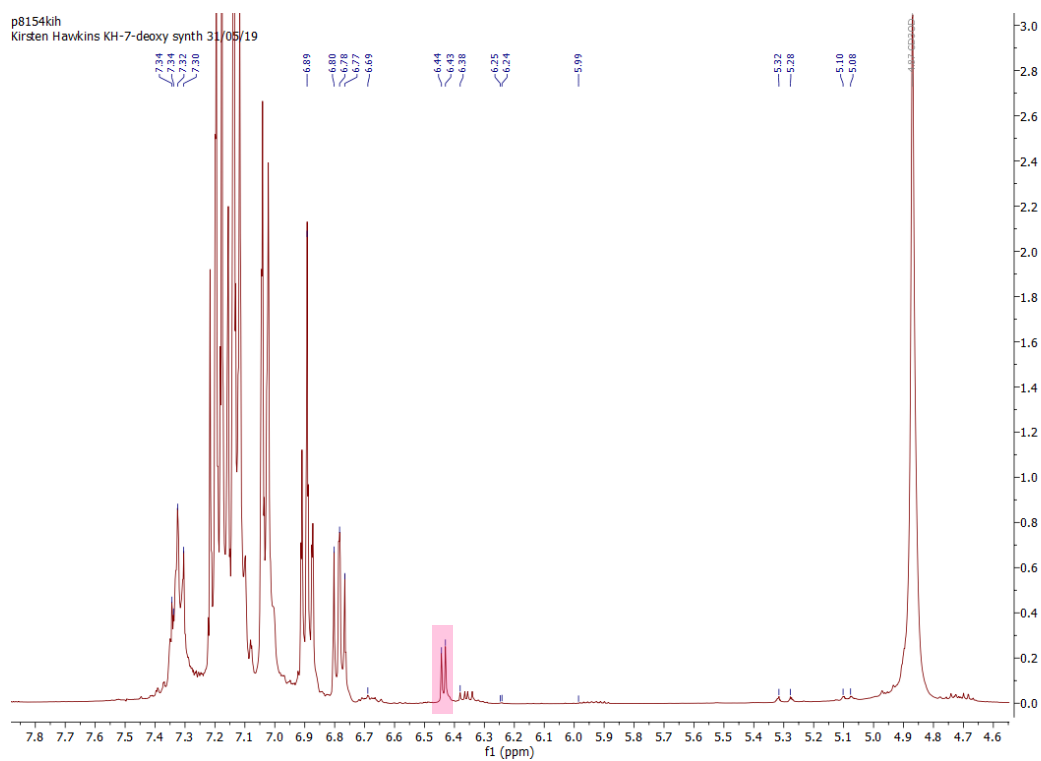
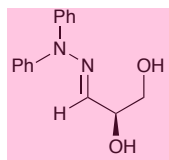


Figure 147: ^1H NMR spectrum of 2-deoxy-D-ribose diphenyl hydrazide standard (**188**)





236

Figure 148: ^1H NMR spectrum of crude reaction taken place on benzyl glutamine amide hydrogel after 7 days, diphenyl hydrazine trapped

It was decided that as this reaction can be slow, the reaction time should be increased to 7 days to determine if any product could be observed. As a result the reaction was repeated but with a duration of 7 days. However after 7 days, once again no product was observed and the gel structure began to break down (Figure 149). It is hypothesised that the reaction did not take place was because enamine formation not taking place due to low concentration of catalyst (10 mol%), as well as an increase in the dispersion of catalyst due to loss of the gel network. It is also possible that modifying D-glyceraldehyde so that it is more electron-withdrawing or hydrophilic could allow the reaction to proceed.

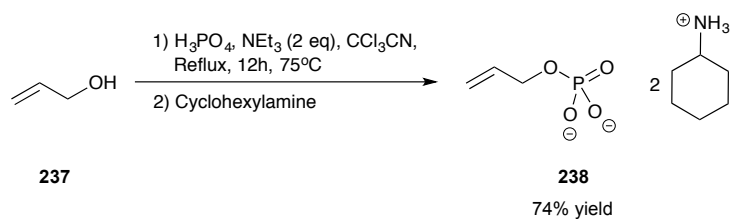


Figure 149: Gels left for 7 days image c at the start of reaction, image d after 7 days

With no success using these gels for the synthesis of 2-deoxy-D-ribose (**186**) or 2-deoxythreopentose (**187**), we decided to turn our attention to the synthesis of diphosphate erythrose and threose derivatives (**98**). This reaction was selected to test because it was already found that the catalytic hydrogel was effective in the dimerization of glycolaldehyde (Chapter 4). Therefore, it was proposed to test the ability of the system to synthesise the phosphate derivatives that are important in the evolution of biological systems as discussed in Chapter 1.

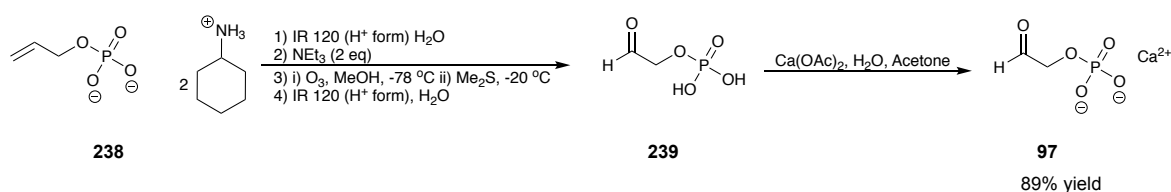
The starting material for this new reaction was glycolaldehyde phosphate. This was synthesised from allyl alcohol (**237**) following a procedure developed by Eschenmoser. The first step of this procedure required allyl alcohol (**237**) to be

refluxed with phosphoric acid under basic conditions then converted to the biscyclohexylamine salt (**238**). (Scheme 49).



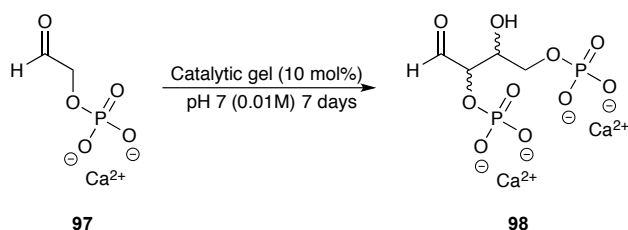
Scheme 49: Synthesis of allyl phosphate biscyclohexylamine salt (**238**)

Ion exchange was performed in water to produce the free phosphoric acid which was mixed with triethylamine to give the triethylamine salt. To produce the aldehyde, ozonolysis was performed followed by ion exchange, then calcium acetate was added to give glycolaldehyde phosphate as the calcium salt (**97**). (Scheme 50).



Scheme 50: Synthesis of glycolaldehyde phosphate calcium salt (**97**)

With the glycolaldehyde phosphate calcium salt (**97**) in hand, we began to perform reactions using the benzylglutamine amide (**230**) gel. To do this, a hydrogel of benzylglutamine amide (**230**) (pH 7, 0.01M) was formed by heating, sonication then cooling. Once the gel had formed, a suspension of glycolaldehyde phosphate calcium salt (**97**) in water (200 μL pH 7, 0.01 M) was added to the surface of the gel and rolled over to ensure the entirety of the gel surface was covered. In the first instance, the reaction was left for 7 days simply to establish if any product could form.



Scheme 51: Dimerisation of glycolaldehyde phosphate calcium salt (**97**)

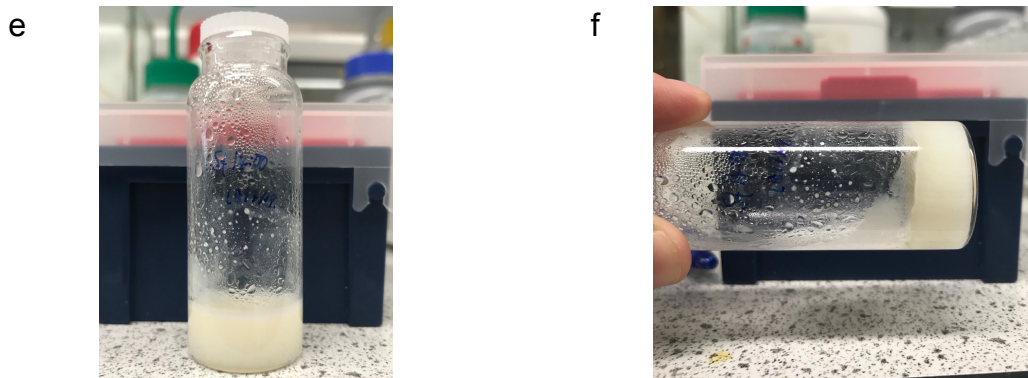
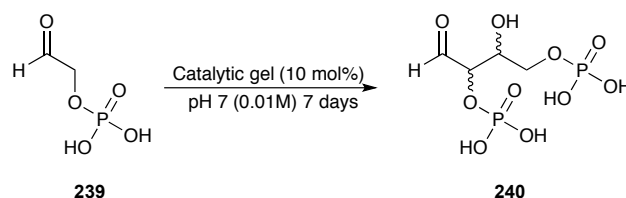


Figure 150: Images of the gel at the start of the reaction with reagents added (e), and after 7 days (f)

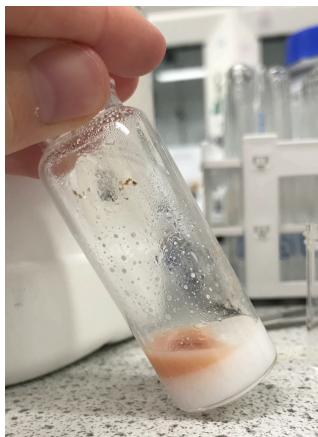
After 7 days, ^1H NMR spectroscopy indicated no reaction had taken place and no product was detected by ESI mass spectrometry. This could be due to the poor solubility of the starting material (**97**), as dianionic phosphates are quite insoluble in water.¹⁷¹

A second approach was taken to try and overcome the insolubility of starting material. Instead of producing the calcium salt of the glycolaldehyde phosphate (**97**), the free phosphoric acid of glycolaldehyde phosphate (**239**) was used, as this was more soluble in water. To ensure that the correct product had been isolated, a small proportion of the glycolaldehyde phosphoric acid (**239**) was transformed into the calcium salt (**97**) so that the ^1H NMR could be directly compared to Eschenmoser's ^1H NMR analysis.⁹⁷ The ^1H NMR data of both the free phosphoric acid (**239**) and the calcium salt of glycolaldehyde phosphate (**97**) showed that the product was clean and more importantly, the correct compound. The free acid was once again dissolved in water (pH7 0.01 M buffer, 200 μL) and added to the surface of the gel. Within 5 minutes, the gel network dissolved. As the gel network broke down, it was decided that after 48h the reaction would be worked up to determine if any reactions had taken place. Analysis by ^1H NMR indicated that no reaction had taken place.



Scheme 52: Dimerization of glycolaldehyde phosphate free acid (**240**)

g



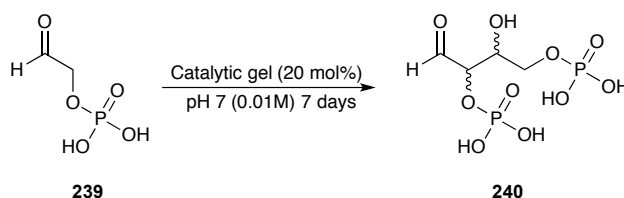
h



Figure 151: Glycolaldehyde phosphate reaction on the gel using the free acid (**239**) at the start (g) and after 48h (h)

Nonetheless a second reaction was set up. This time even, when the gel broke down, it was left for 7 days to determine whether any product would form over a longer duration. Once again, no evidence of new ^1H or ^{31}P signals were found in the ^1H NMR spectrum.

As we hypothesised earlier that loss of the gel network might have resulted in the catalyst being more disperse in solution and therefore make the possibility of reaction less likely, it was decided that the gelator and therefore catalytic loading should be increased to help stabilise the gel network. In addition, if there was breakdown of the gel network there would then be a greater concentration of catalyst in solution. The gelator loading was doubled (8 mg/mL) and gel formation was performed in the same way as previously described. Once the gel had formed, the same quantity of glycolaldehyde phosphoric acid (**239**) in water as used in previous reactions was pipetted onto the surface of the gel. Within a couple of minutes the gel broke down and after a couple of hours the solution was transparent. The reaction was left for 7 days to determine if this increased catalytic loading would allow the reaction to take place.



Scheme 53: Dimerization of glycolaldehyde phosphate (**239**) with higher catalytic and therefore gelator loading of benzylglutamine amide (**230**)



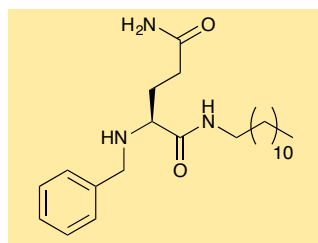
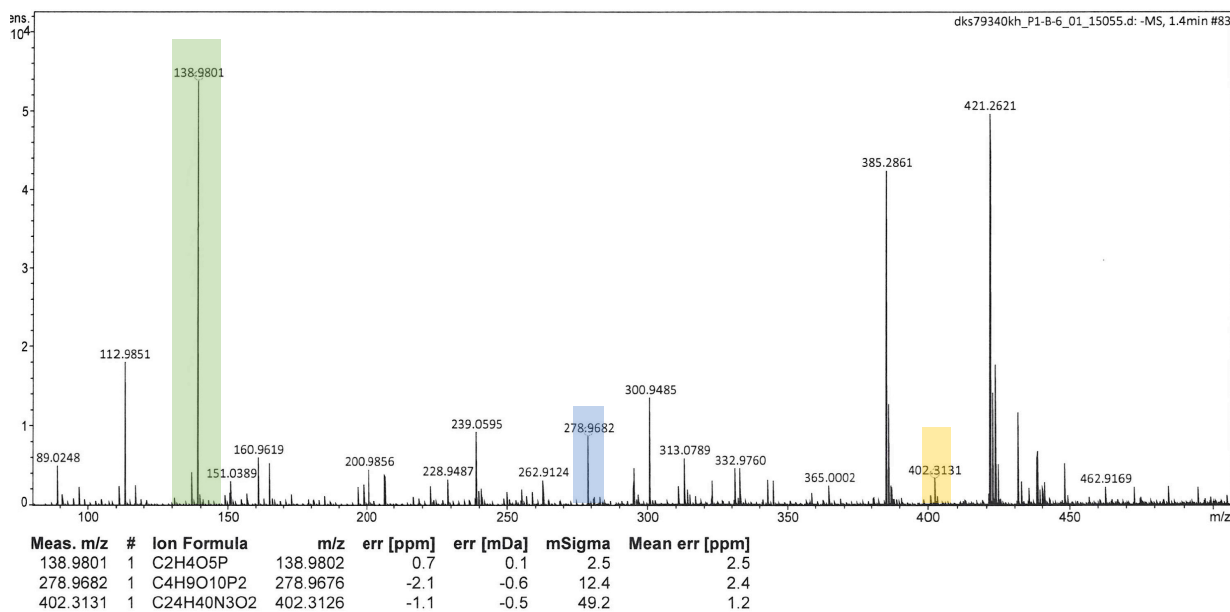
Figure 152: (i) Benzylglutamine amide (**230**) gel before reagents loaded, (j) once reagents (**239**) added resulting in the loss of the gel network

During the 7-day duration of the reaction something unexpected happened; a translucent gel formed. Benzylglutamine amide (**230**) does not usually reform its gel network, therefore it can be assumed that a chemical reaction has taken place, resulting in gelation. The gelation could be due to formation of the desired products, the formation of an intermediate or even a new supramolecular interaction between the catalyst and reagents/products present in solution.

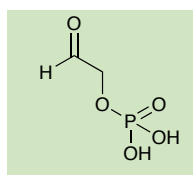


Figure 153: In situ gel during the dimerization of glycolaldehyde phosphate (**239**) catalysed by benzylglutamine amide (**230**)

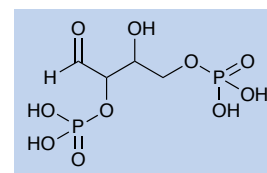
To understand what was causing gelation to take place, a sample was taken and analysed by SEM, ESI negative ion mass spectrometry, IR and NMR (^1H and ^{31}P). The results of mass spectrometry showed that tetrose-2,4-diphosphate (Figure 154) was present in the sample as well as the starting glycolaldehyde phosphate and catalyst.



230



239



240

Figure 154: Electrospray mass spectrum of gel formed *in situ*

Based upon previous work with the diphenyl hydrazine derivatives of threose and erythrose (Chapter 4), we have been able to analyse by ^1H NMR the crude reaction material (Figure 158). The triplet at 5.14 ppm corresponds to the aldehyde proton of glycolaldehyde phosphate (**239**), the resonance frequency for this proton is low as it is present as the hydrate (**243**). We believe that the peaks which appear at 5.26 ppm and 5.31 ppm correspond to the 'aldehyde' proton in the 2,4-diphosphate tetrose products, present as the hydrate form (**241/242**) in the ^1H NMR spectrum therefore the chemical shift is significantly lower than the aldehyde. The J couplings of these peaks are in keeping with each other, 2.6 Hz for the doublet at 5.31 ppm and 3.6 Hz for the doublet at 5.26 ppm. This is the same pattern that we observed in the diphenyl hydrazone protected erythrose (**232/233**) and threose products (**234/235**), where the threose (**234/235**) (5.7 Hz) coupling constant was lower than that of the erythrose (**234/235**) (6.0 Hz). Based upon these similarities we can propose that the peak at 5.31 ppm corresponds to the

erythrose (**242**) product and the peak at 5.26 ppm corresponds to the threose (**241**) product. This gives a diastereomeric ratio of erythrose (**242**) to threose (**241**) of 1:0.69, which is similar to previous work with the non-phosphorylated system. In addition the total percentage conversion to 2,4-diphosphorylated tetrose products (**98**) is 10%. This experiment was carried out twice more to see if the results were consistent (Table 29). In the repeat reactions, we observed higher conversions, but the diastereomeric ratio determined by ^1H NMR is fairly consistent. However, to confirm these findings, standards will need to be made to ensure product assignment is robust

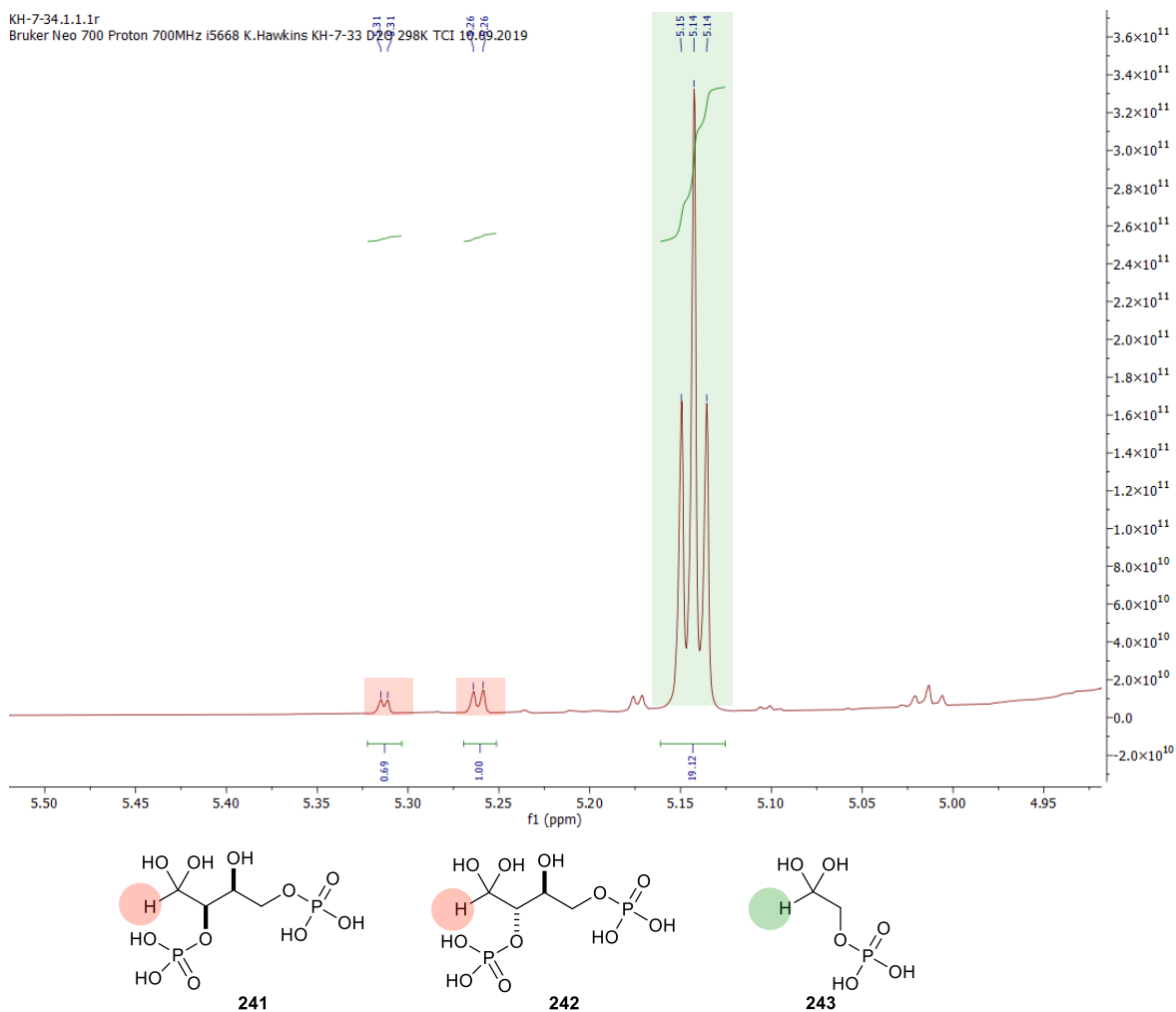


Figure 155: ^1H NMR spectrum of crude glycolaldehyde phosphate (**239**) dimerization ^1H NMR (700 MHz) D_2O

Table 29: Dimerization of glycolaldehyde phosphate (**239**) with benzylglutamine amide (**230**) hydrogel pH7

Run	Conversion %	NMR dr threose:erythrose
1	10	1.00:0.69
2	31	1.00:0.83
3	31	1.00:0.94
Blank run	0	N/A

The network of the gel that assembles *in situ* was analysed by scanning electron microscopy, (SEM), with samples being prepared in the same manner as described in Chapter 3 where the sample is dried and stained. The images showed a very interesting morphology. The morphology is more honeycomb-like and less fibrous compared to other gels shown in this report. The nanofibres in the gel are between 160 nm and 320 nm in width.

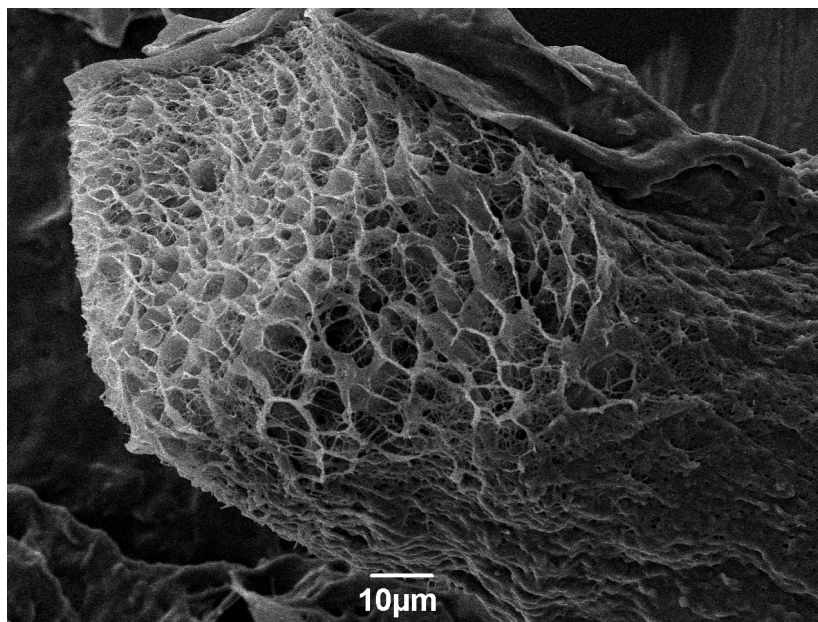


Figure 156: SEM image of gel formed *in situ* 1000 magnification

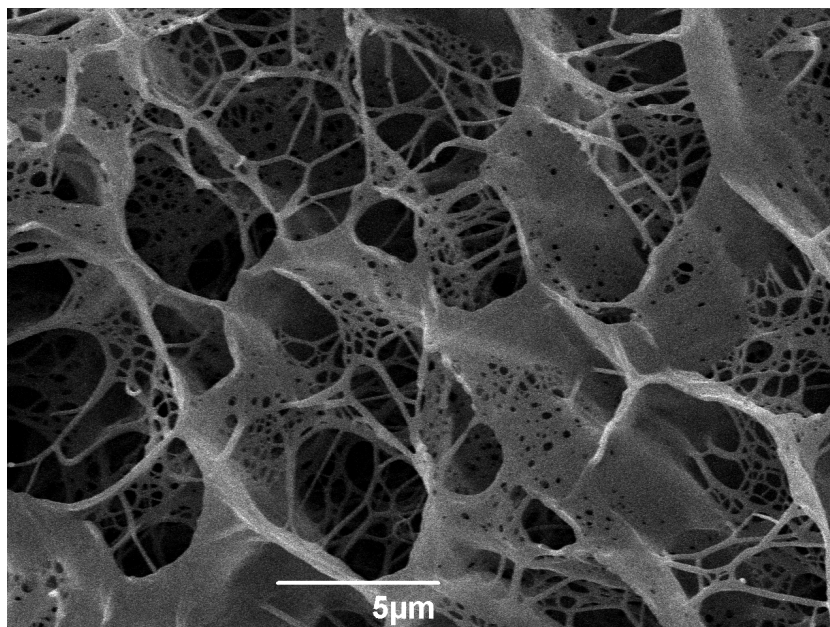


Figure 157: SEM image of gel formed *in situ* 5000 magnification

To analyse the gel by ^1H NMR directly, the dimerization of glycolaldehyde phosphate (**239**) catalysed by benzylglutamine amide (**230**) was repeated in an NMR tube. To do this, deuterated water was added to benzylglutamine amide (**230**) the suspension underwent a heat-sonicate-cycle before the addition of a spike of DMSO (10 μL). The mixture was then transferred to an NMR tube and left to cool. Once the gel had formed glycolaldehyde phosphate (**239**) dissolved in deuterated water was added to the top of the gel in the NMR tube. In the same way that the reaction vial gel dissolved, the gel formed in the NMR tube dissolved completely. The sample was then left for the same duration to allow gel formation to occur ca. 5 days. The results of the NMR experiment showed that 3% of the glycolaldehyde phosphate could be observed as mobile in the gel the benzylglutamine amide (**230**) and any product peaks do not appear in the NMR spectrum therefore must be immobilised in the gel.

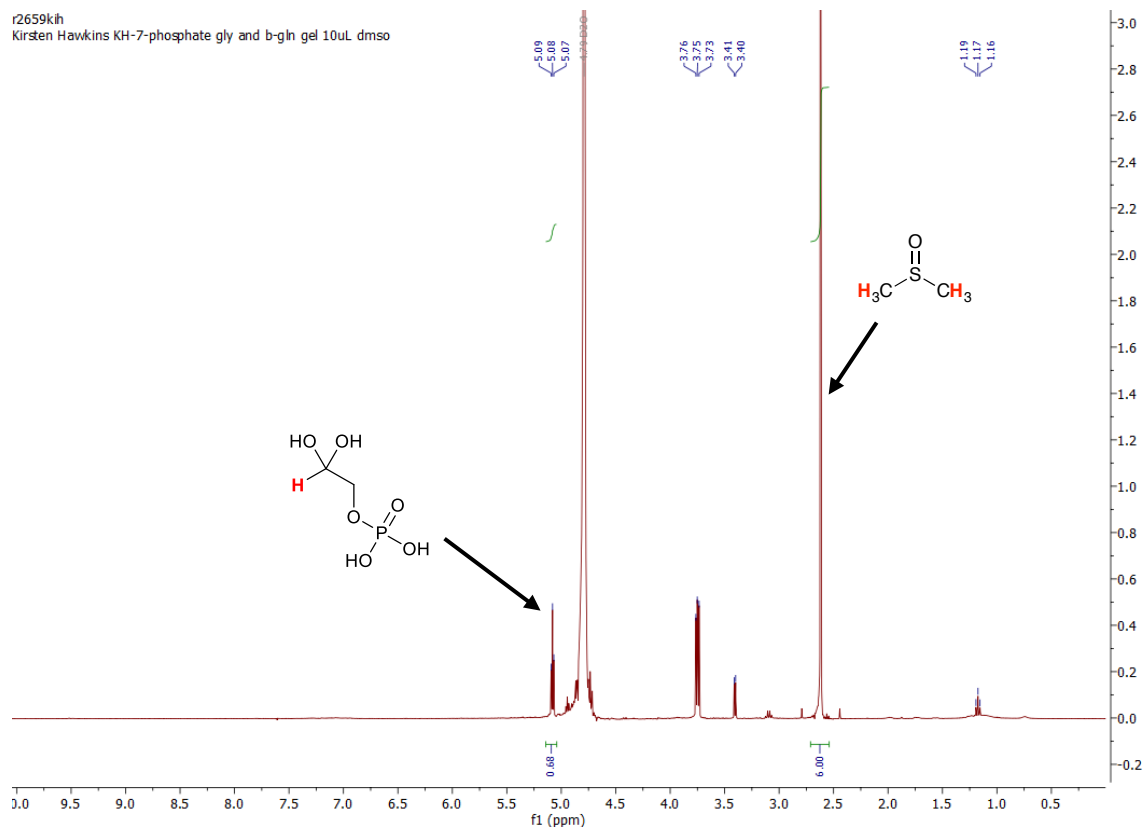
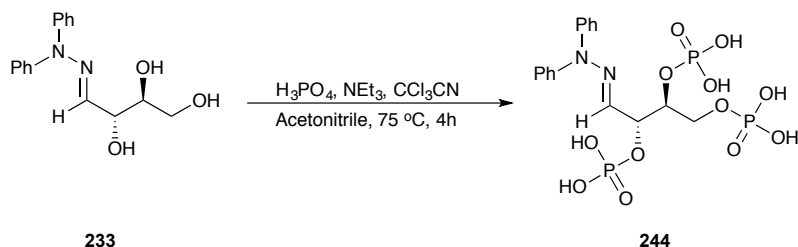


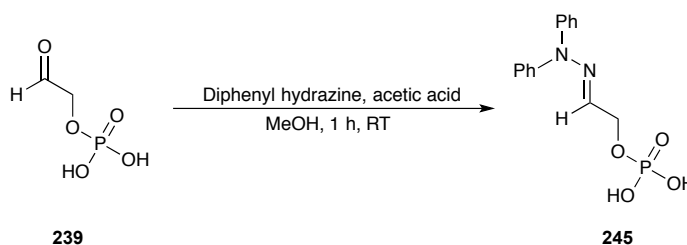
Figure 158: ¹H NMR of hydrogel formed in the catalysis of glycolaldehyde phosphate (**239**) dimerization. 10uL DMSO spike

Now that we have showed that 2,4-diphosphate tetrose sugars (**240**) can be synthesised by benzylglutamine amide (**230**) we wanted to establish whether there was an enantioselectivity. To do this we need to make 5 standards, both enantiomers of threose and erythrose (**240**) and also a standard of the glycolaldehyde phosphate (**239**). These standards need to be UV active so that we can employ HPLC techniques as previously described for determining the ee% of threose and erythrose (Chapter 4). To do this, L-erythrose trapped with diphenyl hydrazine (**233**) was phosphorylated (**244**) it by refluxing in phosphoric acid for 4 h. Unfortunately, no reaction appeared to have taken place as both mass spectrometry and ¹H NMR and ³¹P showed no product. We therefore propose that a different method to exhaustively phosphorylate diphenyl hydrazine trapped erythrose is required.

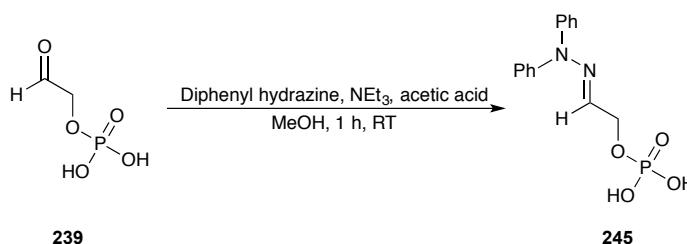


Scheme 54: Method for the phosphorylation of diphenyl hydrazone trapped L-erythrose (**233**)

Glycolaldehyde phosphate (**239**) was reacted with diphenyl hydrazone to try and yield the hydrazone (**245**). Two approaches to this were taken, the first was to trap using the same method as in Chapter 4 (Scheme 55) however this did not produce the desired product. To determine if the diphenylhydrazone was being protonated by the phosphoric acid hence preventing reaction, five equivalents of triethylamine were added (Scheme 56). However this also failed to give the desired product.



Scheme 55: Method 1 of diphenylhydrazone trapping of glycolaldehyde phosphate (**239**)



Scheme 56: Method 2 of diphenylhydrazone trapping of glycolaldehyde phosphate (**239**)

Inspired by the formation of the diphosphate derivatives of threose and erythrose (**98**) we turned our attention to a preliminary experiment to see if the aldol condensation of formaldehyde (**88**) and glycolaldehyde phosphate (**239**) (Scheme 57), originally reported by Eschenmoser,⁹⁷ could take place either in the gel or in solution phase. Analysis of the reaction by ^1H NMR and ESI mass spectrometry showed that no products had been formed. In addition when reagents were added to the surface of the gel the gel structure was destroyed.

required to allow an ee% to be determined, for example by trapping with a different UV active group then phosphorylating exhaustively or by using an enzyme to remove the phosphate groups to yield erythrose and threose, which can then be trapped as the diphenylhydrazine. Furthermore, the synthesis of glycolaldehyde phosphate (**239**) needs to be optimised to ensure that the final product is clean.

6.0 Conclusions and Future work

In Chapter 2, it was shown that simple amino acid amides are able to catalyse a simple aldol condensation reaction between 4-nitrobenzaldehyde and cyclohexanone with good conversion, but limited selectivity thought to be due to the heterogeneous nature of the reaction. In addition it was shown that these single amino acid amides are able to form gels either organogels or hydrogels. However, the gels were unable to survive the catalytic reaction intact. It is therefore suggested that on enamine formation non-covalent interactions between gelators are lost, causing gel breakdown. It would be interesting to investigate this further by exploring a broader range of amino acids to try and understand any key features that might result in a more stable gel. In addition, changing the C12 chain length, either increasing or decreasing, could also reveal some further information about the supramolecular nature of these compounds. For example, with glutamine amide, shortening the chain length might help with solubility in water allowing a more consistent gel to form. Whereas, increasing chain length could make the molecule more surfactant-like therefore catalytically-proficient micellar or vesicle structures might be observed.

In Chapter 3, the spontaneous formation of a hydrogel on mixing 4-nitrobenzaldehyde with glutamine amide was studied and it was found that these two-components formed a Schiff base *in situ* and resulted in a super gelator gelling with 0.6 mg glutamine amide and 1 equivalent of 4-nitrobenzaldehyde in 1 mL of water. However, the two-component hydrogel formed gels more consistently at a total loading of 1.48 mg/mL. It was also found that a 1:1 ratio of 4-nitrobenzaldehyde: glutamine amide formed the best hydrogels, but the aldehyde could be as low as 0.7 eq with respect to glutamine amide. The two-component hydrogel was also found to be able to be tuned depending upon aldehyde selection. Upon changing aldehyde there was a different morphology identified by

SEM and TEM images as well as differences in thermal stability (T_{gel}). In addition it was found that this two-component hydrogel has the ability to reform, which was hypothesised to be related to the dynamic nature of the formation of the Schiff base. Rheological studies of this system need to be improved to help give further insight into physical properties of the gel, especially with regards to the gels ability to reform. It would also be interesting to see how the rheological properties change with aldehyde. This could allow a mix and match approach to be taken with application of gels. Again the effect of chain length and amino acid could also be investigated to see how versatile the two-component system.

In Chapter 4 the Schiff base present in the two-component gel was reduced to produce a second generation of catalytic gelator. This compound was found to be a super hydrogelator gelling at 0.3 mg/mL. The gel was found to have good thermal stability and also a more nano-scale sample-spanning network identified by SEM imaging. In addition, the gelator was also shown to be catalytically active as a monomer for solution phase catalysis of 4-nitrobenzaldehyde and cyclohexanone with good conversion ca. 50% after 72 h, and some selectivity for the *anti*-product over the *syn*-product ca. 2:1. From here the ability of this compound to form gels was combined with its catalytic ability, and was tested as a catalyst for the prebiotically relevant dimerization of glycolaldehyde to produce threose and erythrose using the hydrogel. It was thought that as the dimerization of glycolaldehyde is a water-soluble reaction loss of the gel network should be prevented. Indeed the gel structure remained intact in these studies. It was reasoned that the additional non-covalent interactions between aromatic rings help stabilise the gel. The gel was found to be an effective catalyst, giving diastereoselectivity for threose over erythrose with a 2.2:1 d.r in addition a small enantioselectivity was observed by chiral HPLC for the *D* enantiomer, this was more apparent for threose with ca. 10% at pH 7. This particular area of research discussed has the potential to be expanded further by forming gelators with different amino acids as this could have an impact on both d.r and ee%.

In Chapter 5 the second-generation catalytic gelator was tested further in prebiotically-relevant reactions. Although this specific gelator did not produce any deoxy-ribose products it did turn over the dimerization of glycolaldehyde phosphate. We tentatively suggested selectivity for threose over erythrose and a

typical conversion of ca. 24%. This is highly promising given that the formation of phosphate-modified sugars is a relatively under-explored area of prebiotic chemistry. A significant amount of work needs to be done to fully analyse the results obtained from this process. One of the problems encountered was with making standards of the threose and erythrose 2,4-diphosphates. There is potential here for multiple synthetic approaches to form standards. One approach could utilise the enzyme phosphatase. The reaction mixture could be exposed to this enzyme which would dephosphorylate the sugars formed. The resulting mixture could then be trapped with diphenyl hydrazine and analysed using the method developed in Chapter 4 by chiral HPLC and ^1H NMR to give both diastereo and enantio selectivities. It was also found in Chapter 5 that during the dimerization of glycolaldehyde phosphate, a gel formed *in situ*. This was unexpected and needs to be characterised fully by CD, rheology, T_{gel} as well as establishing the reason for gel formation. It is interesting to speculate that gel formation in prebiotic reaction processes could be an interesting mechanism for driving reactions to completion, or for trapping and amplifying specific products from complex reaction mixtures.

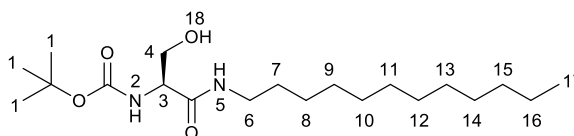
7.0 Experimental

General Experimental:

Unless otherwise noted all compounds were bought from commercial suppliers and used without further purification. Where a solvent is described as “dry” it was purified by PureSolv alumina columns from Innovative Technologies. Melting points were determined using a Stuart SMP3 apparatus. Optical rotations were carried out using a JASCO-DIP370 polarimeter and $[\alpha]_{\text{D}}^{25}$ values are given in $\text{deg. cm}^3 \text{ g}^{-1} \text{ dm}^{-1}$. Infra-red spectra were acquired on a ThermoNicolet Avatar 370 FT-IR spectrometer. Nuclear magnetic resonance spectra were recorded on a Jeol ECS-400, a Jeol 500 Avance III HD 500 or a Jeol AV500 at ambient temperature. Coupling constants (J) are quoted in Hertz. Mass spectrometry was performed by the University of York mass spectrometry service using electron spray ionisation (ESI) technique. Thin layer chromatography was performed on glass-backed plates coated with Merck Silica gel 60 F254. The plates were developed using ultraviolet light, acidic aqueous ceric ammonium molybdate or basic aqueous potassium permanganate. Liquid chromatography was performed using forced

flow (flash column) with the solvent systems indicated. The stationary phase was silica gel 60 (220–240 mesh) supplied by SigmaAldrich. Preparative Thin Layer Chromatography (PTLC) was carried out on 20x20 2000 micron silica plates with UV254 purchased from Uniplate. High Performance Liquid Chromatography (HPLC) was performed using an Agilent 1100 series instrument using the chiral columns indicated and a range of wavelengths from 210-280 nm for detection. Buffer solutions, pH 6 and pH 7 phosphate buffers, were purchased as ready-made solutions from Fisher Scientific.

7.1 Synthesis of L-Boc-serine dodecylamine (248)

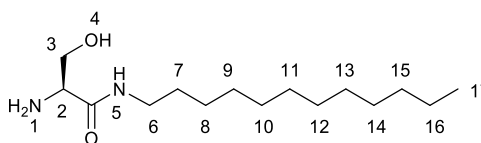


248

Figure 69: Boc-Serine amide

N-(tert-Butoxycarbonyl)-L-serine (Boc-Ser) (400 mg, 1.94 mmol) was dissolved in DCM (50 mL) and stirred at 0 °C for 5 minutes. Then EDC (647 mg, 3.37 mmol, 1.74 eq) DMAP (236 mg, 1.97 mmol) and dodecylamine (359 mg, 1.94 mmol) were added. The mixture was stirred for 2 hours at 0 °C followed by a 12 hour stir at room temperature. The reaction mixture was then washed with 2 M hydrochloric acid solution (20 mL), water, 1 M NaOH (20 mL) and brine (20 mL). The organic solvent was dried over magnesium sulfate then was removed *in vacuo* to yield a white solid (66 % 487 mg, 1.31 mmol). **Mp** 61-63 °C; **IR** ν_{max} (cm⁻¹): 3378 m, 3318 m, 2953 m, 2918 s, 2850 m, 1686 s, 1649 s, 1642 s, 1549 s, 1506 vs, 1468 m, 1443 w, 1390 m, 1367 m, 1336 m, 1317 m, 1303 m, 1269 m, 1237 s, 1164. s, 1099 m, 1076 s, 1054 s, 1030 w, 854 w, 784 w, 722 m, 660 m, 599 s, 551 m, 511 w, 466 w; **[α]_D²⁵** (deg cm³ g⁻¹ dm⁻¹) -32.4 (c = 1.0, chloroform); **¹H NMR** (400 MHz, DMSO-d₆) δ ppm 7.72 (1H, br t, *J*=5.3 Hz, H₅), 6.57 (1H, d, *J* = 8.2 Hz, H₂), 4.78 (1H, t br, *J* = 5.7 Hz, H₁₈), 3.89 (1H, q, *J* = 6.9 Hz, H₃), 3.41-3.57-3.42 (2H, m, H₄) 2.90-3.16 (2H, *sptd*, H₆) 1.45-1.31 (11H, m, H₁, H₇), 1.23 (18H, m, H₈₋₁₆), 0.85 (3H, t, *J* = 7.3 Hz, H₁₇). **¹³C NMR** (100.53 MHz, DMSO-d₆) δ ppm: 170.27 (HN-C=O), 155.28 (C-boc C=O), 78.29 (Boc CH₃-C), 61.97 (C-4), 57.01 (C-3), 31.44 (C-6), 29.10 (CH₂), 28.85 (C-1), 26.35 (C-7-15), 21.75 (C-16) 14.04 (C-17) **ESI-MS** (m/z) cal C₂₀H₄₀N₂NaO₄ 395.2880, found 395.2880 (100% [M+Na]⁺)

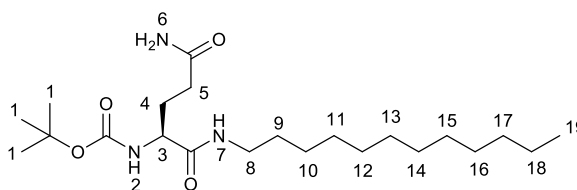
7.2 Synthesis of L-serine dodecylamine (209)



209

L-Boc-Ser amide (**248**) (487 mg, 1.31 mmol) was added to a solution of HCl in dioxane (4.91 mL, 4 M, 15 eq) and stirred for an hour. The solvent was removed *in vacuo* then washed with 1 M NaOH (10 mL) and extracted into DCM (40 mL). The solvent was removed *in vacuo* (313 mg, 1.15 mmol, 88 %). **Mp** = 73-75.5 °C; **IR** ν_{\max} (cm⁻¹): 3299 m, 3156 w, 2935 w, 2919 vs, 2849 s, 1658 vs, 1563 s, 1532 w, 1479 w, 1464 m, 1414 w, 1371 w, 1303 w, 1253 m, 1123 w, 1120 w, 1060 m, 1020 m, 967 w, 922 w, 919 w, 878 w, 722 m, 636 w, 588 w, 514 w, 479 w; **[α]_D²⁵** (deg cm³ g⁻¹ dm⁻¹) -6.4 (c = 1.0, chloroform); **¹H NMR** (400 MHz, DMSO-d₆) δ ppm 8.44 (1H, t, *J* = 5.5 Hz, H₅), 8.14 (3H, br s, H₁), 4.70 (1H, t, *J* = 7.2 Hz, H₄), 3.62 - 3.80 (2H, m, H₆), 3.5-3.46 (2H, m, H₃), 3.14 (1H, q, H₂), 3.09 (2H, m, *J* = 7.8 Hz, H₇), 1.41-1.36 (2 H, m, H₈), 1.24 (18 H, s, H₉₋₁₇), 0.85 (3H, t, *J*=7.8 Hz, terminal H₁₈). **¹³C NMR** (100.53 MHz, DMSO-d₆) δ ppm: 170.27 (HN-C=O), 61.97 (C-3), 57.01 (C-2), 31.44 (C-6), 29.10 (CH₂), 28.85 (C-1), 26.35 (C-7-15), 22.23 (C-16) 14.54 (C-17); **ESI-MS** (m/z) cal C₁₅H₃₃N₂O₂ 273.2537, found 273.2538 (100% [M+H]⁺), and cal C₁₅H₃₃N₂NaO₂ 295.2356, found 295.2357 (31 % [M+Na]⁺)

7.3 Method one for the synthesis of L-Boc-glutamine dodecylamine (249)

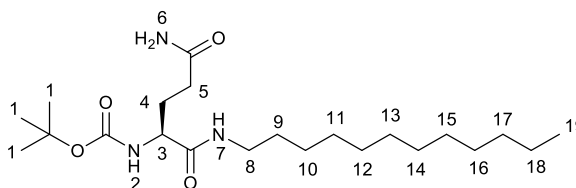


249

Figure 70: Boc Glutamine amide

L-Boc-Gln-OH (0.241 g, 0.977 mmol) was dissolved in THF (6 mL) and stirred at 0 °C for 5 minutes. Then HOBt (0.235 g, 1.74 mmol) and dodecylamine (0.181 g, 0.977 mmol) were added. The mixture was stirred for 2 hours at 0 °C followed by a 12 hour stir at room temperature. The solvent was then removed *in vacuo*, redissolved in ethyl acetate and washed with NaHCO₃ (20 mL), 5% potassium bisulfate (20 mL) and saturated brine (20 mL), the organic layer was dried over magnesium sulphate. The solvent was then removed *in vacuo* yielding a white solid (258.69 mg, 0.625 mmol, 64%). **Mp**: 109-110 °C; **IR** ν_{\max} (cm⁻¹): 3380 w; 3319 w, 3251 w, 3196 w, 3077 w, 2922 m, 2852 m, 1962 w, 1691 s, 1653 vs, 1619 m, 1560 m, 1515 s, 1455 m, 1415 m, 1391 m, 1364 m, 1319 m, 1286 m, 1246 s, 1168 s, 1089 w, 1058 w, 1028 w, 999 w, 866 w, 785 w, 721 w, 638 m, 597 m, 554 m, 481 w, 464 w, 457 w; **[α]_D²⁵** (deg cm³ g⁻¹ dm⁻¹) -9.7 (c = 1.0, chloroform); **¹H NMR** (400 MHz, DMSO-*d*₆) δ ppm 7.71 (1 H, br t, *J*=5.5 Hz, CO-H₇), 7.26 (1H, br s, H₂), 6.78 (2H, br t, *J*=14.7 Hz, H₆), 3.81 (1 H, q, *J*=8.7 Hz, H₃), 1.98 - 2.13 (2 H, m, H₅), 2.93 - 3.13 (2 H, m, H₈), 1.58 - 1.86 (2 H, m, H₄), 1.41 (11 H, m, H₁, H₉), 1.21 (20 H, m, H₁₀₋₁₈), 0.85 (3 H, t, *J* = 8.2, H₁₉); **¹³C NMR** (100.53 MHz, DMSO-*d*₆) δ ppm: 173.79 (H₂N-C=O), 171.55 (HN-C=O), 155.28 (C-Boc C=O), 77.98 (Boc CH₃-C), 52.81 (C-3), 38.37 (C-5), 31.62 (C-4), 31.34 (C-8), 29.05 (CH₂), 28.85 (CH₂), 28.75 (CH₂), 27.87 (CH₂) 26.29 (C-4), 22.13 (C-18) 14.04 (C-19); **ESI-MS** (m/z) calc C₂₂H₄₃N₃NaO₄ 436.3146, found 436.3151 (100% [M+Na]⁺).

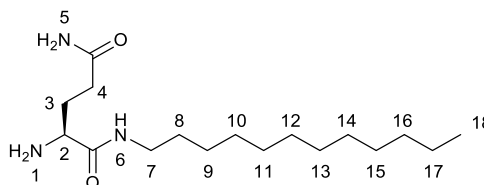
7.4 Method two for the synthesis of L-Boc-glutamine dodecylamine (249)



249

Boc-Gln-OH (482 mg, 1.97 mmol) was dissolved in DCM (30 mL) and stirred at 0 °C for 5 minutes. Then EDC (660 mg, 3.56 mmol) DMAP (239 mg, 1.97 mmol) and dodecylamine (362 mg, 1.97 mmol) were added. The mixture was stirred for 2 hours at 0 °C followed by a 12 hour stir at room temperature. The reaction mixture was then washed with 2 M hydrochloric acid solution (20 mL), water, 1 M NaOH (20 mL) and brine (20 mL). The organic solvent was dried over magnesium sulfate. The organic solvent was removed *in vacuo* to yield a white solid. The organic solvent was removed *in vacuo* to yield a white solid (422.71 mg, 1.02 mmol, 52%). Data matched that reported in 7.2

7.5 Synthesis of L-Glutamine dodecylamine (210)

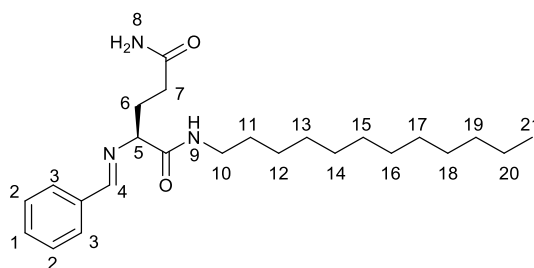


210

To deprotect, L-Boc-Gln amide (**249**) (100 mg, 0.242 mmol) was added to a solution of 4 M HCl in dioxane (15 eq) and stirred for 1 h. Solvent was removed *in vacuo* to yield a white solid (75 mg, 0.241 mmol, 100%). The solid (75 mg) is then deprotonated using NaOH (1 M) and extracted with DCM to give the free amine (40 mg, 0.127 mmol, 53%). **Mp** = 117-119°C ; **IR** ν_{max} (cm⁻¹): 3411 w, 3380 w, 3321 w, 3157 w, 3079 w, 2919 m, 2850 m, 2708 vw, 2564 vw, 2502 vw, 2386 vw, 2024 vw, 2016 vw, 1998 vw, 1962 m, 1691 m, 1651 vs, 1616 m, 1548 m, 1532 m, 1518 m, 1449 s, 1429 m, 1415 m, 1392 w, 1367 m, 1321 w, 1303 w, 1284 m, 1272 m, 1248 m, 1211 w, 1169 m, 1114 w, 1100 w, 1057 w, 1039 w, 1027 w, 984 w, 951 vw, 935 vw, 915 w, 892 w, 861 w, 825 w, 802 w, 792 w, 773 w, 755 w, 730 w, 719

w, 666 w, 631 m, 596 m, 581 m, 561 m, 546 m, 539 m, 494 w, 484 m, 464 w, 457 w; $[\alpha]_D^{25}$ (deg cm³ g⁻¹ dm⁻¹) -25.21 (c = 1.0, chloroform); **¹H NMR** (400 MHz, DMSO-*d*₆) δ ppm 7.75 (1 H, t, *J*=5.5 Hz, H₆), 7.22 (3 H, br d, *J*=3.6 Hz, H₁), 6.67 (3 H, s, H₅), 3.10 – 2.92 (1 H, m, H₂), 2.1-1.95 (2H, m, H₄) 1.76-1.68 (2 H, m, H₃), 1.55-1.45 (2H, m, H₇), 1.41-1.30 (2 H, m, H₈), 1.21 (18 H, m, H₉₋₁₇) 0.85 (3 H, t, *J*=5.5 Hz, H₁₈); **¹³C NMR** (100.53 MHz, DMSO-*d*₆) δ ppm: 174.77 (H₂N-C=O), 174.29 (NH-C=O), 54.48 (C-3), 38.29 (C-4), 31.77 (C-3), 31.34 (C-7), 31.26 (CH₂), 31.19 (CH₂), 29.06 (CH₂), 28.76 (CH₂), 26.44 (C-7), 22.14 (C-18) 14.09 (CH₂-CH₃).; **ESI-MS** (m/z) calc C₁₇H₃₆N₃O₂ 314.2802, found 314.2802 (100% [M+H]⁺).

7.6 Synthesis of (*E*)-2-(benzylideneneamino)-N¹-dodecyl-L-glutamine amide (**231**)

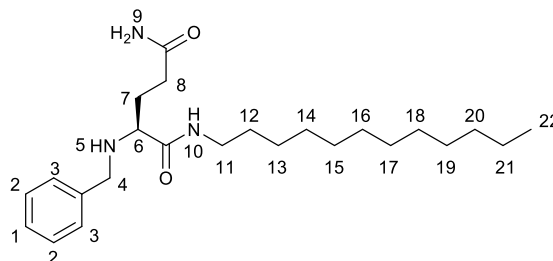


231

To L-glutamine amide (**230**) (351 mg, 1.23 mmol) was added benzaldehyde (0.14 mL, 1.35 mmol, 1.2 eq) followed by 100 mL of water. The suspension was sonicated for 2 minutes then heated until boiling or until fully dissolved to initiate gelation. The solution was then left to cool. Once the solution had gelled, it was extracted into DCM (3x 50 mL) the organic layer was removed *in vacuo* to yield a white solid (413.9 mg, 84% yield 1.03 mmol); **IR** ν_{\max} (cm⁻¹): 3411 w, 3298 m, 2918 s, 2872 w, 2850 m, 1649 vs, 1639 s, 1579 w, 1547 s, 1467 m, 1451 m, 1434 m, 1410 m, 1380 w, 1338 w, 1308 m, 1236 w, 1157 w, 756 m, 720 w, 695 s, 670 m, 623 m, 618 m, 585 m, 559 m, 502 w; **¹H NMR** (400 MHz, DMSO-*d*₆) δ ppm: 8.31 (s, 1H, H₄), 8.33 (d, 2H, *J* = 8.9 Hz, H₃), 7.63 (t, 1H, *J* = 5.9 Hz, H₉), 7.56-7.37 (m, 3H, H₁₋₂), 7.27 (s broad, 1H, H₈), 6.72 (s broad, 1H, H₈), 3.98-3.76 (m, 1H, H₅), 3.31-3.02 (m, 2H, H₁₀), 2.21-1.85 (m, 2H, H₆), 1.44-1.36 (m, 2H, H₇), 1.46-1.32 (m, 2H, H₁₁), 1.28-1.15 (m, 20H, H₁₂₋₂₀), 0.84 (t, 3H, *J* = 7.2 Hz, H₂₁), **ESI-MS** (m/z) cal, C₂₄H₄₀N₃O₂ 402.3115 found 402.3117 (47% [M+H]⁺) and cal C₂₄H₃₉N₃NaO₂ 424.2934 found 424.2936 (100% [M+Na]), **¹³C NMR** (100.53 MHz, DMSO-*d*₆) δ ppm 174.13 (NH₂-C=O), 171.00 (NH-C=O), 162.95 (C-4), 131.59 (C

aromatic), 129.14 (C aromatic), 31.83 (C-7), 30.35 (C-6), 29.26 (CH₂), 26.86 (CH₂), 22.64 (CH₂-CH₃), 14.51 (terminal CH₃);

7.7 Synthesis of 2-Benzylamino-N¹-dodecyl-L-glutamine amide (230)

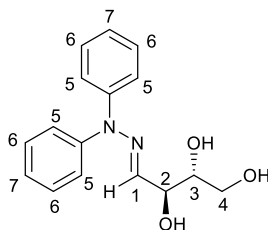


230

To L-glutamine amide (**210**) (200 mg, 0.64 mmol) was added benzaldehyde (81 uL, 0.77 mmol, 1.2 eq) followed by 100 mL of water. The suspension was sonicated for 2 minutes then heated until boiling or until fully dissolved to initiate gelation. The solution was then left to cool. Once the solution had gelled, it was extracted into DCM (3x 50 mL) the organic layer was removed *in vacuo* to yield a white solid. A methanol (10 mL) solution of sodium borohydride (10 eq) was added to the white solid. The solution was left to stir. Once TLC (90:10 DCM:MeOH) indicated that reduction of both residual aldehyde and the imine had taken place the solvent was removed *in vacuo*, then re-dissolved in DCM (20 mL) filtered and washed with ammonium chloride (NH₄Cl) solution. The organic layer was removed *in vacuo* to yield either a clear sticky oil or a white product. If a clear sticky oil was observed diethyl ether 20 mL was added then removed *in vacuo* to yield a white solid. (218 mg, 84% 0.54 mmol). **Mp** 90-91°C; **IR** ν_{max} (cm⁻¹): 3397 m 3301 m, 3213 w, 2955 m, 2919 s, 2851 s, 1655 vs, 1640 s, 1627 s, 1551 s, 1496 w, 1466 m, 1453 m, 1415 m, 1377 m, 1344 m, 1309 w, 1276 m, 1257 m, 1247 m, 1209 w, 1153 w, 1128 w, 806 w, 745 m, 721 m, 696 s, 669 s, 655 s, 611 s, 598 s, 509 m, 465 m **[α]_D²⁵** (deg cm³ g⁻¹ dm⁻¹) -4.64 (c = 1.0, chloroform); **¹H NMR** (400 M Hz, DMSO-*d*₆) δ ppm: 7.85 (1H, t, *J*= 5.7 Hz, H₁₀), 7.30 (2 H, d, H₃), 7.19 - 7.26 (3 H, m, H₁₋₂), 6.70 (2 H, s, H₉), 3.65 (1 H, d, *J*=13.2 Hz, H₄), 3.48 (1 H, d, *J*=13.7 Hz H₄), 3.08 (2 H, q, *J*=6.4 Hz, H₁₁), 2.91 (1 H, t, *J*=6.6 Hz, H₆), 2.22- 1.99 (2 H, m, H₈), 1.77 - 1.58 (1 H, m, H₇), 1.48-1.36 (2 H, m, H₁₂), 1.23 (20 H, m, H₁₃₋₂₁), 0.85 (3 H, t, *J*=6.6 Hz, H₂₂) **¹³C NMR** (100.53 MHz, DMSO-*d*₆) δ ppm 174.07 (NH₂-C=O), 173.58 (HN-C=O), 140.54 (C aromatic), 136.63 (C aromatic), 128.54 (C aromatic),

128.11 (C aromatic), 127.87 (C aromatic), 127.68 (C aromatic), 126.62 (C aromatic), 61.23 (Bnz-CH₂-NH-CH), 51.12 (Bnz-CH₂-NH-CH), 31.32 (CH₂ Chain), 29.22 (CH₂ Chain), 29.03 (CH₂ Chain), 28.74 (CH₂ Chain), 26.39 (CH₂ Chain), 22.12 (CH₂-CH₃), 13.99 (terminal CH₃); **ESI-MS** (m/z) cal C₂₄H₄₂N₃O₂ found 404.3270 (100% [M+H]⁺) and cal C₂₄H₄₁N₃NaO₂ found 426.3091 (21% [M+Na]⁺)

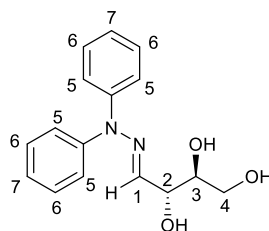
7.8 Synthesis of (2*R*, 3*S*) *E*-4-(2,2-diphenylhydrazone)-butane-1,2,3-triol (232)¹⁴⁶



232

D-Erythrose (20 mg, 0.16 mmol) and *N,N*-diphenyl hydrazine **144** (35 mg, 0.19 mmol) were dissolved in methanol (3 mL) and stirred for 45 minutes at room temperature before concentration in vacuo. Purification via flash column chromatography (95:5 DCM:methanol) gave a brown oil in a 19 % yield (9.12 mg, 0.031 mmol). **IR** ν_{\max} (cm⁻¹): 3307 m, 3062 w, 2929 w, 2158 vw, 2041 vw, 1942.00 vw, 1589 s, 1494 s, 1451 m, 1410 s, 1298 m, 1212 s, 1175 m, 1086 s, 1045 s, 887 m, 781 m, 748 s, 692 vs, 655 s, 645 s, 631 s, 618 s, 597 s, 562 s, 507 s, 456 s; **[α]_D²⁵** (deg cm³ g⁻¹ dm⁻¹) -10.11 (c = 1.0, chloroform) **¹H NMR** (400 MHz, CD₃OD) δ ppm: 7.37-7.34 (4H, m, H₆), 7.12 (2H, t, *J* = 7.4 Hz, H₇), 7.06 (4H, m, H₅), 6.54 (1H, d, *J* = 6.0 Hz, H₁), 4.24 (1H, dd, *J* = 6.0, 5.9 Hz, H₂), 3.67-3.60 (1H, m, H₃), 3.55-3.50 (2H, m, H₄); **¹³C NMR** (100.53 MHz, CD₃OD) δ ppm: 145.2 (C-5), 139.2 (C-4), 130.7 (C-7), 125.4 (C-8), 123.5 (C-6), 75.5 (C-2), 73.7 (C3), 64.3 (C-1); **ESI-MS** (m/z) cal C₁₆H₁₈N₂NaO₃ 309.1210, found 309.1210 (100% [M+H]⁺).

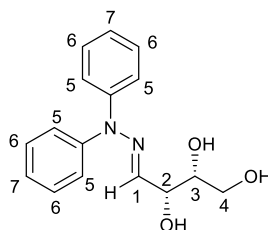
7.9 Synthesis of (2*S*, 3*R*) *E*-4-(2,2-diphenylhydrazone)-butane-1,2,3-triol (233)¹⁴⁶



233

L-Erythrose (20 mg, 0.16 mmol) and *N,N*-diphenyl hydrazine **144** (35 mg, 0.19 mmol) were dissolved in methanol (3 mL) and stirred for 45 minutes at room temperature before concentration in vacuo. Purification via flash column chromatography (95:5 DCM:methanol) gave a brown oil in a 19 % yield (9.12 mg, 0.031 mmol). **IR** ν_{\max} (cm^{-1}): 3337 s, 2948 m, 2840 w, 2324 vw, 2164 w, 2148 vw, 2065 vw, 1980 vw, 1960 vw, 1938 vw, 1651 m, 1639 m, 1591 s, 1496 m, 1450 m, 1406 m, 1318 m, 1214 m, 1175 m, 1016 vs, 749 s, 694 vs, 623 vs, 610 vs, 598 vs, 580 vs, 559 vs, 551 vs, 521 vs, 508 vs, 476 vs, 469 s, 463 s, 456 s; $[\alpha]_{\text{D}}^{25}$ ($\text{deg cm}^3 \text{g}^{-1} \text{dm}^{-1}$) +23.96 ($c = 1.0$, chloroform) **¹H NMR** (400 MHz, CD_3OD) δ ppm 7.37-7.34 (4H, m, H_6), 7.12 (2H, t, $J = 7.4$ Hz, H_7), 7.06 (4H, m, H_5), 6.54 (1H, d, $J = 6.0$ Hz, H_1), 4.24 (1H, dd, $J = 6.0, 5.9$ Hz, H_2), 3.67-3.60 (1H, m, H_3), 3.55-3.50 (2H, m, H_4); **¹³C NMR** (100.53 MHz, CD_3OD) δ ppm: 145.2 (C-5), 139.2 (C-4), 130.7 (C-7), 125.4 (C-8), 123.5 (C-6), 75.5 (C-2), 73.7 (C3), 64.3 (C-1); **ESI-MS** (m/z) cal $\text{C}_{16}\text{H}_{18}\text{N}_2\text{NaO}_3$ 309.1210, found 309.1210 (100% $[\text{M}+\text{H}]^+$).

7.10 Synthesis of (2*S*, 3*S*) *E*-4-(2,2-diphenylhydrazone)-butane-1,2,3-triol (234)¹⁴⁶

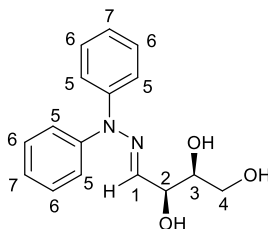


234

L-Threose (20 mg, 0.16 mmol) and *N,N*-diphenyl hydrazine **144** (35 mg, 0.19 mmol) were dissolved in methanol (3 mL) and stirred for 45 minutes at room temperature before concentration in vacuo. Purification via flash column

chromatography (95:5 DCM:methanol) gave a brown oil in a 68 % yield (31 mg, 0.108 mmol). **IR** ν_{\max} (cm^{-1}): 3308 m, 3061 w, 2927 w, 2882 w, 1589 s, 1494 vs, 1451 m, 1410 s, 1296 s, 1212 s, 1175 m, 1155 m, 1090 s, 1070 s, 1037 s, 1002 s, 939 m, 887 m, 782 m, 748 vs, 737 s, 693 vs, 654 s, 630 s, 618 s, 566 s, 507 s, 456 m; $[\alpha]_{\text{D}}^{25}$ ($\text{deg cm}^3 \text{g}^{-1} \text{dm}^{-1}$) -3.46 ($c = 1.0$, chloroform) **$^1\text{H NMR}$** (400 MHz, CD_3OD) δ ppm: 7.35 (4H, dd, $J = 8.4$ Hz, H_6), 7.18 (2H, t, $J = 7.4$ Hz, H_7), 7.05 (4H, m, H_5), 6.51 (1H, d, $J = 5.7$ Hz, H_1), 4.27 (1H, dd, $J = 5.7, 4.4$ Hz, H_2), 3.63 (1H, ddd, $J = 8.0, 5.0, 4.4$ Hz, H_3), 3.63 (2H, dd, $J = 12.5, 5.0$ Hz H_4); **$^{13}\text{C NMR}$** (100.53 MHz, CD_3OD) δ ppm: 145.2 (C-5), 139.2 (C-4), HRMS 130.7 (C-7), 125.4 (C-8), 123.5 (C-6), 75.5 (C-2), 73.7 (C3), 64.3 (C-1); **ESI-MS** (m/z) cal $\text{C}_{16}\text{H}_{18}\text{N}_2\text{NaO}_3$ 309.1210, found 309.1210 (100% $[\text{M}+\text{H}]^+$).

7.11 Synthesis of (2*R*, 3*R*) *E*-4-(2,2-diphenylhydrazone)-butane-1,2,3-triol (235)¹⁴⁶

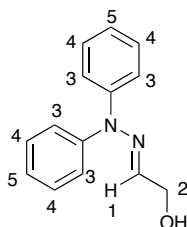


235

D-Threose (60 mg, 0.5 mmol) and *N,N*-diphenyl hydrazine **144** (105 mg, 0.57 mmol) were dissolved in methanol (3 mL) and stirred for 45 minutes at room temperature before concentration in vacuo. Purification via flash column chromatography (95:5 DCM:methanol) gave a brown oil in a 5.5 % yield (8.12 mg, 0.091 mmol). **IR** ν_{\max} (cm^{-1}): 3341.00 m, 3060.00 w, 2928.00 w, 2880.00 w, 2596.00 vw, 2431.00 vw, 2184.00 vw, 1950.00 vw, 1943.00 vw, 1938.00 vw, 1876.00 vw, 1785.00 vw, 1589.00 s, 1493.00 vs, 1455.00 m, 1401.00 m, 1357.00 m, 1295.00 s, 1212.00 s, 1175.00 m, 1156.00 m, 1089.00 s, 1069.00 s, 1035.00 s, 1002.00 m, 995.00 m, 940.00 m, 887.00 m, 782.00 m, 748.00 vs, 737.00 s, 693.00 vs, 660.00 s, 655.00 s, 630.00 s, 598.00 m, 565.00 s, 507.00 s, 477.00 m, 470.00 m, 455.00 m; $[\alpha]_{\text{D}}^{25}$ ($\text{deg cm}^3 \text{g}^{-1} \text{dm}^{-1}$) +13.99 ($c = 1.0$, chloroform); **$^1\text{H NMR}$** (400 MHz, CD_3OD) δ ppm: 7.35 (4H, dd, $J = 8.4$ Hz, H_6), 7.18 (2H, t, $J = 7.4$ Hz, H_7), 7.05 (4H, m, H_5), 6.51 (1H, d, $J = 5.7$ Hz, H_1), 4.27 (1H, dd, $J = 5.7, 4.4$ Hz, H_2), 3.63 (1H, ddd, $J = 8.0, 5.0, 4.4$ Hz, H_3), 3.63 (2H, dd, $J = 12.5, 5.0$ Hz H_4); **^{13}C**

NMR (100.53 MHz, CD₃OD) δ ppm: 145.2 (C-5), 139.2 (C-4), HRMS 130.7 (C-7), 125.4 (C-8), 123.5 (C-6), 75.5 (C-2), 73.7 (C3), 64.3 (C-1); **ESI-MS** (m/z) cal C₁₆H₁₈N₂NaO₃ 309.1210, found 309.1210 (100% [M+H]⁺).

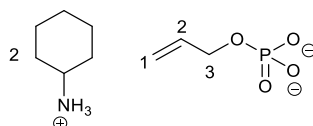
7.12 Synthesis of 2-(2,2-diphenylhydrazone)-ethanol (235)¹⁴⁶



236

Glycolaldehyde dimer (30 mg, 0.25 mmol) and *N,N*-diphenyl hydrazine (55 mg, 0.3 mmol) were dissolved in methanol (3 mL) and stirred for 45 minutes at room temperature before concentration in *vacuo*. Purification via flash column chromatography (95:5 DCM:methanol) gave a brown oil in a 30 % crude yield (17 mg, 0.075 mmol). **¹H NMR** (400 MHz, CD₃OD) δ ppm: 7.40-7.37 (4H, m, H₅), 7.13-7.09 (2H, m, H₄), 7.03 (4H, d, *J* = 7.9 Hz, H₃), 6.49 (1H, t, *J* = 5.0 Hz, H₁), 4.15 (1H, d, *J* = 5.0 Hz). **¹H NMR** corresponded with that reported in literature¹⁷²

7.13 Synthesis of Bis(cyclohexyl-1-ammonium)-allyl-phosphate (238)⁹⁷

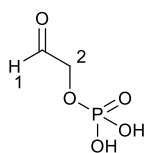


238

To hydrophosphoric acid (1.90g, 19.4 mmol) was added trimethylamine (4.00 g, 39.6 mmol) followed by allyl alcohol (30.00 g, 517 mmol) and trichloroacetonitrile (14.40 g, 100 mmol) which were added dropwise. The mixture was stirred at 75 °C for 12 h under reflux. The solution was then concentrated in *vacuo* to about 15 mL. Water (200 mL) was added and washed twice with diethyl ether (150 mL). The aqueous layer was then mixed with cyclohexylamine (14.40 g, 100 mmol) and solvent was removed in *vacuo* to yield an off white powder. The white powder was then dissolved in water (50 mL) and acetone was added until a white precipitate began to form. The suspension was kept at 4 °C overnight. The precipitate was filtered off and dried to give a consistent weight of 4.8 g, (74%, 14.28 mmol). **Mp**

203-205 °C; **IR** ν_{\max} (cm^{-1}): 2932 m; 2856 m, 2763 m, 2713 m, 2617 m, 2564 m, 2221 w, 2000 vw, 1885 vw, 1823 vw, 1727 vw, 1627 w, 1558 m, 1453 w, 1421 w, 1393 w, 1374 w, 1356 w, 1320 vw, 1288 w, 1265 w, 1246 w, 1192 w, 1139 m, 1085 s, 1064 vs, 1053 vs, 1023 s, 976 vs, 914 s, 890 m, 879 m, 845 m, 815 s, 597 m, 546 s, 487 m, 468 m; **$^1\text{H NMR}$** (400 MHz, D_2O) δ ppm: 6.00-5.90 (1H, m, H_2); 5.34 (1H, dd, $J = 17.3, 1.7$ Hz, H_1), 5.21 (1H, dd, $J = 10.6, 1.5$ Hz, H_1), 4.30 (2H, ddt, $J = 7.0, 5.3, 1.4$ Hz, H_3), 3.21-3.11 (m, 2H, NH_3^+) 2.00-1.37 (20H, m, cyclohexylamine), **$^{13}\text{C NMR}$** (100.53 MHz, D_2O) δ ppm: 135.44 (C-1), 115.61 (C-2), 63.32 (C-3), 50.31 (C-cyclohexylamine), 30.99 (C-cyclohexylamine), 24.32 (C-cyclohexylamine), 23.83 (C-cyclohexylamine); **$^{31}\text{P NMR}$** (161.83 MHz D_2O decoupled) δ ppm: 3.80 (s 1 P)

7.14 Synthesis of 2-(Phosphonoxy)acetaldehyde (**239**)⁹⁷

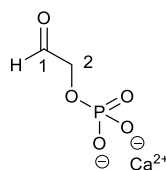


239

Bis(cyclohexyl-1-ammonium)-allyl-phosphate (**238**) (2.5 g, 7.435 mmol) was suspended in water (50 mL) and shaken with ion exchange resin (IR 120 H^+ form) for 30 minutes. The ion exchange resin was filtered off and the filtrate was washed with diethyl ether (250 mL). The aqueous layer was extracted and triethylamine (8.8 mL, 66.9 mmol, 9 eq) was added. Solvent was then removed in *vacuo* to yield an orange oil. The oil was then ozonolyzed in methanol (130 mL) at -78 °C until the solution went either bright blue or colourless. Excess ozone was removed by a continuous flow of oxygen and addition of dimethyl sulphide (1.19 mL, 16.6 mmol, 5 eq) and left to stir at 0 °C for 24 h. After 24 h, the solution was mixed with ion exchange resin (IR 120 H^+ form) and shaken for 30 minutes. The ion exchange resin was filtered off and the solution was washed with ice-cold water (400 mL). Solvent was removed in *vacuo* to yield the free acid as a pale orange oil. (65%, 678 mg, 4.87 mmol). **IR** ν_{\max} (cm^{-1}): 3016.00 w, 2952.00 w, 2896.00 w, 2746 w, 2324 w, 1652 m, 1645 m, 1522 w, 1436 m, 1407 m, 1320 w, 1175 m, 933 vs, 835 s, 711 s, 475 vs, **$^1\text{H NMR}$** (400 MHz, D_2O) δ ppm: 4.98 (1H, t, $J = 5.9$ Hz, H_2); 3.66 (2H, m, H_1), **$^{13}\text{C NMR}$** (100.53 MHz, D_2O) δ ppm: 89.6 (C-1), 88.19 (d C-1). As this is a crude sample peaks are present that cannot be assigned to the final product.

However peaks reported correspond with that reported in literature.⁹⁷ Future work is required to optimise purification.

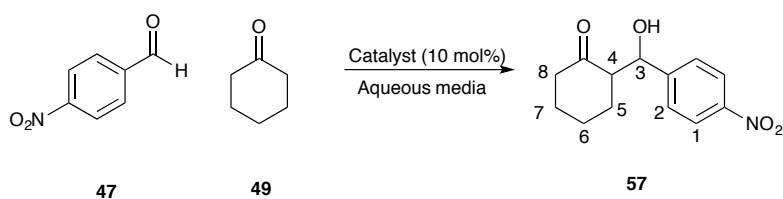
7.15 Synthesis of 2-(Phosphonoxy)acetaldehyde calcium salt (97)⁹⁷



97

To the oil was added water (100 mL) followed by calcium acetate (0.5 g, 1 eq, 2.26 mmol) in water (25 mL) followed by drop wise addition of acetone over 4h. The suspension was left at 4 °C overnight then filtered off to yield a white powder 519 mg (89 % 2.91 mmol). ¹H-NMR (400 MHz, D₂O) δ ppm: 5.09 (1H, t, *J*=4.8 Hz H₁), 3,72 (2H, dd, *J* = 4,9, H₂) IR *v*_{max} (cm⁻¹): 3912 vw; 3886 vw, 3848 vw, 3822 vw, 3816 vw, 3808 vw, 3802 vw, 3791 vw, 3744 vw, 3676 vw, 3670 vw, 3657 vw, 3629 vw, 3350 vw, 2932 m, 2856 m, 2715 m, 2622 m, 2561 m, 2210 w, 2185 w, 2168 w, 2156 w, 1928 vw, 1646 w, 1630 w, 1560 m, 1470 w, 1452 w, 1422 vw, 1393 w, 1355 vw, 1346 vw, 1320 vw, 1284 w, 1262 w, 1192 w, 1156 m, 1133 m, 1066 vs, 1045 s, 1031 s, 995 s, 982 s, 956 m, 927 s, 878 s, 845 m, 817 m, 785 m, 766 m, 714 m, 664 m, 594 m, 580 m, 529 vs, 466 s.

7.16 General procedure for solution phase catalysis of 4-nitrobenzaldehyde (47) and cyclohexanone (49)³⁸

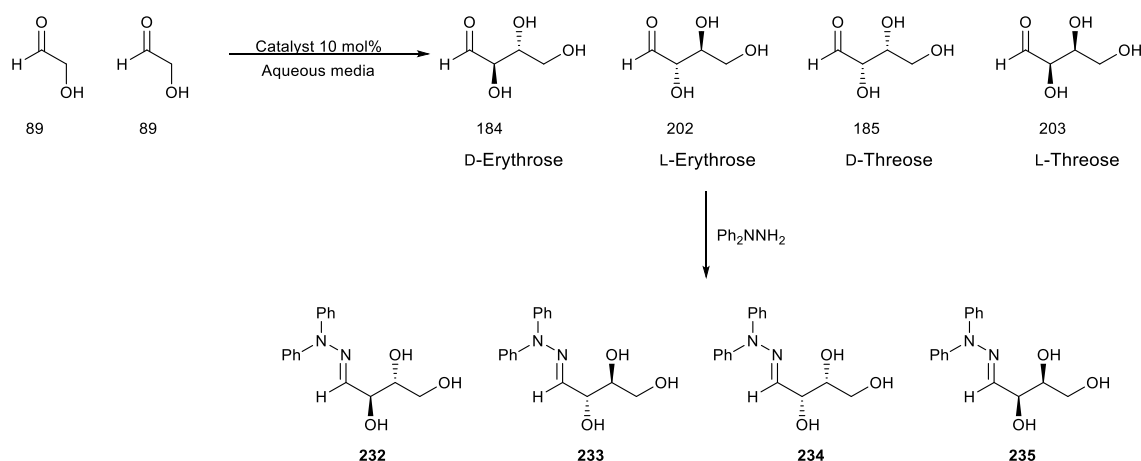


To a solution of amide (0.065 mmol) in water (20 mL) was added a solution of 4-nitrobenzaldehyde (98 mg, 6.5 mmol) in cyclohexanone (6.7 mL, 65 mmol). The reaction was left for 72 h with no stirring. After 72 h the reaction mixture was extracted with DCM then solvent was removed in vacuo to yield a yellow solid crude material. New reactions were set up with the same procedure but only run for 48 h and 24 h before being worked up. The conversion of the reaction was determined by integrating the ¹H NMR of the crude reaction mixture using the

aldehyde peak as a reference. Syn/antiratio was determined by integrating the ^1H NMR of the crude reaction mixture and by comparing the two CH-OH peaks. The enantiomeric excess of the crude product was analysed, via HPLC using a chiralpak IB column; 97:3 Hexane: IPA Flow rate 1 mL/min.

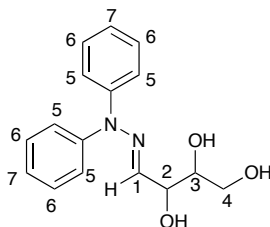
Syn diastereomer: ^1H NMR (400 MHz, CDCl_3) δ ppm: 8.21 (1H, d, J = 8.9 Hz, H_1), 7.49 (1H, d, J = 8.4 Hz, H_2), 5.49 (1 H, br. s, H_3), 3.18 (1 H, br. s, OH), 2.66-2.59 (1 H, m, H_4), 2.52-2.46 (1 H, m, H_8), 2.45 - 2.35 (1 H, m, H_8), 2.15-2.08 (1 H, m, H_7), 1.89-1.82 (1H, m, H_6), 1.76-1.65 (2 H, m, H_5 , H_7), 1.63-1.47 (2 H, m, H_5 , H_6), ^{13}C NMR (400 MHz, CDCl_3) δ ppm: 214.0 (C=O), 149.1 (Ar), 147.1 (C-N), 126.7 (2), 123.8 (1), 70.2 (3), 56.9 (4), 42.7 (8), 28.0 (7), 26.0 (5), 25.0 (6); **Chiral HPLC** syn-diastereomer: Enantiomer 1 tR = 27.9 min, Enantiomer 2 tR = 29.5 min. ^1H NMR (400 MHz, CDCl_3) δ ppm: 8.21 (1H, d, J =8.8 Hz, H_1), 7.51 (1H, d, J = 8.4 Hz, H_2), 4.89 (1H, dd, J =3.2 Hz, 8.35 Hz, H_3), 4.08 (1 H, d, J =3.2 Hz, OH), 2.64-2.54 (1 H, m, H_4), 2.53-2.46 (1 H, m, H_8), 2.42 - 2.31 (1 H, m, H_8), 2.15-2.08 (1 H, m, H_7), 1.89-1.79 (1 H, m, H_6), 1.74-1.64 (1 H, m, H_5), 1.63-1.47 (2 H, m, H_5 , H_6), 1.45-1.34 (1 H, m, H_7); **Chiral HPLC** anti-diastereomer: Enantiomer 1 tR = 34.7 min, Enantiomer 2 tR = 43.3 min. Spectroscopic data are in agreement with the literature.^{38,153}

7.17 General procedure for the dimerization of glycolaldehyde on the hydrogel



To the surface of the benzylglutamine amide (**230**) hydrogel (20 mg, 49.6 μmol , 5 mL) was added glycolaldehyde (59 mg, 0.49 mmol) in water (200 μL) in 10 μL aliquots. After 48 h the reaction was stopped by removed the water *in vacuo*. Once

the water was removed 1.2 eq of diphenyl hydrazone was added in methanol with 1-2 drops of acetic acid. The reaction was left to stir for 1 h at room temperature. After 1 h the solvent was removed to yield a brown oil. The crude oil was analysed by ^1H NMR to determine conversion of glycolaldehyde to tetrose sugars. Then purified by column chromatography (100 % DCM to 8:2 DCM:MeOH) then chiral HPLC was performed on an IC Chiral Pak column (90:10 Hexane:IPA, 40°C, 1 mL/min)

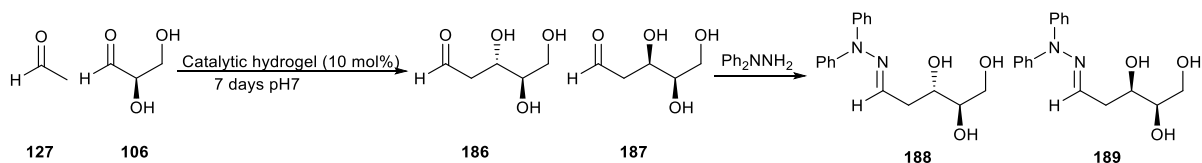


247

Erythrose hydrazone ^1H NMR (400 MHz, CD_3OD) δ ppm 7.37-7.34 (4H, m, H_6), 7.12 (2H, t, $J = 7.4$ Hz, H_7), 7.06 (4H, m, H_5), 6.54 (1H, d, $J = 6.0$ Hz, H_1), 4.24 (1H, dd, $J = 6.0, 5.9$ Hz, H_2), 3.67-3.60 (1H, m, H_3), 3.55-3.50 (2H, m, H_4);

Threose ^1H NMR (400 MHz, CD_3OD) δ ppm: 7.35 (4H, dd, $J = 8.4$ Hz, H_6), 7.18 (2H, t, $J = 7.4$ Hz, H_7), 7.05 (4H, m, H_5), 6.51 (1H, d, $J = 5.7$ Hz, H_1), 4.27 (1H, dd, $J = 5.7, 4.4$ Hz, H_2), 3.63 (1H, ddd, $J = 8.0, 5.0, 4.4$ Hz, H_3), 3.63 (2H, dd, $J = 12.5, 5.0$ Hz H_4); **Chiral HPLC**: L-Erythrose hydrazone tR = 18.414 min, D-Erythrose hydrazone tR = 27.130 min, L-Threose hydrazone tR = 34.082 min, D-Threose hydrazone tR = 21.905 min

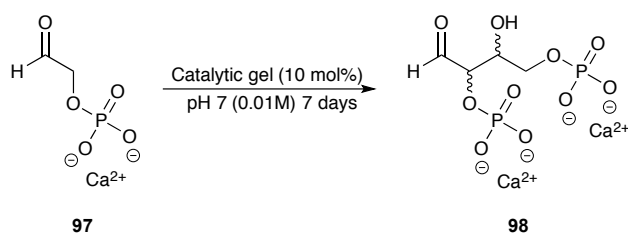
7.18 General procedure of Aldol condensation of D-glyceraldehyde and acetaldehyde on the hydrogel



A stock solution of acetaldehyde (pH 7 phosphate buffer, 0.15 mL acetaldehyde in 2 mL buffer) was prepared. To glyceraldehyde (59 mg, 0.49 mmol) was added the stock solution of acetaldehyde (200 μL), this mixture was then transferred to the surface of the benzylglutamine amide (**230**) hydrogel (20 mg, 49.6 μmol , 5 mL) in 10 μL aliquots. After 48 h the reaction was stopped by removed the water *in*

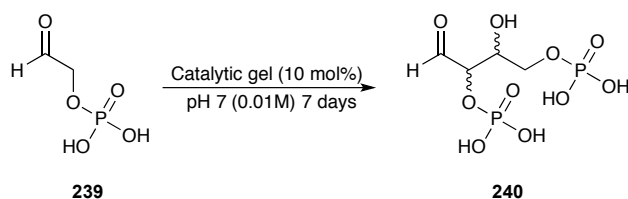
vacuo. Once the water was removed 1.2 eq of *N,N*-diphenyl hydrazine was added in methanol with 1-2 drops of acetic acid. The reaction was left to stir for 1 h at room temperature. After 1 h the solvent was removed to yield a brown oil. ^1H NMR of crude performed in (400 MHz, CD_3OD).

7.19 General procedure for the dimerization of glycolaldehyde phosphate calcium salt on the hydrogel



To the surface of the benzylglutamine amide (**230**) hydrogel (20 mg, 49.6 μmol , 5 mL) was added glycolaldehyde phosphate calcium salt (**97**) (59 mg, 0.49 mmol) in water (200 μL) in 10 μL aliquots. After the required duration (48 h or 7 days) the reaction was stopped by removing water *in vacuo*. The sample was then analysed by ^1H NMR in D_2O to identify any changes.

7.20 General procedure for the dimerization of glycolaldehyde phosphate on the hydrogel



To the surface of the benzylglutamine amide (**230**) hydrogel (20 mg, 49.6 μmol , 5 mL) was added glycolaldehyde phosphate (**239**) (69 mg, 0.49 mmol) in water (200 μL) in 10 μL aliquots. After 48 h the reaction was stopped by removing the water *in vacuo*. The sample was analysed by ESI Mass spectroscopy (negative), ^1H NMR and ^{31}P NMR in D_2O .

7.21 Solvent screening for valine, serine and glutamine amides for gelation

A known quantity of amino acid amide (3 mg) was weighed into a 2.5 mL sample vial to which was added by 0.1 mL of solvent. The vial was then heated until both components dissolved. The vial was then left to cool, 12 hours the tube inversion test was carried out to see if gelation had taken place.

7.22 General procedure for gelation of L-glutamine amide (210) and aldehyde

To a known quantity of L-glutamine amide (**210**) aldehyde (1 eq) was added followed by water (1 mL) to form a suspension. The suspension was heated until oil droplets appeared. The solution was left to cool. Inversion test was then used to establish if a gel had formed. These quantities were changed depending on what being studied.

7.23 Gelation of 2-benzylamino-N¹-dodecyl-L-glutamine amide (230)

Water (1 mL) was added to benzyl glutamine amide (**230**) (1 mg 2.48 μmol) to form a suspension. The suspension was heated until oil droplets appeared then immediately sonicated until the solution became white but no aggregates observed. The solution was left to cool. Inversion test was then used to establish if a gel had formed. This method was the same even on a larger scale of gel formation.

7.24 TEM sample preparation

The gels are prepared as described above in section 7.21 and 7.22. To prepare samples for TEM, a small portion of gel was removed with a spatula and 'drop-cast' onto a heat-treated copper TEM grip. Excess material was removed using filter paper and left to dry for 20 minutes prior to imaging. A uranyl acetate stain was used for contrast. Meg Stark at the Biology Technology Facility, University of

York, carried this out.

7.25 SEM sample preparation

Gels were prepared as described in section 7.11. Gels were then prepared for SEM by freeze-drying; Meg Stark at the Biology Technology Facility, University of York, using the method described below, carried this out. The gel was spread using a mounted needle on a thin piece of copper shim (to act as support); excess liquid was removed with filter paper. The gel was frozen on the copper support by submersion in nitrogen slush (ca. -210°C); after this water was removed from the gel by lyophilising on a Peltier stage, with a maximum temperature of -50°C . Once dry, the gel was knocked off the shim with a mounted needle, and the shim was mounted on an SEM stub using a carbon sticky tab. The sample was then sputter-coated with a thin layer ($< 12\text{ nm}$) of gold/palladium coating to prevent sample charging, before SEM imaging.

7.26: General procedure for Circular dichroism samples with glutamine amide (210) and 4-nitrobenzaldehyde (47)

To glutamine amide (**210**) (1 mg, 3.19 mmol) was added 4-nitrobenzaldehyde (**47**) (1 eq, 480 μg . 3.19 mmol) followed by water (1 mL). The solution was heated until boiling ca. 100°C . Whilst hot an aliquot (450 μL) of the sample was taken and transferred to 1 mm quartz cuvette. The sample was left over night to allow gel formation.

7.27: General procedure for Circular dichroism samples with benzylglutamine amide (230)

Water (1 mL) was added to benzylglutamine amide (1 mg, 0.025 mmol). The solution was heated until boiling ca. 100°C then sonicated for 30 seconds. Whilst hot an aliquot (450 μL) of the sample was taken and transferred to 1 mm quartz cuvette. The sample was left over night to allow gel formation.

7.28: General procedure for rheology samples with glutamine amide (210) and 4-nitrobenzaldehyde (47)

To glutamine amide (**210**) (1 mg, 3.19 mmol) was added 4-nitrobenzaldehyde (**47**) (1 eq, 480 μ g, 3.19 mmol) followed by water (1 mL). The solution was heated until boiling ca. 100 °C. Whilst hot the sample was transferred to a bottomless vial attached to a Petri dish with sealant. The sample was left over night to allow gel formation then transferred to the rheometer plate.

7.29: General procedure for Circular dichroism samples with benzylglutamine amide (230)

Water (1 mL) was added to benzylglutamine amide (**230**) (4 mg, 0.01 mmol). The solution was heated until boiling ca. 100 °C then sonicated for 30 seconds. Whilst hot the sample was transferred to a bottomless vial onto the rheometer plate (pre-heated to 50 °C). Once loaded the rheometer plate was cooled to room temperature. The vial was held in place until the gel began to form, then left for half an hour before removal of the vial.

Abbreviations

Ala	Alanine
aq	Aqueous
Ar	Aromatic
Asp	Asparagine
Atm	Atmosphere
Boc	Tert-butyl oxycarbonyl
br	Broad
Cbz	Carboxybenzy
CD	Circular Dichroism
CMC	Critical micellar concentration
CVC	Critical vesical concentration
Cys	Cystine
d	NMR chemical shift (in ppm)
d	Doublet (NMR)
d.r	Diastereomeric ratio
Da	Dalton
DBS	1,3:2,4-dibenzylidene-D-sorbitol
DCM	Dichloromethane
DLS	Dynamic light scattering
DMSO	Dimethylsulfoxide
DMSOd6	Deuterated dimethylsulfoxide
DNA	Deoxyribonucleic acid
e.e	Enantiomeric excess
EDC	1-ethyl-3(3'-diethylaminopropyl)carbodiimide
eq	Equivalent
ESI-MS	Electrospray ionisation mass spectrometry
G'	Storage modulus
G''	Loss modulus
GC	Gas chromatography
Gln	Glutamine
Glu	Glutamic acid
Gly	Glycine
h	Hour

His	Histidine
HOBt	Hydroxybenzotriazole
HPLC	High performance liquid chromatography
Hz	Megahertz
Ile	Isoleucine
IR	Infa-red
<i>J</i>	Coupling constant
LMWG	Low molecular weight gelator
m	Multiplet (NMR)
m	Medium (IR)
m/z	Mass to charge ratio
mdeg	Millidegrees
Met	Methionine
mg	Micrograms
min	Minute(s)
mL	Microlitres
mL	Millilitres
mmol	Millimole
Mp	Melting point
Ms	Mass spectrometry
Mw	Molecular weight
NaOH	Sodium Hydroxide
nm	Nanometer
NMR	Nuclear magnetic resonance
Pa	Pascal
PdNP	Palladium nanoparticles
PG	Polymer gel
pH	Negative logarithm of the concentration of hydrogen ions
Phe	Phenylalanine
Pro	Proline
q	Quartet (NMR)
RNA	Ribonucleic acid
rt	Room temperature
s	Strong (IR)

s	Singlet (NMR)
SEM	Scanning electron microscopy
Ser	Serine
t	Time or triplet (NMR)
TEM	Transmission electron microscopy
TFA	Trifluoroacetic acid
Tgel	Gel-sol transition temperature
TIPS	Triisopropylsilyl
TLC	Thin layer chromatography
Tyr	Tyrosine
Val	Valine
w	Weak (IR)

8.0 Appendix:

Table 30 Valine amide catalysed aldol condensation of 4-nitrobenzaldehyde and cyclohexanone in water

Solvent	Time h	Conversion %	Crude NMR d.r anti:syn	Gel?
Water	24	45	1.12:1	No
	24	46	1.36:1	No
	24	29	1.21:1	No
Water	48	31	1.32:1	No
	48	45	1.20:1	No
	48	49	1.34:1	No
Water	72	87	0.98:1	No
	72	96	0.94:1	No
	72	81	0.96:1	No

Table 31: Serine amide catalysed aldol condensation of 4-nitrobenzaldehyde and cyclohexanone in water

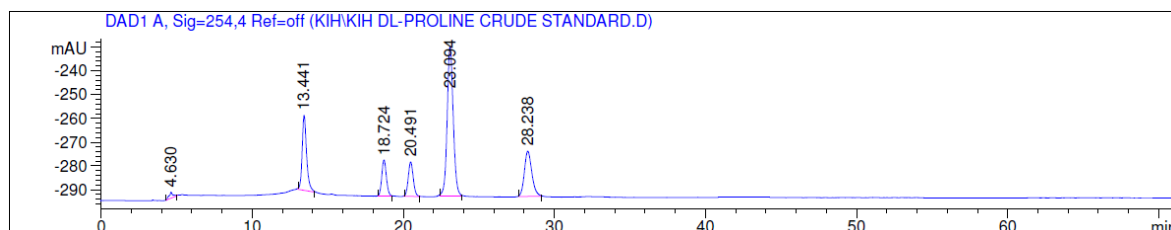
Solvent	Time h	Conversion %	Crude NMR d.r anti:syn	Gel?
Water	24	11	1.21:1	No
	24	10	1.23:1	No
	24	12	1.20:1	No
Water	48	39	1.89:1	No
	48	21	1.48:1	No
Water	72	57	1.81	No
	72	51	2.06	No
	72	41	1.72	No

Table 32: Glutamine amide catalysed aldol condensation of 4-nitrobenzaldehyde and cyclohexanone in water

Solvent	Time h	Conversion %	Crude NMR d.r anti:syn	Gel?
Water	24	45	2.07:1	In-situ
	24	33	2.22:1	In-situ
Water	48	100	1.57:1	In-situ
	48	68	1.59:1	In-situ
	48	100	1.16:1	In-situ
Water	72	99	1.07:1	In-situ
	72	100	1.71:1	In-situ
	72	99	1.33:1	In-situ

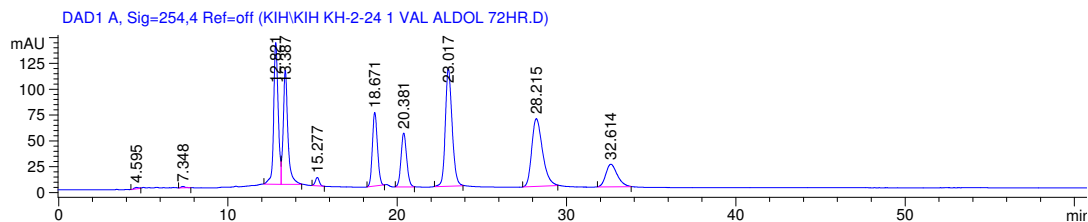
Table 33: L-valine amide catalysis HPLC ee%

Solvent	Time h	Crude HPLC ee%	In situ gel?
Water	72	Syn 10% Anti 4%	No
Water	72	Syn 13% Anti 60%	No
Water	72	Syn 6% Anti 9%	No



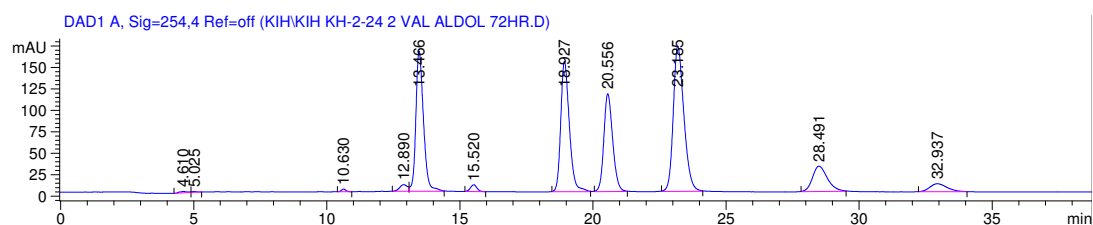
Peak	Retention time (min)	Peak area (%)
1	18.724	8.6364
2	20.491	8.9111
3	23.094	46.5431
4	28.238	17.4865

Figure 159: HPLC trace for stands for the aldol condensation of 4-nitrobenzaldehyde with using D/L proline



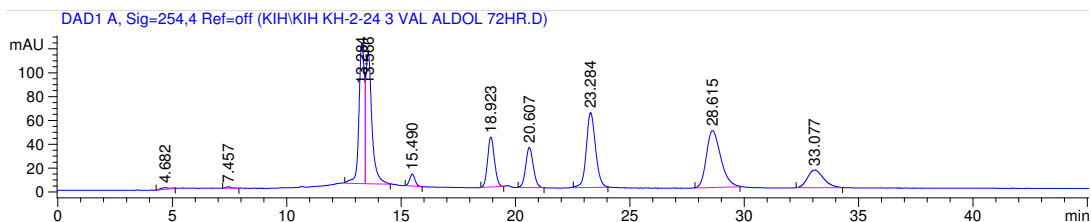
Peak	Retention time (min)	Peak area (%)
1	18.671	10.1111
2	20.381	8.2268
3	23.017	21.6630
4	28.215	19.8831

Figure 160: HPLC trace for aldol condensation of 4-nitrobenzaldehyde with cyclohexanone at 72 h run 1 catalysed by valine amide in solution phase



Peak	Retention time (min)	Peak area (%)
1	18.927	21.4236
2	20.556	16.5732
3	23.185	29.3757
4	28.491	7.2460

Figure 161: HPLC trace for aldol condensation of 4-nitrobenzaldehyde with cyclohexanone at 72 h run 2 catalysed by valine amide in solution phase

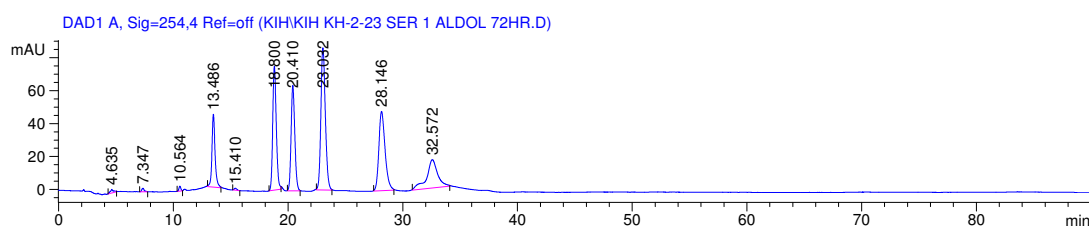


Peak	Retention time (min)	Peak area (%)
1	18.923	8.3673
2	20.607	7.4615
3	23.284	16.8454
4	28.615	19.9830

Figure 162: HPLC trace for aldol condensation of 4-nitrobenzaldehyde with cyclohexanone at 72 h run 3 catalysed by valine amide in solution phase

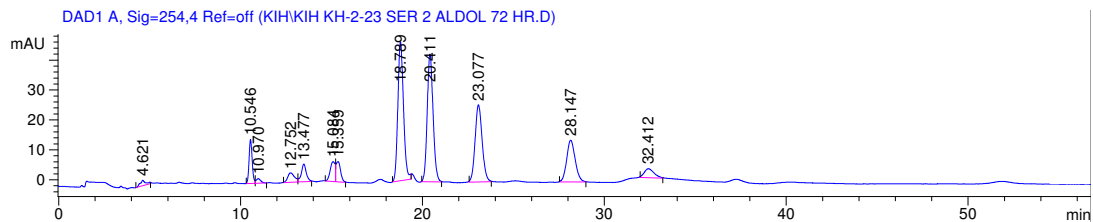
Table 34: L-serine amide catalysed HPLC data

Solvent	Time h	Crude HPLC ee%	In situ gel?
Water	72	Syn 6% Anti 13%	No
Water	72	Syn 2% Anti 21%	No
Water	72	-	No



Peak	Retention time (min)	Peak area (%)
1	18.800	17.3795
2	20.410	15.3711
3	23.092	25.1460
4	28.146	19.4207

Figure 163: HPLC trace for aldol condensation of 4-nitrobenzaldehyde with cyclohexanone at 72 h run 1 catalysed by serine amide in solution phase

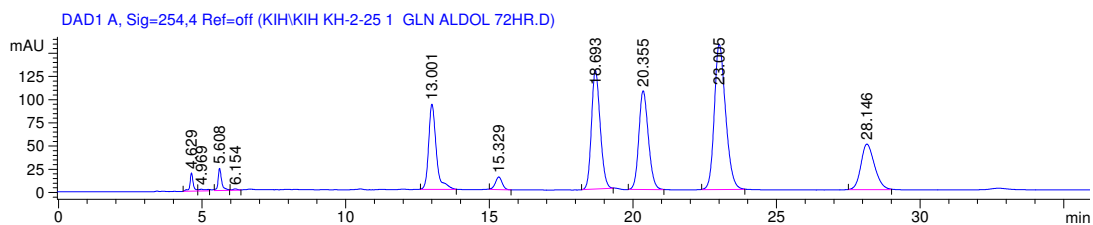


Peak	Retention time (min)	Peak area (%)
1	18.800	25.7135
2	20.410	24.4814
3	23.092	17.8897
4	28.146	11.6784

Figure 164: HPLC trace for aldol condensation of 4-nitrobenzaldehyde with cyclohexanone at 72 h run 2 catalysed by serine amide in solution phase

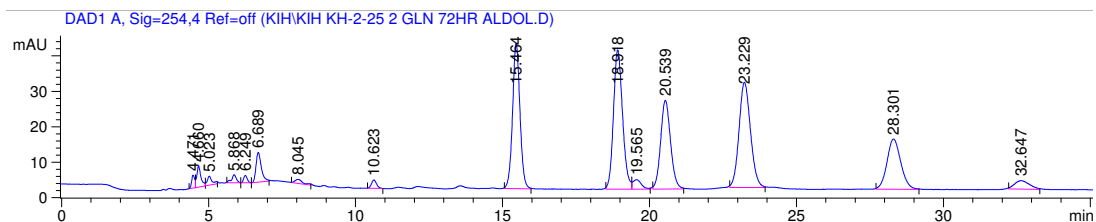
Table 35: L-glutamine amide catalysis HPLC data

Solvent	Time h	Crude HPLC ee%	In situ gel?
Water	72	Syn 5% Anti 45%	Yes
Water	72	Syn 18% Anti 27%	Yes
Water	72	Syn 10% Anti 24%	Yes



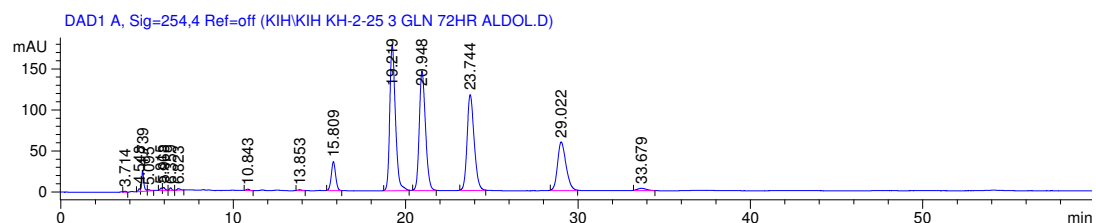
Peak	Retention time (min)	Peak area (%)
1	18.693	20.1493
2	20.355	18.3346
3	23.005	31.9384
4	28.146	12.0856

Figure 165: HPLC trace for aldol condensation of 4-nitrobenzaldehyde with cyclohexanone at 72 h run 1 catalysed by glutamine amide in solution phase



Peak	Retention time (min)	Peak area (%)
1	18.918	21.8651
2	20.539	15.1963
3	23.229	20.8279
4	28.301	11.9392

Figure 166: HPLC trace for aldol condensation of 4-nitrobenzaldehyde with cyclohexanone at 72 h run 2 catalysed by glutamine amide in solution phase

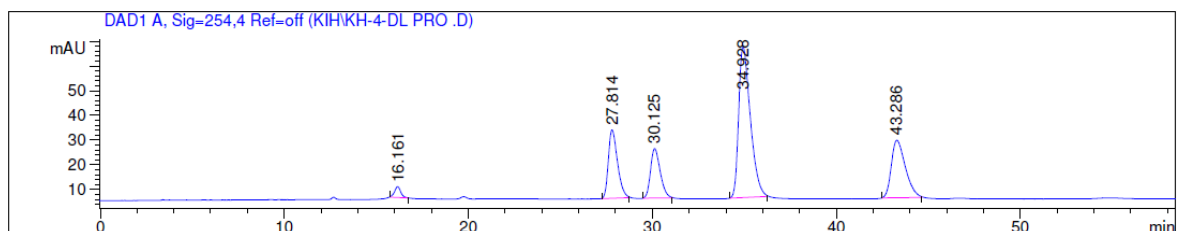


Peak	Retention time (min)	Peak area (%)
1	19.219	28.5837
2	20.948	25.7488
3	23.744	23.3859
4	29.022	14.2308

Figure 167: HPLC trace for aldol condensation of 4-nitrobenzaldehyde with cyclohexanone at 72 h run 3 catalysed by glutamine amide in solution phase

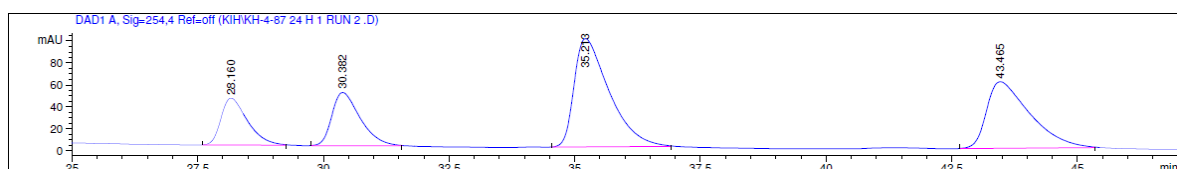
Table 36: Benzylglutamine amide catalysed aldol condensation of 4-nitrobenzaldehyde and cyclohexanone in solution in water

Amide catalyst	Entry	Time h	Conversion %	NMR d.r of crude anti:syn	HPLC of crude ee%
Benzyl glutamine amide	1	24	24	1.99 : 1.00	<i>Anti</i> : 16 % <i>Syn</i> : 11%
	2	24	21	1.95 : 1.00	<i>Anti</i> : 17 % <i>Syn</i> : 7 %
	3	24	25	2.10 : 1.00	<i>Anti</i> : 16 % <i>Syn</i> : 10%
	4	48	24	2.14 : 1.00	<i>Anti</i> : 22 % <i>Syn</i> : 8 %
	5	48	46	2.20 : 1.00	<i>Anti</i> : 15 % <i>Syn</i> : 7 %
	6	48	31	2.10 : 1.00	<i>Anti</i> : 23 % <i>Syn</i> : 12 %
	7	72	42	1.98 : 1.00	<i>Anti</i> : 15 % <i>Syn</i> : 8 %
	8	72	53	2.11 : 1.00	<i>Anti</i> : 16 % <i>Syn</i> : 6 %
	9	72	36	1.93 : 1.00	<i>Anti</i> : 16% <i>Syn</i> : 7%



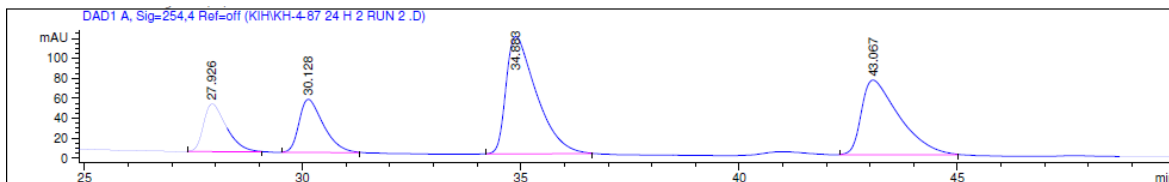
Peak	Retention time (min)	Peak area (%)
1	27.814	16.6655
2	30.125	12.8407
3	34.928	47.1505
4	43.286	21.5095

Figure 168: HPLC standard for the aldol condensation of 4-nitrobenzaldehyde and cyclohexanone using D/L proline as a catalyst



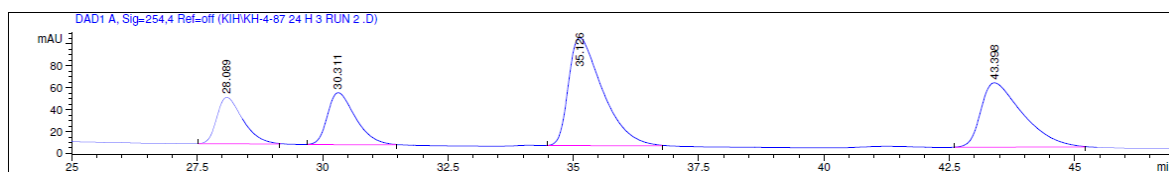
Peak	Retention time (min)	Peak area (%)
1	27.823	2.2277
2	30.058	2.8000
3	34.855	6.5108
4	42.927	4.7606

Figure 169: HPLC trace for aldol condensation of 4-nitrobenzaldehyde with cyclohexanone at 24 h run 1 catalysed by benzyl glutamine amide in solution phase



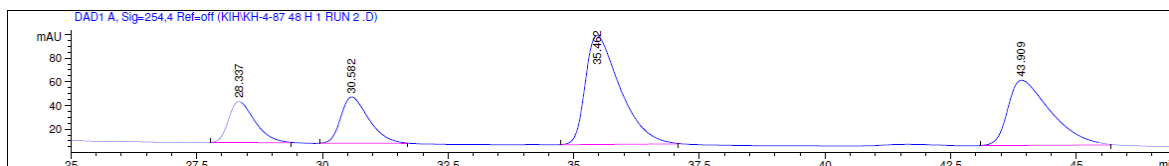
Peak	Retention time (min)	Peak area (%)
1	27.901	2.1275
2	30.157	2.4308
3	35.106	2.8400
4	43.363	2.8793

Figure 170: HPLC trace for aldol condensation of 4-nitrobenzaldehyde with cyclohexanone at 24 h run 2 catalysed by benzyl glutamine amide in solution phase



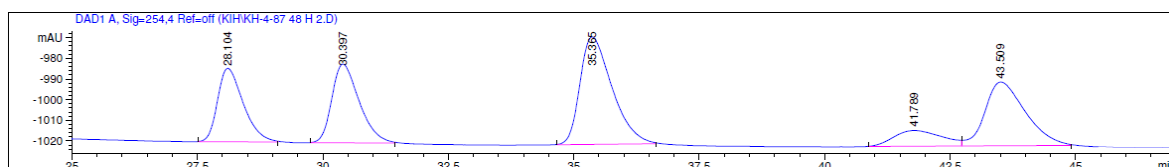
Peak	Retention time (min)	Peak area (%)
1	27.985	2.2724
2	30.231	2.7656
3	35.046	6.2312
4	43.093	4.5699

Figure 171: HPLC trace for aldol condensation of 4-nitrobenzaldehyde with cyclohexanone at 24 h run 3 catalysed by benzyl glutamine amide in solution phase



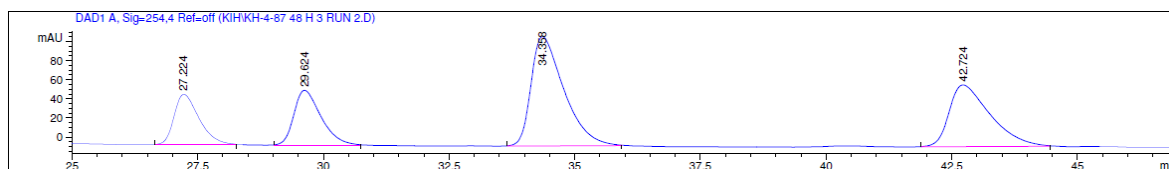
Peak	Retention time (min)	Peak area (%)
1	28.195	1.9041
2	30.471	2.2492
3	35.321	4.7004
4	43.421	3.0202

Figure 172: HPLC trace for aldol condensation of 4-nitrobenzaldehyde with cyclohexanone at 48 h run 1 catalysed by benzyl glutamine amide in solution phase



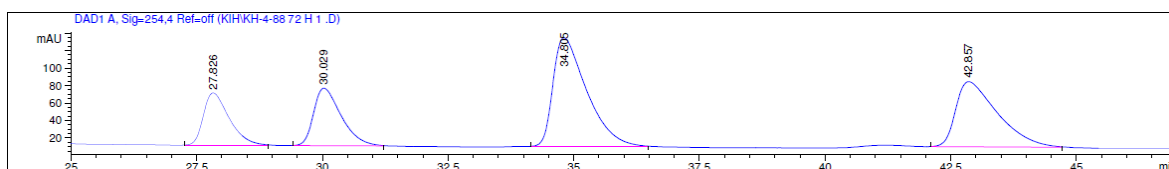
Peak	Retention time (min)	Peak area (%)
1	28.104	2.0422
2	30.397	2.3394
3	35.365	3.7423
4	43.509	2.7861

Figure 173: HPLC trace for aldol condensation of 4-nitrobenzaldehyde with cyclohexanone at 48 h run 2 catalysed by benzyl glutamine amide in solution phase



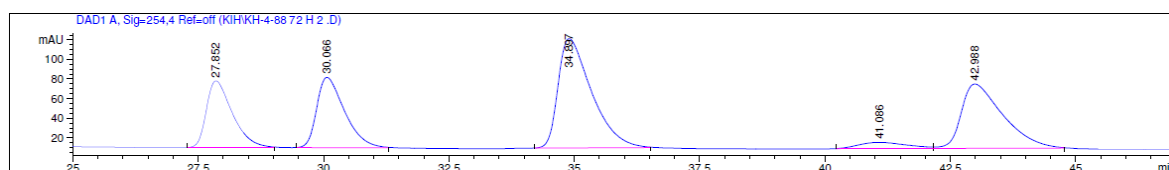
Peak	Retention time (min)	Peak area (%)
1	27.985	2.2724
2	30.231	2.7656
3	35.046	6.2312
4	43.093	4.5699

Figure 174: HPLC trace for aldol condensation of 4-nitrobenzaldehyde with cyclohexanone at 48 h run 3 catalysed by benzyl glutamine amide in solution phase



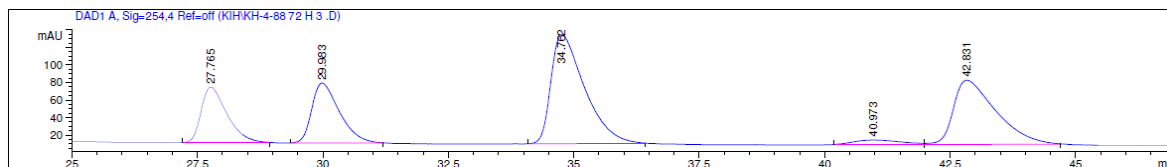
Peak	Retention time (min)	Peak area (%)
1	27.826	3.2861
2	30.029	3.8748
3	34.805	8.901
4	42.857	6.6407

Figure 175: HPLC trace for aldol condensation of 4-nitrobenzaldehyde with cyclohexanone at 72 h run 1 catalysed by benzyl glutamine amide in solution phase



Peak	Retention time (min)	Peak area (%)
1	27.852	5.8943
2	30.066	6.6581
3	34.897	12.4945
4	42.988	9.1192

Figure 176: HPLC trace for aldol condensation of 4-nitrobenzaldehyde with cyclohexanone at 72 h run 2 catalysed by benzyl glutamine amide in solution phase

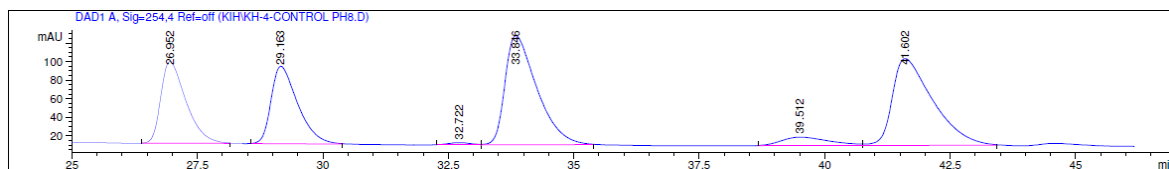


Peak	Retention time (min)	Peak area (%)
1	27.765	4.1753
2	29.983	4.8244
3	34.762	10.6466
4	42.831	7.9042

Figure 177: HPLC trace for aldol condensation of 4-nitrobenzaldehyde with cyclohexanone at 72 h run 3 catalysed by benzyl glutamine amide in solution phase

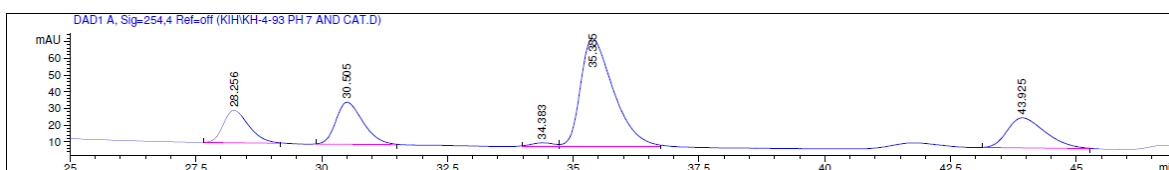
Table 37: Controlled pH reactions

Entry	Catalyst present	Time h	pH	Conversion %	NMR d.r of <i>Anti:Syn</i>	HPLC of crude ee %
1	No	72	8.6	50	2.00:1.00	<i>Anti</i> :1 <i>Syn</i> : 1
2	Yes	24	7	11 %	1.88:1.00	<i>Anti</i> : 51 <i>Syn</i> : 16 <i>Anti</i> : 59 <i>Syn</i> : 19 <i>Anti</i> : 58 <i>Syn</i> : 18
3	Yes	24	4	5 %	1.94:1.00	<i>Anti</i> : 72 <i>Syn</i> : 34 <i>Anti</i> : 73 <i>Syn</i> : 35 <i>Anti</i> : 74 <i>Syn</i> : 34
4	No	24	7	4%	1.98:1.00	<i>Anti</i> : 1 <i>Syn</i> : 1
5	No	24	4	0.3 %	0.84: 1.00	<i>Anti</i> : 1 <i>Syn</i> : 1



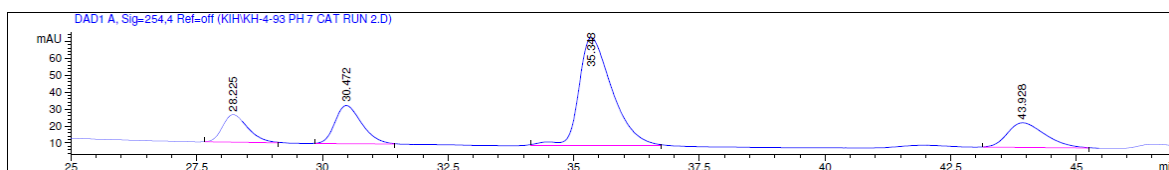
Peak	Retention time (min)	Peak area (%)
1	26.952	4.8631
2	29.163	4.8600
3	33.846	8.2141
4	41.602	8.2927

Figure 178: HPLC trace for aldol condensation of 4-nitrobenzaldehyde with cyclohexanone at 72 h run 1 pH 8.6 buffer control reaction



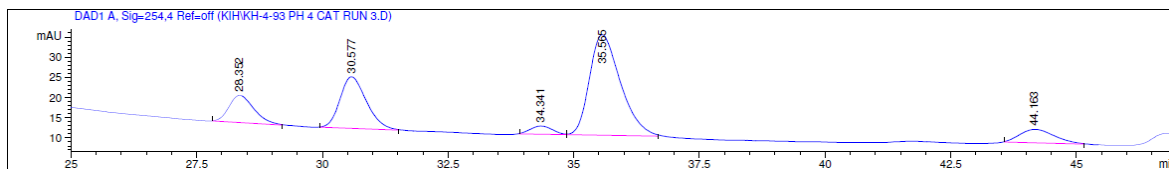
Peak	Retention time (min)	Peak area (%)
1	28.256	0.9415
2	30.505	1.3007
3	35.385	3.9950
4	43.925	1.3105

Figure 179: HPLC trace for aldol condensation of 4-nitrobenzaldehyde with cyclohexanone at pH 7 with benzylglutamine amide control reaction 24 h run 1



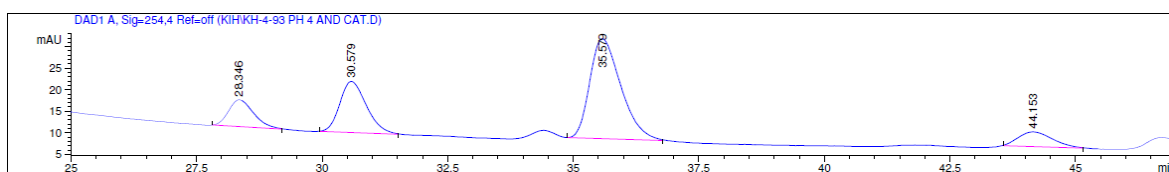
Peak	Retention time (min)	Peak area (%)
1	28.225	0.7741
2	30.472	1.1392
3	35.348	3.9655
4	43.928	1.0305

Figure 180: HPLC trace for aldol condensation of 4-nitrobenzaldehyde with cyclohexanone at pH 7 with benzylglutamine amide control reaction 24 h run 2



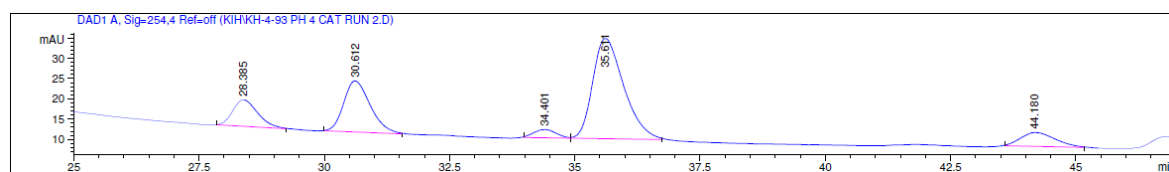
Peak	Retention time (min)	Peak area (%)
1	28.037	0.7642
2	30.351	1.1168
3	35.209	3.7760
4	43.823	1.0078

Figure 181: HPLC trace for aldol condensation of 4-nitrobenzaldehyde with cyclohexanone at pH 7 with benzylglutamine amide control reaction 24 h run 3



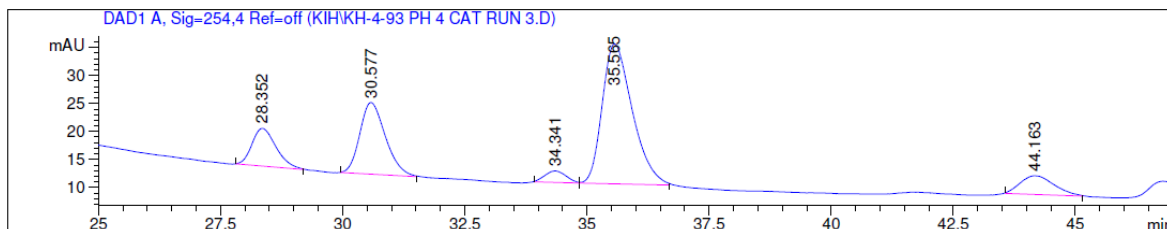
Peak	Retention time (min)	Peak area (%)
1	28.346	0.2419
2	30.579	0.4911
3	35.579	1.1233
4	44.153	0.1805

Figure 182: HPLC trace for aldol condensation of 4-nitrobenzaldehyde with cyclohexanone at pH 4 with benzylglutamine amide control reaction 24 h run 1



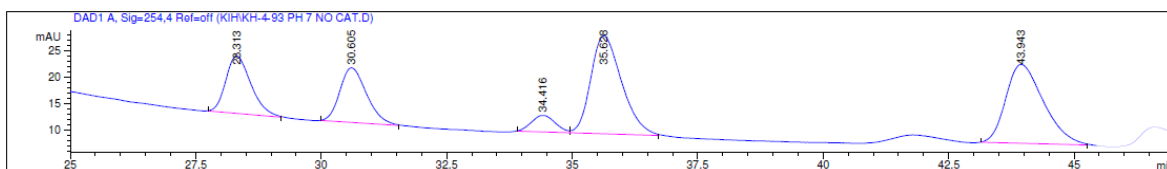
Peak	Retention time (min)	Peak area (%)
1	28.385	0.2389
2	30.612	0.4911
3	35.611	1.1279
4	44.180	0.1743

Figure 183: HPLC trace for aldol condensation of 4-nitrobenzaldehyde with cyclohexanone at pH 4 with benzylglutamine amide control reaction 24 h run 2



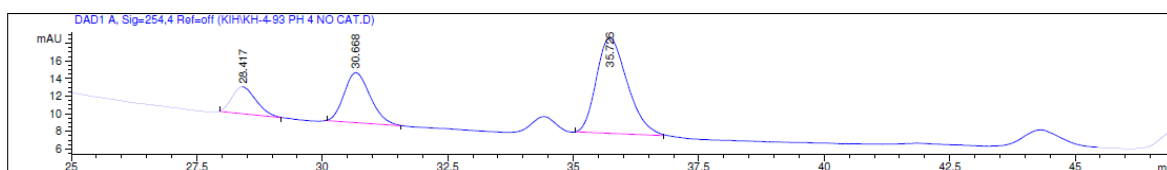
Peak	Retention time (min)	Peak area (%)
1	28.352	0.2420
2	30.577	0.4865
3	34.341	1.1164
4	35.565	0.1683

Figure 184: HPLC trace for aldol condensation of 4-nitrobenzaldehyde with cyclohexanone at pH 4 with benzylglutamine amide control reaction 24 h run 3



Peak	Retention time (min)	Peak area (%)
1	28.313	0.3399
2	30.605	0.3440
3	35.628	0.7141
4	43.943	0.7001

Figure 185: HPLC trace for aldol condensation of 4-nitrobenzaldehyde with cyclohexanone at pH 7 no catalyst control reaction

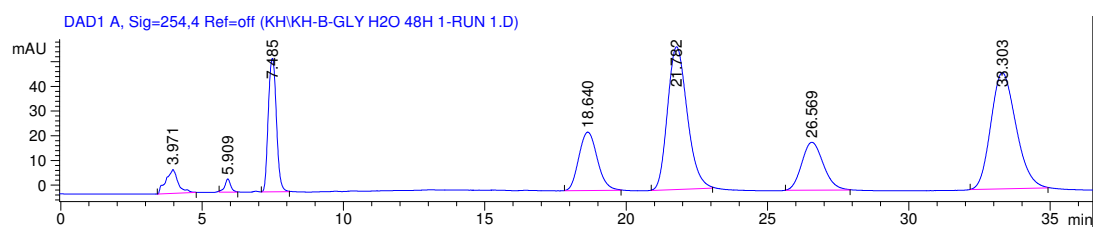


Peak	Retention time (min)	Peak area (%)
1	28.417	0.1765
2	30.668	0.3586
3	35.726	0.8104

Figure 186: HPLC trace for aldol condensation of 4-nitrobenzaldehyde with cyclohexanone at pH 7 no catalyst control reaction

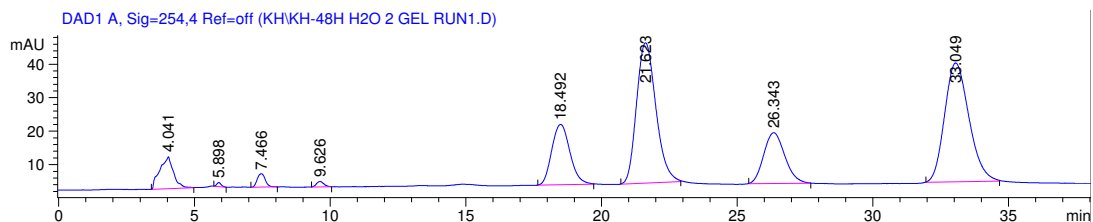
Table 38: Dimerization of glycolaldehyde with benzylglutamine amide data on the hydrogel over 48h

Amide catalyst	Entry	Solvent	Conversion %	Crude NMR	
				d.r Erythrose to Threose	HPLC ee%
Benzyl glutamine amide	1	Water	12	1.00 : 2.77	Ery: 2 % Thr: 2 %
	2	Water	10	1.00 : 2.90	Ery: 2 % Thr: 3 %
	3	Water	7	1.00 : 1.38	Ery: 2 % Thr: 7 %
	4	pH 7	68	1.00 : 2.28	Ery: 3 % Thr: 7 %
	5	pH 7	43	1.00 : 1.94	Ery: 1 % Thr: 6%
	6	pH 7	76	1.00 : 1.95	Ery: 4 % Thr: 10 %



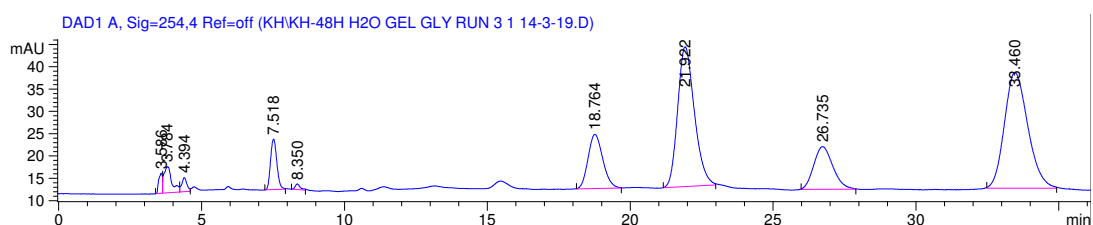
Peak	Retention time (min)	Peak area (%)
1	18.640	11.5690
2	21.782	30.2097
3	26.569	11.1212
4	33.303	31.5698

Figure 187: HPLC trace for dimerization of glycolaldehyde with benzylglutamine amide as a gel 48 h run 1



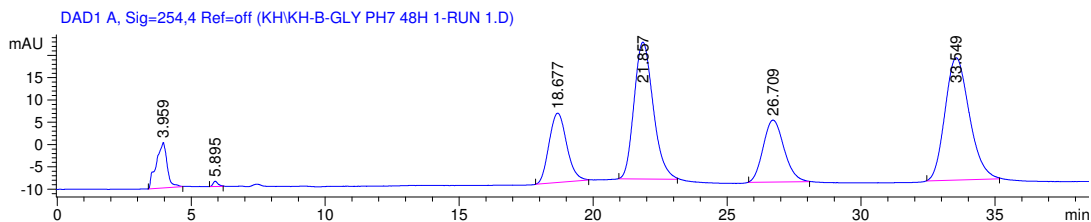
Peak	Retention time (min)	Peak area (%)
1	18.492	13.0411
2	21.623	32.3852
3	26.343	12.7896
4	33.049	34.6036

Figure 188: HPLC trace for dimerization of glycolaldehyde with benzylglutamine amide as a gel 48 h run 2



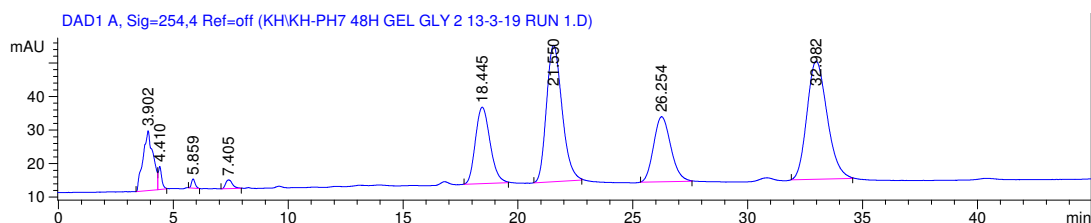
Peak	Retention time (min)	Peak area (%)
1	18.764	10.7850
2	21.922	31.7947
3	26.735	11.1461
4	33.460	36.8207

Figure 189: HPLC trace for dimerization of glycolaldehyde with benzylglutamine amide as a gel 48 h run 3



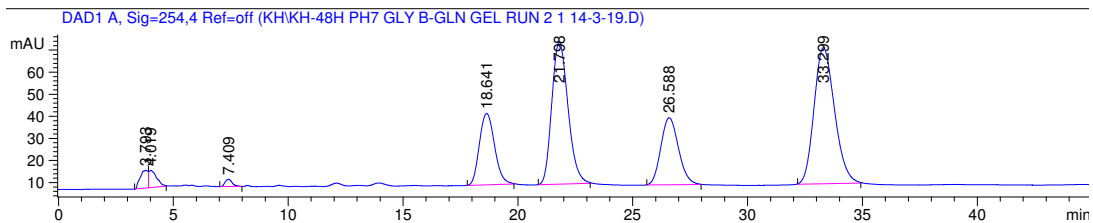
Peak	Retention time (min)	Peak area (%)
1	18.764	14.1906
2	21.922	30.2743
3	26.735	15.0206
4	33.460	34.5193

Figure 190: HPLC trace for dimerization of glycolaldehyde with benzylglutamine amide as a gel 48 h at pH 7 run 1



Peak	Retention time (min)	Peak area (%)
1	18.445	14.8551
2	21.550	28.2334
3	26.254	14.8500
4	34.982	31.7954

Figure 191: HPLC trace for dimerization of glycolaldehyde with benzylglutamine amide as a gel 48 h at pH 7 run 2



Peak	Retention time (min)	Peak area (%)
1	18.641	14.1279
2	21.798	30.0387
3	26.588	15.3826
4	33.299	36.2502

Figure 192: HPLC trace for dimerization of glycolaldehyde with benzylglutamine amide as a gel 48 h at pH 7 run 3

References

- 1 A. R. Hirst, B. Escuder, J. F. Miravet and D. K. Smith, *Angew. Chem Int. Ed.*, 2008, **47**, 8002–8018.
- 2 D. J. Cornwell and D. K. Smith, *Mater. Horiz*, 2015, **2**, 279–293.
- 3 K. Hanabusa and M. Suzuki, *Polym. J.*, 2014, **46**, 776–782.
- 4 L. E. Buerkle and S. J. Rowan, *Chem. Soc. Rev*, 2012, **41**, 6089–6102.
- 5 P. R. A. Chivers and D. K. Smith, *Chem. Sci.*, 2017, **8**, 7218–7227.
- 6 B. O. Okesola and D. K. Smith, *Chem. Soc. Rev.*, 2016, **45**, 4226–4251.
- 7 N. M. Sangeetha and U. Maitra, *Chem. Soc. Rev.*, 2005, **34**, 821–836.
- 8 J. Naskar, G. Palui and A. Banerjee, *J. Phys. Chem. B*, 2009, **113**, 11787–11792.
- 9 K. Y. Lee and D. J. Mooney, *Chem. Rev.*, 2001, **101**, 1869–1879.
- 10 S. Kiyonaka, K. Sugiyasu, S. Shinkai and I. Hamachi, *J. Am. Chem. Soc.*, 2002, **124**, 10954–10955.
- 11 J. C. Tiller, *Angew. Chem Int. Ed.*, 2003, **42**, 3072–3075.
- 12 M. Suzuki, H. Saito and K. Hanabusa, *Langmuir*, 2009, **25**, 8579–8585.
- 13 D. M. Ryan, T. M. Doran and B. L. Nilsson, *Chem. Commun*, 2011, **47**, 475–477.
- 14 M. Halperin-Sternfeld, M. Ghosh, R. Sevostianov, I. Grigoriants, L. Adler-Abramovich and Li, *Chem. Commun.*, 2017, **53**, 9586–9589.
- 15 J. R. Moffat and D. K. Smith, *Chem. Commun*, 2009, 316–318.
- 16 K. Hanabusa, T. Miki, Y. Taguchi, T. Koyama and H. Shirai, *J. Chem. Soc. Chem. Commun.*, 1993, 1382–1384.
- 17 J. G. Hardy, A. R. Hirst, D. K. Smith, C. Brennan and I. Ashworth, *Chem. Commun*, 2004, 385–387.
- 18 A. R. Hirst, D. K. Smith and J. P. Harrington, *Chem. Eur. J.*, 2005, **11**, 6552–6559.
- 19 K. S. Partridge, D. K. Smith, G. M. Dykes and P. T. Mcgrail, *Chem. Commun.*, 2001, 319–320.
- 20 A. R. Hirst, J. F. Miravet, B. Escuder, L. Noirez, V. Castelletto, I. W. Hamley and D. K. Smith, *Chem. Eur. J.*, 2009, **15**, 372–379.
- 21 N. Sreenivasachary and J.-M. Lehn, *Proc. Natl. Acad. Sci. U. S. A.*, 2005, **102**, 5938–5943.
- 22 M. M. Smith, W. Edwards and D. K. Smith, *Chem. Sci.*, 2013, **4**, 671–676.

- 23 J.-M. Lehn, *Supramolecular Chemistry: Concepts and Perspectives*, Weinheim ; New York : VCH, 1995.
- 24 C. J. Pedersen, *J. Am. Chem. Soc.*, 1967, **89**, 7017–7036.
- 25 C. J. Pedersen, *Angew. Chemie Int. Ed. English*, 1988, **27**, 1021–1027.
- 26 A. Lützen, *Angew. Chemie Int. Ed.*, 2008, **47**, 6320–6320.
- 27 M. Raynal, P. Ballester, A. Vidal-Ferran and P. W. N. M. van Leeuwen, *Chem. Soc. Rev.*, 2014, **43**, 1660–1733.
- 28 B. Escuder, F. Llansola and J. F. Miravet, *New J. Chem.*, 2010, **34**, 1029–1224.
- 29 W. Fang, Y. Zhang, J. Wu, C. Liu, H. Zhu and T. Tu, *Chem. Asian J.*, 2018, **13**, 712–729.
- 30 B. Xing, M.-F. Choi and B. Xu, *Chem. Eur. J.*, 2002, **8**, 5028–5032.
- 31 P. Slavík, D. W. Kurka and D. K. Smith, *Chem. Sci.*, 2018, **9**, 8673–8681.
- 32 K. Tanaka, A. Mori and S. Inoue, *J. Org. Chem.*, 1989, **55**, 181–185.
- 33 H. Danda, *Synlett*, 1991, 263–264.
- 34 Y. Shvo, M. Gal, Y. Becker and A. Elgavi, *Tetrahedron: Asymmetry*, 1996, **7**, 911–924.
- 35 M. O. Guler and S. I. Stupp, *J. Am. Chem. Soc.*, 2007, **129**, 12082–12083.
- 36 C. Zhang, X. Xue, Q. Luo, Y. Li, K. Yang, X. Zhuang, Y. Jiang, J. Zhang, J. Liu, G. Zou and X.-J. Liang, *ACS Nano*, 2014, **8**, 11715–11723.
- 37 E.-M. Schön, E. Marqués-López, R. P. Herrera, C. Alemán and D. Díaz Díaz, *Chem. Eur. J.*, 2014, **20**, 10720–10731.
- 38 F. Llansola, J. F. Miravet and B. Escuder, *Chem. Commun.*, 2009, **71**, 7303–7305.
- 39 S. Oltra, C. Berdugo, J. F. Miravet and B. Escuder, *New J. Chem.*, 2015, **39**, 3785–3791.
- 40 T. Tu, W. Assenmacher, H. Peterlik, G. Schnakenburg and K. H. Dötz, *Angew. Chemie Int. Ed.*, 2008, **47**, 7127–7131.
- 41 D. Mazzier, F. Carraro, M. Crisma, M. Rancan, C. Toniolo and A. Moretto, *Soft Matter*, 2016, **12**, 238–245.
- 42 F. Rodríguez-Llansola, B. Escuder and J. F. Miravet, *Org. Biomol. Chem.*, 2009, **7**, 3091–3094.
- 43 W. Notz, F. Tanaka and C. F. Barbas, *Acc. Chem. Res.*, 2004, **37**, 580–591.
- 44 D. S. Tsekova, J. A. Saez, B. Escuder and J. F. Miravet, *Soft Matter*, 2009, **5**, 3727–3735.

- 45 J. F. Miravet and B. Escuder, *Chem. Commun.*, 2005, 5796–5798.
- 46 N. Mase, Y. Nakai, N. Ohara, H. Yoda, K. Takabe, F. Tanaka and C. F. Barbas III, *J. Am. Chem. Soc.*, 2006, **128**, 734–735.
- 47 C. Berdugo, J. F. Miravet and B. Escuder, *Chem. Commun.*, 2013, **49**, 10608–10610.
- 48 M. Tena-Solsona, J. Nanda, S. Oltra, A. Chotera, G. Ashkenasy and B. Escuder, *Chem. A Eur. J.*, 2016, **22**, 6687–6694.
- 49 M. Araújo, S. Díaz-Oltra and B. Escuder, *Chem. Eur. J.*, 2016, **22**, 8676–8684.
- 50 T. R. Chan and V. V. Fokin, *QSAR Comb. Sci.*, 2007, **26**, 1274–1279.
- 51 T. R. Chan, R. Hilgraf, K. B. S. Sharpless and V. V. Fokin*, *Org. Lett.*, 2004, **6**, 2853–2855.
- 52 C. Rizzo, A. Mandoli, S. Marullo and F. D’anna, *J. Org. Chem.*, 2019, **84**, 6356–6365.
- 53 L. E. Orgel, *Orig. Life Evol. Biosph.*, 2003, **33**, 211–218.
- 54 A. Lazcano and S. L. Miller, *Cell*, 1996, **85**, 793–8.
- 55 S. I. Walker, *Nature*, 2019, **569**, 36–38.
- 56 J. L. Bada, *Chem. Soc. Rev.*, 2013, **42**, 2186–2196.
- 57 E. T. Parker, H. J. Cleaves, J. P. Dworkin, D. P. Glavin, M. Callahan, A. Aubrey, A. Lazcano, J. L. Bada and G. F. Joyce, *Proc. Natl. Acad. Sci. U. S. A.*, 2011, **108**, 5526–5531.
- 58 A. Lazcano and J. L. Bada, *Orig. Life Evol. Biosph.*, 2003, **33**, 235–242.
- 59 J. P. Schrum, T. F. Zhu and J. W. Szostak, *Cold Spring Harb. Perspect. Biol.*, 2010, **2**, 1–15.
- 60 K. Ruiz-Mirazo, C. Briones and A. de la Escosura, *Chem. Rev.*, 2014, **114**, 285–366.
- 61 T. P. Kee and P.-A. Monnard, *Beilstein J. Org. Chem.*, 2017, **13**, 1551–1563.
- 62 W. R. Hargreaves, S. J. Mulvihill and D. W. Deamer, *Nature*, 1977, **266**, 78–80.
- 63 M. Rao, J. Eichberg and J. Oró, *J. Mol. Evol.*, 1987, **25**, 1–6.
- 64 M. Rao, J. Eichberg and J. Oró, *J. Mol. Evol.*, 1982, **18**, 196–202.
- 65 D. E. Epps, E. Sherwood, J. Eichberg and J. Oró, *J. Mol. Evol.*, 1978, **11**, 279–292.
- 66 D. E. Epps, D. W. Nooner, J. Eichberg, E. Sherwood and J. Oró, *J. Mol.*

- Evol.*, 1979, **14**, 235–241.
- 67 D. W. Deamer and R. A. M. Pashley, *Orig. life Evol. Biosph.*, 1989, **19**, 21–38.
- 68 D. W. Deamer, *Nature*, 1985, **317**, 792–794.
- 69 C. L. Apel, D. W. Deamer and M. N. Mautner, *Biochim. Biophys. Acta*, 2002, **1559**, 1–9.
- 70 S. E. Maurer, D. W. Deamer, J. M. Boncella and P.-A. Monnard, *Astrobiology*, 2009, **9**, 979–987.
- 71 T. Namani and D. W. Deamer, *Orig. Life Evol. Biosph.*, 2008, **38**, 329–341.
- 72 I. A. Chen, K. Salehi-Ashtiani and J. W. Szostak, *J. Am. Chem. Soc.*, 2005, **127**, 13213–13219.
- 73 K. Adamala and J. W. Szostak, *Nat. Chem.*, 2013, **5**, 495–501.
- 74 K. P. Adamala, A. E. Engelhart and J. W. Szostak, *Nat. Commun.*, 2016, **7**, 11041.
- 75 E. C. Izgu, A. Björkbom, N. P. Kamat, V. S. Lelyveld, W. Zhang, T. Z. Jia and J. W. Szostak, *J. Am. Chem. Soc.*, 2016, **138**.
- 76 G. H. Pollack, *Cells, gels and the engines of life. (A new, unifying approach to cell function) 1st edn.*, Oxford University Press, 2001.
- 77 J. T. Trevors and G. H. Pollack, *Prog. Biophys. Mol. Biol.*, 2005, **89**, 1–8.
- 78 M. Bayoumi, H. Bayley, G. Maglia and K. T. Sapra, *Sci. Rep.*, 2017, **7**, 45167.
- 79 A. J. Dzieciol and S. Mann, *Chem. Soc. Rev.*, 2012, **41**, 79–85.
- 80 R. Krishna Kumar, X. Yu, A. J. Patil, M. Li and S. Mann, *Angew. Chemie Int. Ed.*, 2011, **50**, 9343–9347.
- 81 A. Butlerow, *Comptes Rendus l'Académie des Sci.*, 1861, **53**, 145–147.
- 82 R. Breslow, *Tetrahedron Lett.*, 1959, **1**, 22–26.
- 83 C. Appayee and R. Breslow, *J. Org. Chem.*, 2014, **136**, 3720–3723.
- 84 R. F. Socha, A. H. Weiss and M. M. Sakharov, *J. Catal.*, 1981, **67**, 207–217.
- 85 J. B. Lambert, S. A. Gurusamy-Thangavelu and K. Ma, *Science (80-)*, 2010, **327**, 984–986.
- 86 Y. Furukawa, H.-J. Kim, D. Hutter and S. A. Benner, *Astrobiology*, 2015, **15**, 259–267.
- 87 D. Kopetzki and M. Antonietti, *New J. Chem*, 2011, **35**, 1787–1794.
- 88 G. A. Khoury, R. C. Baliban and C. A. Floudas, *Sci. Rep.*, 2011, **1**, 90.
- 89 K. E. Nelson, M. Levy and S. L. Miller, *Proc. Natl. Acad. Sci. U. S. A.*, 2000,

- 97**, 3868–71.
- 90 H. D. Bean, F. A. L. Anet, I. R. Gould and N. V. Hud, *Orig. Life Evol. Biosph.*, 2006, **36**, 39–63.
- 91 P. E. Nielsen, *Chem. Biodivers.*, 2007, **4**, 1996–2002.
- 92 F. S. Mohammed, K. Chen, M. Mojica, M. Conley, J. W. Napoline, C. Butch, P. Pollet, R. Krishnamurthy and C. L. Liotta, *Synlett*, 2016, **28**, 93–97.
- 93 C. Fernández-García, A. J. Coggins and M. W. Powner, *Life*, 2017, **7**.
- 94 M. Pasek, B. Herschy and T. P. Kee, *Orig. Life Evol. Biosph.*, 2015, **45**, 207–218.
- 95 A. Dass, M. Jaber, A. Brack, F. Foucher, T. Kee, T. Georgelin and F. Westall, *Life*, 2018, **8**, 7.
- 96 C. Gibard, I. B. Gorrell, E. I. Jiménez, T. P. Kee, M. A. Pasek and R. Krishnamurthy, *Angew. Chemie*, 2019, **131**, 8235–8239.
- 97 D. Miiller, S. Pitsch, A. Kittaka, E. Wagner, C. E. Wintner, A. Eschenmoser and G. Ohloffgewidmet, *Helv. Chim. Acta*, 1990, **73**, 1410–1468.
- 98 H. J. Cleaves, *Precambrian Res.*, 2008, **164**, 111–118.
- 99 A. J. Coggins and M. W. Powner, *Nat. Chem.*, 2016, **2**, 1–76.
- 100 S. L. Miller, *Science (80-.)*, 1953, **117**, 528–529.
- 101 S. L. Miller, *J. Am. Chem. Soc.*, 1955, **77**, 2351–2361.
- 102 S. A. Stern and J. E. Colwell, *Astrophys. J.*, 1997, **490**, 879–882.
- 103 Z. Martins, P. Modica, B. Zanda and L. L. S. d’Hendecourt, *Meteorit. Planet. Sci.*, 2015, **50**, 926–943.
- 104 K. Kvenvolden, J. Lawless, K. Pering, E. Peterson, J. Flores, C. Ponnampereuma, I. . Kaplan and C. Moore, *Nature*, 1970, **228**, 923–926.
- 105 J. L. Bada, J. R. Cronin, M.-S. Ho, K. A. Kvenvolden, J. G. Lawless, S. L. Miller, J. Oro and S. Steinberg, *Nature*, 1983, **301**, 494–496.
- 106 M. H. Engel and S. A. Macko, *Nature*, 1997, **389**, 265–268.
- 107 E. L. Shock, *Orig. Life Evol. Biosph.*, 1990, **20**, 331–367.
- 108 R. J.-C. Henet, N. G. Holm and M. H. Engel, *Naturwissenschaften*, 1992, **79**, 361–365.
- 109 A. C. Evans, C. Meinert, C. Giri, F. Goesmann and U. J. Meierhenrich, *Chem. Soc. Rev.*, 2012, **41**, 5447.
- 110 D. Ritson and J. D. Sutherland, *Nat. Chem.*, 2012, **4**, 895–899.
- 111 B. H. Patel, C. Percivalle, D. J. Ritson, D. D. and J. D. Sutherland, *Nat. Chem.*, 2015, **7**, 301–307.

- 112 R. Mahrwald, Ed., *Modern Aldol Reactions*, Wiley-VCH, Weinheim, 2004.
- 113 R. Mahrwald, Ed., *Aldol Reactions*, Springer, New York, 2009.
- 114 H. E. Zimmerman and M. D. Traxler, *J. Am. Soc. Chem.*, 1957, **79**, 1920–1923.
- 115 C. J. Cowden and I. Paterson, in *Organic Reactions*, John Wiley & Sons, Inc., Hoboken, NJ, USA, 1997, pp. 1–200.
- 116 I. Paterson, V. A. Doughty, G. Florence, K. Gerlach, M. D. McLeod, J. P. Scott and T. Trieselmann, 2001, pp. 195–206.
- 117 D. A. Evans, H. P. Ng, J. S. Clark and D. L. Rieger, *Tetrahedron*, 1992, **48**, 2127–2142.
- 118 D. A. Evans, J. S. Clark, R. Metternich, V. J. Novack and G. S. Sheppard, *J. Am. Chem. Soc.*, 1990, **112**, 866–868.
- 119 D. A. Evans, J. Bartroli and T. L. Shih, *J. Am. Chem. Soc.*, 1981, **103**, 2127–2129.
- 120 E. M. Carreira, R. A. Singer and W. Lee, *J. Am. Chem. Soc.*, 1994, **116**, 8837–8838.
- 121 J. Mlynarski and B. Gut, *Chem. Soc. Rev.*, 2012, **41**, 587–596.
- 122 U. Eder, G. Sauer and R. Wiechert, *Angew. Chem Int. Ed.*, 1971, **10**, 496–497.
- 123 C. W. Shoppee, F. P. Johnson, R. E. Lack, J. S. Shannon, Z. G. Hajos and D. R. Parrish, *J. Org. Chem*, 1974, **39**, 1615–1621.
- 124 T. Bui and C. F. Barbas III, *Tetrahedron Lett.*, 2000, **41**, 6951–6954.
- 125 B. List, R. A. Lerner and C. F. Barbas, *J. Am. Chem. Soc.*, 2000, **122**, 2395–2396.
- 126 K. Sakthivel, W. Notz, T. Bui and C. F. III, Barbas, *J. Am. Chem. Soc.*, 2001, **123**, 5260–5267.
- 127 A. Códova, S.-I. Watanabe, F. Tanaka, W. Notz and C. F. Barbas III, *J. Am. Chem. Soc.*, 2002, **124**, 1866–1867.
- 128 A. B. Northrup and D. W. C. Macmillan, *J. Am. Chem. Soc.*, 2002, **124**, 6798–6799.
- 129 N. S. Chowdari, J. T. Suri and C. F. Barbas III, *Org. Lett.*, 2004, **6**, 2507–2510.
- 130 N. Mase, R. Thayumanavan, F. Tanaka and C. F. Barbas III, *Org. Lett.*, 2004, **6**, 2527–2530.
- 131 U. M. Lindström, *Chem. Rev.*, 2002, **102**, 2751–2772.

- 132 S. Kobayashi and K. Manabe, *Acc. Chem. Res.*, 2002, **35**, 209–217.
- 133 A. P. Brogan, T. J. Dickerson and K. D. Janda, *Angew. Chem - Int. Ed.*, 2006, **45**, 8100–8102.
- 134 T. J. Dickerson and K. D. Janda, *J. Am. Chem. Soc.*, 2002, **124**, 3220–3221.
- 135 C. J. Rodgers, T. J. Dickerson, A. P. Brogan and K. D. Janda, *J. Org. Chem.*, 2005, **70**, 3705–3708.
- 136 A. M. Steer, N. Bia, D. K. Smith and P. A. Clarke, *Chem. Commun.*, 2017, **75**, 10333–10470.
- 137 L. Burroughs, M. E. Vale, J. A. R. Gilks, H. Forintos, C. J. Hayes and P. A. Clarke, *Chem. Commun.*, 2010, **46**, 4776.
- 138 L. Burroughs, P. A. Clarke, H. Forintos, J. R. Gilks, C. J. Hayes, M. E. Vale, W. Wade and M. Zbytniewski, *Org. Biomol. Chem.*, 2012, **10**, 1565–70.
- 139 D. J. Ritson and J. D. Sutherland, *Angew. Chem. Int. Ed. Engl.*, 2013, **52**, 5845–7.
- 140 L. E. Snyder, D. Buhl, B. Zuckerman and P. Palmer, *Phys. Rev. Lett.*, 1969, **22**, 679–681.
- 141 J. M. Hollis, F. J. Lovas and P. R. Jewell, *Astrophys. J.*, 2000, **540**, L107–L110.
- 142 J. K. Jørgensen, C. Favre, S. E. Bisschop, T. L. Bourke, E. F. van Dishoeck and M. Schmalzl, *Astrophys. J.*, 2012, **757**, L4.
- 143 A. R. Hirst, I. A. Coates, T. R. Boucheteau, J. F. Miravet, B. Escuder, V. Castelletto, I. W. Hamley and D. K. Smith, *J. Am. Chem. Soc.*, 2008, **130**, 9113–9212.
- 144 J. E. Hein and D. G. Blackmond, *Acc. Chem. Res.*, 2012, **45**, 2045–2054.
- 145 B. M. Soares, A. M. Aguilar, E. R. Silva, M. D. Coutinho-Neto, I. W. Hamley, M. Reza, J. Ruokolainen and W. A. Alves, *Phys. Chem. Chem. Phys.*, 2017, **19**, 1181–1189.
- 146 A. M. Steer, PhD Thesis, Univeristy of York, 2017.
- 147 T. J. Dickerson and K. D. Janda, *J. Am. Chem. Soc.*, 2001, **124**, 3220–3221.
- 148 S. P. Brown, M. P. Brochu, C. J. Sinz and D. W. C. MacMillan, *J. Am. Chem. Soc.*, 2003, **125**, 10808–10809.
- 149 A. Córdova, W. Notz and C. F. Barbas III, *J. Org. Chem.*, 2002, **67**, 301–303.
- 150 J. R. Moffat and D. K. Smith, *Chem. Commun.*, 2008, 2248.
- 151 E. R. Draper, T. O. McDonald and D. J. Adams, *Chem. Commun.*, 2015, **51**,

- 6595–6597.
- 152 Y. Lan, M. G. Corradini, X. Liu, T. E. May, F. Borondics, R. G. Weiss and M. A. Rogers, *Langmuir*, 2014, **30**, 14128–14142.
- 153 M. Penhoat, D. Barbry and C. Rolando, *Tetrahedron Lett.*, 2011, **52**, 159–162.
- 154 U. Scheffler and R. Mahrwald, *J. Org. Chem.*, 2012, **77**, 2310–2330.
- 155 X. Yu, L. Chen, M. Zhang and T. Yi, *Chem. Soc. Rev.*, 2014, **5346**, 5346–5371.
- 156 B. Escuder, M. Llusar and J. F. Miravet, *J. Org. Chem.*, 2006, **71**, 7747–7752.
- 157 V. J. Nebot and D. K. Smith, *Functional Molecular Gels*, Royal Society of Chemistry, Cambridge, 2013.
- 158 J. Makarević, M. Jokić, B. Perić, V. Tomišić, B. Kojić-Prodić and M. Žinić, *Chem. Eur. J.*, 2001, **7**, 3328–3341.
- 159 A. R. Hirst, I. A. Coates, T. R. Boucheteau, J. F. Miravet, B. Escuder, V. Castelletto, I. W. Hamley and D. K. Smith, *J. Am. Chem. Soc.*, 2008, **130**, 9113–9212.
- 160 N. Berova, K. Nakanishi and R. Woody, *Circular dichroism: principles and applications*, Wiley-VCH, 2000.
- 161 P. De Marcellus, C. Meinert, I. Myrgorodska, L. Nahon, T. Buhse, L. Le, S. D 'hendecourt and U. J. Meierhenrich, *Proc. Natl. Acad. Sci. U. S. A.*, 2015, **112**, 965–970.
- 162 C. Menor-Salván and M. R. Marín-Yaseli, *Chem. Soc. Rev.*, 2012, **41**, 5404–5415.
- 163 V. M. Kolb, *Handbook of Astrobiology*, CRC Press, Boca Raton, 2018.
- 164 V. K. Rao, S. S. Reddy, B. S. Krishna, K. R. M. Naidu, C. N. Raju and S. K. Ghosh, *Green Chem. Lett. Rev.*, 2010, **3**, 217–223.
- 165 S. Bhagat, N. Sharma and T. S. Chundawat, *J. Chem.*, 2013, **2013**, 1–4.
- 166 E. R. Draper and D. J. Adams, *Langmuir*, 2019, **35**, 6506–6521.
- 167 L. Burroughs, University of York, 2011.
- 168 S. Pizzarello and A. L. Weber, *Science*, 2004, **303**, 1151.
- 169 A. L. Weber and S. Pizzarello, *Proc. Natl. Acad. Sci. U. S. A.*, 2006, **103**, 12713–7.
- 170 J. Kofoed, J.-L. Reymond and T. Darbre, *Org. Biomol. Chem.*, 2005, **3**, 1850–1855.

- 171 S. Budavari, M. J. O'Neil, A. Smith, P. E. Heckelman and J. F. Kinneary, *The Merck Index*, Merck Research Laboratories Division of Merck & CO., Inc, Whitehouse Station, N.J, 12th edn., 1996.
- 172 G. K. Friestad and S. E. Massari, *Org. Lett.*, 2000, **2**, 4237–4240.